

**Proceedings of the  
North American Congress  
on Biomechanics**

combined with  
The Tenth Annual Conference of  
The American Society of Biomechanics (ASB)  
and  
The Fourth Biannual Conference of the  
Canadian Society for Biomechanics (CSB)/  
Société Canadienne de Biomécanique (SCB)



Montreal (Quebec), Canada  
25, 26, 27 August 1986

Volume I

**Proceedings of the  
North American Congress  
on Biomechanics**

combined with  
The Tenth Annual Conference of  
The American Society of Biomechanics (ASB)  
and  
The Fourth Biannual Conference of the  
Canadian Society for Biomechanics (CSB)/  
Société Canadienne de Biomécanique (SCB)

**Volume I**

**Montreal (Quebec), Canada**

**Published by the Organizing Committee**

**P. Allard and M. Gagnon, Co-chairpersons, G. Drouin,  
M. Duhaime, G. Dumas, C. Gagnon, M. Lamontagne,  
C. Putman, C.-H. Rivard, B. Roy, C. Sicard**



All rights to this publication reserved

This book may not be reproduced in any form without  
permission of the publisher

The rights to individual papers are held by the authors.

**Additional copies of Volumes I  
and II may be obtained from:**

**Secretariat ASB**

Thomas P. Andriacchi  
Secretary-Treasurer  
Dept. of Orthopaedic Surgery  
Rush - Presbyterian - St. Luke's  
Medical Center  
1753 West Congress Parkway  
Room 1471 Jelke  
Chicago, Illinois, 60612

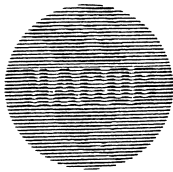
**Secretariat CSB/SCB**

School of Physical and  
Health Education  
Queen's University  
Kingston, Ontario  
K7L 3N6

**Price:**

**\$35.00 (U.S.)** cheque or money order payable to American  
Society of Biomechanics to be forwarded to Secretariat  
ASB.

**\$50.00 (Can.)** cheque or money order payable to Canadian  
Society for Biomechanics to be forwarded to Secretariat  
CSB/SCB.



## **North American Congress on Biomechanics**

### **NACOB**

August 25-26-27, 1986  
Montréal, Québec, Canada

### **CO-CHAIRMEN**

Paul Allard  
Dépt. d'Éducation Physique  
Université de Montréal, PQ  
Micheline Gagnon  
Dépt. d'Éducation Physique  
Université de Montréal, PQ

### **ORGANIZING COMMITTEE**

Gilbert Drouin  
Dépt. de Génie Mécanique  
École Polytechnique  
de Montréal, PQ  
Morris Duhaime  
Dépt. de Chirurgie  
Hôpital Sainte-Justine, PQ  
Geneviève Dumas  
Dept. of Mechanical  
Engineering  
Queen's University, ON  
Carole Gagnon  
Dépt. d'Éducation Physique  
Université de Montréal, PQ  
Mario Lamontagne  
Dépt. de Kinanthropologie  
Université d'Ottawa, ON  
Carol Putnam  
School of Physical Education  
Dalhousie University, NS  
Charles-Hilaire Rivard  
Dépt. d'Orthopédie  
Hôpital Sainte-Justine, PQ  
Benoit Roy  
Dépt. d'Éducation Physique  
Université Laval, PQ  
Claude Sicard  
Dépt. d'Éducation Physique  
Université de Montréal, PQ

The Executive Boards which have governed the American Society of Biomechanics (ASB) and the Canadian Society for Biomechanics (CSB/SCB) during the past year comprise the following members:

### **ASB 1986**

Savio L-Y. Woo  
*President*  
University of California  
San Diego  
Peter R. Cavanagh  
*President-Elect*  
Penn State University  
Thomas P. Andriacchi  
*Secretary-Treasurer*  
Rush-Presbyterian-St. Luke's  
Medical Center  
Paul Allard  
*Meeting Chairperson*  
Université de Montréal  
Carol Putnam  
*Program Chairperson*  
Dalhousie University  
Richard A. Brand  
*Nominating Committee  
Chairperson*  
University of Iowa Hospital  
Ronald F. Zernicke  
*Education Committee  
Chairperson*  
University of California  
Roger M. Enoka  
*Membership Committee  
Chairperson*  
University of Arizona

### **Secretariat ASB**

Thomas P. Andriacchi  
*Secretary-Treasurer*  
Dept. of Orthopaedic Surgery  
Rush-Presbyterian-St. Luke's  
Medical Center  
1753 West Congress Parkway  
Room 1471 Jelke  
Chicago, Illinois, 60612  
(312) 942-5813

### **CSB/SCB 1985-1986**

J. Gavin Reid  
*President*  
Queen's University  
Carol Richards  
*Secretary - Treasurer*  
Université Laval  
Micheline Gagnon  
*Conference Chairperson*  
Université de Montréal  
Susan Tupling  
*Newsletter Editor*  
University of Toronto  
Sandy Thorton-Trump  
*Past Conference Chairman*  
University of Manitoba

### **Secretariat CSB/SCB**

School of Physical and  
Health Education  
Queen's University  
Kingston, Ontario,  
K7L 3N6

**EXECUTIVE BOARD  
1986**

SAVIO L-Y. WOO  
President  
University of California, San Diego  
(619) 452-2676

PETER R. CAVANAGH  
President-Elect  
Penn State University  
(814) 865-3445

THOMAS P. ANDRIACCHI  
Secretary/Treasurer  
Rush-Presbyterian-St. Luke's  
Medical Center  
(312) 942-5813

PAUL ALLARD  
Meeting Chairperson  
University of Montreal  
(514) 343-7934

CAROL PUTNAM  
Program Chairperson  
Dalhousie University  
(902) 424-2152

RICHARD A. BRAND  
Nominating Committee Chairperson  
University of Iowa Hospital  
(319) 356-3472

RONALD F. ZERNICKE  
Education Committee Chairperson  
University of California  
(213) 825-5376

ROGER M. ENOKA  
Membership Committee Chairperson  
University of Arizona  
(602) 621-4850

**PAST PRESIDENTS**

F. GAYNOR EVANS (1977-78)  
ALBERT H. BURSTEIN (1978-79)  
JAMES G. HAY (1980-81)  
STEPHEN A. WAINRIGHT (1981-82)  
ALBERT B. SCHULTZ (1982-83)  
DORIS I. MILLER (1983-84)  
RICHARD A. BRAND (1984-85)

**PAST SECRETARY-TREASURERS**

SAVIO L-Y. WOO (1977-80)  
MALCOLM H. POPE (1980-83)



DEPARTMENT OF ORTHOPEDIC  
SURGERY  
Rush-Presbyterian-St. Luke's  
Medical Center  
1753 West Congress Parkway  
Room 1471 Jelle  
Chicago, Illinois 60612

May 14, 1986

Dear Colleagues:

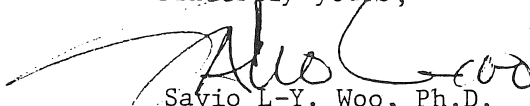
The field of Biomechanics is large, and the investigators are from many disciplines. As a result, numerous difficulties in communication develop. In particular, there are too many meetings which touch upon Biomechanics, and they are scattered in many different professional societies. Thus, the founding members of the American Society of Biomechanics (ASB), in 1977, formed our Society to provide a forum for the exchange of information and ideas among researchers in Biomechanics. The term "Biomechanics" is used to mean the study of the structure and function of biological systems by means of methods of mechanics. ASB consists of members from five loosely divided disciplines. They include: biological sciences, engineering and applied physics, ergonomics and human factors, health sciences, and exercise and sport sciences.

It is a great honor for me to write this note to welcome you to the first combined meeting of the ASB and the Canadian Society of Biomechanics (CSB). This meeting also marks the Tenth Annual Conference of ASB and the Fourth Biannual Conference of CSB. I believe this "crossing the border" meeting will greatly enhance the advances of Biomechanics by bringing investigators from North America under one roof. I am certain that this Congress is only the beginning. I anticipate the combined meeting will blossom and attract increasing numbers of quality papers and participants, as well as to become a focal point for discussion of applications of mechanics to biological and biomedical problems in North America.

The 1986 NACOB is particularly exciting, as we have outstanding invited keynote speakers from Europe including Drs. Cappozzo (Italy), Alexander (United Kingdom), and Huijskes (The Netherlands). Other keynote lecturers will include Drs. Chaffin, Bramble, Norman and Winter from the North American continent. We will also have the Borelli Award lecture by Dr. M.R. Yeadon (Canada). I am sure all will generate new interest, enthusiasm, further participation and collaboration. We thank them sincerely for taking time to join us.

I very much look forward to participating in this three-day conference. The papers are of high quality, and the number of participants is by far the largest for both societies. I look forward to meeting and welcoming you in person during this first North American Congress on Biomechanics.

Sincerely yours,

  
Savio L-Y. Woo, Ph.D.  
President

SOCIÉTÉ CANADIENNE  
DE  
BIOMÉCANIQUE.



CANADIAN SOCIETY  
FOR  
BIOMECHANICS

## WELCOME

The Canadian Society for Biomechanics is pleased to welcome guests and delegates from overseas and across this continent to the North American Congress on Biomechanics in Montreal, Canada. This beautiful city, first discovered in 1535, is located on the Island of Montreal, an extinct volcano. It is the second largest city in Canada and the largest French-speaking city outside of France. We do hope that you find time to tour the city, sample its cuisine and enjoy its night life.

This is the first combined meeting of the American Society of Biomechanics and the Canadian Society for Biomechanics. We are honoured to share in this meeting with our colleagues from the South. The scientific program reflects the breadth and depth of research in biomechanics. May we all benefit in the interchange of information and from the social interaction that will occur. The program provides the opportunity for the fostering of new ideas, rekindling of old friendships and the development of new ones, all of which should well be the main purpose of this Congress.

The organizing committee has provided the forum and now depends on the individual commitment and participation of the delegates to render the Congress successful.

## BIENVENUE

La Société Canadienne de Biomécanique est heureuse de souhaiter la bienvenue aux unités et délégués d'outre-mer et de ce continent pour le Congrès Nord-américain de Biomécanique qui a lieu à Montréal, Canada. Cette belle ville, d'abord découverte en 1535, est située sur l'Ile de Montréal, un volcan éteint. C'est la deuxième plus grande ville du Canada et la plus grande ville francophone à l'extérieur de la France. Nous espérons que vous trouverez le temps de visiter la ville, d'essayer ses styles culinaires et d'apprécier sa vie nocturne.

Il s'agit de la première réunion conjointe de l'American Society of Biomechanics et de la Société Canadienne de Biomécanique. C'est pour nous un honneur de prendre part à cette réunion avec nos collègues du Sud. Le programme scientifique reflète l'ampleur et la profondeur de la recherche en biomécanique. Pussions-nous tous bénéficier des échanges d'information et des interactions sociales qui auront lieu. Le programme donne l'opportunité de stimuler de nouvelles idées, de faire renaître d'anciennes amitiés et d'en développer de nouvelles; tous ces aspects devraient effectivement constituer le but principal de ce Congrès.

Le comité organisateur a fourni un forum et il dépend maintenant de l'engagement individuel et de la participation des délégués d'assurer la réussite du Congrès.

J. Gavin Reid  
Président  
CSB/SCB



## CONGRESS SCHEDULE

Le Grand Hôtel, Montréal

### Sunday Evening, 24 August 1986

19:00 - 22:00 Registration (Foyer du banquet)  
19:00 - 22:00 Welcoming Reception (Cartier A-B)

### Monday, 25 August 1986

07:30 Registration and Information  
(Foyer du banquet)  
08:00 Announcements and Welcoming  
Address (Room A)  
08:15 Keynote Lecture 1  
• **Dr. Donald B. Chaffin** (Room A),  
University of Michigan, Ann Arbor, MI,  
U.S.A.  
08:45 SESSION 1 - Joint Mechanics (Room A)  
SESSION 2 - Human Locomotion IV  
Walking and  
Running (Room B)  
10:15 Intermission  
10:45 Keynote Lecture 2  
• **Dr. Denis Bramble** (Room A),  
University of Utah, Salt Lake City, UT,  
U.S.A.  
11:15 SESSION 3 - Muscle I (Room A)  
SESSION 4 - Human Locomotion IV  
Foot Dynamics (Room B)  
12:30 Lunch  
12:30 ASB Executive Meeting  
CSB/SCB Executive Meeting  
13:30 SESSION 5 - Human Locomotion IV - Poster  
Session I (Régence A)  
14:45 Intermission  
15:00 Borelli Lecture  
• **M.R. Yeadon** (Room A),  
University of Calgary, Calgary, AB, Canada  
15:30 SESSION 6 - Human Locomotion IV  
Rehabilitation (Room A)  
SESSION 7 - Sport (Room B)

### Tuesday, 26 August 1986

08:00 Keynote Lecture 3  
• **Dr. David A. Winter** (Room A),  
University of Waterloo, Waterloo, ON,  
Canada.  
08:30 SESSION 8 - Occupational Biomechanics  
(Room A)  
SESSION 9 - Muscle II (Room B)  
10:00 Intermission  
10:30 Keynote Lecture 4  
• **Dr. R. McNeill Alexander** (Room A),  
University of Leeds, Leeds, United  
Kingdom.  
11:00 SESSION 10 - Human Locomotion IV  
Gait (Room A)  
SESSION 11 - Muscle Control (Room B)  
12:15 ASB Presidential Address and Business  
Meeting (Room B)  
CSB Business Meeting (Room A)  
13:00 Lunch  
14:00 Laboratory Tours  
19:30 Banquet

## Wednesday, 27 August 1986

- 07:00 ASB Executive Meeting
- 08:00 Keynote Lecture 5  
• **Dr. Rik Huiskes** (Room C),  
University of Nijmegen, Nijmegen,  
Netherlands.
- 08:30 SESSION 12 - Spine (Room C)  
SESSION 13 - Human Locomotion IV  
(Room B), Orthopaedic Gait
- 10:00 Intermission
- 10:30 Keynote Lecture 6  
• **Dr. Robert W. Norman** (Room C),  
University of Waterloo, Waterloo, ON,  
Canada.
- 11:00 SESSION 14 - Poster Session II (Régence A)
- 12:15 Lunch
- 13:30 SESSION 15 - Bone Mechanics (Room C)  
SESSION 16 - Human Locomotion IV  
(Room B), Sport
- 15:00 Keynote lecture 7  
• **Dr. Aurelio Cappozzo** (Room C),  
University of Rome, Rome, Italy.
- 15:30 Intermission
- 15:45 SESSION 17 - Human Locomotion IV  
(Room C), Altered Gait  
SESSION 18 - Orthopaedic Fixation (Room B)

Please note the following locations:

Audio-visual room: (Le Royer)

Secretariat: (Vitré)

Exhibits: (Régence A)





## CONGRESS PROGRAM

**Monday, August 25**

### Morning

08:00 - 08:15 Announcements and Welcoming Address  
(Room A)

08:15 - 08:45 **Keynote 1** (Room A)  
**Dr. Donald B. Chaffin**, University of  
Michigan, Ann Arbor, MI, USA.  
LOW BACK MUSCLE MODELS FOR  
LIFTING EVALUATION

### SESSION 1

**- JOINT MECHANICS (Room A)**  
**CHAIRPERSONS:**  
**I.A.F. Stokes & S. Naumann**

08:45 - 09:00 DIFFERENTIATION OF COMPONENTS OF  
RESISTANCE TO PASSIVE MOVEMENT  
USING VOLUNTARY MANEUVERS  
S. Desjardins, C.L. Richards, M. Fillion,  
D. Gravel & V. Piette  
*Hôpital l'Enfant-Jésus and Laval University,  
Quebec, PQ.*

09:00 - 09:15 IN VIVO MEASUREMENTS OF PASSIVE  
MOMENTS OF THE HUMAN HIP  
M. Vrahas, T. Brown, J. Andrews, R. Brand  
& D. Pederson  
*University of Iowa, Iowa City, IA.*

09:15 - 09:30 LOAD TRANSMISSION OF THE WRIST  
JOINT AND PATHOMECHANISM OF  
KIENBÖCK'S DISEASE  
H. Tsumura, S. Himeno, K.N. An & E.Y.S.  
Chao  
*Mayo Clinic, Rochester, MN.*

09:30 - 09:45 ASYMMETRICAL KNEE LAXITIES: AN  
OBJECTIVE EVALUATION  
T.B. Hoshizaki, H. Sveistrup & G. Vagenas  
*McGill University, Montreal, PQ.*

09:45 - 10:00 ANALYSIS OF SQUEEZE-FILM  
LUBRICATION IN HUMAN JOINTS BASED  
ON NON-NEWTONIAN PROPERTIES OF  
SYNOVIAL FLUID  
T.J. Pratt & D.F. James  
*University of Toronto, Toronto, ON.*

10:00 - 10:15

IN-VIVO KINEMATIC PROPERTIES OF THE  
HUMAN SHOULDER COMPLEX  
A.E. Engin & S.M. Chen  
*Ohio State University, Columbus, OH.*

### SESSION 2

**- HUMAN LOCOMOTION IV**  
**- WALKING AND RUNNING**  
**(Room B)**

**CHAIRPERSONS:**  
**S. Olney & P.E. Martin**

08:45 - 09:00

VISUAL ASSESSMENT OF HUMAN GAIT -  
A RELIABILITY STUDY  
A.E. Patla & S.D. Clouse  
*University of Waterloo, Waterloo, ON.*

09:00 - 09:15

KNEE BRACE INFLUENCES ON THE  
SUPPORT PHASE OF RUNNING  
K. Knutzen, P. Schot & B.T. Bates  
*Western Washington University, Bellingham,  
WA and University of Oregon, Eugene, OR.*

09:15 - 09:30

BIOMECHANICAL CHARACTERISTICS OF  
THE SWING LIMB IN MASTERS RUNNERS  
E.M. Roberts, T.K. Cheung, A.A.M. Hafex,  
S.K. Bullard  
*University of Wisconsin, Madison, WI and  
Helwan University, Cairo, Egypt.*

09:30 - 09:45

COMPARISON OF TWO  
ELECTROGONIOMETER PLACEMENTS  
FOR THE MEASUREMENT OF ANKLE  
MOVEMENTS DURING GAIT  
D. Gravel & C.L. Richards  
*Laval University, Quebec, PQ.*

09:45 - 10:00

CHILD AMPUTEE WALKING AND  
RUNNING GAIT: A COMPARISON  
BETWEEN THE SACH AND SINGLE-AXIS  
FOOT COMPONENTS  
B. Brouwer, P. Allard & H. Labelle  
*McGill University, University of Montreal and  
Hôpital Sainte-Justine, Montreal, PQ.*

10:00 - 10:15

QUANTITATIVE THERAPY CONTROL  
USING GAIT ANALYSIS  
S. Luethi, E. Stuessi & B. Segesser  
*Federal Institute of Technology, Zuerich and  
Rennbahn Klinik, Muttentz, Switzerland.*

10:15 - 10:45

**Intermission**

10:45 - 11:15      **Keynote 2 (Room A)**  
**Dr. Denis Bramble**, *University of Utah, Salt Lake City, UT, USA.*  
 MECHANICAL AND PHYSIOLOGICAL ISSUES UNDERLYING LOCOMOTOR AND RESPIRATORY COUPLING IN MAMMALS.

### SESSION 3

- **MUSCLE I (Room A)**  
**CHAIRPERSONS:**  
**F.E. Zajac & M. Lamontagne**

11:15 - 11:30      PHYSIOLOGICAL AND MECHANICAL FACTORS INFLUENCING THE PREDICTION OF MUSCLE FORCES ABOUT THE KNEE JOINT DURING GAIT  
 R.P. Mikosz  
*Rush-Presbyterian - St. Luke's Medical Center, Chicago, FL.*

11:30 - 11:45      ELECTRO-MECHANICAL ADAPTATION TO MUSCULAR STRENGTH TRAINING  
 G.A. Wood, K.P. Singer & A.G. Cresswell  
*University of Western Australia, Australia.*

11:45 - 12:00      PREDICTION OF ANKLE MOMENTS IN GAIT USING CALIBRATED EMG-FORCE-JOINT ANGLE RELATIONSHIPS  
 S.J. Olney, M.P. Griffin, P.A. Costigan & U.P. Wyss  
*Queen's University, Kingston, ON.*

12:00 - 12:15      THE EFFECT OF THE MUSCLES MOMENT ARM ON ITS EMG-FORCE RELATIONSHIPS  
 M. Solomonow, R. Chuinard & R. D'Ambrosia  
*Louisiana State University Medical Center, New Orleans, LA.*

12:15 - 12:30      COMPUTER GRAPHICS OF MUSCLE KINEMATICS AND ELECTROMYOGRAPHY IN GAIT  
 B. McFadyen, D. Winter, B. Day & F. Burkowski  
*University of Waterloo, Waterloo, ON.*

### SESSION 4

- **HUMAN LOCOMOTION IV**  
 - **FOOT DYNAMICS (Room B)**  
**CHAIRPERSONS:**  
**G.A. Valiant & K.R. Williams**

11:15 - 11:30      BIOMECHANICAL ASPECTS OF SHOCK ABSORBING DEVICES  
 A.S. Voloshin  
*Lehigh University, Bethlehem, PA.*

11:30 - 11:45      DISCRETE IN-SHOE PLANTAR STRESS VARIATIONS WITH RUNNING SPEED  
 T.S. Gross & R.P. Bunch  
*Converse Biomechanics Laboratory, North Reading, MA.*

11:45 - 12:00      THE INFLUENCE OF LATERAL HEEL FLARE ON PRONATION AND IMPACT FORCES  
 B.M. Nigg, J. Denoth & R. Glover  
*University of Calgary, Calgary, AB and Federal Institute of Technology, Zurich, Switzerland.*

12:00 - 12:15      EVALUATION OF SHOE-ORTHOTIC INTERACTIONS USING AN IN-SHOE PRESSURE SENSOR SYSTEM  
 J. Hamill, B.T. Bates, M.D. Ricard & M.K. Miller  
*Southern Illinois University, Carbondale, IL and University of Oregon, Eugene, OR.*

12:15 - 12:30      EFFECTS OF FOOT INSERTS ON THE GAIT PARAMETERS OF RHEUMATOID ARTHRITIC PATIENTS  
 P. Allard, W. Loo & H. Tannenbaum  
*University of Montreal, Sainte-Justine Hospital and Montreal General Hospital, Montreal, PQ.*

### Afternoon

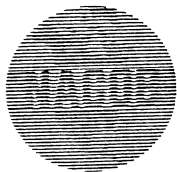
### SESSION 5

- **HUMAN LOCOMOTION IV**  
 - **Poster Session I (Régence A)**  
**CHAIRPERSONS:**  
**G. Drouin & T. Brown**

13:30 - 14:45      PERFORMANCE CHARACTERISTICS OF THE BIOMECHANICS FORCE PLATE  
 D.A. Schieb  
*Kistler Instrument Corporation, Amherst, NY.*

A CLINICALLY VIABLE FORCE PLATFORM MEASUREMENT TECHNIQUE FOR THE VISUAL AND NUMERICAL ASSESSMENT OF FORCE DISTRIBUTIONS BENEATH THE FEET  
 C.D. MacKinnon & C.M. Godfrey  
*Wellesley Hospital, Toronto, ON.*

A TECHNIQUE FOR NORMALIZING CENTER OF PRESSURE PATHS  
 H.U. Motriuk  
*University of Calgary, Calgary, AB.*



A DEVICE FOR THE MEASUREMENT OF  
FIRST RAY MOBILITY

M.M. Rodgers & P.R. Cavanagh  
*West Virginia University Medical Center,  
Morgantown, WV and Pennsylvania State  
University, University Park, PA.*

A KINEMATIC ANALYSIS OF SHANK  
MOTION RELATIVE TO THE CALCANEUS  
DURING THE SUPPORT PHASE OF  
RUNNING

J.R. Engsborg & J.G. Andrews  
*University of Denver, Denver, CO and  
University of Iowa, Iowa City, IA.*

THE FREE MOMENT OF GROUND  
REACTION IN DISTANCE RUNNING AND  
ITS CHANGES WITH PRONATION

J.P. Holden & P.R. Cavanagh  
*Knee Technologies Inc., Cincinnati, OH and  
Pennsylvania State University, University  
Park, PA.*

THE INFLUENCE OF LOAD ON MOVEMENT  
FREQUENCY

R.J. Neal & B.D. Wilson  
*University of Queensland, Australia.*

THE WOBBLING MASS - A RELEVANT  
VARIABLE IN GAIT AND LOAD ANALYSIS

J. Denoth  
*Federal Institute of Technology, Zurich,  
Switzerland.*

THE EFFECTS OF ADDITIONAL LOAD ON  
IMPACT FORCE

B.T. Bates, P. DeVita & J. Hamill  
*University of Oregon, Eugene, OR and  
Southern Illinois University, Carbondale, IL.*

PREDICTION OF OPTIMAL STEP LENGTH  
USING THREE SIMPLE DYNAMIC MODELS  
OF WALKING

M. Hubbard, E.G. Paterson & A.E. Orcutt  
*University of California, Davis, CA.*

A COMPUTERIZED GAIT PROFILE SYSTEM

J.P. Dickey & D.A. Winter  
*University of Waterloo, Waterloo, ON.*

GAIT PATTERNS AND ENERGY  
EXPENDITURE OF PATIENTS AFTER  
RESECTION ARTHRODESIS OF THE KNEE

C. Tylkowski, G. Miller, D. Springfield, N.  
Williamson & W. Enneking  
*University of Florida, Gainesville, FL.*

O<sub>2</sub> CONSUMPTION IN A GAIT  
LABORATORY SETTING

D.L. Wheeler, G.J. Miller & C.M. Tylkowski  
*University of Florida, Gainesville, FL.*

THE DIVERSITY OF NORMAL GAIT

J.C. Wall, J. Charteris & G.I. Turnbull  
*Dalhousie University, Halifax, NS and Rhodes  
University, Grahamstown, South Africa.*

A NEW TECHNIQUE FOR THE  
DETERMINATION OF BODY SEGMENT  
PARAMETERS UTILIZING CAT AND CAD  
PROCEDURES

M.H. Moeinzadeh, S.A. Burns, R.J. Borre &  
G.J. Pijanowski  
*University of Illinois at Urbana-Champaign,  
Urbana, IL.*

CHANGES IN SEGMENT MASS, RADIUS  
AND RADIUS OF GYRATION, FOUR YEARS  
TO ADULTHOOD

R.K. Jensen  
*Laurentian University, Sudbury, ON.*

ESTIMATING SEGMENTAL INERTIAL  
PROPERTIES: MAGNETIC RESONANCE  
IMAGING VERSUS EXISTING METHODS

M. Mungiole & P.E. Martin  
*Arizona State University, Tempe, AZ.*

REGRESSION EQUATIONS FOR  
SEGMENTAL INERTIA PARAMETERS

M. Morlock & M.R. Yeadon  
*University of Calgary, Calgary, AB.*

AN EXPLANATION OF THE UPWARD DRIFT  
IN OXYGEN UPTAKE (UDO) DURING  
PROLONGED SUBMAXIMAL ECCENTRIC  
EXERCISE

R.W. Dick & P.R. Cavanagh  
*Pennsylvania State University, University  
Park, PA.*

CONTRIBUTIONS OF THE ANKLE AND  
KNEE MUSCLES TO SPRINT STARTING

D.G.E. Robertson  
*University of Ottawa, Ottawa, ON.*

VALIDATION OF PLANAR LINK SEGMENT  
MODELS FOR THE STUDY OF UPRIGHT  
BALANCE IN WALKING

J.F. Yang & D.A. Winter  
*University of Waterloo, Waterloo, ON.*

EMG PATTERNS OF THE QUADRICEPS  
DURING TREADMILL RUNNING: A  
DESCRIPTION OF PATELLOFEMORAL PAIN  
SYNDROME

D. MacIntyre & D.G.E. Robertson  
*University of British Columbia, Vancouver,  
BC and University of Ottawa, Ottawa, ON.*

INTEGRATED BIOMECHANICAL & EMG  
ANALYSIS OF STAIR WALKING

B. McFadyen & D. Winter  
*University of Waterloo, Waterloo, ON.*

THE USE OF MULTIPLE REGRESSION IN  
THE DESIGN AND TESTING OF DYNAMIC  
MUSCLE MODELS

J.J. Dowling & R.W. Norman  
*University of Waterloo, Waterloo, ON.*

A DIMENSIONLESS MUSCULOTENDON  
ACTUATOR MODEL FOR USE IN  
COMPUTER SIMULATIONS OF BODY  
COORDINATION: STATIC PROPERTIES

F.E. Zajac, P.J. Stevenson & E.L. Topp  
*Stanford University, Stanford and Veterans  
Administration Medical Center, Palo Alto,  
CA.*

MUSCULOTENDON ENERGETICS OF  
HUMAN JUMPS

M.G. Hoy, F.E. Zajac, E.L. Topp, C.T. Cady,  
M.E. Gordon & W.S. Levine  
*Veterans Administration Medical Center, Palo  
Alto, CA; Stanford University, Stanford,  
CA and University of Maryland, College Park,  
MD.*

ELASTIC ENERGY STORAGE DURING  
SIMPLIFIED JUMPING MOVEMENTS IN  
MAN

M.R. Shorten, R.T. Mueller & L.B. Cooper  
*Nike Sports Research Laboratory, Beaverton,  
OR.*

IN-VIVO PASSIVE RESISTIVE PROPERTIES  
BEYOND THE HUMAN SHOULDER  
COMPLEX SINUS

A.E. Engin & S.M. Chen  
*Ohio State University, Columbus, OH.*

14:45 - 15:00

Intermission

15:00 - 15:30

**BORELLI LECTURE (ROOM A)**

**Dr. M.R. Yeadon**, *University of Calgary,  
Calgary, AB, Canada.*

THE BIOMECHANICS OF TWISTING  
SOMERSAULTS

**SESSION 6**

**- HUMAN LOCOMOTION IV  
- REHABILITATION (Room A)**

**CHAIRPERSONS:**

**J. Sullivan & M.H. Pope**

15:30 - 15:45

FINITE ELEMENT MODEL OF  
ASYMMETRICAL RIB GROWTH IN  
SCOLIOSIS

J. Dansereau, I.A.F. Stokes, J.P. Laible &  
M.S. Moreland  
*University of Vermont, Burlington, VT.*

15:45 - 16:00

THE EFFECT OF LIMITED KNEE-FLEXION  
RANGE ON PEAK HIP JOINT TORQUES IN  
HUMANS TRANSFERRING FROM SITTING  
TO STANDING

S.J. Fleckenstein, R.L. Kirby & D.A.  
MacLeod  
*Dalhousie University and Nova Scotia  
Rehabilitation Centre, Halifax, NS.*

16:00 - 16:15

RELIABILITY AND APPLICATION OF A  
COMPUTERIZED TRIAXIAL  
ELECTROGONIOMETER FOR THE  
EVALUATION OF HEAD MOVEMENTS

F. Malouin & J. Préfontaine  
*Laval University, Quebec, PQ.*

16:15 - 16:30

BIOMECHANICAL ASPECTS OF  
PRECLINICAL DESCRIPTORS OF  
OSTEOARTHRITIS

J. Alexander, A. Bhattacharya, P. Patel & S.  
Brooks  
*University of Cincinnati Medical Center,  
Cincinnati, OH.*

16:30 - 16:45

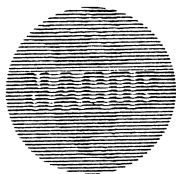
USE OF STATIC PRE-LOADING IN  
ESTIMATION OF DYNAMIC STRENGTH  
WITH THE KIN-COM DYNAMOMETER

V. Piette, C. Richards & M. Fillion  
*Hôpital l'Enfant-Jésus, Québec, PQ.*

16:45 - 17:00

MUSCLE UTILIZATION IN GAIT  
DETERMINED BY A PHYSIOLOGICAL  
CALIBRATION OF EMG

M.C. Normand, C.L. Richards & M. Fillion  
*Université du Québec à Trois-Rivières and  
Hôpital l'Enfant-Jésus, Québec, PQ.*



## SESSION 7

### - SPORT (Room B)

#### CHAIRPERSONS:

**J. Dapena & D.G.E. Robertson**

- 15:30 - 15:45 THREE MODE PRINCIPAL COMPONENT ANALYSIS OF ARM SEGMENT VELOCITIES IN THROWING  
R.J. Neal, C.W. Snyder Jr. & B.D. Wilson  
*University of Queensland, Australia.*
- 15:45 - 16:00 DYNAMICS OF THE SHOULDER AND ELBOW JOINTS OF THE THROWING ARM DURING A BASEBALL PITCH  
M.E. Feltner & J. Dapena  
*Indiana University, Bloomington, IN.*
- 16:00 - 16:15 A MODEL FOR OPTIMIZING THE TIMING OF THE RELATIVE FORCE PATTERNS OF THE ARMS, TORSO, AND LEGS DURING SPRINGBOARD DIVING TAKE-OFFS  
E. Springings, G. Watson, E. Haseganu & D. Derby  
*University of Saskatchewan, Saskatoon, SK.*
- 16:15 - 16:30 AN EXAMINATION OF MECHANICAL ENERGY TRANSFERS AMONGST LOWER EXTREMITY SEGMENTS DURING A KICKING MOTION  
P.E. Martin & W.L. Siler  
*Arizona State University, Tempe, AZ.*
- 16:30 - 16:45 KINEMATICS OF A WORLD RECORD IN THE TRIPLE JUMP  
J.A. Miller Jr. & J.G. Hay  
*University of Iowa, Iowa City, IA.*
- 16:45 - 17:00 FACTORS DETERMINING SQUASH BALL VELOCITY AND IMPLICATIONS FOR THE STROKE  
A.E. Chapman  
*Simon Fraser University, Burnaby, BC.*

**Tuesday, August 26**

## Morning

- 08:00 - 08:30 **Keynote 3 (Room A)**  
**Dr. David A. Winter**, *University of Waterloo, Waterloo, ON, Canada.*  
STRATEGIES AND CONCERNS REGARDING THE ASSESSMENT OF PATHOLOGICAL GAIT

## SESSION 8

### - OCCUPATIONAL BIOMECHANICS

#### (Room A)

#### CHAIRPERSONS:

**J.A.A. Miller & M. Lortie**

- 08:30 - 08:45 A MATHEMATICAL MODEL FOR NECK TENSION AS RELATED TO SOURCE DOCUMENT POSITION  
N. Hamilton  
*University of Illinois, Urbana, IL.*
- 08:45 - 09:00 PRESSURE DISTRIBUTION IN OFFICE SEATING  
S. Reinecke, G. Weisman, A. Stifter & M.H. Pope  
*Vermont Rehabilitation Engineering Center and University of Vermont, Burlington, VT.*
- 09:00 - 09:15 BIOMECHANICAL BASIS OF MUSCULOSKELETAL DISORDERS AMONG VISUAL ARTISTS  
W. Chang., F.J. Bejjani & D. Chyan  
*Hospital for Joint Diseases Orthopaedic Institute, New York, NY.*
- 09:15 - 09:30 ARM LIFT STRENGTH AT DIFFERENT REACH DISTANCES  
S. Kumar & D. Hill  
*University of Alberta, Edmonton, AB.*
- 09:30 - 09:45 WORK-ENERGY REQUIREMENTS FOR TRANSLATING AND TURNING PATIENTS IN BED AS EXECUTED BY NURSING AIDES  
M. Gagnon, F. Akre, M. Lortie, A. Chehade & F. Kemp  
*University of Montreal and Institut de recherche en santé et sécurité du Québec, Montréal, PQ.*
- 09:45 - 10:00 POSTURAL KINEMATICS OF TRUMPET PLAYING  
N. Halpern & F.J. Bejjani  
*Hospital for Joint Diseases Orthopaedic Institute, New York, NY.*

## SESSION 9

### - MUSCLE II (Room B)

#### CHAIRPERSONS:

**R. Wells & M.R. Shorten**

- 08:30 - 08:45 INFLUENCE OF THE AMOUNT OF INFORMATION ABOUT MUSCLE PROPERTIES IN THE COST FUNCTION ON THE ESTIMATE OF INDIVIDUAL MUSCLE FORCES  
W. Herzog *University of Calgary, Calgary, AB.*

- 08:45 - 09:00 SURFACE ELECTROMYOGRAPHY OF ILIOPSOAS  
N. Evans Stüber & R. Wells  
*University of Waterloo, Waterloo, ON.*
- 09:00 - 09:15 ISOKINETIC AND ISOMETRIC STRENGTH ANALYSIS OF HIP MUSCULATURE  
T.D. Cahalan, S.H. Liu & E.Y.S. Chao  
*Mayo Clinic, Rochester, MN.*
- 09:15 - 09:30 SYNERGISTIC BEHAVIOUR OF THE TRICEPS SURAE UNDER SUSTAINED SUBMAXIMAL ISOMETRIC CONTRACTIONS  
A.V. Sirin & A.E. Patla  
*University of Waterloo, Waterloo, ON.*
- 09:30 - 09:45 THE PREDICTION OF MUSCLE FORCE USING EMG AND A MUSCLE MODEL  
S.C. White & D.A. Winter  
*University of Wisconsin, Madison, WI and University of Waterloo, Waterloo, ON.*
- 09:45 - 10:00 BIARTICULAR MUSCLES IN MULTISEGMENT LIMBS  
R.H. Rozendal, G.J. van Ingen Schenau, M. Bobbert & L.H.V. van der Woude  
*Vrije Universiteit, Amsterdam, Netherlands.*

10:00 - 10:30 Intermission

- 10:30 - 11:00 **Keynote 4** (Room A)  
**Dr. R. McNeill Alexander**, *University of Leeds, Leeds, United Kingdom.*  
ELASTIC MECHANISMS IN THE MOVEMENT OF MAMMALS

## SESSION 10

- **HUMAN LOCOMOTION IV**  
- **GAIT (Room A)**  
**CHAIRPERSONS:**  
**C.L. Richards & M.G. Hoy**

- 11:00 - 11:15 BILATERAL ANALYSIS OF THE LOWER LIMBS DURING WALKING IN NORMAL INDIVIDUALS  
S. Ounpuu & D.A. Winter  
*University of Waterloo, Waterloo, ON.*
- 11:15 - 11:30 ASYMMETRY IN LOADING TIMES BETWEEN THE NATURAL AND PROSTHETIC LIMBS IN THE ABOVE-KNEE AMPUTEE  
W. O'Connor  
*Royal Ottawa Regional Rehabilitation Centre, Ottawa, ON.*

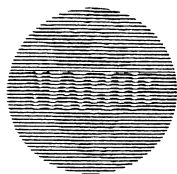
- 11:30 - 11:45 SYSTEM FOR LOCOMOTOR REHABILITATION  
H. Barbeau, L. Finch & M. Wainberg  
*McGill University, Montreal, PQ.*
- 11:45 - 12:00 KINEMATIC ANALYSIS OF GAIT PATTERNS IN UNOPERATED CHILDREN WITH SPASTIC DIPLEGIA  
O. Huk, H. Labelle, M. Duhaime & P. Allard  
*Hôpital Sainte-Justine and University of Montreal, Montreal, PQ.*
- 12:00 - 12:15 HIGH-RESOLUTION REAL-TIME MOVEMENT ANALYSIS AT 100 Hz WITH STROBOSCOPIC TV-CAMERA AND VIDEO-DIGITAL COORDINATE CONVERTER  
E.H. Furnée  
*Delft University of Technology, Delft, Netherlands.*

## SESSION 11

- **MUSCLE CONTROL (Room B)**  
**CHAIRPERSONS:**  
**G.A. Wood & H. Debruin**

- 11:00 - 11:15 THE DEPENDENCE OF THE EMG-FORCE RELATIONSHIP ON THE MUSCLES MOTORUNITS RECRUITMENT RANGE  
M. Solomonow, B.-H. Zhou, R. Baratta, H. Shoji & R. D'Ambrosia  
*Louisiana State University Medical Center, New Orleans, LA.*
- 11:15 - 11:30 FEEDFORWARD POSTURAL CONTROL IN CHILDREN  
C.L. Riach & K.C. Hayes  
*McMaster University, Kingston and Parkwood Hospital, London, ON.*
- 11:30 - 11:45 ELECTROMYOGRAPHIC RESPONSES OF THE LOWER LIMB MUSCULATURE IN SIMULATED POSTURAL AND LOCOMOTOR ACTIVITIES  
R. Wells & N. Evans Stüber  
*University of Waterloo, Waterloo, ON.*
- 11:45 - 12:00 MODULATION OF LIMB DYNAMICS DURING THE LEARNING OF RAPID ARM MOVEMENTS  
K. Schneider, R.F. Zernicke, R.A. Schmidt & T.J. Hart  
*University of California, Los Angeles, CA.*
- 12:00 - 12:15 DOES BICEPS FEMORIS RESPONSE ALWAYS PRECEDE VOLUNTARY ARM RAISES DURING LOCOMOTION IN HUMANS? A.E. Patla  
*University of Waterloo, Waterloo, ON.*





## Wednesday, August 27

### Morning

08:00 - 08:30

**Keynote 5 (Room C)**  
**Dr. Rik Huiskes**, *University of Nijmegen, Nijmegen, Netherlands.*  
 HUMAN JOINT KINEMATICS: A  
 STRUCTURE BASED APPROACH

### SESSION 12

**- SPINE (Room C)**  
**CHAIRPERSONS:**  
**J. Dansereau & A.H. Ahmed**

08:30 - 08:45

QUANTITATIVE ANATOMY OF TRUNK  
 MUSCLES  
 G.A. Dumas, M.J. Poulin, B. Roy,  
 M. Gagnon & M. Jovanovic  
*Queen's University, Kingston;  
 Laval University, Quebec and University of  
 Montreal, Montreal, PQ.*

08:45 - 09:00

CORRELATION OF OBJECTIVE MEASURES  
 OF TRUNK MOTION AND MUSCLE  
 FUNCTION WITH LOW BACK DISABILITY  
 RATINGS  
 J. Triano & A.B. Schultz  
*National College, Lombard, IL and University  
 of Michigan, Ann Arbor, MI.*

09:00 - 09:15

EFFECTS OF CHANGE IN INTRADISCAL  
 FLUID CONTENT ON MECHANICAL  
 RESPONSE OF A LUMBAR MOTION  
 SEGMENT IN COMPRESSION AND  
 EXTENSION  
 A. Shirazi-Adl & G. Drouin  
*Ecole Polytechnique de Montréal, Montréal,  
 PQ.*

09:15 - 09:30

FAILURE OF INTRA-ABDOMINAL  
 PRESSURIZATION TO REDUCE ERECTOR  
 SPINAE LOADS DURING LIFTING TASKS  
 M.H. Krag, K.B. Byrne, L.G. Gilbertson &  
 L.D. Haugh  
*Vermont Rehabilitation Engineering Center,  
 University of Vermont, Burlington, VT.*

09:30 - 09:45

VIBRATION AND IMPACT RESPONSE OF  
 THE SEATED HUMAN  
 M.H. Pope, D.G. Wilder, L. Jorneus, H.  
 Broman, M. Svensson & G. Andersson  
*University of Vermont, Burlington, VT; Ort.  
 Kir. 1, Sahlgrenska Sjukhuést, Goteborg,  
 Sweden; Chalmers Technical University,  
 Goteborg, Sweden; Rush Presbyterian-  
 St.-Luke's Hospital, Chicago, IL.*

09:45 - 10:00

ENERGY TRANSFERS IN THE SPINAL  
 ENGINE  
 S.A. Gracovetsky & S. Iacono  
*Concordia University and Diagnostics  
 Research Inc., Montreal, PQ.*

### SESSION 13

**- HUMAN LOCOMOTION IV**  
**- ORTHOPAEDIC GAIT (Room B)**  
**CHAIRPERSONS:**  
**M. Duhaime & B.T. Bates**

08:30 - 08:45

FUNCTIONAL ANALYSIS OF HIP  
 RESECTION ARTHROPLASTY  
 C.M. Tylkowski, J. Chase, R.W. Petty & G.  
 Miller  
*University of Florida, Gainesville, FL.*

08:45 - 09:00

CHANGE IN ADULT ACQUIRED  
 HEMIPLEGIC GAIT PATTERN FOLLOWING  
 SURGICAL CORRECTION OF EQUINUS  
 R. Sherman, M. Pinzur, P. DiMonte-Levine &  
 J. Trimble  
*Loyola University Medical Center and Hines  
 VA Hospital.*

09:00 - 09:15

ANALYSIS OF CANINE GAIT WITH FORCE  
 PLATFORMS FOLLOWING ANTERIOR  
 CRUCIATE LIGAMENT REPAIR: A PILOT  
 STUDY  
 B.T. Meller, M.T. Manley, P. Hurley & S.  
 Yoshia  
*Cleveland Clinic Foundation, Cleveland, OH.*

09:15 - 09:30

GAIT OF PATIENTS WITH TOTAL KNEE  
 REPLACEMENTS (TKR)  
 U.P. Wyss, S.J. Olney, I. McBride & T.D.V.  
 Cooke  
*Queen's University, Kingston, ON.*

09:30 - 09:45

EFFECTS OF PROXIMAL TIBIAL  
 OSTEOTOMY ON KNEE JOINT LOADING  
 B. Cairns, S. Naumann, P. Tepperman & V.  
 Kekosz  
*University of Toronto, Toronto, ON.*

09:45 - 10:00

BIOMECHANICAL ASSESSMENT OF THE  
 RESULTS OF KNEE SURGERY  
 M.W. Whittle & R.J. Jefferson  
*University of Oxford, Headington, Oxford,  
 England.*

10:00 - 10:30

Intermission

10:30 - 11:00

**Keynote 6 (Room C)**

**Dr. Robert Norman**, *University of Waterloo, Waterloo, ON, Canada.*

CAN BIOMECHANICAL SCIENCE BE EFFECTIVE IN AN ELITE ATHLETE DEVELOPMENT PROGRAM?

A COMPARISON OF ACTUAL INTERNAL DISPLACEMENTS OF HUMAN SPINAL MOTION SEGMENTS PRODUCED BY IN VITRO LOADING AND FINITE ELEMENT MODEL PREDICTIONS

M.H. Krag, R. Seroussi, D.G. Wilder, K.B. Byrne & I. Tausch

*Vermont Rehabilitation Engineering Center and University of Vermont, Burlington, VT.*

THE MECHANICAL EFFECT OF SUSTAINED SIMULATED SEATING ON THE LUMBAR MOTION SEGMENT

D.G. Wilder, R.E. Seroussi, J. Dimnet & M.H. Pope

*University of Vermont, Burlington, VT and Ecole Centrale de Lyon, Lyon, France.*

PARAVERTEBRAL MUSCLE RECRUITMENT IN LATERAL SPINE CURVES

J.A.A. Miller, A.B. Schultz, H. Steen & I. Bjerkreim

*University of Michigan, Ann Arbor, MI and Sophies Minde Orthopaedic Hospital, University of Oslo, Norway.*

THE ANALYTICAL MEASUREMENT OF VERTEBRAL ROTATION

V.J. Raso, D.L. Hill, J.B. McIvor & G.G. Russell

*Glenrose Rehabilitation Hospital and University Hospital, Edmonton, AB.*

ESTIMATIONS OF FORCE AND MOMENT GENERATING CAPACITY OF TRUNK MUSCULATURE FROM CT SCAN MEASURES

S.M. McGill, R.W. Norman & N. Patt  
*University of Waterloo, Waterloo and St. Michael's Hospital, Toronto, ON.*

OBJECTIVE DETERMINATION OF TRUNK MUSCLE DIMENSIONS USING ULTRASOUND: IMPLICATIONS FOR LOW BACK PAIN RESEARCH

M.H. Krag, L. Miller, K.B. Byrne, L.G. Gilbertson & G.B. Johnson  
*Vermont Rehabilitation Engineering Center and University of Vermont, Burlington, VT.*

EFFECT OF LOAD HEIGHT, WEIGHT AND DISTANCE FROM THE BODY ON KNEE AND LUMBAR SPINE FORCES DURING LIFTING

M. Parnianpour, L. Pavlidis, F.J. Bejjani & M. Nordin  
*Hospital for Joint Diseases Orthopaedic Institute, New York University, New York, NY.*

**SESSION 14**

**- Poster session II (Régence A)**

**CHAIRPERSONS:**

**C. Putnam & G. Dumas**

11:00 - 12:15

JOINT SURFACE GEOMETRY AND ESTIMATION OF JOINT FORCES

I.A.F. Stokes  
*University of Vermont, Burlington, VT.*

SIMULATION OF KNEE JOINT MECHANICS IN TWO DIMENSIONS

G.T. Yamaguchi, M.G. Hoy & F.E. Zajac  
*Stanford University, Stanford and Veterans Administrations Medical Center, Palo Alto, CA.*

PRESSURE DISTRIBUTION ON ARTICULAR SURFACE: APPLICATION TO MUSCLE FORCE DETERMINATION AND JOINT STABILITY EVALUATION

S. Himeno, K.N. An, H. Tsumura & E.Y.S. Chao  
*Mayo Clinic, Rochester, MN.*

EMG ENVELOPES FROM NORMAL AND ANTERIOR CRUCIATE LIGAMENT DEFICIENT INDIVIDUALS

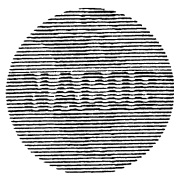
R. Shiavi, H. Borra, M. Frazer & T. Limbird  
*Vanderbilt University, Nashville, TN.*

THE EFFECT OF DEGREES OF FREEDOM ON VARUS-VALGUS KNEE LAXITY

J.M. Hollis, M.A. Gomez, M. Inoue, E.M. Burleson & S.L-Y. Woo  
*University of California, Veterans Administration Medical Center, San Diego, CA.*

A TWO DIMENSIONAL ANALYSIS OF THE CONTRIBUTION OF THE ABDOMINAL MUSCLES TO TRUNK FLEXION

D.J. Morton & J.G. Reid  
*Queen's University, Kingston, ON.*



THE USE OF TRUNK MUSCLE  
ELECTROMYOGRAPHY TO HELP  
VALIDATE A SIMPLE PHYSICAL MODEL  
FOR LIFTING TASKS

R.E. Seroussi & M.H. Pope  
*University of Vermont, Burlington, VT.*

A 3-D ANALYTICAL MODEL FOR THE  
CANCELOUS BONE OF HUMAN LUMBAR  
VERTEBRAE

H. Vaillancourt, G. Drouin & G. McIntyre  
*Ecole Polytechnique de Montréal, Montréal, PQ.*

THE SOFT TISSUE SYSTEM AT THE HEEL  
REGION OF THE FOOT: ITS MECHANICAL  
BEHAVIOR AND FUNCTION

S.E. Robbins & A. Hanna  
*Concordia University, Montreal, PQ.*

A MECHANICAL TEST FOR THE  
MODULUS OF TRABECULAR BONE  
TISSUE

J.L. Ku, S.A. Goldstein, K.W. Choi, S.  
Stein, L. Degnore & L.S. Matthews  
*University of Michigan, Ann Arbor, MI.*

MONITORING SYSTEM FOR HARRINGTON  
ROD IN VIVO STRESS EVOLUTION

N. Charbonneau, G. Drouin, G. Dumas &  
C.H. Rivard

*Ecole Polytechnique de Montréal and  
Sainte-Justine Hospital, Montréal, PQ.*

BENDING AND TORQUE STIFFNESS OF A  
NEW NAIL WITH SPREADING  
MECHANISM FOR FEMORAL FRACTURES

C. Krettek, N. Haas & L. Gotzen  
*Hannover Medical School, Hannover, Federal  
Republic of Germany.*

MATHEMATICAL MODELS FOR  
PREDICTING BONE DENSITY FROM  
STRESS HISTORY

D.R. Carter, D.P. Fyhrie & R.T. Whalen  
*Stanford University, Stanford and Veterans  
Administration Medical Center, Palo Alto, CA.*

SCALING OF LONG BONE FRACTURE  
STRENGTH WITH ANIMAL MASS

F. Selker & D. Carter  
*Stanford University, Stanford, CA.*

SCALING OF LONG BONE TORSION  
STRENGTH DURING GROWTH

T.S. Keller, D.R. Carter, J.A. Main, A.M.  
Strauss & D.M. Spengler  
*V.A. Medical Center, Nashville, TN;  
Stanford University, Stanford, CA and  
Vanderbilt University, Nashville, TN.*

THE ROLE OF COLLAGEN CROSSLINKS IN  
THE AGE RELATED CHANGES IN  
MECHANICAL PROPERTIES OF PIG  
DIGITAL TENDONS

R.E. Shadwick  
*Agricultural and Food Research Council,  
Bristol, United Kingdom and University of  
Calgary, Calgary, AB.*

EVALUATING THE DYNAMIC  
PERFORMANCE OF POSITION  
MEASUREMENT SYSTEMS

Z. Ladin  
*Boston University, Boston, MA.*

ANTICIPATORY POSTURAL  
ADJUSTMENTS IN CHILDREN:  
DEVELOPMENTAL CHARACTERISTICS

L. McCarthy, J. Frank, J. Brown & S. Maki  
*University of Waterloo, Waterloo, ON.*

MOBILITY OF HALO-VEST ON THORAX:  
COMPARATIVE BIOMECHANICS OF 7  
CURRENT AND 1 EXPERIMENTAL VEST  
DESIGN

M.H. Krag & B.D. Beynon  
*Vermont Rehabilitation Engineering Center  
and University of Vermont, Burlington, VT.*

**Afternoon**

**SESSION 15**

13:30 - 13:45

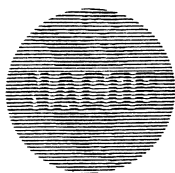
**- BONE MECHANICS (Room C)  
CHAIRPERSONS:**

**M.H. Krag & R. Black**

THE INFLUENCE OF PHYSICAL ACTIVITY  
ON BONE DENSITY

R.T. Whalen, D.R. Carter & C.R. Steele  
*Veterans Administration Medical Center, Palo  
Alto and Stanford University, Stanford,  
CA.*

13:45 - 14:00	REGIONAL VARIATIONS IN THE COMPRESSIVE PROPERTIES OF HUMAN LUMBAR VERTEBRAL TRABECULAE: INFLUENCE OF TISSUE PHYSICAL CHARACTERISTICS T.S. Keller, T.H. Hansson, M.M. Panjabi & D.M. Spengler <i>V.A. Medical Center, Nashville, TN; Sahlgren Hospital, Gothenburg, Sweden; Yale Medical School, New Haven, CT and Vanderbilt University, Nashville, TN.</i>	13:45 - 14:00	MUSCULAR AND "MECHANICAL" MOMENTS OF FORCE IN SWING MOTION E.M. Roberts, J.L. Lin & R.P. Moorman <i>University of Wisconsin, Madison, WI.</i>
14:00 - 14:15	MORPHOLOGICAL AND MECHANICAL RESPONSES OF LONG BONE TO WEIGHTLESSNESS S. Shaw, R. Zernicke, A. Vailas & R. Grindeland <i>University of California, Los Angeles and NASA-Ames Research Center, Moffett Field, CA.</i>	14:00 - 14:15	AN EMPIRICAL MODEL TO CALCULATE THE EFFECTS OF WIND AND ALTITUDE ON THE TIMES OF 100 METER SPRINT RACES J. Dapena & M.E. Feltner <i>Indiana University, Bloomington, IN.</i>
14:15 - 14:30	MECHANICAL PROPERTIES OF BONE ALLOGRAFTS K. Cowling, J. Mukherjee, R.W. Soutas-Little, R. Hubbard & J. Forsell <i>Michigan State University, East Lansing, MI and Edward Sparrow Hospital, Lansing, MI.</i>	14:15 - 14:30	IDENTIFICATION OF SKATEBOARD RIDER CONTROL STRATEGIES M. Hubbard & H. Fujikawa <i>University of California, Davis, CA.</i>
14:30 - 14:45	THE VISCOPLASTIC BEHAVIOR OF CORTICAL BONE M. Fondrk, E. Bahniuk, D.T. Davy, C. Michaels & P. Pallone <i>Case Western Reserve University, Cleveland, OH.</i>	14:30 - 14:45	MEASUREMENTS OF THE ROTATIONAL FRICTION OF COURT SHOES ON AN OAK HARWOOD PLAYING SURFACE G.A. Valiant, L.B. Cooper & T. McGuirk <i>Nike Sports Research Laboratory, Beaverton, OR.</i>
14:45 - 15:00	ESTIMATION OF MECHANICAL PROPERTIES OF BONE USING COMPUTED TOMOGRAPHY E. Schneider, P. Weber, B. Gasser & S.M. Perren <i>University of Bern, Bern, Switzerland.</i>	14:45 - 15:00	THE USE OF AUGMENTED FEEDBACK TO MODIFY PEDALLING MECHANICS D.J. Sanderson & P.R. Cavanagh <i>Pennsylvania State University, University Park, PA.</i>
<b>SESSION 16</b>		15:00 - 15:30	<b>Keynote 7 (Room A)</b> <b>Dr. Aurelio Capozzo</b> , <i>University of Rome, Rome, Italy</i> MECHANICAL LOADING OF THE HUMAN SKELETAL SYSTEM
13:30 - 13:45	BIOMECHANICAL CORRELATES WITH RUNNING ECONOMY IN ELITE DISTANCE RUNNERS K.R. Williams & P.R. Cavanagh <i>University of California, Davis, CA and Pennsylvania State University, University Park, PA.</i>	15:30 - 15:45	Intermission
		<b>SESSION 17</b>	
		- <b>HUMAN LOCOMOTION IV</b> - <b>ALTERED GAIT (Room C)</b> <b>CHAIRPERSONS:</b> <b>M. O'Rian &amp; M. Hubbard</b>	
		15:45 - 16:00	THE KINEMATICS OF UPHILL AND DOWNHILL WLAKING J.C. Wall & J. Charteris <i>Dalhousie University, Halifax, NS and Rhodes University, Grahamstown, South Africa.</i>
		16:00 - 16:15	ELECTROMYOGRAPHIC PATTERNS DURING VISUALLY PERTURBED GAIT A.W. Smith & D.A. Winter <i>University of Waterloo, Waterloo, ON.</i>



- 16:15 - 16:30 THE GAIT OF PACERS  
B.D. Wilson, R.J. Neal & J.S. Groenendyk  
*University of Queensland, Brisbane, Australia.*
- 16:30 - 16:45 A PRELIMINARY STUDY OF THE  
TEMPORAL GAIT KINEMATICS OF  
AFRICAN OCCUPATIONAL HEADLOAD  
CARRIERS  
J. Charteris, P.A. Scott & J.C. Wall  
*Rhodes University, Grahamstown, South African and Dalhousie University, Halifax, NS.*
- 16:45 - 17:00 A COMPARISON BETWEEN FORWARD  
AND BACKWARD WALKING  
B.T. Bates & S.T. McCaw  
*University of Oregon, Eugene, OR.*

#### SESSION 18

##### - ORTHOPAEDIC FIXATION (Room B)

##### CHAIRPERSONS:

**D.R. Carter & C.H. Rivard**

- 15:45 - 16:00 A BIOMECHANICAL ANALYSIS OF GRAFT  
FATIGUE FRACTURE IN A RESECTION  
ARTHRODESIS  
N.R. Williamson, C. Tylkowski,  
G. Piotrowski, G. Miller & D. Springfield  
*University of Florida, Gainesville, FL.*
- 16:00 - 16:15 ANALYSIS OF BONE MODEL MATERIAL  
FOR EXTERNAL FRACTURE FIXATION  
EXPERIMENTS  
T.J. Hein, A. Perissinotto, R.N. Hotchkiss &  
E.Y.S. Chao  
*Mayo Clinic, Rochester, MN.*
- 16:15 - 16:30 MECHANICAL PERFORMANCE OF  
PROPHYLACTIC KNEE BRACES  
S. Meyer, D. Anderson, M. Jimenez, T.  
Brown & R. Brand  
*University of Iowa, Iowa City, IA.*
- 16:30 - 16:45 FRACTURE GAP MOTION IN EXTERNAL  
FIXATION  
B. Fleming, T. Kristiansen, G. Neale, S.  
Reinecke & M. Pope  
*Vermont Rehabilitation Engineering Center  
and University of Vermont, Burlington, VT.*
- 16:45 - 17:00 FATIGUE EVALUATION OF A NEW SPINAL  
FIXATION DEVICE  
M.H. Krag, B.D. Beynnon, M.H. Pope, J.W.  
Frymoyer & L.D. Haugh  
*Vermont Rehabilitation Engineering Center  
and University of Vermont, Burlington, VT.*

## **Keynote Lectures**





Dennis M. Bramble, Department of Biology, University of Utah  
Salt Lake City, Utah, 84112 USA

## INTRODUCTION

This paper is intended to present an overview of current problems concerning the biomechanical and physiological basis of locomotor-respiratory coupling (LRC) in running mammals. Of particular interest are the distinctions between quadrupedal species and humans which arise from difference in body design, posture, and locomotor kinematics. Despite these differences, however, it now appears that both quadrupeds and humans closely integrate gait and breathing patterns in order to: (a) avoid mechanical interference; (b) exploit locomotor forces for respiratory purposes; (c) appropriately scale pulmonary ventilation to the metabolic requirements of the locomotor machinery.

## REVIEW AND THEORY

LRC has only recently been recognized as a widespread and important mechanism in mammals (1). Precise phase-locking of locomotor and respiratory cycles has now been reported in several divergent species, including horses, hares, dogs, and humans (1,2). Quadrupedal mammals tend to exhibit a constant 1:1 coupling ratio (= strides/breath) when running at faster speeds. Humans, in contrast, may utilize up to 6 ratios (e.g., 4:1, 3:1, 2:1) but normally do not exhibit the 1:1 pattern of quadrupeds (3). The kinematics of quadrupedal running, especially the periodic impulsive loading of the forelimbs and thorax, seems to constrain respiration to a simple 1:1 synchronization with the gait cycle. Bipedalism in humans confers greater flexibility in respiratory patterning during running. The choice of any particular coupling ratio seems to depend upon physiological state including such associated parameters as running speed and metabolic demand. Recent theoretical considerations suggest that rhythmic stimulation of mechanoreceptors in the chestwall and diaphragm are possibly key elements in the neurophysiological integration of the locomotor and respiratory cycles in exercising mammals (4).

## METHODOLOGY

Qualitative and quantitative data on LRC have been obtained from freely running subjects (1,3). A small stereophonic tape recording system carried by the subject is used to record breathing sounds on one channel and gait information from limb-mounted accelerometers on the other. High speed cine recordings are used to obtain kinematic detail on limb and trunk motion.

## RESULTS AND DISCUSSION

Recent investigations of mammalian LRC have helped to clarify the mechanical and physiological correlates of this phenomenon. Among the more important findings are the following.

I. Locomotor induced displacements of a "visceral piston" probably have a central role in the mechanical coupling of breathing and gait. Due to its mass and direct attachment to the muscular diaphragm, the liver is the principal component of the piston. In galloping mammals, horizontal cranial and caudal inertial displacements of the piston are associated with exhalation and inhalation respectively. Piston motions in running humans are essentially vertical and are more complex than in quadrupeds. Nonetheless, correlated respiratory and locomotor profiles indicate that piston action is important to pulmonary mechanics in human runners. Further, the data suggest that the dynamics of the visceral piston may be partly responsible for the double-peaked ground reaction force so characteristic of footstrike in human subjects (5,6).

II. Preliminary mathematical modeling indicates that piston mechanics may constrain the maximum economical stride frequency of running mammals to those approximately equal to the natural frequency of the piston system itself (4). This could help to explain the empirical fact that stride frequency in quadrupedal mammals remains nearly constant and independent of running speed above the trot-gallop transition (7).

III. The linking of locomotor and respiratory parameters may provide exercising mammals with a simple but effective means of matching lung ventilation to running speed and, hence, metabolic power requirements. Theoretically, this can be accomplished by simply making breath frequency and tidal volume proportional to (respectively) stride frequency and stride length. Recently published data for exercising horses (2) confirm the predictions of this model. More experiments will be required to determine whether a basically similar (but more complex) relationship exists in humans.

IV. Preliminary data indicate that for humans there is an optimal coupling ratio for sustained running at a particular speed (or range of speeds). Suboptimal coupling patterns appear to result in excessive lung ventilation and possibly excessive energy expenditure. The system of alternate coupling ratios seen in human runners may constitute a gearing system whose purpose is to minimize the energetic cost of both respiration and locomotion. Such a strategy would be analogous to the changing of gait (e.g., trot to gallop; Fig. 1) in quadrupedal runners, an act which is known to minimize the cost of transport (8).

V. The scaling of stride frequency and stride length against speed is strikingly different for quadrupedal and human runners of equal body size. As Figure 2 shows, the expected stride frequency of an experienced human runner is approximately 85 min<sup>-1</sup> at a speed of 5 meters sec<sup>-1</sup>, whereas that of

a quadruped is nearly  $150 \text{ min}^{-1}$ . At this speed the respiratory frequency of the quadruped is (with 1:1 coupling) equal to its stride frequency ( $\sim 150 \text{ min}^{-1}$ ), but the breathing frequency of the human is only  $30\text{--}45 \text{ min}^{-1}$  depending upon the coupling ratio. Hence, at sustainable aerobic running speeds ( $< 6 \text{ m/sec}$ ), a human respire much more slowly and with a relatively much larger tidal volume than does a quadruped moving at the same speed.

It also appears that the fundamental differences in locomotor kinematics of quadrupedal and human runners account for the use of multiple coupling ratios in the latter. Figure 2 is a simple working model which illustrates how stride and ventilation frequency as well as tidal volume and minute lung ventilation are expected to change with increasing running speed in a well-conditioned, elite distance runner. The model suggests that abrupt changes from one breathing pattern to another (e.g., 3:1 to 2:1) are triggered by an upper limit (= threshold value) on tidal volume. The model predicts that such switches in coupling ratio are accompanied both by a sudden increase in ventilation frequency and a correlated drop in tidal volume. Preliminary experimental data seem to support the model.

#### CONCLUSION

Both empirical and experimental data indicate that locomotor and respiratory patterns and mechanics in running mammals are strongly coupled and highly interdependent. Such close integration presumably favors mechanical efficiency and reduces the overall cost of locomotor exercise. Major differences exist in the pattern of locomotor-respiratory coupling exhibited by quadrupedal and human runners. These stem mainly from important differences in the body design and locomotor kinematics of the two groups.

#### References

1. Bramble, D.M., et al. *Science* 219:251-256, 1983.
2. Hörnicke, H., et al. *Equine Exercise Physiology*, D.H. Snow (ed.), Burlington Press, Cambridge (1983), pp. 7-16.
3. Bramble, D.M. *Modelling and Control of Breathing*, Whipp, B.J. and D.M. Wiberg (eds.), Elsevier, New York (1983), pp. 213-220.
4. Bramble, D.M. *Nonlinear Oscillations in Biology and Chemistry*, Lect. Notes in Biomath., H.G. Othmer (ed.), Springer-Verlag (in press).
5. Cavanagh, P.R. et al. *J. Biomech.* 13:397-406, 1980.
6. Dickinson, J.A., et al. *J. Biomech.* 18:415-422, 1985.
7. Heglund, N.C. et al. *Science* 186:1112-1113, 1974.
8. Hoyt, D.F. et al. *Nature* 292:239-240, 1981.

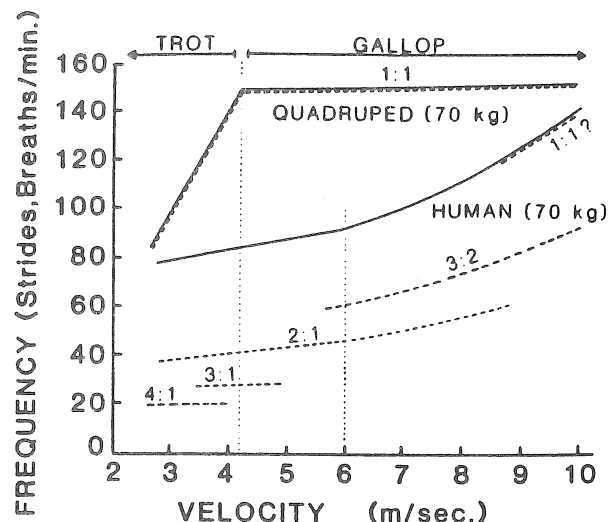


Figure 1. Scaling of coupled stride (solid lines) and respiratory (dashed lines) frequencies against speed in quadrupedal and human runners of equal body mass (70 kg). Speed ranges of various coupling ratios in the human are approximate.

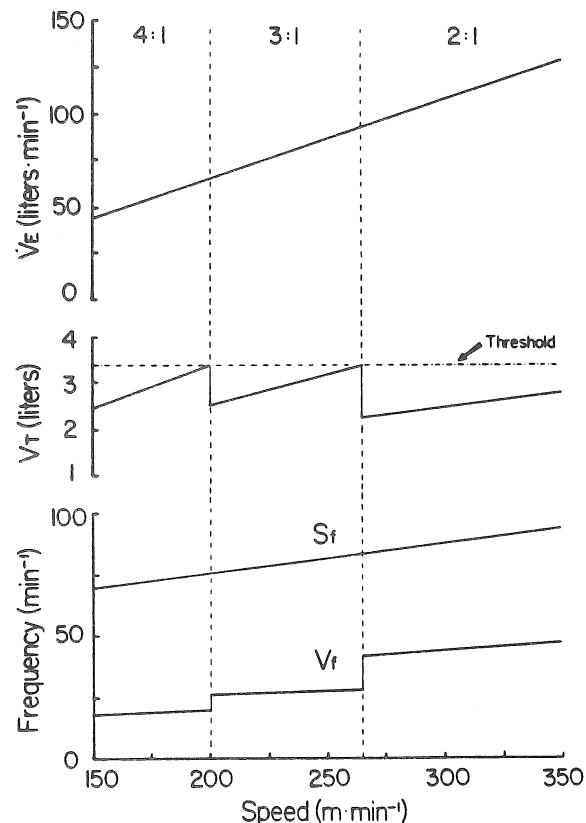


Figure 2. Schematic model of possible interplay of stride ( $S_f$ ) and ventilation ( $V_f$ ) frequency with tidal volume ( $V_T$ ) and minute lung ventilation ( $\dot{V}_E$ ) in a human runner. See text for discussion.

# STRATEGIES AND CONCERNS REGARDING THE ASSESSMENT OF PATHOLOGICAL GAIT

D. A. Winter

Department of Kinesiology  
University of Waterloo  
N2L 3G1

## INTRODUCTION

Clinical gait laboratories have proliferated during the past decade and a wide range of assessments of pathological gait are being reported. Some justified criticisms have been levied; many laboratories merely monitor the progress or lack of progress of patients and are not actively providing information critical to surgical or therapy decisions. Most laboratories are not able to quantify the degree of abnormality at both the motor and kinematic level and few are documenting the adaptations that patients are making that may confound planned therapy. Also, this author would question the validity of some therapy which automatically assumes that a patient must be forced to achieve a more normal gait (in spite of evidence that indicates that an abnormal pattern is safer or more optimal).

The purposes of this paper are: (i) to document basic information about normal gait that will influence our diagnostic procedures, (ii) to summarize the scientific steps to arrive at a definitive diagnosis at the motor level, and (iii) to comment on some potentially erroneous rehab strategies.

## Diagnosis at the Motor Level

Much of the pessimism regarding clinical gait labs is based on the fact that too much effort has focussed on descriptive measures (velocity, cadence, symmetry, joint angles) which are limited to monitoring changes of global measures of the abnormal movement pattern. They don't diagnose the cause of the pattern they observe. It is only at the kinetic and EMG level (suitably correlated with the abnormal pattern) can we achieve a cause-effect diagnosis.

Because so many muscles are involved in gait, we are faced with a serious indeterminacy problem: there are an infinite number of muscle force patterns that can produce the same moment of force profile. The "bad news" that results from this indeterminacy is that normal subjects will have a wide range of motor patterns, so wide that it may be difficult to define what really is normal. The "good news" is that this variability means flexibility and is indicative of tremendous plasticity in the neural control system to adapt to pathological situations.

## Normal Kinematic and Kinetic Patterns

Statistically reliable kinematic and kinetic patterns for normals are required for comparison with our pathological profiles.

Figure 1 is a typical set of profiles of moments of force for fast walking adults. Because the kinetic profiles vary considerably with cadence and body mass, we have subdivided our database into three cadence groups and have normalized all of our kinetic curves by dividing by body mass. Further normalization for body height and sex resulted in insignificant improvements to the inter-subject profiles. We now have available normalized profiles of moment of force, joint mechanical power and EMG patterns for 16 muscles against which our patients can be compared.

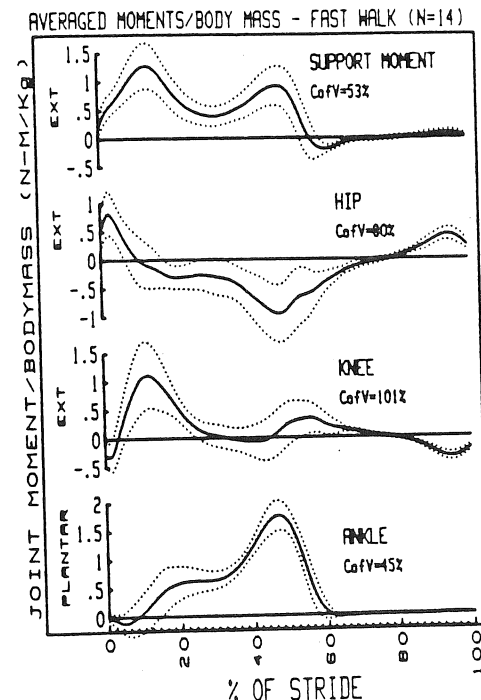


Figure 1: Normalized moment of force profiles for fast walking normals. Mean curve (solid) and  $\pm$  standard deviation (dotted) for 14 subjects is plotted. The coefficient of variation is a measure of the inter-trial variability expressed as a percent of the amplitude of the signal.

## Strategy for Diagnosis

Based on many years experience, we have developed a fairly routine strategy to arrive at a specific diagnosis for each individual patient. The first step is to observe all movement abnormalities; we use TV and summa-

rize the total gait pattern using a computerized gait profile form (Figure 2). Details of the use of this form are presented in another paper in this Congress. It is sufficient to note that the \* alerts us as to phases of the gait cycle that are out of normal range.

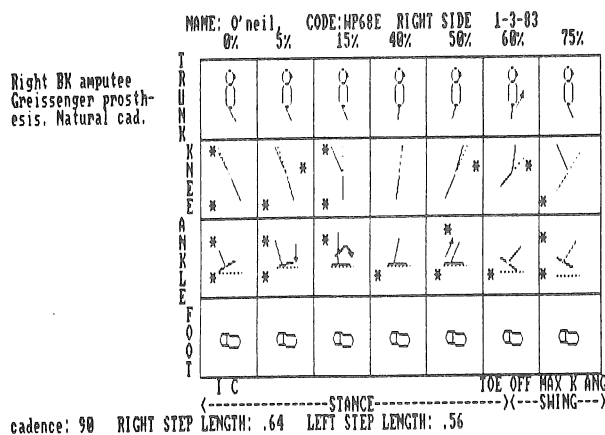


Figure 2: Computerized Gait Profile Form with the profile of the B/K amputee described in the example diagnosis.

TABLE 1

Observed Abnormality	Possible Causes	Biomechanical and Neuromuscular Evidence
Short step-length	Weak push-off prior to swing	Below normal plantarflexor moment or power generation or EMG during push-off
	Weak hip flexors at toe-off and early in swing	Below normal hip flexor moment or power or EMG during late push-off and early swing
	Excessive deceleration of leg in late swing	Above normal hamstring EMG or knee flexor moment or power absorption late in swing
	Above normal contralateral hip extensor activity during stance	Hyperactivity in EMG of contralateral hip extensors
Stiff-legged weight bearing	Above normal ankle, knee or hip extensors early in stance	Above normal EMG activity or moments in hip extensor or plantarflexors early in stance

The second step is to list all possible causes of the observed abnormal movement. Table 1 gives a summarized version of two commonly observed abnormalities: short step length and stiff-legged weight bearing. Then, the final challenge is to examine the patient's biomechanical profiles and, by comparison with those from normals, we should be able to pinpoint the exact cause of the abnormal gait patterns, and also show any compensating patterns.

#### Example Diagnosis

The Computerize Gait Profile for B/K amputee wearing a Gressinger prosthesis is presented in Figure 2. From this profile, the following information was extracted: (i) entire lower limb was extended more than normal at HC. Flat foot did not occur until 15%; initial knee flexion was reduced, (ii)

push-off (50%) was weak, HO was delayed and knee flexion was delayed, and (iii) normal hip extensor pull-off occurred. As this patient was a B/K amputee, his foot could not plantarflex after HC, thus, the delay noted in (i). The fact that he had any observable push-off is somewhat surprising. The biomechanical analyses of joint powers is presented in Figure 3, and which correlates completely with the profile information. Normals are plotted with a solid line and the amputee with a dashed line. A1 power shows the amputee's ankle mechanism (a spring) storing energy, and a small amount is returned during push-off (A2). The amputee had little knee flexion early in stance, therefore did not have a K1 burst. When his knee did break in late stance, he had to use above normal knee extensor power (K3) to control excessive flexion. At the hip, the pull-off power (H3) by the hip flexors was slightly above normal and was the major compensation for the lack of a strong push-off

POWER GEN/ABS (GRESSINGER PROSTHESIS vs. NORMALS)

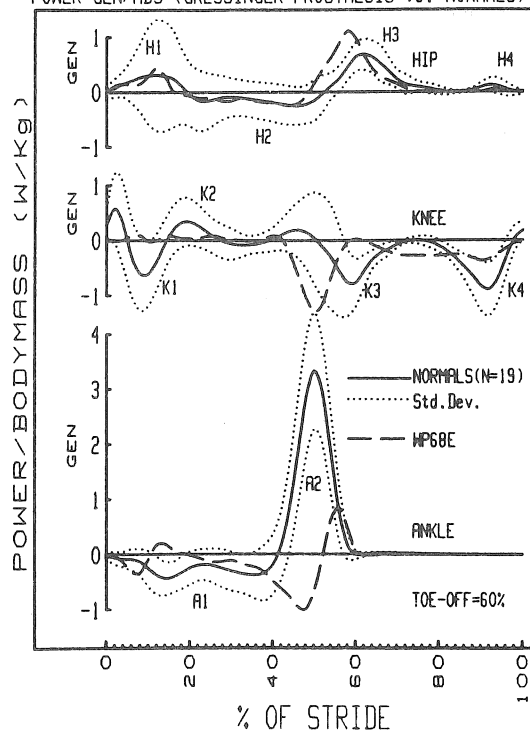


Figure 3: Mechanical power generation and absorption at the ankle, knee and hip for the B/K amputee (dashed line) compared with that for normals (solid line for average, dotted line for s.d.).

#### Conclusions

A systematic and scientific approach has been presented for the diagnosis of pathological gait at the motor level. The procedure not only pinpoints the abnormal motor or biomechanical patterns but also identifies the compensating motor patterns in the residual muscles. Caution is, therefore, suggested when therapy is prescribed which does not recognize these adaptations. For example, forcing an amputee to walk more symmetrically, may undo a new optimal pattern; or, lack of prescribed exercise for newly-compensating muscles may result in early fatigue.

R. McNeill Alexander  
Department of Pure & Applied Zoology  
University of Leeds, Leeds LS2 9JT, U.K.

The elastic properties of materials are exploited in mammals, in several distinct ways.

The ligamentum nuchae in the necks of ungulates serves as a muscle antagonist, helping to support and raise the head (1). The paw pads of mammals serve as shock absorbers (2). Elastic structures serve as catapults in jumping insects (3), but no catapults seem to have been identified in mammals.

This paper is concerned mainly with another function of elastic structures, as pogo-sticks. A running man or a hopping kangaroo loses kinetic energy (KE) and potential energy in the first half of each step and regains them in the second half (4). Each leg exerts a braking action and then an accelerating one, both in bipeds and in quadrupeds. Energy is saved by using muscles and tendons like the springs of pogo-sticks, to absorb energy and then return it. The tendons are particularly important (5). Some distal leg muscles of ungulates have vestigial muscle fibres but retain strong tendons which serve as passive springs. Tendon is an excellent material for such functions because it returns, in its elastic recoil, 93% of the work done stretching it (6). Mechanical tests on feet of donkeys, deer and wallabies have supplied data for rough estimates of energy savings (7), and similar tests are being made on human feet.

The KE fluctuations discussed so far are of external KE, that is of KE associated with movement of the centre of mass. As speed increases, internal KE becomes increasingly important: this is KE associated with movements of feet and other parts relative to the centre of mass. Transition from symmetrical gaits to galloping enables mammals to use an aponeurosis in the back as a spring, storing energy as the legs are halted at the end of a swing and returning it in an elastic recoil (8).

There seems to be scope for saving energy by tendon elasticity in the swimming of whales, but a preliminary analysis suggests that the tendons are more compliant than would be optimal.

#### References

1. Dimery, N.J., et al. J.Zool., Lond. (A) 206: 341-351, 1985.
2. Alexander, R.McN., et al. J.Zool., Lond. (A) 209: in the press, 1986.
3. Bennet-Clark, H.C. J.exp.Biol. 63: 53-83, 1975.
4. Cavagna, G.A., et al. Am.J.Physiol. 233: R243-261, 1977.
5. Alexander, R.McN. Am.Zool. 24: 85-94, 1984.
6. Ker, R.F. J.exp.Biol. 93: 283-302, 1981.
7. Ker, R.F. et al. J.Zool., Lond. (A) 208: 417-428, 1986.
8. Alexander, R.McN. et al. J.Zool., Lond. (A) 207: 467-482, 1985.





## **Sessions' Papers**



S. DESJARDINS, C.L. RICHARDS, M. FILION, D. GRAVEL and V. PIETTE

Centre de Recherche en Neurobiologie  
Hôpital de l'Enfant-Jésus  
1401, 18<sup>e</sup> Rue, Québec, G1J 1Z4

## INTRODUCTION

Several authors have measured visco-elastic resistance to passive movement (PM) at different joints. Such et al. (3) measured knee joint "stiffness" during slow sinusoidal leg oscillations. Effects of neuromuscular responses (NMR) in stretched or shortened muscles were not obvious in these measures. However, when Sahrman et al. (2) imposed ramp movements at the knee joint, NMR were observed, and were often stronger during muscle shortening than during lengthening. Such NMR recorded during PM may influence measures of visco-elastic resistance in systematic ways.

Using a KIN-COM isokinetic exercise system, we repeated part of the methodology of Sahrman et al. (2). At 30°/s, NMR were observed in the quadriceps (Q), and were stronger during muscle shortening than during lengthening. Comparing these results with those taken while performing voluntary maneuvers inhibiting Q-NMR revealed that Q-NMR effects are not negligible: measures of the resistance to movement were significantly modified during the maneuver. We therefore suggest that NMR contribute significantly to the total limb response to passive movement, that they can therefore cause over or underestimation of resistance measures, and that NMR effects can be separated from visco-elastic resistance to movement through specific voluntary maneuvers.

## METHODS

Subjects (6 males; one female) sat on a special bench; the backrest angle being set at 110° with the horizontal. Seat length was adjusted to allow full knee flexion. Upper body movement was restricted by seat belts. Electromyographic (EMG) activity of right quadriceps (Q) and hamstrings muscles were recorded during movements. Movement at the knee was produced by a torque arm attached to the KIN-COM dynamometer. In each movement cycle, the torque-arm rotated the leg from 90° flexion to 0° extension, and back to 90° flexion. Ten such cycles were termed a Movement Condition (MC). EMG responses to imposed movement, force of resistance and angular displacement signals were simultaneously recorded. A data session began with the subject completely relaxed (PM30). During subsequent MC, different voluntary maneuvers were performed: the Jendrassik maneuver during each extension or flexion phase (JE30, JF30 respectively); lightly swinging the opposite leg (SOL).

## RESULTS

We compared force values recorded during the MC: JE30, JF30 and SOL (angle for angle) with those of PM30. Figs. 1 and 2 show the size and direction of shifts to the PM30 force/angle curve caused by these MC. Points plotted negative to the PM30 line indicate forces tending to extend the leg that are

greater than those recorded during PM30. Thus, comparatively less resistance to passive leg extension (Fig. 1) and more resistance to flexion (Fig. 2) is encountered. Points plotted positive to the PM30 line would have the opposite effect. Force values at 0 and 90 degrees were excluded from the analysis. Q-NMR were usually present during PM30 and were either facilitated or inhibited (compare pairs of cols. 1-3 of Fig. 3). Q-NMR were larger during extension than flexion (compare cols. 1A, 2A and 3A, Fig. 3). During JE30 (Fig. 1), a progressive decrease in resistance to extension was seen on Q muscle shortening. In contrast, during SOL, an increased resistance to extension (Fig. 1) and decreased resistance to flexion was seen (Fig. 2). Both force deviations in Fig. 1 and the SOL-induced force deviation in Fig. 2 were significant ( $p < 0.05$ ).

## DISCUSSION

These data partly confirm observations of Sahrman et al. (2), in that neuromuscular responses in the quadriceps (Q) were observed at velocities of 30°/s during both Q shortening and Q lengthening. However, no NMR were seen in hamstrings musculature. Further, a maneuver that inhibits Q-NMR (SOL, Fig. 3) results in significant shifts to the force-angle curve describing resistance to movement. Thus Q-NMR, normally present during PM30 influence records of resistance to movement. They cause underestimation of the resistance to extension, and overestimation of resistance to flexion afforded by purely passive tissues. Since Agarwal and Gottlieb (3) and Wilke (4) described response to PM as being sensitive to reflex contractions or muscular activation, maneuvers such as SOL are valuable in separating the different components of resistance (neuromuscular from viscoelastic) for independent study. Since Q-NMR were angle dependent and repeatable, they may not necessarily be perceived as such in the force records. High gain EMG analysis is necessary to identify such activations, which can be eliminated by use of maneuvers such as SOL.

## CONCLUSIONS

The major conclusion of this paper is the demonstration of significant neuromuscular activity in Q muscles during passive extension and flexion. These NMR were not obvious from the force/angle curves alone and were seen to be present in the force-deviation/angle curves during a maneuver that inhibits Q-NMR (SOL). Components of resistance due to muscle activation and passive viscoelasticity can be separated (at least at the knee joint at low movement velocity) by SOL.

# REFERENCES

1. Such, C.H., et al. Ann. Rheum. Dis. 34: 286-291, 1975.
2. Sahrman, S.A., et al. Proceedings of World Confederation for Physiotherapy: 7th Int'l Meeting, Montreal, Canada: 403-410, 1974.
3. Agaral, G.C., et al. J. Biomed. Eng. 99: 166-170, 1977.
4. Wilke, D.R. J. Physiol. 10: 249-280, 1950.

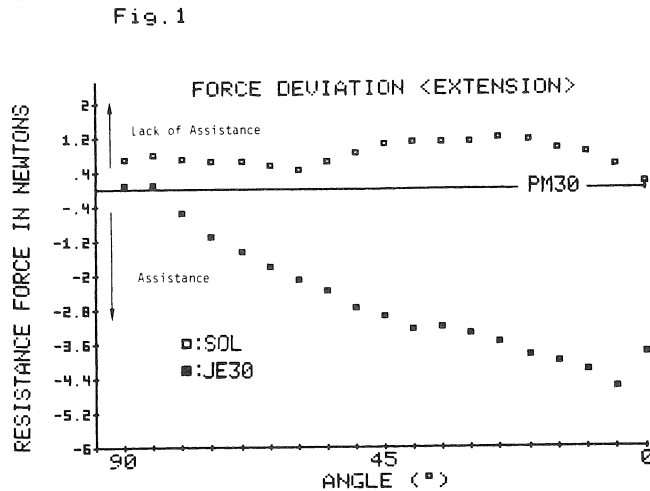


Fig. 1 Force-deviation/angle graph compares limb resistance to imposed knee extension during PM30 to that of JE30 (■) and to that of SOL (□). Smoothly increasing Q-NMR with extension correspond to progressively greater assistance to extension movement. SOL removes Q-NMR and thus removes this assistance.

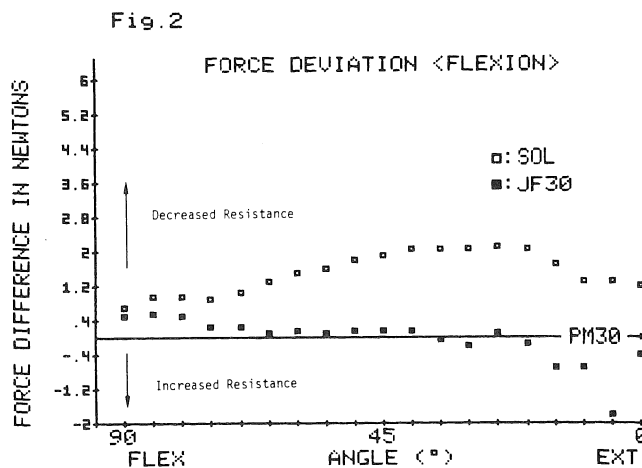


Fig. 2 Force-deviation/angle graph compares limb resistance to imposed knee flexion during PM30 to that of JF30 (■) and to that of SOL (□). SOL removes Q-NMR and thus removes an increased resistance to flexion present in the PM30 condition.

Fig. 3

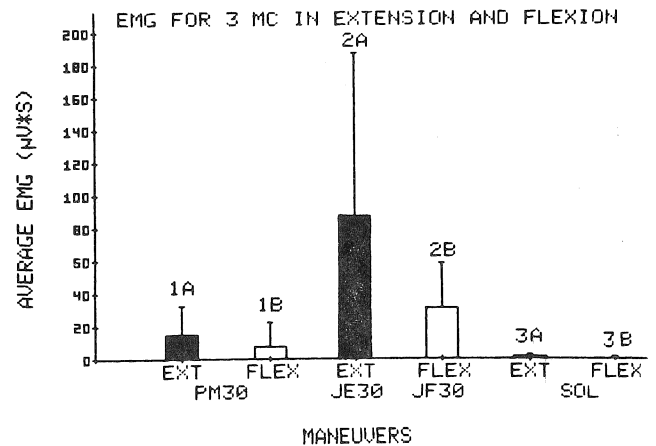


Fig. 3. The Q NMR responsible for the above effects are shown as histograms corresponding to mean EMG amplitude during the extension phase. Q-NMR are greater during extension than flexion, (compare A vs B across cols) and show a trend dependent on MC. For Extension: JE30 > PM30 > SOL. Similar trends are seen for flexion: JF30 > PM30 > SOL.

Acknowledgments: This work was supported by a grant from l'Institut de recherche en santé et sécurité du travail du Québec (IRSST). We thank D. Tardif and Lise Laroche for technical assistance.

# IN VIVO MEASUREMENTS OF PASSIVE MOMENTS OF THE HUMAN HIP

M. Vrahas, T. Brown, J. Andrews, R. Brand, D. Pedersen  
Department of Orthopaedic Surgery, Biomechanics Laboratory  
The University of Iowa, Iowa City, Iowa 52242

## INTRODUCTION

Most investigators studying the kinetics of gait have assumed that inactive muscles and other passive structures contribute little to the total intersegmental moments generated during gait. Recent work by Yoon and Mansour, however, has suggested that the contribution of these passive structures is appreciable [1]. In this pilot study we measured in vivo the flexion/extension moment generated by noncontractile elements at the hip in five normal male subjects. By varying knee flexion angles, and rotating the hip through an arc of 60 degrees, the "passive" hip moments were evaluated at positions corresponding to those of normal gait. At positions similar to those seen at toe off and at heel strike, moments ranged from 2.1Nm to 11.6Nm, and from -5.5Nm to -2.5Nm respectively (negative moment = extension moment). Also important, knee joint flexion angles clearly affected the passive moments at the hip.

## REVIEW AND THEORY

Studying stiffness characteristics, Wright et al. measured the passive moment of the human metacarpophalangeal joint [2]. Wright found the magnitude of the passive moment to be dependent on angular displacement, but not on angular velocity, and from this suggested that viscous elasticity contributed less than 1/10th of the total passive moment generated during the experiments. They further noted, however, the measured moment decreased by 50% if the finger was held motionless for two minutes, suggesting that time, somehow, affected the structures generating the passive moment. More recently, Yoon and Mansour measured in vivo the passive flexion/extension moment at the human hip [1]. These investigators also found the magnitude of the measured moments to be independent of angular velocity, but did not study the effect of holding the hip motionless for prolonged periods of time. More importantly, from their measurements Yoon and Mansour suggested that the passive moment could comprise as much as 50 to 100% of the total flexion/extension moment generated during gait [1]. Because of the significance of these data, we felt it important to attempt to repeat the Yoon and Mansour work.

## METHODOLOGY

The experimental subject assumed a lateral decubitus position on a bench, the pelvis being constrained against rotation. A second table supporting a vertical shaft manually positioned above the patient, and clamped so that the axis of the shaft aligned with the center of rotation of the subject's hip. The subject's leg was suspended from a bar attached to this shaft so that rotations of the shaft flexed and extended the hip. Through a system of pulleys, linear motion of a strain-gaged beam, mounted on a hydraulic MTS ram, caused the vertical shaft to rotate. The MTS ram was programmed to follow a triangular wave form,

resulting in constant angular velocity flexion and extension of the subject's hip.

Five normal male subjects, aged 25 to 40, were evaluated. A continuous measurement of passive hip moment was recorded as the patient's hip was rotated through an arc of 60 degrees. Similar measurements were made for each of five different knee flexion angles (0,20,40,60,80 degrees). All measurements were duplicated at angular velocities of 11, 34, and 80 degrees/second, the latter being a velocity typical of normal gait and the former two being the velocities reported by Yoon and Mansour.

## RESULTS

The measured passive moments at selected hip flexion angles for each of the five knee positions studied in one subject are presented in Figure 1. Table 1 presents the measured passive moments, for all five subjects, for combinations of hip/knee flexion angles commonly seen during gait. There were no appreciable differences in the passive moments measured at different angular velocities, and no decay was noted in the magnitude of the measured moment when the hip was held flexed for 2 minutes.

## DISCUSSION

Comparisons of our work to the few similar published studies, and the internal consistencies of our data suggest that our results are reasonable. The measured moments for a given hip/knee flexion angle (Table 1) are similar from subject to subject. The trends in the moment values corresponding to the different stages of gait are also similar from subject to subject.

Consistent with other investigators, we found passive moment measurements to be insensitive by changes in velocity within the tested range [1,2]. In contrast to the observations made by Wright [2], however, maintaining the hip at 60 degrees of flexion did not lead to a decay in the magnitude of the measured moment. Differences in experimental technique, or in the nature of the metacarpophalangeal passive elements when compared to the nature of the passive elements at the hip could explain the discrepancies. However, it is difficult to imagine a time-dependent portion of the moment independent of changes in angular velocity.

Our data shows a clear relationship between measured hip passive moments, and knee flexion angles. This observation generally similar to the conclusion made by Yoon and Mansour, and implies an important contribution of muscles in general, and two-joint muscles in particular, to the passive moments measured at the hip.

Finally, our passive moment measurements at hip/knee angles corresponding to toe off (range = 2.1Nm to 11.6Nm) were similar to those observed by

Yoon and Mansour. At hip/knee angles corresponding to heel strike, however, our measured moments (-2.5Nm to -5.5Nm) were significantly lower than those reported by those investigators (range = 20Nm - 40Nm).

Further investigations will include the effects of age and disease on the passive moments at the hip joint.

#### CONCLUSIONS

1. The magnitudes of passive moments measured at the hip insensitive to the angular velocity at which they are measured.
2. Changes in knee flexion angles have a substantial affect on the passive moments measured at the hip.
3. At hip/knee flexion angles corresponding to those seen at toe off and at heel strike, measured passive hip moments ranged from 2.1Nm to 11.6Nm and from -2.5Nm to -5.5Nm respectively.

#### References

- [1] Yoon, Y., et al. J. Biomech. 15(12):905-910.
- [2] Wright, V., et al. Ann. Rheum. Dis. 20:36-45.
- [3] Murry, A. J. Phys. Med. 46:290-333.

Supported in part by NIH Grants AM14486 and AM07075.

Figure 1

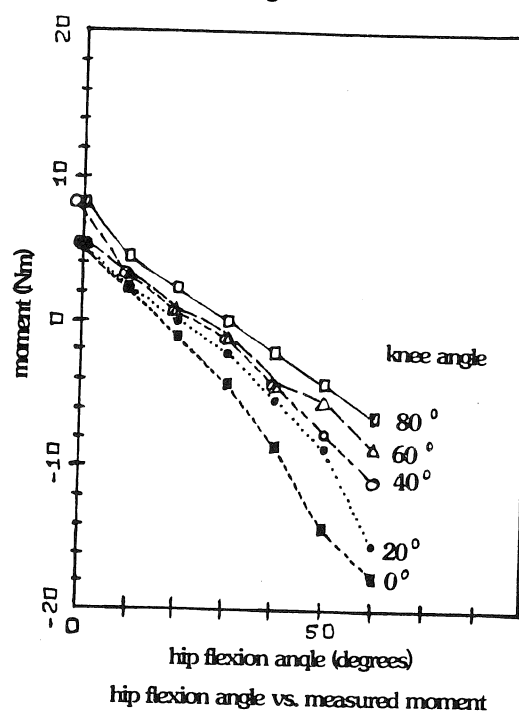


Table 1

%gait hip/knee angle	0%	20%	40%	60%	80%	100%
	0/30	20/20	0/0	10/40	30/60	30/0
SUB.1	-3.8	0.0	3.8	6.3	0.0	-2.5
SUB.2	-2.5	0.0	2.5	5.1	1.3	-3.8
SUB.3	-4.4	0.0	5.5	11.6	1.1	-2.1
SUB.4	-4.4	-1.1	0.0	2.1	1.1	-3.2
SUB.5	-5.5	-1.1	1.1	5.3	4.2	-2.1
Mean	-4.1	-.4	2.5	6.1	1.5	-2.7

passive moments for selected hip/angles in Nm

# LOAD TRANSMISSION OF THE WRIST JOINT AND PATHOMECHANISM OF KIENBÖCK'S DISEASE

H. Tsumura, S. Himeno, K. N. An, E. Y. S. Chao  
Orthopedic Biomechanics Laboratory  
Mayo Clinic/Mayo Foundation  
Rochester, MN 55905

## INTRODUCTION

The wrist joint is a complex articulation including carpal bones, metacarpals, and the distal radius and ulna, interconnected by ligaments and capsules. Load transmission through these structures is quite complicated. Analysis of the way load is transmitted is essential for improved understanding of normal wrist function as well as pathomechanics of wrist disorders.

In this paper, force transmission through the wrist joint is studied by considering it as a two-dimensional, multibody contact problem. Loads applied on the metacarpal and transmitted through the capitate and lunate to the radius are demonstrated.

The lunate, as the keystone of the wrist, is found to be highly stressed. The high stress is considered to be a major cause of aseptic necrosis of the lunate, known as Kienböck's disease.

## REVIEW AND THEORY

The high incidence of Kienböck's disease in hand workers, such as carpenters, strongly suggests that some high stress might be related to the lunate during these hand activities (Dorman, 1949).

Photoelastic studies and other techniques of inserting pressure sensors into the joint have been attempted to reveal such high stress on the lunate and pressure at the joint. However, complicated geometries of the bone and joint make these experiments quite difficult and unreliable.

Computer analysis of such problems is promising. Conventional finite element analysis has been attempted. However, computing time, even in the case of a contact problem of two bodies, is too extensive to be feasible. A simplified, discrete model, originally described by Kawai et al (1977), was thus adopted for this study. The bones are assumed to be rigid plates with "joint springs" around the articulating surfaces and interconnected by "ligamentous springs" representing the ligaments and capsule.

This model could be used to calculate, with short computing time, the distribution of contact stress on all joint surfaces and the tension in each ligament.

## METHODOLOGY

Bone contours are digitized from ordinary dorso-palmar views of wrist roentgenograms using a sonic digitizer. The locations of ligament origins and insertions are also digitized based on bone landmarks. Data are stored in a VAX 11/750 computer system for analysis and display (Fig. 1).

The bones are modeled as rigid-shell structures covered with cartilage on joint surfaces. Because of the large difference in Young's modulus between bone

and cartilage, the most deformation takes place in the cartilage layer. Therefore, in the present model, the bones are considered to be rigid elements, with spring elements attached to the joint surfaces to represent the cartilage.

Global stiffness equations are obtained and solved using the ordinary finite element method by summing individual stiffness matrices. After the displacement of the reference point of each rigid element is calculated, the relative displacement of any spring on the element can then be obtained. The degrees of freedom with such modeling remain relatively small. In this wrist study, 240 springs are used on 30 degrees of freedom (Fig. 1).

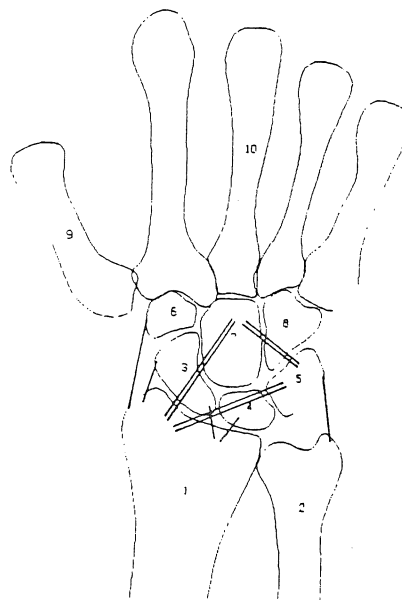


Fig. 1 The wrist model used in this study. Numbers indicate serial numbers of elements. A carpal bone is formulated as a polygonal element. Lines show ligaments.

During calculation, if tension on a "joint spring" or compression on a "ligamentous spring" is detected, the spring is removed, and subsequent iteration continues until no spring removal takes place. After final iteration, the deformation of each element and the normal stress distribution are displayed graphically.

The spring stiffnesses used in this paper are:  
1) Joint springs: 10 N/mm<sup>2</sup> in the normal direction and 0 N/mm<sup>2</sup> tangential to the joint contact surface for each 1 mm of surface length. The spring stiffness between the lunate and fiber cartilage on the end of the ulna is one-half the stiffness of the others.  
2) Ligamentous springs: 40 N/mm for three major ligaments, 10 N/mm for other minor ligaments, and no stiffness in the tangential direction.



The radius and ulna are fixed for all degrees of freedom. Metacarpal bones (designated by "10" in Fig. 1) treated as en bloc were loaded vertically with one unit of force at the location of the middle finger.

### RESULTS

The present method, formulated based on the principle of minimum strain energy, can give pressure distribution on the joint with any arbitrary contour. Pressure distribution and peak pressure of a special hinge joint have been analyzed and compare exactly with those reported by Pauwels (1963).

The stress distribution and force transmission of the wrist joint is shown in Figure 2. Load from the metacarpal was transmitted mainly from the capitate through the lunate and the ulnar side of the scaphoid to the radius. Obviously, the lunate is surrounded by high compressive stress.

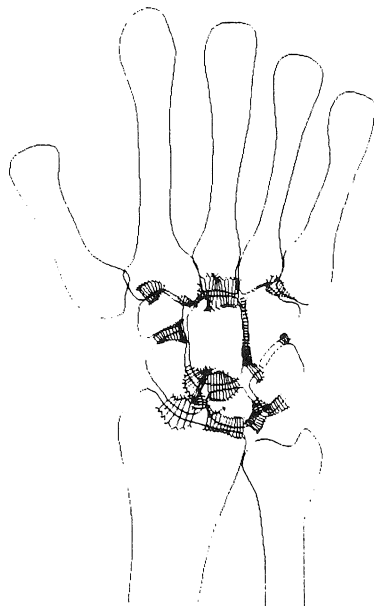


Fig. 2 Load transmission through the normal wrist joint. Note compressive stress around the lunate. All ligaments but one were slackened.

For the condition when the ulna is short relative to the radius, the ulnar support should be less. The spring stiffness along the ulnar side of the lunate is decreased to a fifth of the original conditions. Compressive stress on the ulnar side of the lunate decreased and increased along the radio-lunate joint (Fig 3). This uneven stress might be more unfavorable to the lunate and is considered to be an inducing factor of Kienböck's disease.

### DISCUSSION

Stress distribution on the joints and ligaments is very important in considering wrist pathologies such as aseptic necrosis, injury and instability problems. The method presented in this paper gives some insight into these problems.

The simplification adopted in this method is justified by the fact that bones can be considered as rigid bodies, and most deformation takes place in their cartilage layer. Calculations for intraosseous stress are thus avoided, resulting in a great saving in computing time.

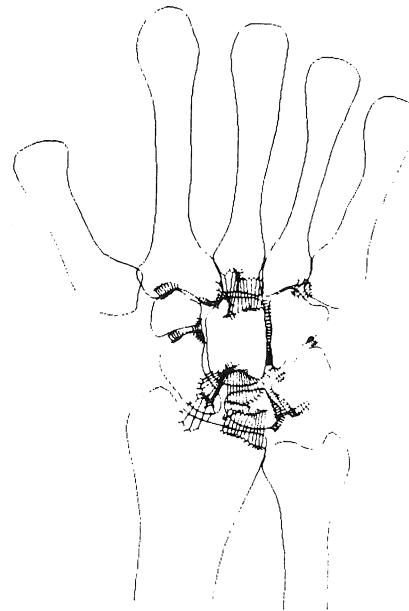


Fig. 3 Load transmission through the wrist joint when ulnar support to the disc was decreased to a fifth of normal. Note decreased pressure along the disc and oppositely increased pressure on the radio-lunate joint.

Unfortunately, only a small amount of data on mechanical properties of the wrist components is available now. The authors had to make several assumptions on this point as mentioned before. However, relative stiffness is considered in the present method, rather than the absolute value itself. Furthermore, a sensitivity study, in which relative stiffnesses of the members was varied several times from original values, had little effect on the conclusions.

### REFERENCES

1. Dorman A.: The results of Treatment in Kienböck's Disease, JBJS, 31-B: 518-520, 1949
2. Pauwels, F: Biomechanics of Locomotive Apparatus, Springer Verlag, 1980
3. Kawai T et al: A New Element in Discrete Analysis of Plane Strain Problems, Seisan kenkyu., 29:204-207, 1977

# ASYMMETRICAL KNEE LAXITIES: AN OBJECTIVE EVALUATION

T.B. Hoshizaki, H. Sveistrup and G. Vagenas  
Biomechanics of Sports Laboratory  
McGill University  
Montreal, Canada H2W 1S4

## INTRODUCTION

Orthopedic surgeons, physiotherapists and trainers are usually faced with the situation of having to evaluate structural damage to the knee without the benefit of pre-injury measures. Evaluation of the structural damage to the knee is therefore accomplished by comparing laxity values for the injured knee with normative laxity values for uninjured knees as well as with the patients contralateral knee values. Assessing the extent of structural damage in the knee by comparing it with the contralateral knee is only valid if structural symmetry in knee joints exists. This assumption has yet to be validated by experimental data. However, there is a convincing argument for the presence of structural and functional asymmetries in the lower limbs of normal persons (1,2,3). This study was designed to identify and measure the degree of asymmetry in knee joint laxity measures represented by AP30, VV20 and IE90 stress tests.

## REVIEW AND THEORY

The techniques used for diagnosis and evaluation of the injured knee have undergone tremendous technical advances. The sophistication of the subjective clinical evaluation has moved from the unstandardized knee evaluation to increasingly complex procedures. It has also been established that knee laxity abnormalities can be more accurately and precisely identified and quantified when biomechanical methods of testing are used as opposed to diagnostic tests of a subjective nature (4). One recently developed biomechanical device that employs an objective measuring technique is the Genucom Knee Analysis System.

Anatomical and functional asymmetries are characteristic of the human body rather than the anomaly (1,2,3). It can be theorized that the function of the knee joint is affected by the presence of such asymmetries thereby imposing an asymmetrical status on the function of the ligaments and other supporting structures of the knee. As a result, knee stability may differ between the left and right leg in normal (uninjured) populations. The common clinical assumption that normal right-left differences are negligible was found invalid by an experimental study (5) which demonstrated the presence of significant laxity asymmetries. This characteristic has serious clinical significance from the point of view of diagnosis of knee injuries.

## METHODOLOGY

Nine females and nine males were tested with the Genucom which consists of a reclining seat supported on a force platform capable of recording force application in the three orthogonal planes and an electrogoniometer used to digitize and locate the knee with respect to an absolute reference axis and to record displacements of the femur within the soft tissue of the thigh and of the tibia with respect to the femur. The subject was braced at the hip and

lower torso to minimize lateral movement of the trunk during force application and at the distal thigh to minimize femoral/thigh movement during force application. Seven points on the tibia/femur were digitized in order to attain a representation of the knee in a relaxed, 90 degree flexed position. The distal thigh was then manipulated through each of the three orthogonal planes in order to determine femoral movement within the soft tissue of the thigh. Actual data collection consisted of repeated measures of the AP30, VV20 and IE90 tests with force application to the tibia only. Figure 1 shows a representative output identifying tibial displacement plotted along the abscissa with force applied plotted along the ordinate. The force-displacement curves of both legs for the same subject are overlaid. Three trials of each test were averaged to give a mean value for each dependent variable. The total range of displacement in each plane was calculated to obtain the dependent variable measures. AP translation was recorded at a 12.24 Nm torque and IE rotation was recorded at a 8.16 Nm torque. The loads employed in testing represent the loads used in clinical diagnosis.

## RESULTS AND DISCUSSION

Statistical analysis required the subjects knees to be designated as superior or inferior based on general variable laxity. The knee was designated as superior if the values for 2 of 3 variables (AP, VV, IE) were less than the contralateral knee. The designation of superior/inferior is simply a classification and does not represent a statistical analysis of the knee. Initial data analysis was performed using SPSSx multivariate analysis of variance. A 2x2 MANOVA was used to identify differences between legs, sex and test for a sex by leg interaction. A significant difference was identified for the sex factor supporting the report of Markolf (5) who identified a tendency for women to manifest greater laxity than men.

When symmetry for knee laxity measures was tested, the data revealed significant differences between the knees. This data was not supported by Markolf (5) who reported no discernable tendency for one knee to be more stable than the other but that random interchanges of relative laxity were observed. However, Markolf's (5) conclusions are not surprising because he compared the left knee with the right knee neglecting to compare superior knees with inferior knees. Following the significant MANOVA, one-tailed univariate F-tests for the three dependent variables collapsed across groups were calculated identifying significant differences between legs for each of the three tests.

The results of the analysis support the existence of knee asymmetry as identified by a combination of the three variables used in this study. The findings have serious implications for the use of contralateral knee laxity values for comparison when assessing knee joint damage.

If, as is demonstrated by the results of this study, the two knees are asymmetrical pre-injury, the diagnosis may be misleading. Often the correct diagnosis

depends on changes in laxity of a few millimeters and given an injury to the "tight" knee, the knee designated as superior in the study, the laxity of the injured knee may increase to approach, equal or be slightly greater than the laxity of the contralateral knee. The increase in the laxity of the injured knee may be significant when compared to its original laxity but may not be significantly different from the healthy contralateral knee. This could allow both 1st, 2nd and 3rd degree injuries to go undetected or even misdiagnosed.

#### REFERENCES

1. Latimer, B.H., et al. Anat Rec. 152:217-224, 1965.
2. Subotnick, I.S. J Amer Pod Assoc. 66:720-723, 1976.
3. Friberg, O. J Sports Med. 22:485-488, 1982.
4. Kalenak, A., et al. JAMA. 234:1143-1145, 1975.
5. Markolf, K.L., et al. J Bone Joint Surg. 60A: 664-674, 1978.

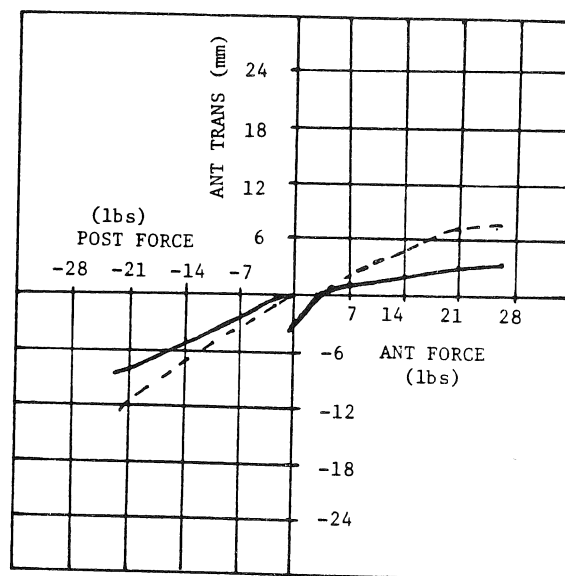


Figure 1. Sample output of anterior-posterior relative displacement-force graphical output. (Solid line indicates right leg; dashed line indicates left leg.)

Table 1. Summary of MANOVA and Univariate F-Tests

MANOVA Results (N 18)  
(females 9, males 9)

Effect	Multivariate F	P
Sex	10.25	.001
Leg	6.04	.007
Sex x Leg	0.23	.88

#### Univariate F-Tests

	N	Superior		Inferior		Diff	F	p*
		M	SD	M	SD			
AP30	18	9.94	3.26	11.65	4.09	-1.71	9.36	.004
VV20	18	9.50	2.55	10.68	2.63	-1.18	3.67	.036
IE90	18	40.31	8.30	42.67	8.38	-2.36	3.77	.035

\* 1-tailed significance

ANALYSIS OF SQUEEZE-FILM LUBRICATION IN HUMAN JOINTS  
BASED ON NON-NEWTONIAN PROPERTIES OF SYNOVIAL FLUID

T.J. Pratt and D.F. James  
Department of Mechanical Engineering,  
Institute of Biomedical Engineering  
University of Toronto  
Toronto, Ontario M5S 1A4

INTRODUCTION

A number of mechanisms have been proposed to explain physiological lubrication, but none appears to be satisfactory for the most severe form of lubrication - squeeze-film lubrication - in which the opposing articular surfaces approach each other head on. Articular surfaces do not wear and therefore presumably do not touch, but analyses of squeeze flow in joints, incorporating the known mechanisms of lubrication, seem to suggest that the surfaces are likely to contact, and thus it is suspected that another mode of lubrication is operative. To test this hypothesis, experiments were planned to measure the decrease in gap distance under a constant load in vitro. To determine if an extra mechanism is operative, it is necessary to know how the squeeze-film process depends on the known mechanisms, particularly on the non-Newtonian properties of the fluid. To that end, a technique was developed to predict gap decrease for an arbitrary shear-thinning fluid, and that work is the subject of this paper. The technique can be applied to many non-Newtonian fluids, but the calculations reported here are for synovial fluid in the talus-tibia joint in the human ankle.

SQUEEZE-FILM LUBRICATION

The basic squeeze-film situation is shown in Figure 1. The disks are assumed to remain parallel as they approach each other under a constant load  $F$ . It is also assumed that  $h \ll R$ , so that the flat surfaces accurately model curved articular surfaces. The goal of the analysis is to find  $h(t)$  for an arbitrary fluid in the gap.

PRIOR WORK

Analytical solutions for  $h(t)$  are available for Newtonian and power-law fluids (For the latter, the shear stress varies as  $\dot{\gamma}^n$ , where  $\dot{\gamma}$  is the shear rate and  $n$  is an experimentally-determined constant). Power-law fluids model the shear-thinning behaviour of polymer solutions reasonably well, but they do not take into account the Newtonian-like behaviour of these fluids at very low and very high rates of shear. To cover the complete range of behaviour, numerical techniques have been developed by Brindley et al(1) and McClelland and Finlayson(2). Because these techniques require specialized software and because the available results from them do not apply to joints, and new numerical technique was devised for the present situation.

DEVELOPMENT OF A FINITE ELEMENT TECHNIQUE

In the analysis to derive an equation for  $h(t)$ , no inertial terms are included in the governing equations because the Reynolds number, based on physiological parameters, is less than 0.1. Because  $h \ll R$ , unsteady effects also can be neglected. Non-Newtonian fluids like polymer solutions can develop normal stresses and these were considered in the momentum balance. Analyses showed that, for synovial fluid under physiological load conditions, the normal stresses in shear and in extension are each at least several orders of magnitude smaller than the pressure created by the load. Hence synovial fluid can be treated as an inelastic fluid whose only relevant property in lubrication is viscosity.

The viscosity of synovial fluid depends markedly on shear rate (as is the case for many polymer solutions) and this behaviour was modelled by treating the fluid as a number of Newtonian fluids, as shown in Figure 2. In the gap, each Newtonian fluid lies in a region bounded by lines of constant shear rate. As indicated in Figure 3, each of these regions was further sub-divided into "finite-element" rectangles in the  $r$ - $z$  plane.

Stokes equation was solved for each rectangle, incorporating the viscosity appropriate for that rectangle. Velocities were matched at horizontal edges and the pressure at vertical edges, to yield the pressure distribution  $p(r)$ . When this distribution was integrated and matched to the load  $F$ , a non-linear 1st-order ordinary differential equation for  $h(t)$  was derived. Solving this equation numerically was not straightforward because the coefficients change in a complex way and there are multiple solutions.

The accuracy of the technique was verified by letting the fluid have power-law characteristics and comparing the answers to the exact results for a power-law fluid.

APPLICATION TO THE TALUS-TIBIA JOINT

The technique was applied to the talus-tibia joint in the ankle. The equivalent radius  $R$  of this joint was estimated to be 1.5 cm and the load was set at 334 N, half the weight of a 68 kg person. The final gap distance was set to 2  $\mu$ m, the mean height of asperities on the articular surface, and the time for the two surfaces to contact was calculated. Using the viscosity versus shear rate data for synovial fluid (3), a contact time of about 0.2 sec was found.

## CONCLUSION

Since standing loads are applied to the ankle for much longer than 0.2 second, it appears that some other mechanism promotes lubrication (unless the surfaces contact but somehow do not wear). In future experiments to explore this possibility, the present technique should be useful in providing a frame of reference for the experimental data.

## References

1. Brindley et al., J. Non-Newt. Fluid Mech., 1, 19, 1976.
2. McClelland, M.A. and Finlayson, B.A., J. Non-Newt. Fluid Mech., 13, 181, 1983.
3. Zeidler et al, Rheol. Acta., 18, 151, 1979.

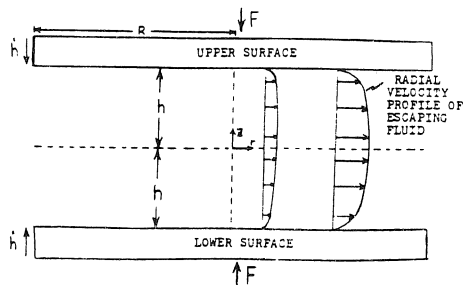


Figure 1. View in the  $r$ - $z$  plane of the squeeze-film flow field.

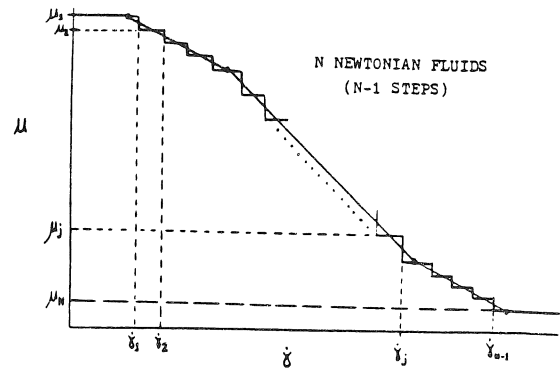


Figure 2. The shear-thinning fluid is modelled as  $N$  Newtonian fluids.

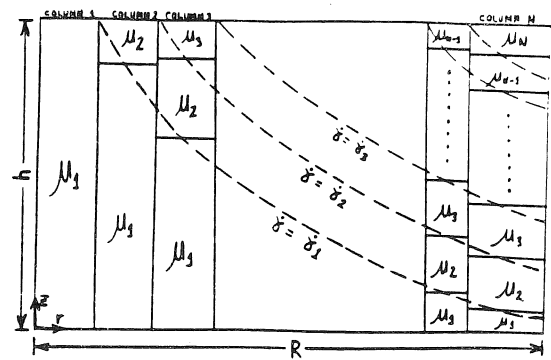


Figure 3. A fluid of constant viscosity (Newtonian) is contained between each pair of dashed lines of constant  $\dot{\gamma}$ . The fluid in each rectangular element is assumed to have a constant viscosity.

# IN-VIVO KINEMATIC PROPERTIES OF THE HUMAN SHOULDER COMPLEX

A.E. Engin  
Department of Engineering Mechanics  
The Ohio State University  
Columbus, Ohio 43210, USA

S.M. Chen  
Department of Engineering Mechanics  
The Ohio State University  
Columbus, Ohio 43210, USA

## INTRODUCTION

In multi-segmented mathematical models of the human body, one area of particular concern is the proper biomechanical description and simulation of major articulating joints. Among these joints, the most complicated and least successfully modeled one has been the shoulder complex mainly due to the lack of an appropriate biomechanical data base as well as the anatomical complexity of the shoulder region. The term "shoulder complex" refers to the combination of the shoulder joint (the glenohumeral joint) and the shoulder girdle which includes the clavicle and scapula and their articulations. This paper presents statistically meaningful data on the range of extreme allowable motion of human shoulder complex for the normal male population of ages 18 thru 32. Ten subjects were randomly chosen to form the sample. The sample mean and sample standard deviation were obtained in a systematic way and were expressed in functional expansion form relative to a locally-defined joint axis system as well as relative to the torso-fixed coordinate system in the form of globographic representation.

## REVIEW AND THEORY

In a recent study (1, 2), the senior author and his associates proposed a new kinematic data collection methodology by means of sonic emitters and data analysis technique based on selection of the "most accurate" data set. By applying this technique, this paper reports the three-dimensional kinematic study on the shoulder complex sinus, i.e., the range of extreme allowable motion of the humerus with respect to torso. The basic components of the data acquisition system used in the study are the sonic digitizer, digitizer sensor assembly with four microphones, torso restraint system, and the arm cuff with six sonic emitters. Since only three emitters are needed to describe the location and orientation of the upper arm with respect to the torso, three out of six emitters can be totally blocked from the view of the sensor assembly without losing kinematic data. A selection criterion (1) was used for the "most accurate" three emitters in cases where more than three emitters produce non-zero data, i.e., when they are not acoustically blocked from the sensor view. Note that with all six emitters giving good readings, there are 20 local axis systems (emitter triads) which can be defined.

## METHODOLOGY

The procedure for determination of the shoulder complex sinus involves the following basic steps: (1) immobilizing the body segment (torso) to be treated as the fixed body and defining the fixed body axis system as shown in Fig. 1, (2) having the subject move the upper arm along the maximal voluntary range of motion (stop contour) and

monitor, with respect to the fixed body axis system, the 3-D coordinates of a distal point on the moving body segment; this point on the elbow joint is selected as being on the humeral longitudinal axis at the level of the humeral condylar maximal width, (3) fitting the 3-D coordinates to a sphere using a least-squares technique, thus establishing a center for the best-fitted sphere and an idealized link length (radius of the sphere), (4) fitting a plane to the same 3-D coordinates using a least-squares technique; the normal to this plane (specified by the spherical coordinates  $(\phi_n, \theta_n)$  as shown in Fig. 1) establishes the pole of a local joint axis system ( $z_{jt}$ -axis) about which the shoulder complex sinus, designated by the spherical coordinates  $(\phi, \theta)$  of the vector connecting the center of the sphere with the distal elbow point, can be expressed as a single-valued functional relationship, i.e.,  $\theta = \theta(\phi)$ . The local joint axis system is uniquely obtained in this study by first rotating the fixed body axis system by an angle  $\phi_n$  about the  $z_{FB}$ -axis and then rotating the intermediate (primed) axis system by an angle  $\theta_n$  about the  $y'$ -axis.

As mentioned before, the shoulder complex sinus can be expressed as a single-valued function, i.e.,  $\theta = \theta(\phi)$ , with respect to the local joint axis system. We consider each individual local joint axis system, defined by  $(\phi_n, \theta_n)$  as an index attributable to the individual anatomical variations in overall joint articulating structure as well as muscle/ligament orientations, and subjective kinematic behavioral variations in the circumscription mannerism. Therefore, not to be biased, each individual shoulder complex sinus should be expressed as  $\theta = \theta(\phi)$  with respect to each individual joint axis system for the purposes of statistically comparing these  $\theta(\phi)$  data sets.

To facilitate the statistical analysis of the huge experimental raw data  $(\phi, \theta)$  collected from the ten subjects, we first expand each subject's sinus by the method of least squares in the following form:

$$\theta(\phi) = \sum_{n=1}^5 \cos^{n-1} \phi (C_{2n-1} + C_{2n} \sin \phi). \quad (1)$$

In this analysis we shall consider  $\theta$  as a random variable and  $\phi$  as an independent variable. It is reasonable to assume that, for each value of  $\phi$ , the random variable  $\theta(\phi)$  is normally distributed with population mean,  $\mu_\theta(\phi)$ , and variance,  $\sigma_\theta^2(\phi)$ , and our task here is to establish estimates of  $\mu_\theta(\phi)$  and  $\sigma_\theta^2(\phi)$  from the sample mean,  $\bar{\theta}(\phi)$  and sample variance,  $S_\theta^2(\phi)$ , of the ten-subject sample.

Since the basis functions on the right-hand side of Eq. (1) are independent and non-random, their coefficients  $C_1, C_2, C_3, \dots, C_{10}$  are independent random variables whose distributions

are also normal with population means  $\mu_{C_1}, \mu_{C_2}, \mu_{C_3}, \dots, \mu_{C_{10}}$  and population variances  $\sigma_{C_1}^2, \sigma_{C_2}^2, \sigma_{C_3}^2, \dots, \sigma_{C_{10}}^2$ . We shall denote their corresponding sample means by  $\bar{C}_1, \bar{C}_2, \bar{C}_3, \dots, \bar{C}_{10}$  and sample variances by  $S_{C_1}^2, S_{C_2}^2, S_{C_3}^2, \dots, S_{C_{10}}^2$ . Note that unlike  $\theta$  which is a function of  $\phi$ , these coefficients are independent of  $\phi$ . Consequently, for each value of  $\phi$ , we have from Eq. (1), the population mean

$$\begin{aligned}\mu_{\theta}(\phi) &= E[\theta(\phi)] \\ &= \sum_{n=1}^5 \cos^{n-1} \phi \{E[C_{2n-1}] + E[C_{2n}] \sin \phi\} \\ &= \sum_{n=1}^5 \cos^{n-1} \phi \left( \mu_{C_{2n-1}} + \mu_{C_{2n}} \sin \phi \right) \quad (2)\end{aligned}$$

and the population variance

$$\begin{aligned}\sigma_{\theta}(\phi) &= \text{VAR}[\theta(\phi)] \\ &= \sum_{n=1}^5 \cos^{2(n-1)} \phi \{ \text{VAR}[C_{2n-1}] \\ &\quad + \text{VAR}[C_{2n}] \sin^2 \phi \} \\ &= \sum_{n=1}^5 \cos^{2(n-1)} \phi \left( \sigma_{C_{2n-1}}^2 + \sigma_{C_{2n}}^2 \sin^2 \phi \right) \quad (3)\end{aligned}$$

where we have utilized

$$\text{COV}(C_i, C_j) = 0 \text{ for all } 1 \leq i < j \leq 10 \quad (4)$$

since all the coefficients  $C_k, 1 \leq k \leq 10$ , are independent. Therefore, if we know the means and variances for the ten coefficients, we can calculate the mean and variance for  $\theta(\phi)$ .

From statistical theory, an estimate for  $\mu_{C_i}$  is

$$\bar{C}_i = \frac{1}{10} \sum_{j=1}^{10} (C_i)_j \quad (5)$$

where  $(C_i)_j$  stands for the  $i^{\text{th}}$  coefficient for the sinus expansion function  $\theta(\phi)$  of the  $j^{\text{th}}$  subject. An unbiased estimate for  $\sigma_{C_i}^2$  is

$$S_{C_i}^2 = \frac{1}{9} \left\{ \sum_{j=1}^{10} (C_i)_j^2 - \frac{1}{10} \left[ \sum_{j=1}^{10} (C_i)_j \right]^2 \right\} \quad (6)$$

Thus, an estimate for  $\mu_{\theta}(\phi)$  from Eq. (2) is

$$\bar{\theta}(\phi) = \sum_{n=1}^5 \cos^{n-1} \phi \left( \bar{C}_{2n-1} + \bar{C}_{2n} \sin \phi \right) \quad (7)$$

and an unbiased estimate for  $\sigma_{\theta}^2(\phi)$  from Eq. (3) is

$$S_{\theta}^2(\phi) = \sum_{n=1}^5 \cos^{2(n-1)} \phi \left( S_{C_{2n-1}}^2 + S_{C_{2n}}^2 \sin^2 \phi \right) \quad (8)$$

## RESULTS

Figure 2 displays the least-squares fitted data for sinuses of all ten subjects. This figure also shows curves for the sample mean,  $\bar{\theta}(\phi)$ , and those corresponding to  $\bar{\theta}(\phi) \pm S_{\theta}(\phi)$ . Figure 3 shows their corresponding globographic representations in the

torso-fixed coordinate system, i.e., the spherical coordinates on the globe are referred to the fixed body axis system. Therefore, the  $(0^\circ, 90^\circ)$  coordinate on the globe corresponds to the emergent point of the  $x_{fb}$ -axis, and the  $(90^\circ, 90^\circ)$  coordinate corresponds to the emergent point of the  $y_{fb}$ -axis.

## References

1. Engin, A.E., et al. J. Biomech. Engng. 106:204-211, 1984.
2. Engin, A.E., et al. J. Biomech. Engng. 106:212-219, 1984.

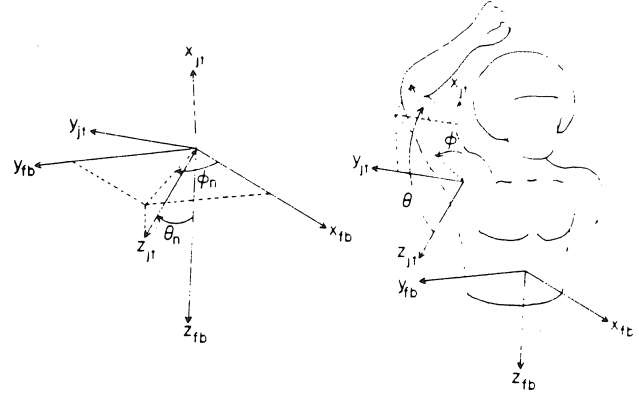


Figure 1. Relative Orientation of the fixed body ( $x_{fb}, y_{fb}, z_{fb}$ ) and locally-defined joint ( $x_{jt}, y_{jt}, z_{jt}$ ) axis system.

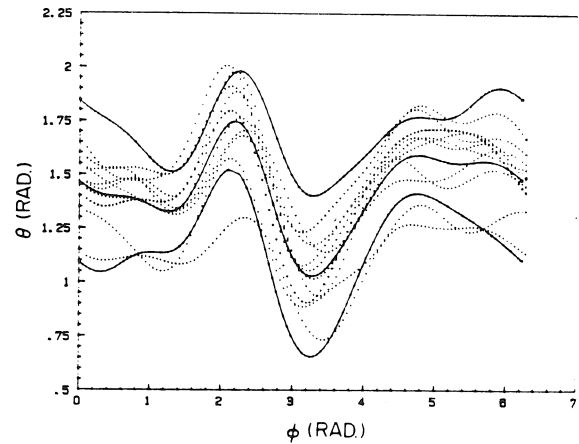


Figure 2. Curve-fitted data for shoulder complex sinuses of all subjects (dotted curves). Solid curves are for  $\bar{\theta}$  and  $\bar{\theta} \pm S_{\theta}$ .

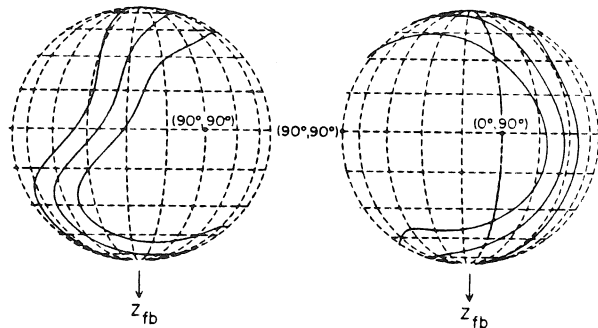


Figure 3. Globographic representations of  $\bar{\theta}$  and  $\bar{\theta} \pm S_{\theta}$ .

# PHYSIOLOGICAL AND MECHANICAL FACTORS INFLUENCING THE PREDICTION OF MUSCLE FORCES ABOUT THE KNEE JOINT DURING GAIT

R.P. Mikosz  
Department of Orthopedic Surgery  
Rush-Presbyterian-St. Luke's Medical Center  
Chicago, Illinois 60612

## Introduction

The prediction of human muscle forces has been the subject of many investigators. In vivo measurement of muscular forces in humans is currently impractical. Thus, either indirect measurements (such as electromyography - EMG) or mathematical prediction of muscle forces on a macroscopic scale are the only alternatives. The prediction of individual muscle forces about the knee requires not only knowledge of the physiological factors influencing muscle contraction, but also must account for intricate anatomy such as the patellar mechanism, the rolling and gliding movement of the tibial-femoral articulation and the geometrically complex articulating surfaces. These factors play a major role in changing the mechanical effect of the muscles about the knee joint. The physiological factors influencing muscle contraction are dependent upon the force developed in the muscle, the length of the muscle and the shortening velocity of the muscle during locomotion. The relationship between force and velocity is described in Hill's equation and is fundamental to muscle mechanics. This paper reports on the development of a three-dimensional statically indeterminate stochastic muscle model of the human knee joint and a study of factors which influence the response of individual muscle forces about the joint.

## Methodology

The model includes the proximal portion of the tibia and the distal portion of the femur represented mathematically as rigid bodies. Thirteen muscles included in the model are represented by potential force vectors directed tangential to the points of attachment at the femur and tibia. The patellar ligament angle changes with knee flexion according to data experimentally obtained (4). The model also includes a mathematical expression of the patellar mechanism. The ratio of tensions in the quadriceps tendon and the patellar ligament were incorporated into the model using experimental data obtained by Ellis, et al. 1980. The combined influence of the ligaments was modelled as torsional bending elements with bending stiffnesses in the abduction-adduction and internal-external rotational direction. The contact area between the tibia and femur was represented as the geometric center of the contact area (3).

The model enforces moment equilibrium at the knee joint. This assumption seemed reasonable since the muscles crossing the

knee joint are in an ideal position to resist external moments. By introducing the contact areas as an unknown, the moment equilibrium equations are non-linear. A Quasi-Newton algorithm for finding the minimum of an N'th order non-linear function in n variables was used. The trial solution required by the algorithm were pre-conditioned using EMG data, flexor-extensor moment directions and relative moment magnitude for a given activity.

The solution method examines the hypothesis that physiological solutions can be obtained by a process other than optimization. Using this technique, the solution space is narrowed by imposing physiological and anatomical constraints on both initial trial solutions and the final solution. The trial solution space is assumed to behave randomly in nature within the bounds of the constraints. This randomness is reflected in the final solution, thus, making this a stochastic model.

An important characteristic which influences the force generated by muscle is that physiologically the maximum force generated by muscle depends on the velocity of contraction of the muscle and the length of the muscle. This relationship between force and velocity, known as Hill's equation (2), is fundamental to muscle mechanics and has been incorporated into the model.

The model was used to simulate experiments (1) designed to study the relationship between external moments acting about the knee joint and EMG activity of 12 muscles crossing the knee joint. The external moments were applied in four directions of load; flexion, extension, combined flexion and combined extension. Four increments of loading were applied in each case for moments tending to produce flexion and for moments tending to produce extension. Moments tending to produce abduction and adduction were applied in combination with the largest and smallest flexion and extension moments. The above moments were applied at knee flexion angles of 10°, 20° and 40° for a total of 47 different load situation.

## Results

Correlation coefficients were combined for all 47 load situations between EMG activity and muscle force. The quadriceps muscles were highly correlated ( $r > 0.94$ ) while the hamstrings were correlated to a lesser extent ( $r < 0.75$ ). The sartorius, gracilis, and gastrocnemius lateralis all



had correlation coefficients of  $r=0.41$  and  $r=0.46$ , respectively. There was a significant relationship between EMG activity and muscle force ( $p<0.05$ ) for all muscles with correlation coefficients of ( $r>0.29$ ). From myoelectric experiments (1) quadriceps myoelectric activity decreased with increasing knee flexion (Fig. 1). At  $10^\circ$  of knee flexion, the EMG activity was 90% maximum and decreased to 25% maximum EMG activity at  $40^\circ$  of knee flexion. When the contact point was free to move in the model, the quadriceps muscle force was correlated to the EMG measurements. However, when the contact point was fixed at the geometric center of the tibial plateau, quadriceps force decreased by only 15% and did not correspond to in vivo results.

The calculation of muscle length and muscle contraction velocity on the prediction of muscle force during the gait cycle indicated that maximum demands on muscles occur at optimum times during the walking cycle. For example, an evaluation of level walking (1.13 m/sec) was used to compare the force, muscle length and muscle velocity of contraction to Hill's equation (Fig. 2). The largest force occurred in the biceps femoris when the muscle was at the greatest length during the gait cycle and at zero velocity.

#### Discussion and Conclusions

A stochastic model has been developed which takes into account some of the anatomical and physiological features of the knee joint. Mathematically, this approach differs from others in the sense that it does not involve a cost function, rather it is a constrained stochastic model. Further, it includes mechanical features of the knee such as the relative tibial-femoral movement and a mathematical representation of the patellar mechanism. By incorporating the velocity tension relationship for muscle, the influence of the effects of velocity of muscle contraction on developed muscle tension were determined.

The model has also been useful in demonstrating why certain mechanical as well as physiological features are necessary to produce physiological muscle forces at the knee joint. A very important aspect of the model was the capability to simulate the moving contact point between the tibia and femur which increased the mechanical advantage of the quadriceps muscles by 50% which correspond to in vivo EMG measurements. A moving contact point for a normal knee supplies a mechanical advantage by increasing the lever arm. This can greatly reduce the forces required by the quadriceps muscles to balance a fixed moment.

During normal gait, the largest demands on muscles to generate forces occur at phases of the cycle where the muscle has its greatest length and is at zero velocity. According to Hill's equation, at zero velocity muscle can generate its maximum force. Thus, it appears that for normal walking the kinematics place the muscles in a position where the demand to generate force is minimized. Thus, variations from

the kinematics of normal gait would likely change this delicate relationship between muscle force, length and velocity of contraction and produces less energy efficient gait.

It should be emphasized that there exists many possible solutions which will satisfy equilibrium. By placing boundaries on the solution and by pre-conditioning the trial solution, it was possible to converge to an equilibrium solution which was within physiological limits without an optimization criterion.

#### References:

1. Andriacchi, T.P., et al. J. Orthop. Res., 1:266-275, 1984.
2. Hill, A.V., Proc. Roy. Soc. Lond. Ser.B., 126:136-195, 1938.
3. Iseki, F., et al. Keio J. Med. 25:37-44, 1976.
4. Matthews, L.S. et al. Acta. Orthop. Scand. 48:511-516, 1977.

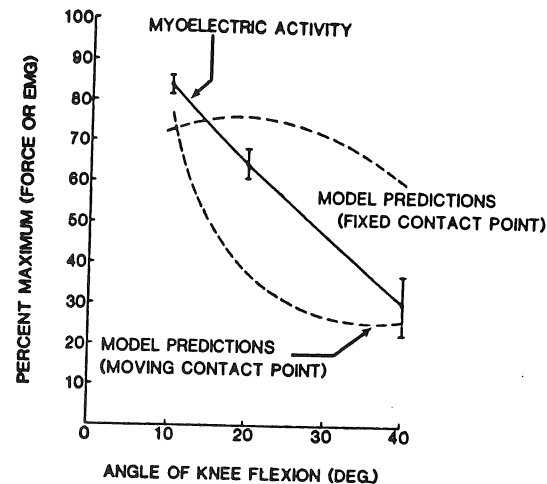


Figure 1. Relationship between myoelectric activity and quadriceps force for a fixed and moving contact point for knee flexion angles of 10, 20, 30 and 40 degrees.

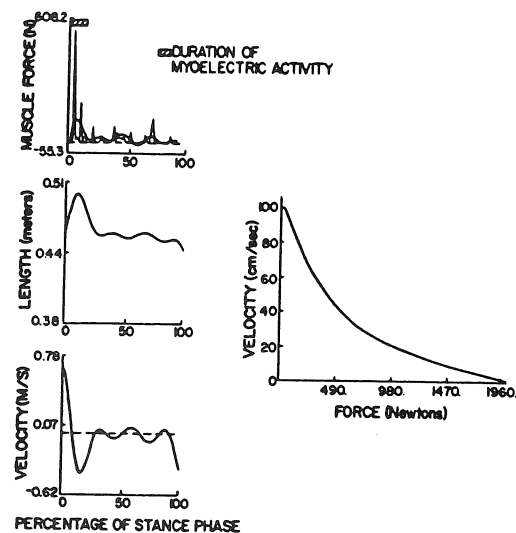


Figure 2. Graphs of model predicted muscle force for the biceps femoris, muscle length and muscle vel. of contraction vs. % of stance phase for level walking at 1.13 m/sec. According to Hill's equation (vel. vs force) max. force is developed at zero vel.

This work was supported by NIH Grants: AM7375 and AM20702.

# ELECTRO-MECHANICAL ADAPTATION TO MUSCULAR STRENGTH TRAINING

Graeme A. Wood, Kevin P. Singer and Andrew G. Cresswell

Department of Human Movement Studies  
University of Western Australia  
Nedlands, W.A. 6009  
AUSTRALIA

## INTRODUCTION

Recent studies from our laboratory have shown significant changes in electro-mechanical delay (EMD) and rate of tension development in voluntary muscle activity following short periods of strength training achieved by both resistive exercise and electrical muscle stimulation (EMS). These changes can be accounted for both in terms of an alteration in motor unit firing patterns (m.u. synchronisation) and increased muscle stiffness, and can occur in the complete absence of gross morphological changes measured by computerised tomography.

## REVIEW AND THEORY

Initial gains in human muscular strength are often accompanied by an alteration in electromyographic (EMG) activity, and can occur in the complete absence of muscle hypertrophy (1,2). It has been our contention that this altered EMG activity is indicative of motor unit synchronisation insofar as cross spectral analysis of electromyograms recorded from two regions of the contracting muscle had shown increased coherency in the lower frequency (<90Hz) bandwidth following the first few weeks of training (2,3). Further, changes in spinal excitability patterns have been found to accompany these strength gains (4,5) and suggest that a strong neural adaptive response has occurred.

Whether these neural changes can completely account for the increased muscle tension developed is not known, but a recent study conducted in our laboratory suggested that other muscle properties may need to be considered. In that study biceps brachii electromechanical delays were examined in a forearm flexion task during eccentric and concentric contractions, both before and again after six weeks of high resistance (isokinetic) training. While significant reduction in EMD's were observed under both conditions (see Figure 1), by far the most dramatic change occurred during concentric contractions, and these changes correlated very highly with the strength gains obtained. Since the comparatively longer delays associated with concentric contractions have been attributed to an added stretch phase (6), it was hypothesised that the series elastic properties of the trained muscle may undergo some change resulting in reduced muscle compliance. This question has been more closely examined during a subsequent strength training study which utilised electrical muscle stimulation (EMS) as the treatment condition.

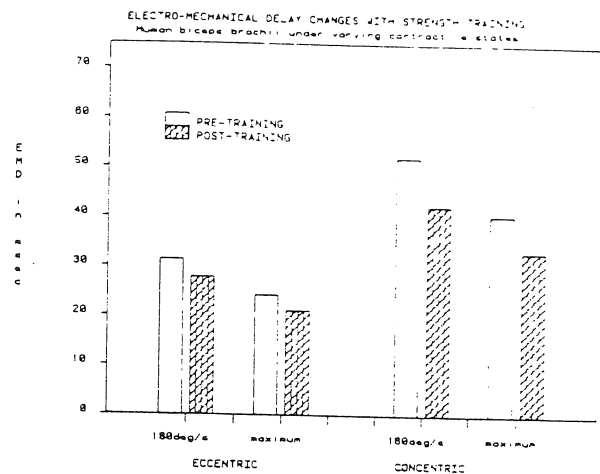


Figure 1: Electro-mechanical delays recorded during an elbow flexion/extension task at two speeds, both before and after six weeks of high resistance (isokinetic) training.

## METHODOLOGY

Eight male subjects displaying unilateral disuse atrophy of the quadriceps muscle group resulting from former knee joint trauma were tested in both limbs for maximum knee extension strength, rate of torque development, and muscle compliance using a Rotagyn dynamometer. Muscle compliance was assessed through the application of a brief torque impulse to the lever arm of the dynamometer during the administration of a maximum knee extension test. A weight was released which impacted with the lever arm and the resulting angular perturbation and impacting force were used in the calculation of muscle compliance [in degrees/(N.m)]. Insofar as the intention was to assess intra-individual changes associated with strength development, no correction was made for system inertia, or visco-elasticity.

Electromyographic activity was recorded from m. vastus lateralis during maximal knee extension tests, using a bipolar electrode plate that permitted recordings from two anatomically discrete motor unit regions (3). Force, angular position and EMG signals were captured on a laboratory computer (PDP-11), and interactive software was used for data reduction. Electromyographic data were subsequently transformed into a Fourier representation, and cross spectral analyses of the two signals were undertaken. The degree of coherency between these two signals was used as an index of motor unit synchronisation.

Strength training consisted of a daily application (15 min.) of EMS using a portable muscle stimulator. In order to examine the neural adaptation versus muscle hypertrophy question a bilateral CT scan of the mid-thigh region was also taken at the beginning and end of EMS treatment.

## RESULTS AND DISCUSSION

The results of this study are summarised in Figure 2 and some aspects have been reported elsewhere (2). All criterion measures showed significant improvement as a result of the EMS training except muscle cross-sectional area. Measures of muscle compliance showed good agreement with those reported by Shorten (7) using an in-vivo added compliance technique (8). There was no apparent relationship between muscle compliance and knee torque registration, a finding that can probably be attributed to the high levels of muscle activation during testing (9).

A significant reduction in the muscle compliance of the treated limb was found to accompany the four weeks of EMS, whereas the non-affected limb showed little change. This increase in musculo-tendinous stiffness would be expected to have an important influence on electro-mechanical delays and rate of tension development, variables which both showed improvement following the course of EMS. The implications of this increased stiffness for motor control are not clear, but its possible effects on joint stress/stability and injury propensity certainly warrant further investigation.

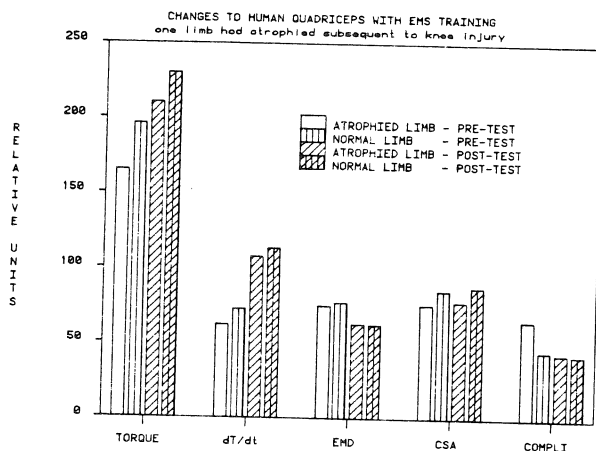


Figure 2: Changes in knee extensor torque (in N.m), rate of torque development (dT/dt, in N.s<sup>-1</sup> x 10<sup>2</sup>), electromechanical delay (in msec), muscle cross-sectional area (CSA, in cm<sup>2</sup>), and angular muscle compliance (in deg/N<sup>-1</sup>.m) following four weeks of EMS treatment. All changes are statistically significant (p<.05) except CSA.

## References

1. Moritani, T. and H.A. deVries, Am. J. Phys. Med., 58: 115-130, 1979.
2. Singer, K.P. and G.A. Wood, NZJ Sports Med., 13(3): 105-109, 1985.
3. Wood, G.A., et al., Austr. Phys. Eng. Sci. Med., 6: 71-75, 1983.
4. Milner-Brown, H.S. et al., EEG clin. Neurophysiol., 38: 245-254, 1975.
5. Wood, G.A., et al., Biomech. IX-A, 368-371, 1985.
6. Cavanaugh, P.C. and Komi, P.V., Europ. J. Appl. Physiol., 42: 159-163, 1979.
7. Shorten, M.R., Biomech. IX-B, 313-318, 1985.
8. Wilkie, D.R., J. Physiol., 110: 249-280, 1950.
9. Cnockaert, J.C. et al., Biomech. VI-B, 73-78, 1978.

\* SHUMAK Industries, Naracoorte, SA 5271, Australia.

This research was supported in part by the Sir Robert Menzies Foundation of Australia.

PREDICTION OF ANKLE MOMENTS IN GAIT USING CALIBRATED  
EMG-FORCE-JOINT ANGLE RELATIONSHIPS

S.J. Olney,\* M.P. Griffin,\*\*  
P.A. Costigan,\* U.P. Wyss,\*  
Queen's University, Kingston, Ontario, K7L 3N6

\* School of Rehabilitation Therapy  
\*\* Department of Mathematics and Statistics

INTRODUCTION

Information from electromyography (EMG) of major muscle groups and joint position was used to determine ankle joint moments during the stance phase of gait. The model predicted the moment by multiplying the instantaneous EMG by a factor depending on angle and angle squared, previously obtained by calibration. Although a quadratic term in angle provided a significantly better fit of EMG-force-angle data, its use did not improve moment predictions substantially over those of a two-position calibration. Errors over four strides were fairly consistent and within an acceptable range for many practical applications.

REVIEW AND THEORY

While some researchers have expressed considerable skepticism concerning the existence of verifiable mathematical models relating EMG to force in the presence of movement(1) the notion has received recent support from Hof(2) and Olney and Winter(3). In the latter case the active state and the series elastic element were lumped together in a linear second-order low-pass filter of the EMG. Force-angle and force-velocity constants were linear. Although the reported errors in predictions of ankle and knee moments were small, the method required the calculation of net muscle moments from a standard link segment kinetic analysis and the derivation of force-length and force-velocity constants for each step.

The purposes of the present study were gain direction for further progress by:

- 1) exploring the feasibility of using an EMG-force-angle calibration factor determined by a minimum number of calibrations.
- 2) if item 1 was successful, assessing the increase in error that would result from use of only two ankle positions for EMG-force-angle calibrations.
- 3) assessing whether co-contraction during calibration contractions is of sufficient magnitude to require inclusion of antagonist muscle groups in the development of predictive equations.
- 4) by examining residual errors from the fitted walking model, to assess the nature and magnitude of the force-velocity component.

METHODOLOGY

EMG electrodes were fixed to prepared skin over the bellies of soleus and tibialis anterior muscles. Matching the EMG of the walking contractions, the subject performed repeated isometric contractions of the ankle plantarflexors and ankle dorsiflexors while fastened in a calibration bench. The signals from the EMG and the force transducer were sampled, A/D converted and stored during an eight-second period. The raw EMG

signals were rectified and passed through a second-order low-pass filter using values incremented by .2 Hz until correlations between the processed signal and the force signal were optimal. The EMG data for each muscle were processed using this filter.

Three ramp contractions were performed at each of four ankle angles while force and EMG data were collected. The slope of the EMG-force curves were determined for each trial. The body was modelled as four segments. Cine, force plate and EMG data were collected while the subject walked, and a standard four-segment link segment analysis performed(4). The EMG-force calibration data were fitted to angle and the resulting equation used to predict the ankle moments. This was repeated using only two positions. The net predicted moments were compared with the net moments derived from link segment analysis.

RESULTS AND DISCUSSION

A significant improvement in fit of EMG-force angle data was obtained by using a quadratic term in joint angle (Figs. 1 & 2) for both tibialis anterior and soleus. Use of tibialis anterior data did not improve the fit to the soleus data, but in fitting the tibialis anterior data, consideration of soleus activity improved the fit significantly. The two-position linear fit is also shown in Figs. 1 and 2.

The quadratic equation for prediction of instantaneous ankle moment caused by one muscle group was:

$$M(t) = E(t)L a [1 + b \theta(t) + c \theta^2(t)]$$

where  $M(t)$  is the instantaneous muscle moment at time  $t$ ,  $E(t)$  is the instantaneous amplitude of the representative muscle.  $L$  is the moment arm length, determined by incrementing values to minimize prediction errors on the first trial;  $\theta(t)$  is the ankle angle, derived from the cine film;  $a$ ,  $b$  and  $c$  are constants derived from the fitted EMG-force-angle equation.

An example of the predicted ankle moment is shown in Fig. 3. The deviations of the predicted curves from link-segment curves over the four steps appear in the Table. The root mean square errors range from 7.1 to 13.8 N.m, a result that compares favourably with previous work(3) but has the advantage of not requiring fitting to kinetic data for each stride. The small decrement in prediction with use of a linear prediction equation also appears in the Table, and a typical example is shown in Fig. 4. The residual errors, plotted in Fig. 5 revealed no identifiable pattern.

References

1. Perry, B. et al. CRV Rev. Biomed. Eng. 7: 1-22, 1981.

2. Hof, A. Human Movement Science 3: 114-153, 1984.
3. Olney, S.J. et al. J. Biomechanics 18: 9-20, 1985.
4. Olney, S.J. et al. Arch Phys. Med Rehabil 67: 92-98, 1985.

Acknowledgement: Supported by MRC (MA-8178)

Table. RMS errors (N.m) in net moment prediction during stance.

Trial	Quadratic	Linear
G1	7.1	7.4
H1	13.8	14.0
I1	9.1	9.1
J1	11.6	12.7

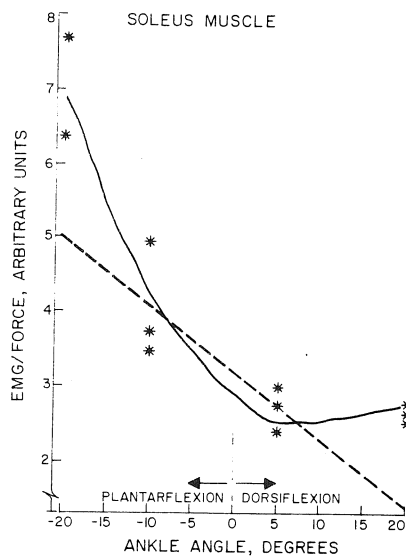


Figure 1. Quadratic and linear fits of EMG-force-angle calibration data for soleus muscle.

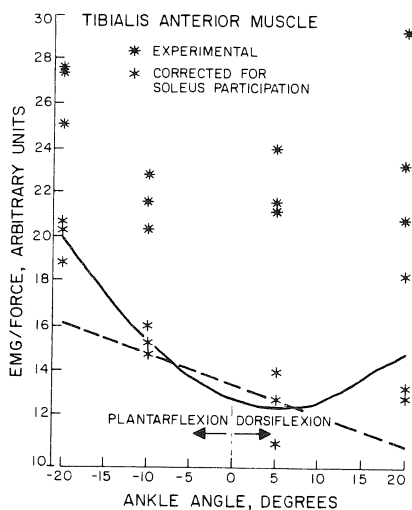


Figure 2. Quadratic and linear fits of EMG-force-angle calibration data for tibialis anterior muscle.

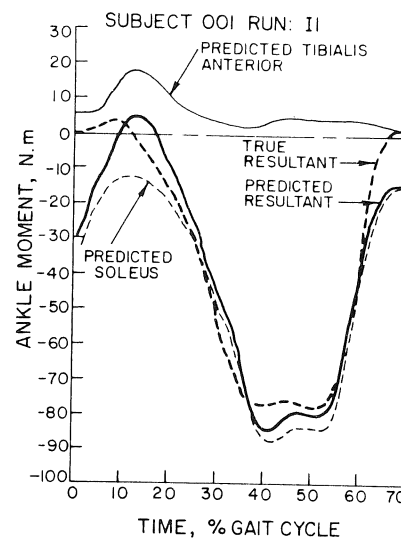


Figure 3. Predicted ankle moment over stance with resultant from link segment analysis.

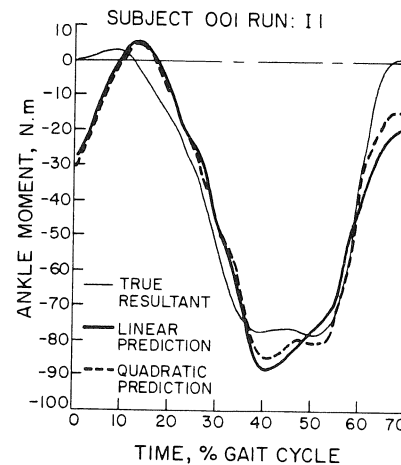


Figure 4. Ankle moments predicted from quadratic and linear equations.

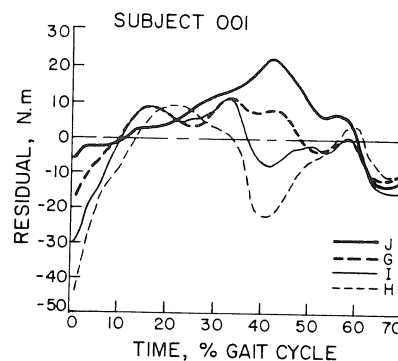


Figure 5. Residual errors for four trials.

# THE EFFECT OF THE MUSCLES' MOMENT ARM ON ITS EMG-FORCE RELATIONSHIPS

M. Solomonow, R. Chuinard and R. D'Ambrosia  
Bioengineering Laboratory  
Department of Orthopaedic Surgery  
Louisiana State University Medical Center  
New Orleans, Louisiana 70112

## INTRODUCTION

The dependence of the EMG-force relationships of the elbow flexors and extensors on the joint angle, gravity vector, and the muscle's moment arm about the joint was defined for each muscle group acting as an agonist or antagonist. This information can substantially improve and augment kinesiological assessment, testing of joint integrity, and design of an electrical stimulation system for restoring function to the paralyzed extremity of stroke and spinal-cord-injured patients. On analysis of the data obtained during isometric and quasi-isometric conditions, the slope of the normalized EMG-force curves of the agonist was found to be independent of joint angle or gravity whereas the slope of the antagonist was sensitive to both joint angle and gravity. Further analysis showed that the normalized EMG-force of the antagonist was inversely related to its moment arm over the physiological range of elbow angles ( $0^\circ$  -  $150^\circ$  flexion).

Our conclusions demonstrate the regulatory role of the antagonist in promoting the functional integrity of the joint as well as its augmentive role to the ligaments in maintaining stability.

## REVIEW

The EMG-force relationships of various muscles have been of substantial interest to many investigators over the last three decades, and excellent reviews of this area were recently given (1,2). Most of the studies related the normalized full-wave rectified and low-pass filtered EMG with the force generated at the hand during isometric conditions at a single elbow angle. Under such conditions the generated force is not only due to the agonist muscle but is compounded with the contributions of the antagonist, ligament laxity, gravity, proprioceptive reflexes, and muscle length or its associated joint angle. To improve the currently available body of knowledge, we set up an experimental study to identify the dependency of the EMG-force relationships of the elbow's antagonistic muscle pair on gravity, joint angle (muscle length), and ligament laxity.

## METHODOLOGY

Twelve healthy young students, all right-handed, were seated in a specially designed frame that had the capabilities to measure elbow flexion/extension forces via a bidirectional load cell in the vertical plane (including gravity) or horizontal plane (excluding the effect of gravity). Simultaneous surface EMG from the agonist and antagonist muscle groups were recorded for force range of 20% to 100% of MVC (max. voluntary contraction) in 10 increments, and at joint angles of  $45^\circ$ ,  $90^\circ$ , and  $135^\circ$  flexion.

We also obtained flexion/extension torque, joint angle, and simultaneous EMG from agonist/antagonist muscles during quasi-isometric conditions with the Cybex system at 10 degrees/sec. rate. The similarity and validity of data in the isometric and quasi-isometric data were verified for one subject.

## RESULTS & DISCUSSION

The normalized EMG-force curves for the agonist in the range of 20%-100% of MVC were linear ( $p < .05$ ) and of the same slope (1.16) regardless of elbow angles or the orientation of the gravity vector.

The EMG-force curves for the antagonist were linear ( $p < .05$ ) for the range of 20%-100% MVC, but showed sensitivity to gravity and to joint angle. The variation with gravity orientation reflected increased antagonist (flexors) activity during elbow extension; (gravity forces were contained) and decreased antagonist (extensors) on activity during flexion to compensate for gravity force's effect. The increase and decrease of antagonist activity were most pronounced at  $90^\circ$ , where the effect of gravity was maximal on the longest effective moment arm of the forearm.

During flexion/extension on the horizontal plane with the absence of gravity forces, the EMG of the antagonist normalized with respect to its MVC value at each joint angle when acting as agonist was inversely related to the curve of its tendon's moment arm at each angle, as shown in figures 1 and 2 respectively.

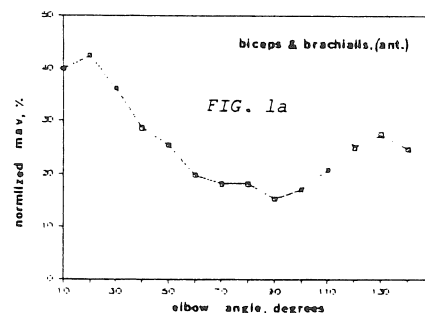
Separate testing showed that the agonist/antagonist muscles are possibly connected in a reflex arc to the joint's ligament and augment the ligament's functions in maintaining joint stability. Biomechanical analysis shows that force components generated by the agonist tend to distract the joint but are opposed, and therefore contained, by force components generated by the antagonist.

## CONCLUSIONS

The activity of the elbow antagonist was shown to have a regulatory role on the joint, which tends to compensate for external gravity forces and to maintain joint stability as augmentation to its associated ligaments.

## References

1. Perry, J., and Bekey, G.A. Crit. Rev. Biomed. Eng. 7:1-22, 1981.
2. Basmajian, J., and DeLuca, C. Muscles Alive, 5th. Edition, Williams & Wilkins, Baltimore, 1985.



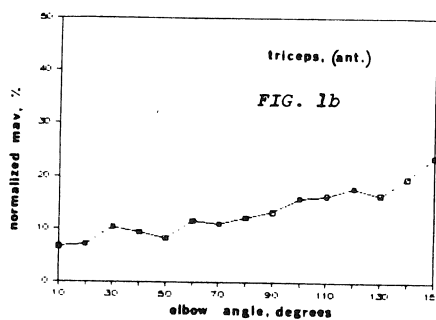


FIGURE 1,a&b

Showing the normalized MAV of the biceps and triceps as a function of elbow angle when acting as antagonists.

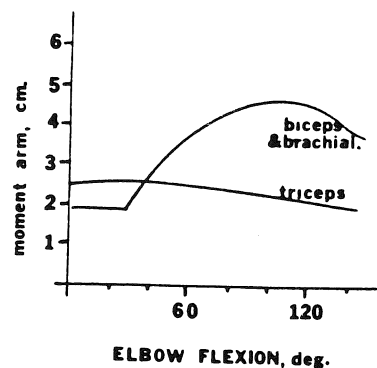


FIGURE 2

Showing the moment arm of the biceps and triceps as a function of elbow angle.

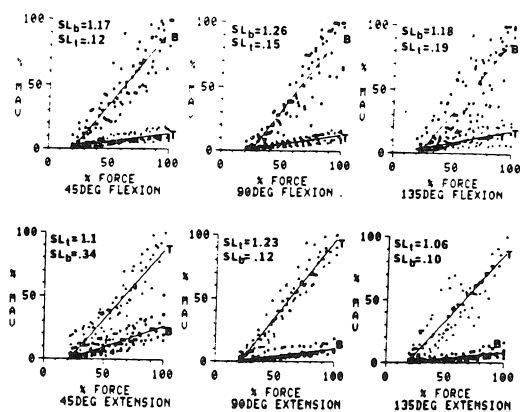


FIGURE 3

Showing the simultaneous MAV of the agonist and antagonist during elbow flexion (upper row) and extension (lower row), B-Biceps, T- Triceps, SL- slope of linear regression fit line to the data from six subjects ( $p < .05$ ).

Bradford McFadyen  
David Winter  
Dept. of Kinesiology

Brad Day  
Forbes Burkowski  
Dept. of Computer Science

University of Waterloo,  
Waterloo, Ontario, N2L 3G1

## INTRODUCTION

One of the most difficult tasks in science is to present data in a form which is both meaningful and applicable. This task is made even more difficult when groups with varying backgrounds are involved. The study of human locomotion is of interest to kinesthetologists, bio-engineers, physiotherapists and medical doctors to name a few. A common basis to all of these groups is the human anatomy. Based on this premise, this paper presents a method of graphically presenting kinematic and electromyographic data in a form for clinical and teaching application.

## METHODOLOGY

Body marker coordinates for a desired walking stride were selected from the U of W gait laboratory data base. A sagittal plane model was used to calculate muscle length changes at each frame relative to estimated resting values. Details of the model are provided in the Appendix. Muscle origins, insertions and pivot points were based on data from the doctoral works of Dostal (1979) and White (personal communication). Central finite difference was used to calculate the velocity of contraction, and each value, in accordance to its polarity, was then coded as shown in Table 1 to indicate the type of contraction involved at each frame.

Corresponding linear enveloped EMG data were matched to the cine frames selected and then coded with respect to relative intensity of activity at each frame. A five level scale was used for these codes as shown in Table 2.

The codes for both contraction type and level of muscular activity were then combined with the appropriate labels indicating one of six leg muscles. For example, an eccentric contraction of the tibialis anterior at full activity would be coded "T-5". These final codes were stored in a data file for later use.

A processor called the AURORA II provided appropriate memory capacity, animation and graphics capabilities to display sixteen (16) colours and continuous viewing of a simulated lower limb similar to that shown in Figure 1 (the actual image excludes printing of the codes). The muscle codes were used by the graphics program to apply the appropriate colour and intensity of colour to each of the six muscles for each frame. Red was used to indicate an eccentric contraction (negative velocity), green for a concentric contraction and yellow for an isometric state. The isometric state was set at an absolute value of velocity less than five percent of maximum. The colour intensity levels paralleled the level of muscular activity such that no activity resulted in no colour being displayed for that muscle and maximum activity produced the brightest colour.

Programs to interpolate the EMG data, calculate length changes and produce the muscle codes were written in IBM pc Basic. Graphics programs and programs to download data to the Aurora II processor were written in Waterloo Port. Based on the coordinates of the joint centres, a computer graphics program was written to draw the lower limb and outline

muscles for each frame to be stored in the AURORA II processor.

## RESULTS

The display offers stop-frame analysis of each frame, continual viewing at a variety of different speeds and the ability to step or view the data in reverse order. A single stride could be viewed as many times as desired. Newer versions of the programs also indicate frame occurrence and magnitude of maximum EMG for each muscle.

## DISCUSSION

This method provides a way to represent kinematic and electromyographic data in a form that is comprehensible to a wide range of human movement scientists and clinicians. As such, the graphic presentation has ready application to both teaching and clinical assessment. The addition of better models, kinetic variables and the representation of other body segments will only serve to improve this method.

Table 1: Codes for type of contraction

CODE	INTERPRETATION
+	concentric contraction (positive velocity above 5% of maximum)
=	isometric contraction
-	eccentric contraction (negative velocity with absolute value above 5% of maximum)

Table 2: EMG activity level codes

CODE	INTERPRETATION
1	muscle off
2	activity from 15 percent to 35 percent of maximum
3	activity from 35 percent to 55 percent of maximum
4	activity from 55 percent to 75 percent of maximum
5	activity from 75 percent to maximum activity.



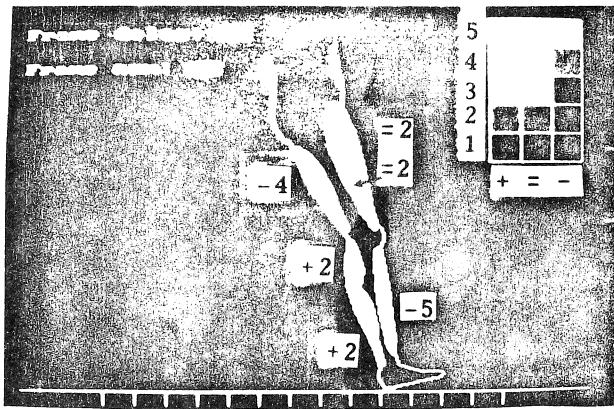


Figure 1: Graphic image of lower limb and muscles.  
Colour codes are normally indicated in the top right hand corner.

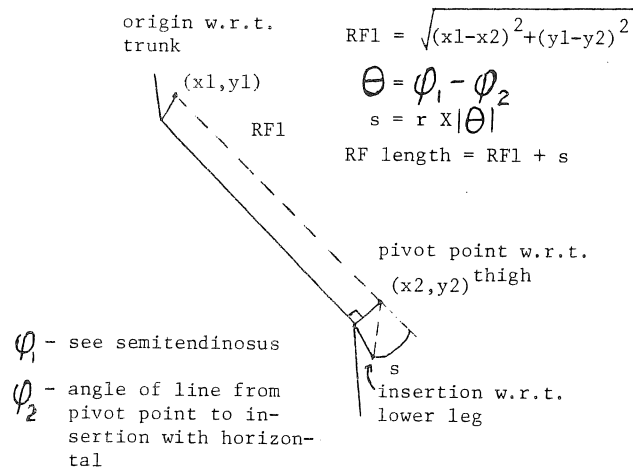
#### References:

1. Frigo, C, & Pedotti, A. Biomechanics VI-A:355-360, 1978.

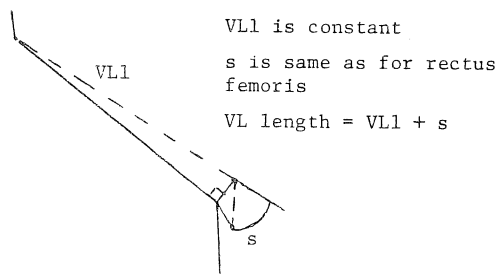
#### APPENDIX

The calculation for individual muscle lengths is provided below. Other models, for example (1) exist. Resting length was determined by finding the initial point of flat foot within the walking cycle (this could be modified for other types of gaits), simulating upright posture and applying the following calculations.

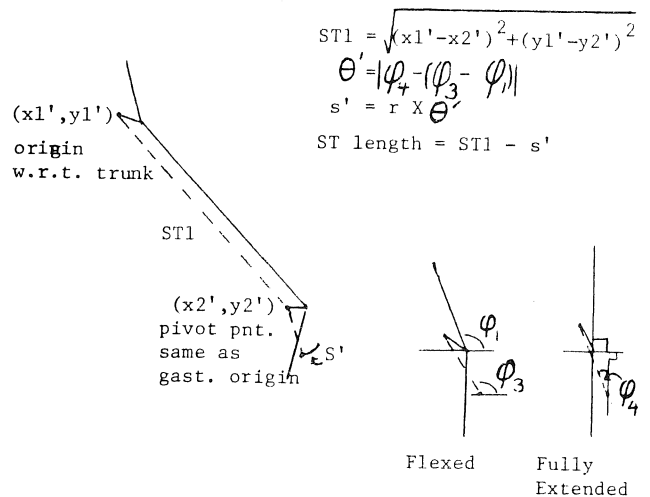
#### Rectus Femoris:



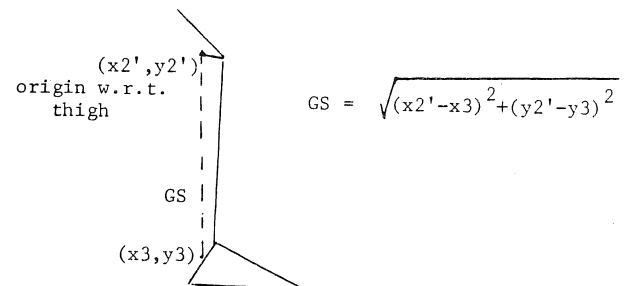
#### Vastus Lateralis:



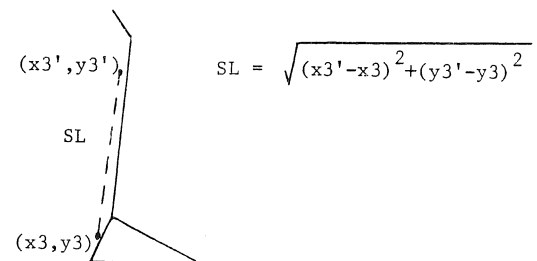
#### Semitendinosus:



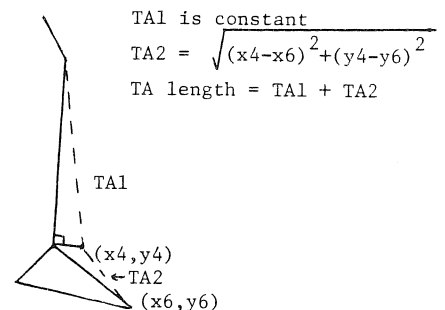
#### Medial Gastrocnemius:



#### Soleus:



#### Tibialis Anterior:



ACKNOWLEDGEMENTS: We acknowledge the support of the Medical Research Council (MT 4343) and partial support of B.McFadyen through a National Health Fellowship.

# THE BIOMECHANICS OF TWISTING SOMERSAULTS

M.R. Yeadon  
Biomechanics Laboratory  
University of Calgary  
Calgary, Alberta T2N 1N4

## INTRODUCTION

The free rotational motions of a rigid body comprise two distinct modes which are characteristic of the motions of a rod and a disc. In the rod mode the twist angle steadily increases whereas in the disc mode the twist angle oscillates about a mean value. Twisting techniques are evaluated using a simulation model of aerial movement and the mechanics are discussed in terms of the rigid body modes. The capabilities of asymmetry techniques for producing and removing sustained aerial twist are established. For twist initiated during the contact phase it is shown that symmetrical configuration changes around the quarter twist position can increase the twist significantly. Modified simulations of filmed movements are used to determine the contributions of the various techniques to the twist produced. The instability of rotations about the intermediate principal axis is shown to be a natural consequence of there being two modes of motion and techniques for maintaining stability in non-twisting layout somersaults are evaluated using hypothetical simulations.

## REVIEW AND THEORY

Cinematographical studies of twisting somersaults are useful for obtaining indications of the techniques which appear to be used but, without an accompanying mechanical analysis, the conclusions that can be drawn are limited. Experimental studies have shown that both aerial and contact techniques are capable of producing one twist in a somersault (Bartee, 1977; Moorse, 1966) but the particular techniques used are largely a matter of conjecture. Theoretical models of airborne movement are capable of evaluating twisting techniques but the accuracies of such models need to be established before there can be confidence in the results. The three models which have been evaluated using data taken from actual performances have established the following:

- (1) One cycle of hula movement of the hips is capable of producing a half twist in a plain jump (Kosa et al., 1972)
- (2) Asymmetrical arm movements are capable of producing a full twist in both piked and straight backward somersaults (Van Gheluwe, 1981)
- (3) A sustained aerial twist may be produced in a forward somersault by making a partial hula movement as the body extends from the piked position (Yeadon et al., 1985)

The above results constitute the present state of knowledge on twisting technique.

For a rigid body in free-fall the conservation of angular momentum gives rise to the following equations (Whittaker, 1937):

- (1)  $\dot{\phi} = h(A\sin^2\psi + B\cos^2\psi)/AB$
- (2)  $\dot{\theta} = -h(A-B)\cos\theta\sin\psi\cos\psi/AB$
- (3)  $\dot{\psi} = (h/C - \dot{\phi})\sin\theta$

where A,B,C are the principal moments of inertia ( $A \geq B \geq C$ ), h is the angular momentum and  $\dot{\phi}, \dot{\theta}, \dot{\psi}$  are the rates of change of the somersault angle  $\phi$ , the tilt angle  $\theta$  and the twist angle  $\psi$ . The three equations may be integrated to give two general solutions which will be named the ROD MODE and the DISC MODE.

In the rod mode the tilt angle  $\theta$  nutates between values  $\alpha$  and  $\beta$  which have the same sign and are defined by the equations:

$$(4) \cos^2\alpha = (h^2/C - 2T)/(h^2/C - h^2/A)$$

$$(5) \cos^2\beta = (h^2/C - 2T)/(h^2/C - h^2/B)$$

where T is the rotational energy. Equations (1) and (3) show that in the rod mode the twist angle  $\psi$  increases monotonically with time.

In the disc mode the tilt angle  $\theta$  oscillates between  $\alpha$  and  $-\alpha$  where  $\alpha$  is given by equation (4). Equations (1) and (3) show that in the disc mode the twist angle oscillates so that the average rate of twist is zero.

The critical value of  $\alpha$  separating the two modes is  $\alpha_0$  which is defined by the equation:

$$(6) \cos^2\alpha_0 = (h^2/C - h^2/B)/(h^2/C - h^2/A)$$

For  $\alpha > \alpha_0$  the motion will be in the rod mode and for  $\alpha < \alpha_0$  the motion will be in the disc mode. Figure 1 shows how the two modes approach each other for values of  $\alpha$  close to  $\alpha_0$ . Each of the two motions may be described as a quadruple somersault with two distinct half twists. In the rod mode these half twists have the same direction whereas in the disc mode the half twists have opposing directions.

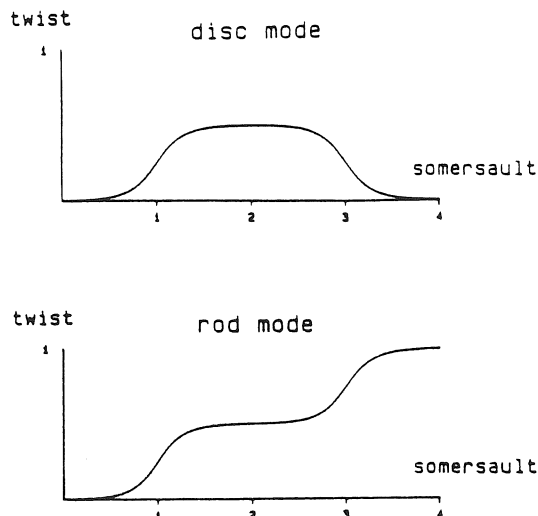


Figure 1. Disc mode and rod mode solutions

## METHODOLOGY

In order to evaluate the effects of changing from one mode of motion to the other, a computer simulation model of the human body in free-fall is used. The model is an extension of that used in Yeadon et al. (1985) and comprises 11 segments with 17 degrees of freedom. By modifying the configurations obtained from film of twisting somersaults, it is also possible to determine the contributions of different techniques to the twist produced in actual performances.

## RESULTS AND DISCUSSION

Figure 2 shows the effect of delaying arm adduction in the flight phase when twist has been established in the contact phase. In (a) the arms are adducted immediately after take-off and the tilt angle between the twist axis and the plane normal to the angular momentum vector remains close to  $10^\circ$  throughout the motion. In (b) the nutation effect increases the tilt angle to its maximum value at the quarter twist position when the arms are adducted. In this case the tilt angle is approximately  $14^\circ$  and the twist rate is correspondingly greater.

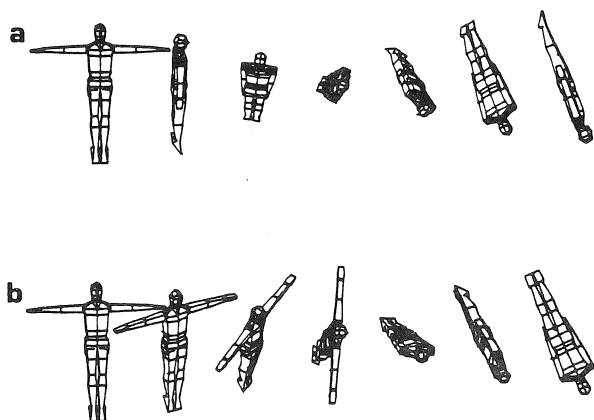


Figure 2. Different timings of arm adduction

By piking at around the quarter twist position more dramatic effects can be produced. As the body pikes the motion changes from the rod mode to the disc mode and the tilt angle starts the oscillation between positive and negative values. By varying the timing of the piking movement the tilt angle can be increased, decreased or even reversed in sign. By extending from the pike at the appropriate time of the oscillation cycle the twist rate may be increased, decreased or even reversed in direction. If piking occurs close to a whole number of half twists, the twist angle will oscillate with relatively small amplitude so that it will appear that the twist has stopped.

If no twist is produced during the contact phase the somersaulting motion may be converted into a twisting somersault by producing a non-zero tilt angle during flight (equation (3)). If the body is initially piked, tilt may be produced by asymmetrical movements of the arms, chest or hips. Prior to the extension from the pike the oscillation effect in the disc mode will increase or decrease the tilt angle depending on the initial direction of somersault.

For asymmetrical arm movements this effect is small so that the technique may be used in both forward and backward somersaults. For asymmetrical chest and hip movements, however, the oscillation effect is of major importance and increases the tilt angle in forward somersaults but decreases the tilt in backward somersaults. Thus asymmetrical movements of the chest or hips are only effective in producing twist in piked forward somersaults. Each of the three asymmetry techniques is capable of producing twist rates of up to 5 twists per somersault.

Since the simulations used to establish these results may be reversed in time it may be concluded that all three techniques are capable of removing tilt when the final direction of somersault is backward whereas only asymmetrical movements of the arms are effective when the final somersault direction is forward.

By modifying the configurations of nine filmed twisting somersaults the resulting simulations showed that twist produced during the contact phase made only small contributions even when the twist was apparent in the early part of the flight phase. The contributions of asymmetry techniques were consistent with the results of the simulations described earlier.

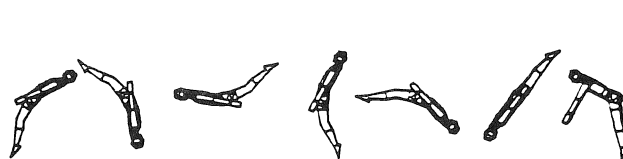


Figure 3. Maintaining stability using an arch

In order to prevent the buildup of twist in layout non-twisting somersaults an arched position may be adopted as shown in Figure 3. In this situation the motion is in the disc mode and is stable. If the body has less arch than that shown in Figure 3 instability becomes a problem but can be controlled by asymmetrical arm movements providing the feedback delay is not greater than about one quarter of a somersault.

## REFERENCES

- Bartee, H.H. 1977. A cinematographical analysis of twisting about the longitudinal axis when performers are free of support. Ph.D dissertation. Texas A & M University.
- Kosa, F. et al. 1972. A study of mechanism of non-inertial twist. Bulletin of Institute of Sport Science 10, 69-81.
- Moorse, A.C. 1966. A cinematographical analysis of a full twisting backward somersault. Modern Gymnast 8,1,12-13.
- Van Gheluwe, B. 1981. A biomechanical simulation model for airborne twist in backward somersaults. Journal of Human Movement Studies 3,5-20.
- Whittaker, E.T. 1937. A treatise on the analytical dynamics of particles and rigid bodies. Cambridge University Press.
- Yeadon, M.R. et al. 1985. The production of a sustained aerial twist during a somersault without the use of asymmetrical arm action. In Biomechanics IX-B, 395-400. Champaign: Human Kinetics.

# SEGMENT INVOLVEMENT IN THROWING: A THREE-MODE JOINT PLOT ANALYSIS

Robert J. Neal, Conrad W. Snyder\* & Barry D. Wilson.

Departments of Human Movement Studies and Psychology\*  
University of Queensland, AUSTRALIA

## INTRODUCTION

When the intention of an effective movement is to generate maximum speed at the distal end of a kinematic linkage, there may be different sequential requirements at phases in the motion. Throwing and kicking a ball or striking a golf or tennis ball are examples of such activities. A number of authors (2,3,5) have proposed a kinetic link theory in which the sequential order of any movement for maximal speed begins with the large, strong, proximal muscles that are then followed by the small, weak, distal muscles.

Little empirical evidence has been provided to support the linkage theory although many authors, when discussing their results, have made reference to it. Postulates regarding the summation of speed, force, and angular momentum in the sequencing of movement, all of which bear on the validity of the kinetic link theory, have been presented to account for specific empirical relationships among the mechanical variables implicated by the theory.

This study examines the variance attributions and interactions of segmental arm action in throwing under different load conditions by applying three-mode component analysis to the velocity measures of the arm segments during a softball throw for maximum distance. The purposes of this study were to examine the counteractions, synergies, and time relationships of the different arm segments in terms of velocity.

## METHOD

Subjects were filmed while performing two throws for maximal distance under each of three load conditions by a Photosonics cine camera operating at 50 fps. Three softballs of masses 180g, 802g and 1316g were used to provide the different load conditions. Film was digitally analyzed to obtain the kinematics of the three segments of interest, the upper arm, the forearm and the hand. These data were interpolated to a common time base of 28 frames because not all subjects completed the throw in the same period of time.

Three-mode principal component analysis (4,6) reduces the larger, observed data set to a smaller quantitative portrait of underlying relationships among the original classification levels. The data are arranged in terms of three classification sets: 28 time periods, 6 arm segment velocity measures, and 36 experimental units (12 athletes throwing three differently weighted balls).

## RESULTS AND DISCUSSION

Velocity measures, reflecting the motion of the hand, forearm and upper arm were reduced to a three component configuration accounting for 55%, 27% and 7% of the total variance respectively. The first component was interpreted as directional velocity (forward-down versus backward-up) and the second component was interpreted as proximal versus distal velocity (from upper arm to hand). The different ball weights had little differential effect on the structure relationships, and trials under the different loads grouped together almost as replicates even though individuals displayed different patterns of action.

Two idealized throwing actions or person types (1 & 2), indicative of a sidearm whip and an over the top of the shoulder action, respectively were identified. These two types accounted for 39% and 27% of the variance respectively. For person type 1, the upper arm dominates the early phase while the movement of the upper arm and the hand become equally apparent in the early-middle phase with shoulder rotation back and down and hand motion up. The upward movement of the hand dominates the late-middle phase but the upper arm and hand contrast equally again late in the throw with the upper arm moving up and the hand coming down. The end of the throw is marked equally by the upper arm going back as the hand goes forward. Thus, the ball is whipped out by the distal segment as the shoulder noticeably recoils in some cases. For person type 2 the upper arm is less influential in the throw (in terms of velocity changes) than for person type 1 and one sees evidence of a summation of the arm segment velocities as the throw progresses. The important actions of type 2 throwers are the coordinated changes in velocity for the forearm and the hand. These relationships are shown in figure 1 in which the component scores for the time periods are projected into the segment velocity space. The influence of the segments at each time during the throw is determined by the distance from the origin of a perpendicular line drawn to a vector originating from the origin of the C1C2 space and passing through the time period.

## CONCLUSIONS

Although there are wide individual differences in throwing action, two general styles are discernible in terms of the velocity changes over the throwing action: one is characterized by segment and time contrasts and the other exhibits time contrasts but with some evidence of segment synergy.

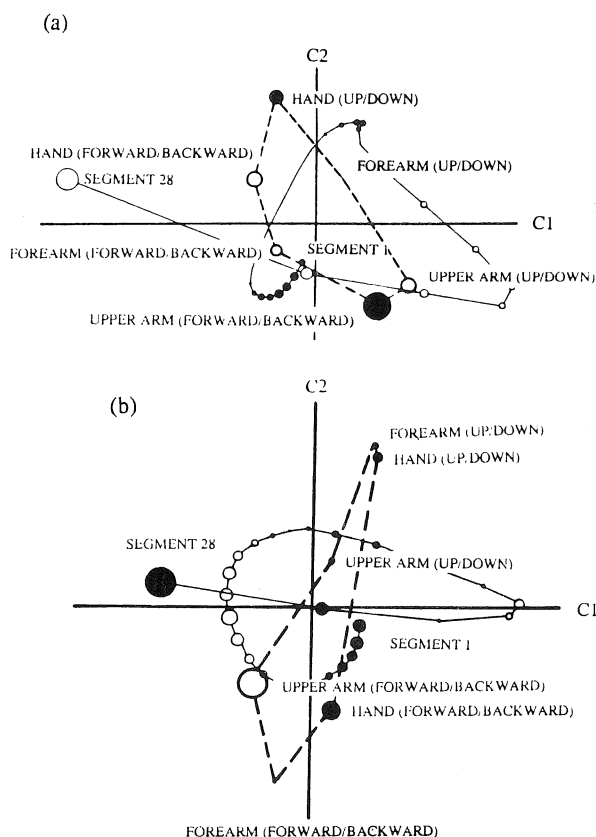


Fig. 1. The component scores for the time periods plotted into the velocity measures space for person type 1 (a) and person type 2 (b).

Regardless of the general style, there appear to be important time phase contrasts in the early versus late-middle phases and the early-middle versus late phases. That is, whatever segment velocity relationships are established in the early phase they are countered in direction in the late-middle phase, while retaining the same segment configuration. Those established in the early-middle phase are countered in direction in the late phase. Thus, these contrasts are critical in all motions; the segment velocity relationships established in these phases constitute the "throwing style."

In the first style, the velocity of the upper arm is negatively related to the velocity of the hand. These contrasts characterize a whip-like throwing action. At release, the hand lies outside the line of the body and the wrist is snapped, as the shoulder recoils. The staggered sequence of velocity peaks in the direction of the throw proceeding from the upper arm, to the forearm, to the hand, is similar to that recommended by Ariel (1) for a "successful and well-executed throw." But these athletes reach this kinematic virtue with less than an optimal style. In the second general throwing style, the segment relationships are characterized by a positive relationship between the velocities of the forearm and hand. These styles are relatively invariant with respect to different loads.

Execution time for the throw varied, but the segment velocity relationships were consistent across the different conditions.

## References

1. Ariel, G. (1976) Computerized biomechanical analysis of throwers at the 1975 Olympic Javelin Camp. *Track & Field Quart. Rev.* 76:45-49.
2. Bunn, J.W. (1972) *Scientific Principles of Coaching* Prentice-Hall, Englewood Cliffs, N.J.
3. Dyson, G. (1973) *The Mechanics of Athletics* (6th ed.), University of London Press, London.
4. Law, H.G., Snyder, C.W., Jr., Hattie, J.A., and McDonald, R.P. (Eds.) (1984) *Research Methods for Multimode Data Analysis*. Praeger, New York.
5. McCloy, C.H. (1960) The mechanical analysis of motor skills. *Science of Medicine of Exercise and Sports* (Edited by Johnson, W.R.), pp. 54-64. Harper and Row Publishers, New York.
6. Tucker, L.R. (1966) Some mathematical notes on three-mode factor analysis. *Psychometrika* 31: 279-311.

# DYNAMICS OF THE SHOULDER AND ELBOW JOINTS OF THE THROWING ARM DURING A BASEBALL PITCH

Michael E. Feltner & Jesús Dapena  
Department of Physical Education, Indiana University, Bloomington, IN 47405.

## INTRODUCTION

To fully understand the mechanics of any body motion, it is necessary to develop a model that links the kinematics of the motion with the kinetic parameters responsible for the production of the observed motion, including the net forces at the joints, and the joint torques (indicative of the underlying muscular activity). This paper reports the results of such an analysis conducted for the shoulder and elbow joints of the throwing arm during baseball pitching. The torques and forces at these joints were calculated, along with selected kinematic data, and were used to develop a tentative interpretation of the roles of these torques and forces in the generation of the motions of the throwing arm.

## REVIEW AND THEORY

Qualitative descriptions of the kinematics of the throwing arm during the baseball pitch have appeared in most kinesiology textbooks, and quantitative kinematic data have been reported by numerous investigators (2) (4) (5). However, no studies on the kinetic parameters at the joints of the throwing arm during full-effort baseball pitching have been reported.

## METHODOLOGY

Fastball pitches of eight male collegiate baseball pitchers were filmed using the DLT method of three-dimensional (3D) cinematography. 3D coordinate data of the relevant body landmarks were obtained using standard film analysis procedures, and were smoothed via quintic spline functions. Vector algebra techniques were then used to calculate the three angles (abduction/adduction, horizontal abduction/adduction, and internal/external rotation) defining the position of the upper arm relative to the trunk, and the elbow flexion/extension angle. The inverse dynamics approach of kinetic analysis (1) was used to calculate the resultant joint torques and forces at the shoulder and elbow joints. The computed joint torque and force data were ultimately expressed in terms of two anatomically relevant reference frames defined at the shoulder and elbow joints, respectively.

## RESULTS AND DISCUSSION

All subjects showed similar kinematic and kinetic patterns. The plots presented in Figures 1-4 correspond to the subject with the fastest ball velocity at the instant of release.

Analysis of Figures 1-4 demonstrates that forces and torques of small magnitude bring the upper arm into a position of approximately  $15^\circ$  of adduction,  $10^\circ$  of horizontal abduction, and  $0^\circ$  of internal/external rotation, with the elbow joint flexed at approximately  $90^\circ$ , at the instant of stride foot contact. From this position, the elbow is moved forward by a horizontal adduction torque at the shoulder. Somewhat later, the

pitcher starts an abduction torque that lifts the elbow.

While the upper arm is subjected to the motions of horizontal adduction and abduction, it also undergoes a motion of external rotation that eventually takes it to an extremely externally rotated position ( $30^\circ$ ) -- see Figure 1. Surprisingly, this external rotation takes place against the action of an internal rotation torque exerted at the shoulder joint.

The external rotation of the upper arm could be explained by the following mechanism. The muscles on the anterior part of the shoulder joint exert a horizontal adduction torque (Fig. 3). This leads to a counterclockwise angular acceleration of the arm in an overhead view, and consequently to a forward linear acceleration of the c.m. of the arm (G in Fig. 5). This linear acceleration of the c.m. requires a forward force at the shoulder joint (F in Fig. 5), and this force exerts a counterclockwise torque (external rotation) with respect to the c.m. of the flexed arm in the view along its longitudinal axis (Fig. 5). Thus, through this indirect mechanism, the muscles that exert horizontal adduction torque also encourage external rotation.

In normal baseball pitching, the external rotation effects of this horizontal adduction torque evidently outweigh the effects of the internal rotation torque (T in Fig. 5) exerted by the shoulder musculature. As the arm externally rotates further, the abduction musculature begins to contract, and assists in producing the continued external rotation of the upper arm, based on a mechanism similar to that described previously.

While the arm externally rotates, part of the internal rotation torque that resists against it is transmitted through the humerus to the elbow joint, where it is reflected in a large varus torque exerted by the upper arm on the forearm (Fig. 4). This large varus torque is probably exerted mainly through tensile forces in the ligaments and articular capsule of the medial elbow joint, and through compressive forces on the bones of the lateral elbow joint, although the muscles originating on the medial epicondyle of the elbow could contribute to this torque while they performed their primary actions. This phenomenon, termed medial tension overload or valgus extension overload, and the injuries associated with it have been discussed extensively in the literature [(3), (6), for example].

The extension torque exerted at the elbow joint is quite small (average peak value, 20 Nm), and this strongly suggests that the rapid elbow extension prior to ball release (Fig. 2) is not due primarily to the action of the triceps, but to the elbow joint force exerted by the upper arm on the forearm. For instance, a force pointing from the elbow joint toward the shoulder joint would lead to elbow extension. Such a force could be associated with the centripetal acceleration of the upper arm as it rotates about the

shoulder joint, or to a linear acceleration of the trunk to the left (viewed from the rear). In any case, the small magnitude of the elbow extension torque suggests that the acceleration of the ball may be due to mechanisms other than muscular activity of elbow extension.

#### References

1. Andrews, J.G. Med. Sci. Sp. Exer. 14:361-367, 1982.
2. Atwater, A.E. Exer. Sp. Sci. Rev. 7:43-85, 1979.
3. Barnes, D.A., et al. Am. J. Sp. Med. 6:62-67, 1978.
4. Gainor, B.J., et al. Am. J. Sp. Med. 8:114-118, 1980.
5. Pappas, A.M., et al. Am. J. Sp. Med. 13:216-222, 1985.
6. Wilson, F.D., et al. Am. J. Sp. Med. 11:83-88, 1983.

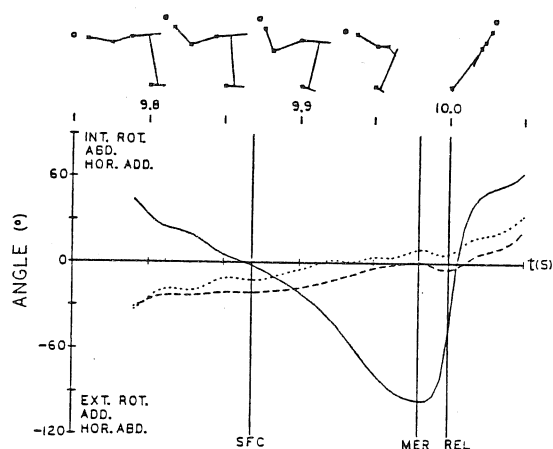


Figure 1. Shoulder angular displacement: int/external rotation (solid curve); abd/adduction (dashed curve); horizontal abd/adduction (dotted curve). The three vertical lines represent the instants of stride foot contact (SFC), maximum external rotation (MER), and ball release (REL), respectively. The side view stick figures represent the positions of the subject, and the crosses indicate joints on the right side of the body.

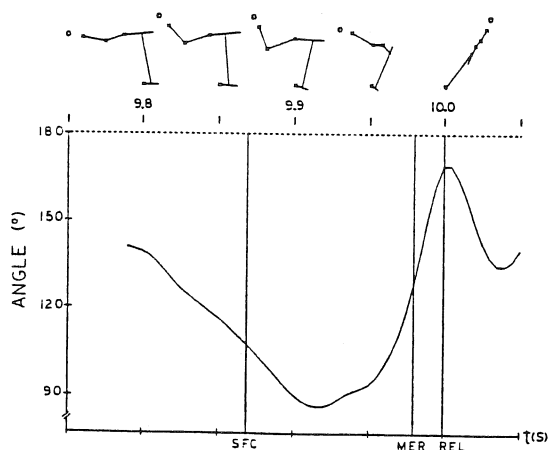


Figure 2. Angle of elbow flexion/extension.

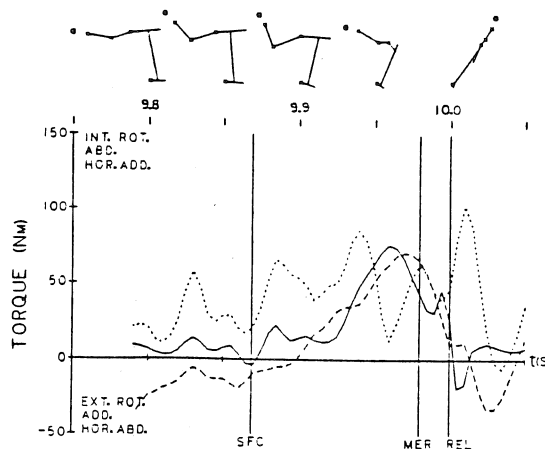


Figure 3. Resultant joint torques at the shoulder joint: int/ext rotation (solid curve); abd/adduction (dashed curve); horizontal abd/adduction (dotted curve).

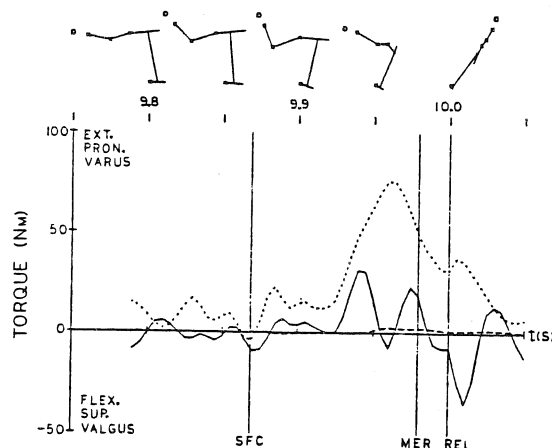


Figure 4. Resultant joint torques at the elbow joint: flexion/extension (solid curve); pron/supination (dashed curve); valgus/varus (dotted curve).

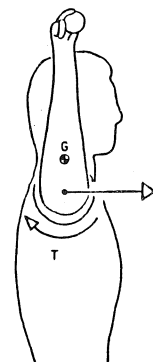


Figure 5. Sketch showing the force (F) produced indirectly by the horizontal adduction musculature, and the internal rotation torque (T) exerted by the internal rotation musculature of the shoulder.

E. Sprigings<sup>1</sup>, G. Watson<sup>2</sup>, E. Haseganu<sup>2</sup>, and D. Derby<sup>2</sup>

<sup>1</sup>College of Physical Education; <sup>2</sup>Department of Mechanical Engineering, University of Saskatchewan, Saskatoon, Sask. S7N 0W0

## INTRODUCTION

The amount of time in the air is of fundamental importance to the success or failure of any diver's performance. Today's aerial maneuvers have become so demanding and complex that fractions of a second often decide whether a dive can be completed as planned. Whether adequate time in the air is achieved for any dive depends on the diver's vertical velocity at the time of take-off. Thus one of the main objectives for any diver becomes one of searching for a way to increase his vertical take-off velocity without unduly jeopardizing his development of angular momentum during the take-off phase.

## REVIEW AND THEORY

Miller (1) has shown that the shoulder, hip and knee musculature of a diver have the capacity to alter the springboard's external reaction force during the depression and recoil stages. For example, if during board contact the muscles of the shoulders were to accelerate the arms upwards with respect to the shoulder joint, and the rest of the body remained rigid, the board would experience a force in the downward direction. On the other hand if the relative arm acceleration was downward, the resulting force on the board would be less which in turn means that the upward external reaction force from the board on the diver is reduced. For both situations mentioned the force on the board resulting from the arm acceleration would be in addition to that produced by the diver's weight and inertial force. A similar story would be true for the torso and legs with the only difference being that their relative acceleration would be measured with respect to the hip joint and metatarsophalangeal joint respectively.

It has generally been assumed that the more a diver can depress the diving board, the greater will be the resulting vertical take-off velocity. Thus it is reasonable to assume that the relative upward acceleration of the arms and legs should take place during the downward deflection (i.e. depression) of the board. However, it was evident from the work of Miller (1,2) that the duration of the relative upward acceleration of both the arms and legs was less than the total time of board depression. This observation raised the question as to whether the amount of board deflection and subsequent vertical take-off velocity was sensitive to the precise positioning of the relative upward acceleration phase of the arms and legs within the time interval of board depression. The basic problem is then one of determining how a given leg and arm force pattern might best be shifted in time so as to produce the greatest possible take-off velocity. That is, with which stage of board contact should a particular phase of the armswing or leg extension pattern be synchronized?

Sprigings and Watson (3) in their initial study examined only the timing pattern of the arms. That is, the diver's body was modelled as a two segment body consisting of arms as one segment and the remainder of the body as the second segment. The diving board was modelled simply as a massless spring and the displacement of the board was assumed to be the same as that of the rigid head-torso-leg segment. This two segment model of a diver was solved mathematically in closed form for the optimal timing pattern of the armswing. The results of this initial study indicated that for a normal armswing, the beginning of the upward relative acceleration phase of the arms should coincide with the initial instant of board contact. The obvious questions which this initial study raised were: (a) would the results for the arms differ if the force patterns due to the hip and knee extensors were also included in the analysis? (b) could the springboard stiffness be theoretically tuned so as to produce a best performance for any individual diver.

## METHOD

The research strategy used in this study, as well as in the initial study was to search for the optimal timing of an already learned movement pattern; namely, the swing of the arms and the flexion-extension of both the hip and the knee. No attempt was made to suggest modifications to the shape of the relative force curves of either the arms or the legs. The advantages of tackling the problem in this manner, were considered to be three-fold. Firstly, it pushed aside the extreme difficulty of trying to optimize the torque patterns of a given subject's armswing and leg flexion-extension based on some unknown maximum capability (4,5,6). Secondly, it reduced the problem to a level where any suggested corrections in performance could easily be implemented by the athlete. Thirdly, it was felt that any corrections in performance offered by this approach would not jeopardize the diver's other objective which was the development of angular momentum during take-off.

The diver was modelled as a three segment body with each segment capable of only linear vertical movement (Fig. 1). Segment 1 consisted of the two arms; segment 2 consisted of the head and torso; and segment 3 consisted of the two legs. The diving board was modelled as an undamped spring-mass system, since experimental tests by the authors had shown that the damping coefficient for a typical springboard was very small.

In the model shown in Fig. 1, the absolute forces  $f_1$ ,  $f_2$  and  $f_3$  are unknown and indeed only  $f_1$  can be conveniently measured. The relative forces  $F_A$ ,  $F_T$  and  $F_L$  were obtained from film and are shown in Figures 2,3,4. For this system at any moment in time, there are four relationships

$$\begin{aligned} M_1 \ddot{Y}_1 &= f_1 - gM_1 \\ M_2 \ddot{Y}_2 &= -f_1 + f_2 - gM_2 \\ M_3 \ddot{Y}_3 &= -f_2 + f_3 - gM_3 \\ M_4 \ddot{Y}_4 &= -f_3 - gM_4 - KY_4 \end{aligned}$$



which must be satisfied by  $f_1, f_2, f_3$ , and  $Y_4$ . The values of  $f_1, f_2, f_3$ , and  $Y_4$  for any instant are in turn generated from the relative segment force equations.

$$\begin{vmatrix} 1+M_1/M_2 & -M_1/M_2 & 0 & 0 \\ -1 & 1+M_2/M_3 & -M_2/M_3 & 0 \\ 0 & -1 & 1+M_3/M_4 & KM_3/M_4 \\ 0 & 0 & 0 & 1 \end{vmatrix} \begin{vmatrix} f_1 \\ f_2 \\ f_3 \\ Y_4 \end{vmatrix} = \begin{vmatrix} F_A \\ F_T \\ F_L \\ f(K, t, V_{4i}, Y_4) \end{vmatrix}$$

This system of equations not only allows the modelling of the measured dive but allows the testing of a different coordination of the muscle effort from the three major groups.

The effective mass of the springboard was determined experimentally and found to be 7.9 Kg. The numeric value of the mass of the 3 body segments were computed using Dempster's (7) percent body segment values.

The method used to search for an optimal timing sequence for the armswing and leg flexion-extension of both the hip and knee consisted of allowing the computer (VAX 11/780) to try all the combinations possible within predefined limits. Basically this meant that the relative force patterns of the hip (Fig. 2) and the knee (Fig. 3) were held constant in time while the relative force history pattern of the arms (Fig. 4) was time stepped through all reasonable possibilities. For each and every shift of the armswing pattern, computations were performed to determine the vertical take-off velocity of the diver's total body center of gravity (CG) under the imposed boundary conditions. The timing pattern which produced the greatest take-off velocity was taken to be best. For the purposes of our study, take-off velocity was considered to correspond to the point in time when the springboard had returned to its point of zero deflection. After the 'best' timing pattern of the armswing had been determined for a given hip and knee pattern, the hip force pattern was time stepped through while keeping the timing of the knee force pattern and the present best arm force pattern constant. The same time stepping was then done with the knee force pattern while holding the current 'best' timing of the arm force pattern and current 'best' timing of hip force pattern constant. The entire process was continually repeated until the optimal timing patterns for arms, hips, and knees had been determined.

#### References:

1. Miller, D., et al. Med. & Sci. in Sports and Ex. 16:234-242, 1984.
2. Miller, D. Proc. II Biannual Conference of the CSB, Kingston, Ont., 24-25, 1982.
3. Sprigings, E., et al. Biomechanics IX-B, 389-394, 1985.
4. Bauer, W. Biomechanics and Performance in Sport, 129-143, 1980.
5. Hatze, H. J. Sports Sci., 1:3-12, 1983.
6. Hatze, H. Human Movement Sci., 3:5-25, 1984.
7. Dempster, W., WADC Technical Report 55-159, Wright Patterson Air Force Base, OH, 183-194, 1955.

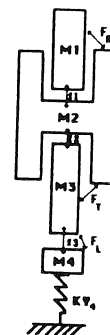


Figure 1. Linear model of a three segment diver and a spring-mass board. (M1=arms, M2=head+torso, M3=legs, M4=effective board mass,  $f_1, f_2, f_3$  = the absolute contact forces between the segments;  $KY_4$  = spring force of board,  $F_A, F_T, F_L$  = the relative forces between the segments)

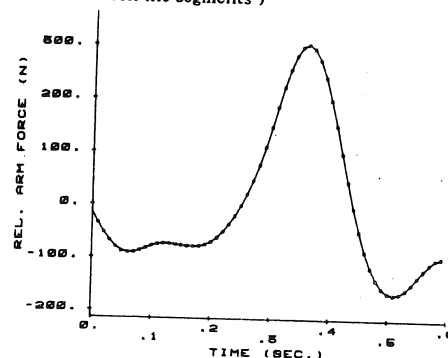


Figure 2. Relative force curve of the arms with respect to the shoulder joint.

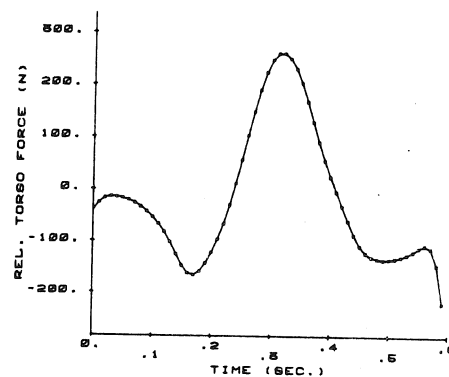


Figure 3. Relative force curve of the torso and head with respect to the hip joint.

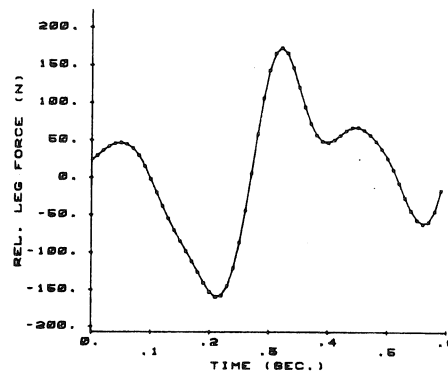


Figure 4. Relative force curve of the legs with respect to the MP joint of the foot.

AN EXAMINATION OF MECHANICAL ENERGY TRANSFERS AMONGST  
LOWER EXTREMITY SEGMENTS DURING A KICKING MOTION

Philip E. Martin and William L. Siler  
Exercise and Sport Research Institute  
Arizona State University  
Tempe, Arizona 85287

INTRODUCTION

The concept of mechanical energy transfer has been used in analyses of many types of movements, but remains a measure whose significance is not clearly defined. The purpose of this project was to compare two methods for calculating measures of mechanical energy transfers within and between body segments for a simple kicking motion. The first was based on a mechanical energy analysis while the second utilized a kinetic approach. The results demonstrated that the measures of energy transfer during the kick were quite different for the two methods. These results are discussed in terms of the advantages and disadvantages of each method and of their implications for considerations of the aerobic demand (economy) of an activity.

REVIEW AND THEORY

When evaluating energy transfer during movement, there are two analytical approaches that have been used. The first of these two, which has been used by many researchers (e.g., 1,2,3), involves the calculation of the potential and kinetic energy components of each of the body segments. From these components, the mechanical work done by the body can be calculated assuming no energy transfer, within segment transfer only, or within and between segment transfer. The differences in these work measures then reflects the energy transfer values of interest.

In contrast, the second analytical method utilizes a kinetic approach to quantify the work done by joint reaction forces and moments. (4,5,6) As a result, this method provides the means to examine not only the roles of the reaction forces and moments in energy transfer between adjacent segments, but also their role in generating and dissipating energy to and from segments.

While both analytical approaches have been used in analyses of human movement, there has been no comparison as to how the mechanical energy transfer measures from the two approaches compare. Since energy transfer is generally considered to have an impact on the economy of movement, there seems to be a need to more fully understand the significance of these measures reflecting segmental interactions.

METHODOLOGY

Fourteen healthy college aged males each performed two trials of a simple kicking motion. The initial position assumed by the subjects was one in which body weight was supported totally on the left foot. The

right leg was then positioned such that the knee was flexed to 90 degrees with the thigh oriented vertically. Upon command, the subject then initiated a rapid swing or kick of the right leg.

All trials were filmed with a single high speed camera at 80 frames per second. Smoothed coordinate data for the hip, knee, ankle, toe, and heel of the right leg that were generated from the film were used to calculate necessary velocity and acceleration characteristics of the segments and joints of the leg. Standard link segment mechanics were then used to derive estimates of the joint reaction forces and the net moments for the ankle, knee, and hip.

The mechanical energy approach for calculating energy transfers used procedures outlined by Pierrynowski et al. (1). Using this method, the instantaneous energy levels of the foot, shank, and thigh were calculated as the sum of the translational and rotational kinetic and potential energy components. The work done on the leg was then calculated by assuming no energy transfer, within segment transfer only, and within and between segment transfer. These results then provided the data necessary to calculate the energy transfers within segments ( $T_w$ ), between segments ( $T_b$ ), and within and between segments ( $T_{wb}$ ).

To calculate energy transfer measures using the kinetic approach, the procedures of Quanberry et al. (5) and Robertson and Winter (6) were used. Based on these procedures, the instantaneous rate at which the joint reaction forces and moments do work on the segments of the leg were calculated. While joint powers reflect a simple transfer of energy between interacting segments ( $T_j$ ), the moment powers represent a more complex interaction since muscles are capable of doing positive and negative work on segments and of transferring energy from a segment to its neighbor. Once the energy transfer component ( $T_m$ ) was partitioned from the positive and negative work measures for the moment, it was combined with the energy transfer due to the joint reaction force to generate a total measure of transfer ( $T_{jm}$ ) for this method.

RESULTS

The results of the analysis of the kicking motion are displayed in Figure 1. For the energy transfers within and between the three segments of the leg as calculated from the mechanical energy approach ( $T_w$ ,  $T_b$ , and  $T_{wb}$ ), the figure illustrates that the kick was nearly half completed before a significant rise in the energy transferred both within and between segments occurred.

The energy transfer curves for the reaction forces and moments ( $T_j$ ,  $T_m$ , and  $T_{jm}$ ) demonstrate that energy transfer occurred steadily throughout the motion based on this method of calculation. A comparison of the total measures of transfer for the two methods ( $T_{jm}$  and  $Twb$ ) shows that the final transfer values were quite similar ( $T_{jm} = 239$  J,  $Twb = 238$  J). This result is misleading, however, since the kinetic measure of transfer reflects the function of the reaction forces and moments and thereby represents between segment functions only. The between segment energy transfer for the mechanical energy approach ( $Tb = 126$  J) represented only half of the total energy transferred for that method. In addition, it should be noted that while the group mean values for total transfer for the two methods were quite similar, individual subjects often displayed differences in the magnitudes of these two transfer measures.

#### DISCUSSION

Much has been made of the body's tendency to minimize the aerobic demand of many movements by adopting a particular movement pattern. (e.g., 1,7,8,9) It has been suggested that the amount of mechanical energy transferred amongst segments influences the economy of movement. Williams (10) and Shorten et al. (2) found statistically significant relationships between the economy of running and the mechanical energy transferred between body segments. In both studies, these measures of energy transfer were calculated using the mechanical energy approach.

While the mechanical energy approach represents a reasonably simple analysis based on kinematic data, the assumptions used in calculating energy transfer are purely mathematical rather than being based on a logical consideration of the nature of body segment interactions. Shorten et al. (2) noted this in stating "that any selection of transfers to be permitted or excluded is largely arbitrary without a knowledge of muscle activity patterns during the movement." (p.215) In addition, the approach provides no information pertaining to the source and mechanisms responsible for energy transfer.

In contrast, the kinetic approach represents a more complicated analysis in terms of data collection and processing. While this approach does not directly reflect the work due to muscle and bone-on-bone forces, it more closely reflects the nature of the mechanisms associated with segmental interactions and thereby provides the user with an indication as to the sources of the energy transfer. Williams (11) also noted this in stating that the kinetic method "seems to be a promising approach for deriving more definitive assessments of the amount and location of energy transfer." (p.322) Unlike the mechanical energy approach, however, the kinetic method does not provide a specific measure of within segment energy transfer.

In summary, this analysis has demonstrated that the two established methods for calculating mechanical energy transfers produce differing results. Because the kinetic approach focuses more directly on the mechanisms associated with segmental interactions, it is believed that this represents a more appropriate method of analysis, particularly with respect to considerations of the economy of motion.

#### References

1. Pierrynowski, M.R., et al. *Ergonomics* 23:147-156, 1980.
2. Shorten, M.R., et al. *Engin. in Med.* 10:213-217, 1981.
3. Norman, R., et al. *Int. J. Sport Biomech.* 1:253-262, 1985.
4. Elftman, H. *Amer. J. Physiol.* 125: 339-356, 1939.
5. Quanberry, A.O., et al. *J. Hum. Movt. Studies* 1:59-67, 1975.
6. Robertson, D.G.E., et al. *J. Biomech.* 13: 845-854, 1980.
7. Ralston, H.J. *Int. Zeit. Angew. Physiol.* 17:277-283, 1958.
8. Nubar, Y., et al. *Bull. Math. Biophys.* 23:377-390, 1961.
9. Sparrow, W.A. *J. Motor Behav.* 15:237-261, 1983.
10. Williams, K.R. *Diss. Abstr. Int.* 41: 4332A.
11. Williams, K.R. *Med. Sci. Sports Exerc.* 17:317-325, 1985.

#### Acknowledgement

This study was supported by a Faculty Grant-In-Aid, Arizona State University.

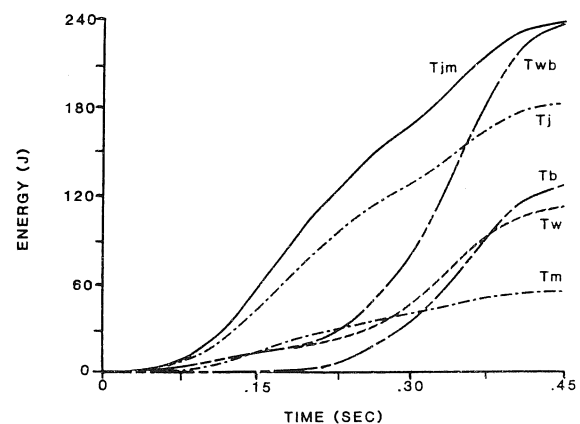


Figure 1. Sample mean curves for measures of energy transfer.  $Tw$ ,  $Tb$ , and  $Twb$  represent energy transfer within, between, and within and between segments, respectively, as calculated using the mechanical energy approach.  $Tm$ ,  $Tj$ , and  $Tjm$  represent energy transfers attributed to the joint moments, reaction forces, and their sum, respectively.

## KINEMATICS OF A WORLD RECORD IN THE TRIPLE JUMP

John A. Miller, Jr. and James G. Hay  
Department of Exercise Science and Physical Education  
The University of Iowa  
Iowa City, IA 52242 USA

### INTRODUCTION

The triple jump at the 1985 TAC (U.S. national) Championships was filmed. Jumps by Willie Banks (17.97 m) and Mike Conley (17.71 m) were, respectively, a new world record and the third best ever. The purposes of the analysis were: (1) to determine selected kinematic data for a world record triple jump, and (2) to compare these data with corresponding data for previous performances by the same athlete and for performances by other elite triple jumpers. The distance of the jump phase, 6.69 m, set Banks' world record apart from those of his predecessors. A comparison of the phase distances and phase ratios for the 1985 TAC jumps with those for the best analyzed jump by Banks, Conley and Joyner at some previous meets revealed that, as they increased their effective distances, all three decreased the emphasis they placed on the step phase. There appeared to be a difference between the better and the lesser elite jumpers in the way they changed their horizontal velocity during the periods of support following the takeoff into the hop. The best athletes seem to use a "pawing" (or active) landing prior to takeoff into the step phase and a "blocking" landing prior to takeoff into the jump phase.

### METHODOLOGY

The subjects were the athletes who finished in the first four places at the 1985 TAC Championships, respectively, Willie Banks, Mike Conley, Charles Simpkins and Al Joyner.

Two motion-picture cameras, filming at nominal rates of 100 frames per second, were used to record the performance of the subjects on each trial. The first camera was used to record the subjects' performances during the last stride and the hop phase of the triple jump. The second camera was used to record the performances during the step and jump phases.

The filmed records of the best jumps of Banks, Conley and Joyner, and the third best jump of Simpkins were analyzed. The official distances of these jumps were 17.97 m, 17.71 m, 17.46 m and 17.51 m, respectively. Ten frames of the films for each trial were digitized (2).

### RESULTS AND DISCUSSION

The distances for the hop, step and jump phases of the analyzed jumps for each of the subjects are presented in Table 1. The longest hop phase was recorded by Conley. His 6.61 m hop phase exceeded those of Banks, Simpkins, and Joyner by 0.31 m, 0.25 m, and 0.36 m, respectively. At the completion of the step, Banks trailed all subjects in distance covered. At that stage Conley had traveled 0.54 m farther than Banks. A 6.69 m jump phase allowed Banks to overtake his competitors and establish a world record.

A comparison of the phase distance recorded for Banks with those recorded for world records since 1910 (3) showed that his hop and step distances were above average ( $\bar{X}$  = 6.21 m and 4.54 m). His jump distance was the largest ever recorded for a world record and exceeded the nearest value (de Oliveira's 6.43 m) by 0.26 m. Thus, it was the distance of the jump phase that set Banks' world record apart from those of his predecessors.

Table 2 contains a comparison of the phase distances and phase ratios for the 1985 TAC jumps with the best analyzed jump by Banks, Conley and Joyner at some previous meets. No additional data was available on Simpkins. For each subject, the effective distance of the triple jump increased. The increase was achieved in the same manner, in each case -- through increased hop, decreased step and increased jump distances. It is of some interest to note that, as they increased their effective distances, all three subjects decreased the emphasis they placed on the step phase. With Banks and Conley, the decreased emphasis on the step phase was accompanied by an increased emphasis on the already-dominant phase of their techniques, the jump and hop, respectively. With Joyner, it was accompanied by an increased emphasis on the jump phase. Although the small sample size in this study does not permit any conclusive statement to be made on the issue, the observed shifting of emphasis from the step phase to other phases suggests that in elite triple jumping, maximizing the length of the step phase may not be conducive to maximizing the overall distance.

Fukashiro and Miyashita (1) estimated the horizontal and vertical velocities at takeoff that would be necessary for an 18 m triple jump (Table 3). The estimates for the horizontal velocities were in surprisingly close agreement with the data for Banks' near-18 m jump. In all instances, the predicted value was within five percent of the measured value. The estimates for the corresponding vertical velocities were not in such close agreement with the measured values. The manner in which Fukashiro and Miyashita estimated the velocities undoubtedly contributed to the differences observed when estimated and measured values were compared. Given the procedures (and, in particular, the phase ratio -- 36.9%:29.1%:34.0%) on which their method rests, it seems remarkable that the estimates of Fukashiro and Miyashita are as close as they are to the values recorded for Banks.

A comparison was made between the absolute (and relative) changes in horizontal velocity during the period of support prior to each phase using the data of the present study and that reported in a study of Olympic finalists by Hay and Miller (2) (Table 4). In all instances, the horizontal velocity decreased during each period of support. In the present study, the magnitude of the relative change in horizontal velocity increased with each successive period of support. This pattern was defined as Technique I.

In the Olympic study (2), the magnitude of the relative change in horizontal velocity increased from the hop to the step and then decreased slightly from the step to the jump. This pattern was defined as Technique III.

Technique I was used in the present study by the three subjects with the longest jumps -- Banks, Conley and Joyner -- and Technique III was used by Simpkins. In the Olympic study six subjects used Technique I and six subjects used Technique III. Within the top six finishers, five used Technique I, and within the bottom six finishers, five used Technique III. Thus, for this limited sample of elite athletes, the better athletes -- those with the longest distances -- tended to use Technique I.

The tendency for the better athletes to decrease their horizontal velocity during the period of support preceding the jump more than during the period of support preceding the step presumably reflects the differing requirements of the phases to follow. At the end of the hop, one of the athlete's principal concerns is to minimize the braking effect due to the horizontal ground reaction forces evoked during the landing and, thus, to maintain as much forward momentum as possible. To this end, coaches frequently recommend a backward-sweeping (or "pawing") action as the foot is brought to the ground -- a so-called "active landing". At the end of the step, the athlete's concern is less with the maintenance of forward momentum than it is with maximizing the length of the jump phase. In this case, a blocking action, akin to that used in the high jump, might yield better results than the pawing action of an active landing. This suggestion is supported by the findings of Tiupa et al. (4) who studied the takeoff techniques of male long jumpers. On the basis of their data, they rejected the view that "increased takeoff effectiveness must result from minimizing the loss in horizontal speed" and concluded instead that a "locking" or braking action of the leg was important to success in the event.

#### Acknowledgements

The authors wish to express their appreciation to the United States Olympic Committee for financial support and to The Athletics Congress of the USA for making it possible to gather the data at the 1985 TAC Championships.

#### References

1. Fukashiro, S., et al. *Med. Sci. Sports Exerc.* 15(4):309-312, 1983.
2. Hay, J.G., et al. *Int. J. Sport Biomech.* 1:185-196, 1985.
3. McNab, T. *Triple Jump*, 1968.
4. Tiupa, V.V. *Theory and Practice of Physical Culture*, 11-14, 1982.

Table 1  
Triple Jump Phase Distances

Athlete	Hop (m)	Step (m)	Jump (m)
Willie Banks	6.30	4.96	6.69
Mike Conley	6.61	5.19	5.98
Charles Simpkins	6.36	5.40	5.72
Al Joyner	6.25	5.39	5.94

Table 2  
Triple Jump Phase Distance to Effective Distance Ratios  
and Phase Distances for Best Analyzed Jump

Athlete	Meet	Effective Distance of Jump (m)	Hop/ Effective Distance (%)	Step/ Effective Distance (%)	Jump/ Effective Distance (%)
			(Hop Distance) (m)	(Step Distance) (m)	(Jump Distance) (m)
Willie Banks	TAC 1985	17.95	35.1 (6.30)	27.6 (4.96)	37.3 (6.69)
	UCLA-Pepsi 1982	17.62	34.8 (6.13)	29.3 (5.17)	35.9 (6.32)
Mike Conley	TAC 1985	17.78	37.2 (6.61)	29.2 (5.19)	33.6 (5.98)
	TAC 1983	17.36	34.7 (6.03)	31.7 (5.50)	33.6 (5.83)
Al Joyner	TAC 1985	17.58	35.6 (6.25)	30.7 (5.39)	33.8 (5.94)
	TAC 1983	17.19	36.1 (6.20)	31.6 (5.43)	32.3 (5.55)

Table 3  
Horizontal and Vertical Velocities at Takeoff

Study (Jump Distance)	Hop (m/s)	Step (m/s)	Jump (m/s)
Horizontal Velocity			
Present Study (17.97 m)	9.5	8.7	7.3
Fukashiro and Miyashita (18.00 m)	9.9	8.6	7.3
Vertical Velocity			
Present Study (17.97 m)	2.2	1.7	2.8
Fukashiro and Miyashita (18.00 m)	2.6	2.1	2.8

Table 4  
Mean Absolute and Relative Changes in Horizontal  
Velocity during the Support Period preceding  
the Takeoff into each Phase

Study	Hop m/s (%)	Step m/s (%)	Jump m/s (%)
Present Study	-0.7 (-6.8)	-1.1 (-11.5)	-1.6 (-18.8)
Hay and Miller (1985)	-0.6 (-6.0)	-1.4 (-14.4)	-1.1 (-13.6)

Arthur E. Chapman  
Simon Fraser University  
Burnaby, British Columbia  
Canada V5A 1S6

## INTRODUCTION

The initial purpose of this research was to assess the relative importance of selected kinematic variables to the velocity of ball projection in the squash stroke of an expert. A further purpose was to consider the implications of the results for the technique of the stroke. Analysis of film revealed that angular velocity of the racquet is the primary determinant of ball velocity. The expert achieves large angular velocities by forearm pronation and supination with an abducted wrist joint. This action requires emphasis when beginners are taught.

## REVIEW AND THEORY

Despite the existence of considerable literature describing the squash stroke, no scientific analysis appears to have been performed. One particular quality shown by top-class players of the international game is the ability to project the ball at a high velocity. The advantages of this ability are obvious in the context of an opponent's time to react. The mechanical properties of the racquet and strings are clear determinants of the kinetic energy generated in a ball. However, for any given racquet it is the kinematics of the stroke which will determine ball velocity. Consider a racquet moving in a horizontal plane with absolute angular velocity 'w' and translational velocity of the wrist joint over the grip 'V<sub>G</sub>'. If the distance between the grip and the point of contact with the ball is 'r', then the velocity of the point of contact 'V<sub>P</sub>' parallel to V<sub>G</sub> is:

$$V_P = V_G + rw$$

This formula allows the relative effects of translational and rotational velocities to be examined.

## METHODS

One top-class squash player was filmed (500frames.s<sup>-1</sup>) performing forehand and backhand drives with one racquet fixed with marking tape. The camera was located 3.36m above the horizontal plane of motion of the racquet and a grid of known dimensions was located on the floor beneath the camera and performer. The zoom lens was adjusted to fill the frame of the film with the racquet. The ball was dropped from a point in line with the camera lens and the performer struck the ball at the top of its rebound. Following digitization of points of interest the following variables were calculated: velocity of the ball following contact, V<sub>B</sub>; velocity of the point of contact on the racquet, immediately prior to contact,

parallel to the ball direction, V<sub>P</sub>; distance between point of contact and the wrist joint r; velocity of the wrist parallel to ball direction, V<sub>G</sub>; and angular velocity of the racquet immediately prior to ball contact, w.

The same subject was filmed (200 frames.s<sup>-1</sup>), while performing forehand and backhand strokes, from a position perpendicular to the direction of ball projection. The view captured the entire stroke. Numerous bodily landmarks were digitized and the horizontal and vertical components of their velocities were calculated, in two dimensions.

## RESULTS

Figure 1 shows that V<sub>P</sub> was highly dependent upon rw (corr.c/e=0.97 slope=0.92) and w (corr.c/e=0.95,) and independent of V<sub>G</sub> (corr.c/e=-0.092). Figure 2 shows that the velocity of the ball V<sub>B</sub> was similarly highly dependent upon V<sub>P</sub> (corr.c/e=0.94, slope=1.39). These results are from pooled data because separate analysis of forehand and backhand strokes failed to reveal significantly different relationships. Figure 3 illustrates the horizontal velocities of the wrist (WR) and the butt of the grip of the racquet (BR) from a film of the second performance. Ball contact occurred at the peak of the trace labelled TH. Upon impact the reduced velocity of the butt relative to the neck indicates significant forearm pronation since the wrist joint was abducted. Figure 4 further illustrates pronation in the sense that the top side of the head of the racquet (TS) travels faster on impact than the bottom side (BS).

## DISCUSSION

Since the velocity of the ball is 1.39 times greater than that of the point of contact on the racquet, the interaction of mechanical properties of ball, racquet and person are important determinants of ball velocity. Little can be said about this aspect because the ball stays on the racquet for about 3ms while sampling occurred every 2ms. In the majority of the strokes the racquet did not bend until after the ball had left. Therefore the velocity of the ball appears to be due partly to the recoil of the strings working against the inertia of the racquet. Ninety-four percent of variance in V<sub>P</sub> was accounted for by the value rw while 90% was accounted for by w alone. This makes the angular velocity of the racquet prior to contact a strong factor determining ball velocity whereas the point of contact is of less importance. This is further exemplified by the fact that the velocity of the grip accounts for none of the variance of V<sub>P</sub>. The

point of contact clearly is important for other features of the stroke including comfort and vibration-induced injury. The data from the isolated view of the racquet indicates that the top of the head of the racquet (TH) travels faster than the butt of the grip due to the angular velocity. The manner in which this is achieved is shown in Figure 3. The reduction in the velocity of the butt of the racquet was characteristic of all strokes performed, and also of those performed by a second expert studied. Therefore, not only does angular velocity of the racquet rank highly as a major factor in ball velocity, it is associated with a concomitant reduction in the velocity of the wrist joint. It seems that the angular velocity of the racquet is increased at the expense of translational velocity of the wrist. Whether the wrist velocity is reduced

either consciously or as a reaction to angular acceleration is a question which must await a full three-dimensional kinetic analysis. For experts in the game of squash, angular velocity of the racquet is achieved by pronation (forehand) and supination (backhand) of the forearm since the angle between the racquet and the forearm is almost  $90^\circ$ . This may not be the case with other striking activities.

Sampling rates in the order of 5,000 frames.s<sup>-1</sup> are required for reasonable resolution of the dynamics of interaction between ball and racquet. Typical questions to answer concern the relative importance of string type and tension and viscoelastic properties of the racquet for velocity of ball projection.

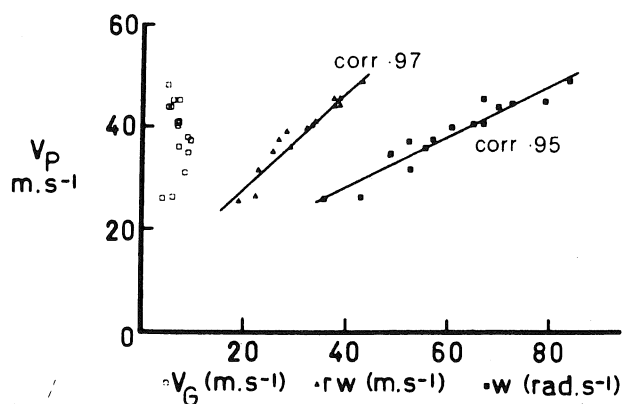


Figure 1. The relationship between velocity of the point of ball contact on the racquet ( $V_p$ ) and velocity of the wrist ( $V_g$ ), the product of radius of rotation and angular velocity ( $rw$ ) and angular velocity alone ( $w$ ).

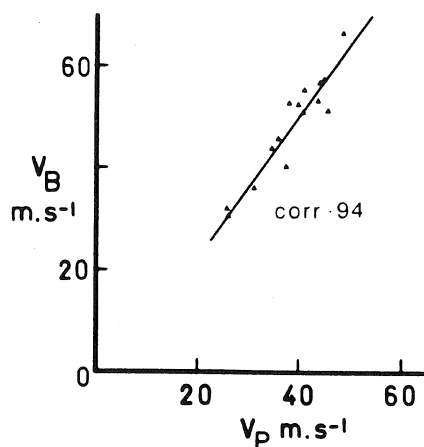


Figure 2. The relationship between velocity of the ball after contact ( $V_b$ ) and velocity of the point of ball contact prior to contact ( $V_p$ ) in the same direction as  $V_b$ .

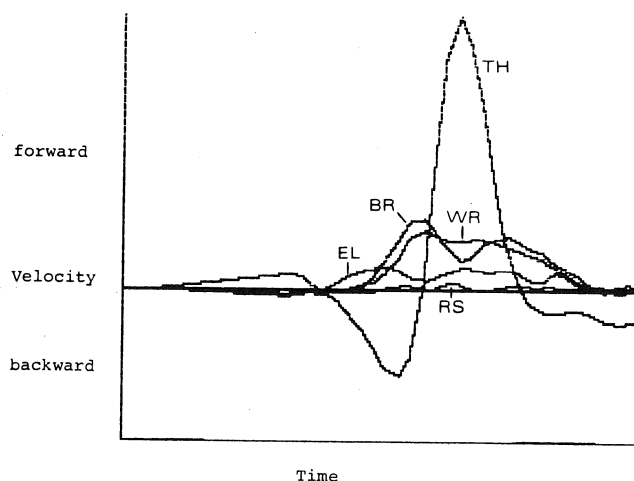


Figure 3. Horizontal velocities of various points on the body and racquet in the direction of ball projection during a forehand drive. These are shoulder (RS), elbow (EL), wrist (WR), butt of racquet grip (BR) and tip of racquet head (TH).

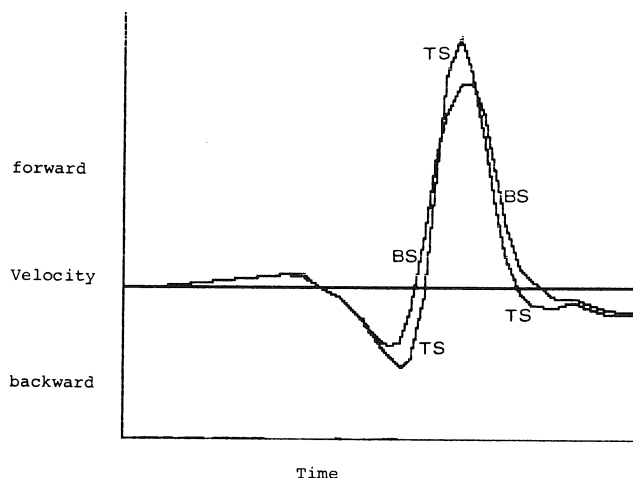


Figure 4. Horizontal velocities of the top side (TS) and bottom side (BS) of the racquet head in the direction of ball projection during a forehand drive.

Nancy Hamilton  
Department of Physical Education  
University of Illinois  
Urbana, IL 61801

## INTRODUCTION

It was the purpose of this study to produce a mathematical model for the prediction of neck muscle tension based on source document placement at a word processing work station. Such a model should reflect tension which exists in both static and dynamic situations. To produce such a model, electromyographic measures of neck muscle tension during both reading and typing tasks were examined. Results from these measures were used to develop a series of regression equations which constitute the mathematical model. The model produced should allow source document effects to be modified through work station design modifications.

## REVIEW AND THEORY

Tension in the neck and shoulder region is a major contributing factor to tension related work reduction phenomena. Cervicobrachial syndrome, tension myalgia, and headaches are often results of such tension and may result in significant loss of job time or efficiency.<sup>(1)</sup> While a number of investigations have been done on work station design factors which contribute to or relieve various forms of tension, little has been done in relation to source document placement. It is the source document as primary visual task in word processing, however, that is the most critical factor in the establishment of head position. Since head position dictates the amount of tension which will exist in the neck muscles, it is necessary to study the causal factor in head positioning as it relates to such tension. Studies done previously have been focused on reports of pain as a result of constrained head positions.<sup>(2,3)</sup> Few studies have been done which attempt to measure the actual level of muscle tension which may contribute to this pain.<sup>(4)</sup>

## METHODOLOGY

Subjects for this study were 20 adult volunteers with varying degrees of typing skills. Each subject was asked to perform a reading task and a typing task in each of six source document positions. During task performance, the levels of muscular tension in the neck extensor muscles and in the sternocleidomastoid muscles were sampled using electromyographic techniques. These tension levels were then compared to the subject's resting level of tension for control and then transformed into a percentage of the maximum level of tension produced in a voluntary isometric contraction.

The document positions which were used in this study consisted of those positions observed to be the most common in the work place. Documents were placed flat on the work station table next to the keyboard and on a document stand to the side of the monitor. Each of these positions was tested bilaterally. In addition, source documents were placed above the keyboard between keyboard and

monitor and above the keyboard in place of the monitor. Each document position was described in terms of both vertical and horizontal angular displacement from work station center.

In addition to EMG data, film was taken to establish head position for each document position. Head positions were established in terms of angle of head flexion, lateral flexion angle, and angle of rotation. Head position was then compared to both source document placement and level of muscular tension.

## RESULTS AND DISCUSSION

ANOVAs performed for neck tension by document position indicated significant differences in tension measures. Tension in the neck extensors varied with changes in both horizontal and vertical displacement angles of the source document. The highest levels of muscle tension were found in the two placements which had documents flat on the table to the side of the keyboard. These two positions also produced the greatest angles of head flexion and rotation.

The lowest levels of neck tension were produced in the two central document positions, which also produced the smallest head flexion angles and the least rotation. Levels of tension differed significantly between typing and reading tasks only in the extreme document positions, that is, central and flat on the table.

To produce the mathematical model, tension in each of the muscle groups was regressed on horizontal and vertical document angles. The regressions for both extensor groups were found to be significant in both the reading and typing conditions. The tension regressions produced four equations. The model was further enlarged to include equations in which neck tension was regressed on measures of head position, adding four more equations. The complete model consists of these eight equations, four for typing and four for reading.

This model is as follows:

### Reading

Tension on document position

$$\text{Left extensor} = -.0025V + .000036H^2 + .00453V^2 + 2.2235$$

$$\text{Right extensor} = -.1127V + .000016H^2 + .0063V^2 + 1.729$$

Tension on head position

$$\text{Left extensor} = .0729F + .115L + .048R + 3.169$$

$$\text{Right extensor} = .177F + .0684L + .0764R + 3.287$$

### Typing

Tension on document position

$$\text{Left extensor} = 0.09496V - .000032H^2 + .00443V^2 + 5.17$$

$$\text{Right extensor} = -.0123V - .0022H^2 + .00206V^2 + .2189H + 7.03$$

Tension on head position

$$\text{Left extensor} = .219F - .0897L + .0245R + 5.83$$

$$\text{Right extensor} = .148F + .231L + .058R + 8.25$$

where V = vertical document angle, H = horizontal document angle, F = head flexion angle, L = head lateral flexion angle, R = head rotation.



## CONCLUSIONS

From this study, it was concluded that source document positioning plays a significant role in the production of tension in the neck extensor muscles. This tension may be a result of head position, with head position related directly to document position.

Source document placement is often overlooked in the design of computer work stations, yet can be a causal factor in work related discomfort. Through the use of modelling techniques such as developed here, it would be possible to predict the levels of tension which might be experienced for a given document placement. In work station design, various document locations might be assessed for tension levels or head position, looking for an optimum placement. In constrained work stations, where there is little document placement flexibility, it would be possible to predict the levels of tension which might occur, and to modify break schedules or work intensity for tension relief.

## References

1. Maeda, K., J. Hum. Ergology, 6:193-202, 1977
2. Hunting, W., et al. Ergonomics, 24:917-931, 1981
3. Ong, C. N., et al. J. Hum. Ergology, 10:161-171, 1981
4. Gray, F. E., et al., Ergonomics, 9:245-256, 1966

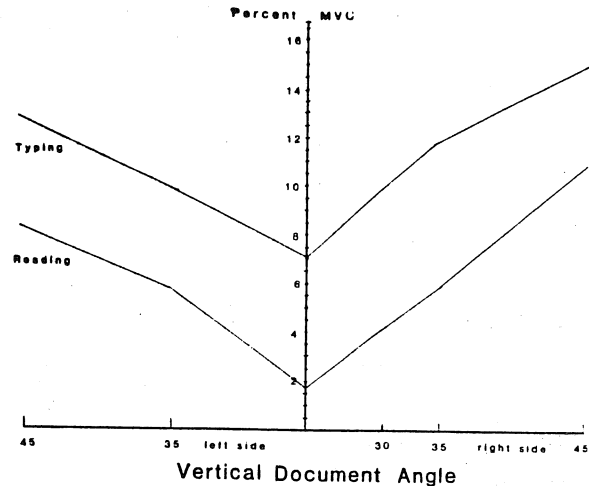


Figure 2. Right extensor tension with vertical document position.

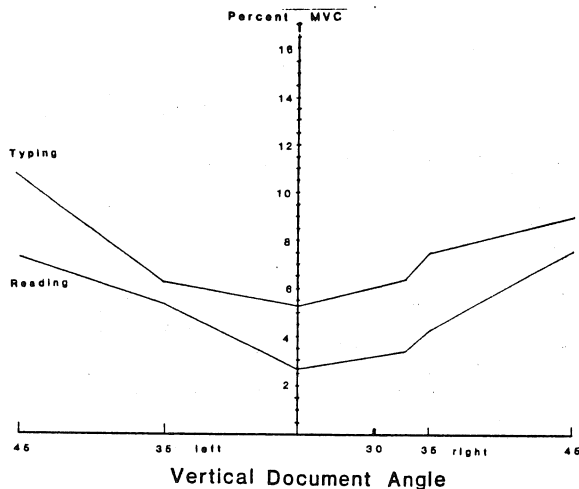


Figure 1. Left extensor tension with vertical document position.

## PRESSURE DISTRIBUTION IN OFFICE SEATING

S. Reinecke, G. Weisman, A. Stifter, M. H. Pope  
Vermont Rehabilitation Engineering Center  
The University of Vermont, Burlington, Vermont 05401

### INTRODUCTION

Seated postures have been recognized as contributing to an increase of low back pain in the workplace (2). Researchers have studied a number of factors which will aid in the design of the "ideal chair" (1, 4,5,6). These factors include anthropometrics, muscle activity, comfort, and pressure distribution.

Although pressure distribution has been investigated in various types of seating, commercially available office chairs have not been studied. Pressure studies have used specially-made experimental chairs, wheelchairs, and wheelchair cushions (3). Jurgens (5) noted that pressure distribution is not the sole determinant of seating quality, but it is a significant component of human seated support.

Pressure distribution information suggests how and where a particular seat supports the body. Using a pressure mat on automobile seats, Kamiyo et al. (6) reported that static pressure distribution patterns distinguished comfortable from uncomfortable seats.

Seating support has been identified as an important factor in determining posture, but pressure distribution may vary with the specific posture assumed. For example, Hertzberg (4) observed a backward shift in force contours when backrest inclination changed from 90° to 115°. Also, he found that differences in buttock pressure between 90° and 105° of backrest tilt show reductions in overall weight and redistribution of the weight backwards. However, pressure distribution has not been systematically assessed in relation to variations in posture; pressure studies performed thus far have used chairs in which one is constrained to a fixed position.

This study describes the pressure distribution of several commercially available office chairs. Pressure measurements were obtained with an air cell transducer on seat pans and backrests; pressure contour maps were then generated for each of the chairs.

### MATERIALS AND METHODS

Six commercially available office chairs were obtained for this study. The six chairs were all different and comprised three types:

Posture Tilt Chair. Commonly called a stenographer's chair, this model incorporates a moving backrest with a stationary seat pan.

Swivel Tilt Chair. Back and seat pan are fixed and thus move as a unit, as in a common rocking chair.

Synchronous Tilt Chair. Back and seat pan move simultaneously and in a fixed ratio. For example, for every 3° of back inclination, the seat pan may tilt backward 1°.

Chair #1: Posture tilt. Half backrest.

Chair #2: Same as Chair #1. Armrests.

Chair #3: Same as Chair #2 but full backrest.

Chair #4: Swivel tilt. Full backrest. Seat pan/backrest unit pivoted about hinge 24cm behind front of seat pan. Armrest.

Chair #5: Posture tilt. Half backrest. Seat pan tilt adjustable from 5° to 8° backward tilt. No armrests.

Chair #6: Synchronous chair. Full backrest. Seat pan tilt adjustable from 5° to 8° backward tilt. Seat pan hinged at front of seat.

The following adjustments were made to the chairs.

(1) Seat pan height was adjusted for all chairs such that the tibia was at 90° to the femur. The femur was horizontal to the floor when individuals were seated erect, with feet flat on the floor.

(2) Backrests of Chairs #1, #2, #3 and #5 were adjusted in height such that the convex curve of the backrest was positioned at the lordosis of the subject when seated erect.

(3) Backrest angles were locked in place during each test for all chairs except #4, due to variability in the spring force of backrest.

Eight subjects (4 males, 4 females) participated in the study. Each subject was positioned at 70°, 90°, and 120° forward flexion. The angle was measured from a horizontal plane to the floor. Chairs #5 and #6 were also tested with seat pans adjusted in the two most extreme positions.

Pressure distribution was measured on seat pans and backrests using two Oxford Pressure Monitors manufactured by Talley Medical Equipment Ltd, Oxford, England. The device uses 25 pneumatic load cells in a 5 x 5 matrix on a 30cm x 30cm mat. Pressures were first recorded at the seat pan; the mat was then removed and secured to the backrest where pressures were again recorded. Air cell transducers allow for description of pressure distribution at the user-chair interface. However, since interpretation of the absolute values obtained for pressure can present problems (8,9), distribution was assessed qualitatively in the present study. Readings from the pressure mat were entered into an AT&T PC computer where values of pressure were linearly interpolated. Sixteen hundred points within the 30cm x 30cm area of the mat were calculated for both the seat pan and backrest, and isobaric contour lines were drawn for each experimental condition.

Data were evaluated by studying pressure patterns of all chairs at each flexion angle. Data mappings were arranged so that comparisons (of location and of the relative "high" and "low" pressure points) could be made between the various flexion angles as well as between chairs. Four observers individually studied the mappings, documenting similarities and differences among chairs and among postures.

### RESULTS

Several pressure distribution patterns were exhibited by all six chairs and are consistent with previous findings (4,5,6,8). The points of highest pressure were found under the ischial tuberosities and under the thighs. Seat pan pressures were generally reduced in all chairs as posture changed from 70° to 120° forward flexion.

Pressure on the backrest was minimal for all chairs in the 70° position. As subjects moved from 70° to 120°, back pressure moved up, becoming localized in the scapular region at the 120° position.

The posture tilt chairs as a group (Chairs #1, #2, #3 and #5) showed higher seat pan pressures than the other types of chairs.

Chairs #1, #2 and #3 showed very similar seat pan distributions. The armrests of Chairs #2 and #3 had no apparent effect on the distribution. The full back of Chair #3 caused higher pressure at the bottom of the backrest due to interference with the buttocks. The backrest tended to hinder upper back support in all three positions. The half backrest of Chairs #1 and #2 allowed space for the buttocks at the back of the seat pan. No back support was noted for Chair #4 at the 70° position and pressure distribution was judged more uniform at the backrest and seat pan than in any of the other chairs evaluated. Seat and back pressures for Chair #4 were the lowest of all the chairs. A tendency for pressure to increase under the thighs as the subject moved from 70° to 120° was noted.

Chair #5 showed an increase of pressure under the thighs as the seat pan was tilted back from 5° to 8°.

Although Chair #6 had a full backrest, it did not have the same effect as Chair #3 of buttock pressure on the backrest. This appeared to be due to the fact that the bottom of the backrest was concave enough so as not to contact the buttocks. Although this chair was tested in two positions of seat pan tilt, increased thigh pressure, as in Chair #5, was not observed.

#### DISCUSSION

All chairs tested showed the same general seat pan pressure distribution as has previously been described in the literature. The finding that the seat pan pressure is reduced and moves rearward with increasingly inclined postures confirms Hertzberg's (4) single observation in a special seat. Although the relative values of pressure may have been affected, the addition of armrests did not seem to change the distribution of pressure on the seat pan.

Two often-cited characteristics of good seating are adequate back support and the ability to allow for movement or altered posture (2). Keegan (7) suggested that risk of low back pain is increased by seated postures which necessitate a decrease in the trunk-thigh angle with consequent flattening of the lumbar curve. Such postures may promote stretching of the posterior longitudinal ligaments and may thus contribute to posterior protrusion of a degenerated lumbar disc. Ligament stretch is minimized in sitting postures when the backrest helps position the spine in a relatively "normal" lordosis. Andersson et al. (1) have reported that proper lumbar supports absorb part of the weight of a reclined individual, thus reducing the load on the lumbar spine. Lumbar supports also help prevent flattening of the spine and corresponding disc pressure.

Disc pressure is also reduced with increased backrest inclination. In a reclined position, muscle activity is reduced and loads are transferred to ligamentous structures. Thus, from a biomechanical perspective, one would recommend that chairs be designed to position the spine in lordosis and to support it through the range of motion of the chair.

The chairs tested here have not been found to provide adequate support to the back in the forward flexed position, a position which is typical in the workplace (e.g., when working at a desk or bench). These six chairs appear to support the lordotic curve of the spine best when an individual maintains an upright, erect posture. However, when reclined, the pressure distribution patterns show that support is displaced upward, toward the scapular region instead of remaining at the lordosis. The swivel tilt chair provided the best lordotic support, perhaps because of the fixed relationship of the back to the seat

pan. However, an increase of pressure under the thighs was observed as the feet left the floor. The backrest pivots of the other chairs do not coincide with the anatomical pivot of the trunk, and thus may cause a shear motion between the backrest and the back of the seated individual. This phenomenon was demonstrated by Warren et al. in the case of reclining wheelchairs (10). To replace the traditional single pivot, they subsequently designed a four-bar linkage which reduces the amount of shearing motion.

#### CONCLUSIONS

1. Pressure distribution on the seat pans of six commercially available office chairs have been found similar to that described for other types of chairs and experimental seats.

2. The backrests of these chairs offer little or no support when one is seated in a forward-flexed position, typical of working postures at desks and workbenches.

3. As the backrest is reclined to 120° the support moves from the lordosis region of the spine to the scapular region. Thus, less support is provided for maintaining the lordosis in reclined positions.

4. The swivel tilt type of chair appears to be the best in supporting the lordosis in the reclined position with a concomitant increase in thigh pressure.

#### References

1. Andersson, G.B.J., Ortengren, R.: Myoelectric back muscle activity during sitting. *Scand J Rehab Med, Suppl.* 3:73-90. 1974.
2. Chaffin, D.B., Andersson, G.: *Occupational biomechanics*. John Wiley & Sons, New York, 1984
3. Ferguson-Pell, M.W., Bell, F., Evans, J.H.: *Interface pressure sensors: Existing devices, their suitability and limitations*. *Bedsore biomechanics*, Univ. Park Press, London, pp. 189-197, 1976.
4. Hertzberg, H.T.E.: *The human buttocks in sitting: Pressures, patterns, and palliatives*. Air Force Technical Report 720005, Aerospace Medical Research Laboratory, U.S. Air Force.
5. Jurgens, Von H.W.: Die Verteilung des korperdrucks auf sitzflache und ruckenlehne als problem der industr. ergonomics, 12(2):198-205, 1969
6. Kamiyo, K., Tsujimura, H., Obara, H., Katsumata, M.: Evaluation of seating comfort. SAE Technical Paper. Passenger Car Mtg, Troy, Mich, 1982.
7. Keegan, J.J.: Alterations of the lumbar curve related to posture and seating. *JBJS* 35-A(3), 1953.
8. Palmieri, V.R., Haelen, G.T., Cochran, G.V.B.: A comparison of sitting pressures on wheelchair cushions measured by air cell transducers and miniature electronic transducers. *Bull. Prost. Rsch.* 17, 1980.
9. Reger, S.I., Chung, K.S.: Comparative evaluation of pressure transducers for seating. RESNA 1985 Conf.
10. Warren, G.C., Stone, T.C., Sims, L.A.: PVA hinge for power recline wheelchairs. RESNA 1983 Conf.

#### Acknowledgement

This work was supported in part by a grant from the National Institute of Handicapped Research, U.S. Department of Education.

# BIOMECHANICAL BASIS OF MUSCULOSKELETAL DISORDERS AMONG VISUAL ARTISTS

W. Chang, F.J. Bejjani, D. Chyan  
Orthopaedic Center for the Arts  
Hospital for Joint Diseases Orthopaedic Institute  
New York, New York, U.S.A.

## INTRODUCTION

Little information is available on musculoskeletal disorders among professional artists. A questionnaire survey by the same authors of seventy-five randomly selected professional visual artists from the New York city area revealed a high incidence of low back, neck, and shoulder complaints. In order to assess the relationship between the artist's working conditions and the development of musculoskeletal disorders, a video analysis of a standard visual artist's workplace was performed. The results of the video analysis demonstrated some biomechanical factors that may contribute to the musculoskeletal complaints among visual artists.

## METHODOLOGY

The video analysis was conducted on-site at the School of Visual Arts in New York City. Fourteen senior drawing students, of equally high artistic ability (according to their teachers), were randomly selected and video taped while they were at work. There were 8 males and 6 females, with a corresponding age of  $19.7 \pm 1.7$  years. Nine were right-handed and five left-handed. They all sat on the traditional drawing "horse", with their drawing boards either on the "horse" or resting on their laps. They used various drawing tools: paint brushes of different sizes, crayons, pencils, nail tacks, etc. The students were divided into two groups according to the size of their paintings: Group I (6 subjects) were doing small detailed still life drawings on 15 x 15 cm papers; and Group II (8 subjects) were doing large live model drawings on 60 x 80 cm papers.

All subjects were given black turtle neck shirts and head bands to wear. Phosphorescent markers were placed on the head, neck, shoulder, elbow, low back, and wrist of the subject's dominant side. Markers were also placed on a vertical pole and on the drawing board. Using a fixed position Panasonic VHS video-camera, each subject was filmed for 15 minutes alternatively in the straight lateral plane and in the oblique dorsal plane at 55 degrees from the coronal plane. There was a 4-minute pause in between filmings. Anthropometric measurements of the dominant upper extremity segments were made (neck, arm, forearm lengths, and palm size) and a nonsignificant difference was found between the two groups.

The video data was then digitized at a sampling rate of 2 frames per 15 seconds, every other minute, for measurement of the following six angles: back flexion, neck flexion, shoulder flexion, shoulder rotation, shoulder abduction, and elbow flexion. For each of these angles, three sample discrete angular velocities were computed for each of three periods: 1st - 3rd minute; 6th - 9th minute; and 12th - 15th minute. A multiple analysis of variance, with contrast testing using the GLM procedure of the SAS package, was performed on the discrete angular velocities of all six angles to test the effects of group, sex, and time periods. A p value of 0.05 or less was considered significant.

## RESULTS

Group I artists had a significantly lower coefficient of variation than Group II artists in back and neck flexion angles (tables 1 and 2). The back and neck were significantly more flexed in Group I than in Group II.

Using free body analysis (1), the theoretical muscle tensions in the trapezium, erector spinae, and mid-deltoid for the neutral position, Group I, and Group II artists were calculated (table 3). The average mode angles of neck flexion, back flexion, and shoulder abduction were used for calculations. The centers of mass of body segments were obtained from Barter's tables (2). The results show sustained muscular tensions of up to 131% of total body weight in the back, 10.4% in the neck, and 23.2% in the shoulder. The calculated muscle tensions in Group I and II artists were several times greater than those of the neutral position because of increased torque in the body segments due to increased moment arm when sitting stooped forward with the neck flexed and shoulders abducted.

The multiple analysis of variance did not show any difference in back, neck, or elbow discrete angular velocities. There was also no difference among discrete shoulder angular velocities, in rotation, abduction and flexion, within each time period. There was, however, a significant difference among the three time periods, such as discrete shoulder angular velocities increased between the first and second periods and decreased between the second and third (table 4, figure 1). Shoulder velocities were found to be significantly higher among males than females ( $p=0.001$ ). No difference was found between Groups I and II.

## DISCUSSION

This study demonstrated high loads sustained for long periods of time in the neck, back, and shoulder muscles of a typical visual artist group at work. Shoulder fatigue over time was suggested by the significant decrease in shoulder rotation and abduction angular velocities between the middle and final time periods. These findings correlate well with the high incidence of low back, neck, and shoulder discomforts found in this population.

## References

1. Wiktorin, C.H., et al. Introduction to Problem Solving in Biomechanics. Lea & Febiger, Philadelphia, 1986.
2. Barter, J.T., Technical Reports: 57-260, 1957. Wright-Patterson, OH.

ANGLES (deg)	Mean (SD)		Mode		C.Var.	
	I	II	I	II	I	II
Back Flexion	26 (5)	15 (5)	26	15	18	50
Neck Flexion	35 (10)	20 (8)	39	18	28	53
SHOULDER	Flexion	38 (8)	36 (13)	36	40	22 40
	Rotation	20 (12)	29 (13)	21	32	59 49
	Abduction	24 (17)	22 (13)	23	31	75 60
Elbow Flexion	79 (9)	77 (11)	66	78	14	14

Table 1 Average mean (standard deviation), mode, and coefficient of variations for back, neck, shoulder, and elbow angles in Groups I and II artists.

ANGLES		Mean	Mode	Min.	Max.	Range	C.V.
Back Flexion	F	9.86	8.44	13.89		n.s.	86.47
	p	0.01	0.013	0.003			0.000
Neck Flexion	F	6.65	9.81	5.18		n.s.	6.27
	p	0.02	0.01	0.04			0.06
Shoulder Flexion	F		n.s.	8.63		n.s.	
	p			0.01			
Shoulder Rotation	F		n.s.	5.68		n.s.	
	p			0.03			
Shoulder Abduction	F				29.30	29.30	n.s.
	p				0.000	0.000	
Elbow Flexion	F		n.s.	14.75		n.s.	
	p			0.009			

Table 2 One-way analysis of variance illustrating the difference between Groups I and II, in back, neck, shoulder, and elbow angles (see table 1).

## MUSCLE TENSION (% Body Weight)

	Neutral	Group I	Group II
Trapezium	2.5%	10.4%	6.4%
Erector Spinae	36%	131%	92%
Mid-Deltoid (elbow flexed)	0%	17.6%	23.2%

Table 3 Theoretical muscle tension of the trapezium, the erector spinae, and the mid-deltoid, as a percentage of total body weight; a comparison of the neutral upright position, Group I and Group II postures (as determined using the mode angles shown in table 1).

Note: The values for the deltoid tension are underestimated because only straight shoulder abduction is considered.

Shoulder Angular Velocities (Deg/sec)	1st - 3rd minute	6th - 9th minute	12th - 15th minute
FLEXION	5.7 (0.9)	11.9 (1.9)	12.3 (1.7)
	t=2.77 p=0.006	t=0.19 n.s.	
ROTATION	3.7 (0.6)	17.0 (2.4)	9.2 (1.5)
	t=5.55 p=0.000	t=3.27 p=0.001	
ABDUCTION	6.9 (1.3)	14.4 (2.0)	6.3 (1.0)
	t=3.56 p=0.001	t=3.81 p=0.000	

Table 4 Average (standard error) shoulder flexion, rotation, and abduction velocities in the first, second, and third time periods with results of the contrast analysis (t and p values).

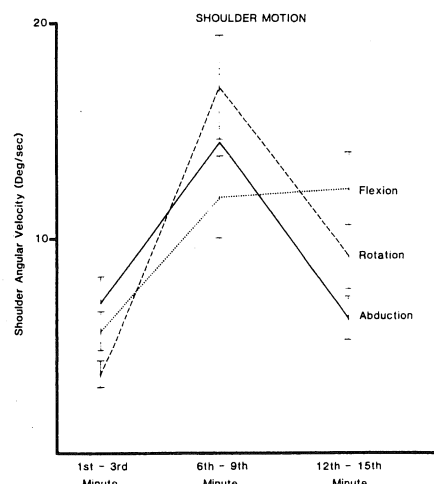


Figure 1 Graph of the three average shoulder angular velocities (with their standard errors) over the three time periods, for all subjects (n=14).

S. Kumar and D. Hill

Department of Physical Therapy, University of Alberta, Edmonton, Alberta, Canada T6G 2G4

## INTRODUCTION

Static Strength has been widely used for manual materials handling tasks design in an effort to curb incidences of low-back pain. However all manual materials handling tasks are dynamic in nature. Therefore, in the present study 11 normal males and 10 normal females without any history of low-back pain were tested for their isometric and isokinetic strength between knuckle to shoulder height in a standing posture. Such tests were performed in midsagittal plane at half, three quarters and full reach distance. The strength was tested by a special strength tester designed and fabricated for this purpose. The results revealed significant difference between the isometric and isokinetic strength. There was a significant difference between the strength values at half reach, three quarters reach and full reach for both isometric and isokinetic conditions.

## REVIEW AND THEORY

Manual materials handling has been extensively associated with low-back pain. The Workers' Compensation Board of Alberta reported that the new back claims for the years 1983 and 1984 were 45.4 and 42.7 per cent of the total claims. On the assumption of equal cost per claim regardless of the body part, the cost of these claims can be estimated to be \$113.7 million and \$99.7 million for the years 1983 and 1984 respectively for Alberta alone. Chaffin (1974) showed that due to increased strength requirement on the job the low-back injuries increased. Such a finding led to the generation of pre-employment strength testing criteria for job allocation (Chaffin et al 1978). They made strength measurements in static mode in three standardized postures. Kumar and Chaffin (1985) have demonstrated that static strengths were significantly greater than the isokinetic lifts for back lifts as well as arm lifts. However, the differences due to different distances have not been investigated. The current study reports these aspects for arm lifts.

## METHODOLOGY

Eleven normal males with mean age 22.5 years, mean weight 73.3 kg and mean height 177.6 cm and ten normal females with mean age 22.3 years, mean weight 58.5 kg and mean height 162.7 cm without any back disorder were used for this study. These subjects were asked to perform isokinetic lifts in standing posture from knuckle

height to shoulder height in a sagittally symmetrical plane at half reach, three quarters reach and full reach distances. The lifts were begun at 10 cm below the knuckle height and terminated past the shoulder height. The data was, however, collected from knuckle height to shoulder height only. The subjects were instructed to exert their maximum effort throughout the range of motion. For isometric tests the initial position of isokinetic test was chosen as the test position. In addition the subjects were also tested in standard posture arm lift (Chaffin et al 1977) for isometric strength.

The strength tester was designed for performing a two handed isometric or isokinetic lift. The handle bar of the strength tester could be adjusted to any height for isometric test. For isokinetic test it provided a constant speed motion regardless of applied force. The speed of motion could be adjusted using servo control mechanism. The constant velocity was achieved by coupling the handle bar through a nonstretchable canvas strap and a one way clutch to a shaft rotating at fixed pre-set speed. The clutch uncoupled the mechanical resistance of the motor driven system until the threshold speed was reached. This allowed a resistance free movement of the handle bar below the pre-set speed. When the speed threshold was reached the clutch engaged the constant speed shaft and controlled the speed with high resistance. The force applied on the handle was measured by a load cell (Interface Model SM 500-500 lb) which was inserted between the handle bar and the canvas strap. The output of the load cell was fed to a HP 9826 computer through a force monitor (ST-1) and a data acquisition system (HP 3054A) with an A to D converter. A displacement potentiometer was used to measure the displacement of the handle bar and its output similarly processed and fed to the computer. A customized software was developed to acquire and log data at 50 Hz. The excursion distance between knuckle and shoulder height was divided into ten equal intervals and data at each interval point was extracted, tabulated and plotted. Isometric and isokinetic strength values were also normalized against the standard posture arm lift peak strength.

## RESULTS

The isometric as well as isokinetic strengths of males were significantly higher than those of females (Fig. 1). The isometric strength was invariably significantly higher than the isokinetic strength among males as well as females (Fig. 1). Both isometric as well as isokinetic strength declined as the reach distance increased from half reach to full reach. (Figs 2 and 3). The relative magnitude of isometric and isokinetic strength with increasing reach distance normalized against the standard posture peak isometric strength is shown in Table 1.

TABLE 1. Relative magnitude of strength expressed as per cent of standard posture peak isometric strength

		Strength Category	2/4 Reach	3/4 Reach	4/4 Reach
F	Isometric		144	107	66
	Isokinetic		107	85	62
M	Isometric		166	85	52
	Isokinetic		93	68	46

F = Female M = Male

## DISCUSSION

Since the most jobs carried out in the industry are not in static mode and are performed at different reach distances away from the body the isokinetic strength measured at standardized distances may be valuable in designing tasks. The current study clearly demonstrates that the strength characteristics are subject to significant variation when conditions change from isometric to isokinetic mode or when the effort lever arm is altered. Increasing the velocity of movement causes a further reduction in strength (Kumar and Chaffin 1985). Based on these findings it is suggested that the dynamic strength measures be incorporated in job design considerations.

## References

1. Chaffin, D.B. J. Occup. Med., 16:248-254, 1974
2. Chaffin, D.B. et al. J. Occup. Med., 20:403-408, 1978
3. Kumar, S. et al. Biomechanics X In press

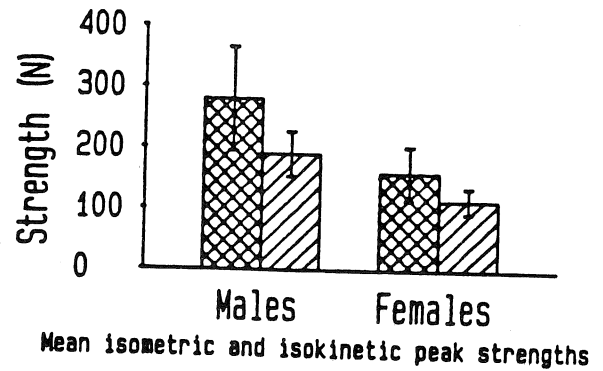
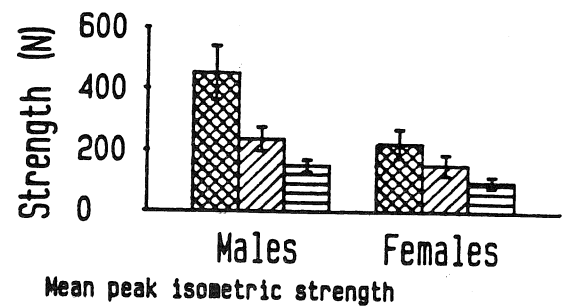
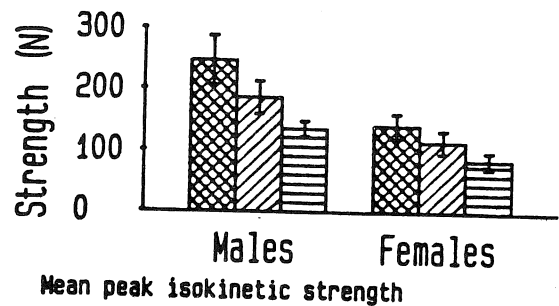


FIGURE 1



■ 2/4 Reach ▨ 3/4 Reach ▤ 4/4 Reach

FIGURE 2



■ 2/4 Reach ▨ 3/4 Reach ▤ 4/4 Reach

FIGURE 3

Gagnon\*, M., Akre\*, F., Lortie\*\*, M., Chehade\*, A. and Kemp\*, F.

\* Department of Physical Education, University of Montreal, Montreal, Quebec, Canada

\*\* IRSST, 505 de Maisonneuve W., Montreal, Quebec, Canada

Several studies are undertaken in our group to evaluate the spinal loading associated with various types of motion undertaken by nursing aides for handling patients. This type of analysis was justified by the high risk of low-back injuries recognized in many professions. These injuries are extremely costly for the society. The nursing aides constitute a group particularly liable to low-back injuries and the turning of patients in bed was identified as potentially risky (Lortie, 1985). In this hospital, the task was executed with the aid of a piqué (a waterproof fabric placed under the patient) and consists of two phases: a translation of the patient towards the side of the bed followed by a rotation after which the patient lies on his/her side. This study was undertaken to examine selected factors affecting the execution of the task for their effects on spinal loading and work-energy requirements. Only the work-energy data are presented in this paper. It is believed that any biomechanical assessment of work operations cannot exclude a complete assessment of mechanical work, if one intends to provide meaningful recommendations for the workers.

#### METHODOLOGY

Fifteen female nursing aides participated in this study. A total of 8 tasks were examined and the subjects made two repetitions for each task. These tasks included several variations in the mode of execution (Figure 1) which allowed comparisons to be made for the following main effects: direction of pull (horizontal and vertical: tasks 3 and 4), velocity of execution (rapid and slow: tasks 4 and 6), knee position (supported or not supported on the bedside: tasks 3 and 5), position of legs (asymmetric and symmetric: tasks 3 and 7) and height of bed (low and high: tasks 4 and 8). The treatments also included a free task, that is, the one usually executed by the nursing aide and a manual task for which the piqué was not utilized. Statistical analysis of variance with repeated measures on the subjects and the repetitions were conducted: the repetition effects were generally found not significant and the mean of the repetitions was then used to conduct new analyses of variance with repeated measures on the subjects only; the pre-determined comparisons described above were examined with univariate tests; tasks 1 and 2 were compared with each other and with all other tasks by Scheffé tests. A 0.1 level of probability was chosen.

The subjects were photographed with a Locam camera; three force platforms were used to record the external forces on both feet and the knee(s). The data were synchronized, recorded and processed on a mini-computer PDP11-23. Dynamic segmental analyses were performed: joint coordinates were smoothed and differentiated by means of quintic splines. The external hand forces were thus determined for further calculations of external work exerted on the patient.

The total work included the internal and external works; the energy transfers between and within seg-

ments and the relative contribution of the different body segments in producing work were evaluated according to the procedures reported by Pierrynowski et al. (1980). The external work was calculated by integrating the power exerted at the hand as a function of time, the power being the scalar product of force and velocity at the hands.

#### RESULTS AND DISCUSSION

The results are presented in Tables 1 and 2. An horizontal pull was associated with a much larger amount of work (about 35%) attributed to increases in both internal and external works. This was attributed to a larger duration of the movement and more segmental amplitude (see L5/S1 displacement). This task was very differently organized as the lower limbs and trunk worked relatively more whereas the upper limbs worked less when compared to a vertical task. A rapid execution of motion was related to more mechanical work (about 15%) attributed to increases in kinetic energies and therefore, increases in internal work. When the knee was supported on the bedside, the total work was not affected but one could observe a shift between internal and external works, that is, an increase in external work (higher hand forces and velocities) and a decrease in internal work (less segmental amplitude: see displ. at L5/S1). A symmetric position of the legs induced a larger relative contribution of the trunk and a smaller contribution of the legs in producing work but these differences were very small. The work-energy requirements were not affected by the height of the bed ( $\Delta = 10$  cm).

The free task presented the characteristics of the horizontal tasks (3, 5, 7) for the kinematic factors and the work-energy parameters. This task was generally associated with the trunk in a more vertical position, a slower motion, less segmental displacement and consequently with less mechanical work, when compared to the horizontal tasks. The manual task did not present any important differences for work-energy parameters even though this task was significantly different from all others with the trunk in an excessively flexed position and larger vertical forces exerted on the patient.

The turning of patients in bed is not a conservative motion: depending on the task, between 1/4 and 1/3 of the energy was conserved during the process. The main source was an exchange between potential and kinetic energies within segments; there was very little evidence of energy transfers between segments as they all acted in phase. The only important distinction was observed for the slow velocity of execution (task 6) where the reduction in kinetic energies was reflected in a very drastic reduction in transfers of energy within the segments.

On the basis of this study, one should recommend to work vertically (also corroborated by data on spinal loading), at a slower velocity, with the legs in an asymmetric position.



## References

1. Lortie, M. 1985. L'identification des activités à risque en milieu hospitalier, Proceedings of the 18th Annual Meeting, Ass. Can. d'Ergonomie, Hull, pp. 119-122.
2. Pierrynowski, M.R. et al. 1980. Ergonomics, 23, pp. 147-156.

The authors are indebted to IRSST for its financial support.

Figure 1. Illustrations of the tasks

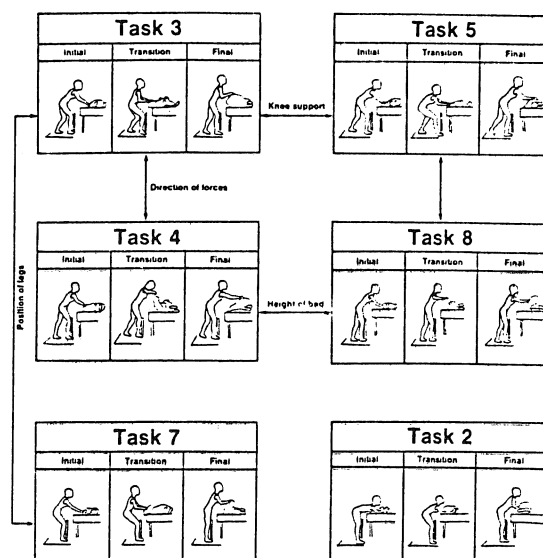


Table 1. Selected kinematic and kinetic factors for the tasks (N = 15)

TASKS	VARIABLES	1*	2*	3*	4*	5*	6*	7*	8*
		Free	Manual	$F_H-V_R-B_L-$ $K_S-L_A$	$F_V-V_R-B_L-$ $K_S-L_A$	$F_H-V_R-B_L-$ $K_N-L_A$	$F_V-V_S-B_L-$ $K_S-L_A$	$F_H-V_R-B_L-$ $K_S-L_T$	$F_V-V_R-B_H-$ $K_S-L_A$
Duration of motion (s) <sup>a</sup>	$\bar{X}$	2.1	1.9	1.7	1.4	2.0	2.0	1.7	1.5
	S.D.	0.4	0.4	0.3	0.3	0.4	0.4	0.3	0.3
Initial trunk angle to vert. (°) <sup>b</sup>	$\bar{X}$	27.3	67.8	35.6	37.6	40.8	37.1	34.4	29.8
	S.D.	8.8	5.3	9.2	9.5	9.5	9.9	7.6	10.0
Hor. displ. L5/S1 (cm) <sup>c</sup>	$\bar{X}$	14.5	14.8	16.6	7.2	24.4	5.9	16.1	4.5
	S.D.	9.1	9.0	7.7	4.3	9.9	4.8	8.1	3.4
Max. vert. hand force (N) <sup>d</sup>	$\bar{X}$	130	181	143	142	98	138	143	136
	S.D.	26	39	25	30	89	26	51	27

\*  $F_H$ ,  $F_V$ : hor., vert. force;  $V_R$ ,  $V_S$ : rapid, slow velocity;  $B_L$ ,  $B_H$ : low, high bed;  $K_S$ ,  $K_N$ : knee supported, non supported;  $L_A$ ,  $L_T$ : legs apart, together.

<sup>a</sup> Sign. diff.: 3-4; 4-6; 3-5; 1-3; 1-4; 1-7; 1-8; 2-4; 2-8

<sup>b</sup> Sign. diff.: 4-8; 3-5; 1-2; 1-3; 1-4; 1-5; 1-6; 1-7; 2-3; 2-4; 2-5; 2-6; 2-7; 2-8

<sup>c</sup> Sign. diff.: 3-4; 3-5; 1-4; 1-5; 1-6; 1-8; 2-4; 2-5; 2-6; 2-8

<sup>d</sup> Sign. diff.: 3-5; 1-2; 2-3; 2-4; 2-5; 2-6; 2-7; 2-8

Table 2. Work-energy parameters for the tasks (N = 15)

TASKS	VARIABLES	1*	2*	3*	4*	5*	6*	7*	8*
		Free	Manual	$F_H-V_R-B_L-$ $K_S-L_A$	$F_V-V_R-B_L-$ $K_S-L_A$	$F_H-V_R-B_L-$ $K_N-L_A$	$F_V-V_S-B_L-$ $K_S-L_A$	$F_H-V_R-B_L-$ $K_S-L_T$	$F_V-V_R-B_H-$ $K_S-L_A$
Total work (J) <sup>a</sup>	$\bar{X}$	222	192	262	195	278	166	274	177
	S.D.	73	55	62	55	63	43	77	48
External work (J) <sup>b</sup>	$\bar{X}$	113	98	133	100	122	91	134	92
	S.D.	32	25	31	27	28	28	40	26
Internal work (J) <sup>c</sup>	$\bar{X}$	108	95	129	98	155	74	139	86
	S.D.	47	36	40	34	51	19	50	30
Energy conserved within segments (%) <sup>d</sup>	$\bar{X}$	20	21	25	23	25	14	24	23
	S.D.	7	5	6	6	5	6	6	5
Energy conserved between segments (%) <sup>e</sup>	$\bar{X}$	9	9	10	10	10	11	9	10
	S.D.	7	5	8	4	6	6	6	6
Internal work: lower limbs (%) <sup>f</sup>	$\bar{X}$	11	13	14	9	15	10	12	10
	S.D.	4	4	3	3	3	3	3	3
Internal work: upper limbs (%) <sup>g</sup>	$\bar{X}$	21	17	19	31	18	31	19	31
	S.D.	8	7	8	6	8	7	7	8
Internal work: trunk-head (%) <sup>h</sup>	$\bar{X}$	68	70	66	60	68	58	69	59
	S.D.	6	4	7	5	7	5	6	6

\*  $F_H$ ,  $F_V$ : hor., vert. force;  $V_R$ ,  $V_S$ : rapid, slow velocity;  $B_L$ ,  $B_H$ : low, high bed;  $K_S$ ,  $K_N$ : knee supported, non supported;  $L_A$ ,  $L_T$ : legs apart, together.

<sup>a</sup> Sign. diff.: 3-4; 4-6; 1-5; 1-6; 1-7; 2-3; 2-5; 2-7

<sup>b</sup> Sign. diff.: 3-4; 3-5; 1-3; 1-6; 1-7; 1-8; 2-3; 2-5; 2-7

<sup>c</sup> Sign. diff.: 3-4; 4-6; 3-5; 1-5; 2-5; 2-7

<sup>d</sup> Sign. diff.: 4-5; 1-3; 1-6; 2-6; 3-4

<sup>e</sup> Sign. diff.: None

<sup>f</sup> Sign. diff.: 3-4; 3-7; 1-5; 2-4

<sup>g</sup> Sign. diff.: 3-4; 1-4; 1-6; 1-8; 2-4; 2-6; 2-8

<sup>h</sup> Sign. diff.: 3-4; 3-7; 1-4; 1-6; 1-8; 2-4; 2-6; 2-8

# POSTURAL KINEMATICS OF TRUMPET PLAYING

N. Halpern and F.J. Bejjani

Orthopaedic Center for the Arts,  
The Hospital for Joint Diseases Orthopaedic Institute.  
New York University,  
Program in Ergonomics and Occupational Biomechanics.  
New York, New York, U.S.A.

## INTRODUCTION

The medical literature has focused mainly on functional cardiac, respiratory and stomatologic limitations in trumpet playing (1,2). However, the whole body participates in generating the air pressure that drives the horn. Inadequate playing posture while sustaining high intrathoracic pressure interferes with sound production, mainly in the high register, where higher air pressures are generated. Moreover, inadequate playing pressure is known to cause acute and chronic injuries, i.e. syncopes and various hernias. The music literature is controversial on the issue of body posture in trumpet playing. Thus, the study of postural kinematics is essential for a biomechanical profile of trumpet playing, in an attempt to improve performance and prevent injuries to occur.

In a previous paper, the authors demonstrated that standing postures of trumpeters, while playing various notes, were not related to the musical task (3). However, changing from low to high notes was accompanied by a decrease in the lumbar lordosis and an increase in knee flexion.

The purpose of this paper is to address the kinematics of trumpet playing as a whole body posture. The role of the trumpeter's anthropometry is also assessed. The findings suggest that anthropometric, as well as physiologic, constraints may act as functional limitations of the trumpeter's performance.

## METHODOLOGY

Sixteen virtuosi male trumpet players were asked to perform various musical pieces (3). Sagittal plane standardized photographs were obtained at each of the following notes: low C, high F, and high F sustained. Various body segment angles were then obtained: Those with an anterior apex (head, neck, lumbar spine and popliteal fossa) were given a positive sign; and those with a posterior apex (thoracic spine and pelvis) were given a negative sign. Various anthropometric data were collected.

In order to obtain an integrated measure of whole body posture, the vectorial sum of the above angles was computed for the neutral posture and the three note-related playing postures. Oneway ANOVA, with contrast analysis, was used to compare the four postures.

In order to evaluate the effect of anthropometry and neutral posture on each of the three playing postures, a multiple regression analysis was conducted, using the GLM procedure of the SAS package.

## RESULTS

The oneway ANOVA model describing the note effect on whole body posture was statistically significant ( $F = 5.31$ ,  $p = 0.001$ ). A significant difference was found between low C and high F postures. Differences between neutral and low C postures, and between high F and high F sustained postures only showed a significant trend (Table 1).

Table 2 shows the estimated coefficients of the following regression equations:

$$C = 34 + 0.14P - 2.6N + 1.1L + 7.8S - 0.08S^2$$

$$F = -245 + 0.25P - 3.8N + 1.7L + 15.5S - 0.15S^2$$

$$Fs = -519 - 0.14P - 5.8N + 3.1L + 27.3S - 0.27S^2$$

where:

- P, C, F and Fs are the vectorial sums of body segments angles for neutral posture, and low C, high F and high F sustained playing postures respectively.
- N, L, and S are the neck, leg and spine lengths respectively.

	P	C	F	Fs
MEAN	330.5°	337.1°	331.7°	327.1°
(S.D.)	10.9°	11.5°	13.3°	17.6°
F	2.81	4.57	3.4	
p	0.09	0.03	0.06	

Table 1. Mean and standard deviation of the vectorial sums of body segment angles in neutral posture (P) and three note-related playing postures: C, F and Fs; F ratios, p values of the oneway contrasts of P vs C, C vs F and F vs Fs.

	Low C		High F		High F Sustained	
	Estimate	SE	Estimate	SE	Estimate	SE
Posture P	0.15	6.11	0.26	16.44	-0.14	11.1
	(0.12)	(0.21)	(0.12)	(0.00)	(0.14)	(0.1)
Neck	2.56	10.00	3.73	19.97	5.66	35.60
Length N	-0.80	(0.003)	-0.66	(0.001)	-0.90	(0.001)
Leg	1.09	6.63	1.72	15.55	3.15	47.32
Length L	-0.34	(0.005)	-0.37	(0.001)	-0.39	(0.001)
Spine	7.83	n.s.	15.55	5.95	27.30	(0.001)
Length S	(5.13)		5.48	(0.019)	19.69	(0.001)
S <sup>2</sup>	-0.08	n.s.	-0.19	8.87	-0.27	35.26
	(0.005)		(0.05)	(0.005)	(0.06)	(0.001)
Intercept	34.36	n.s.	2.45	n.s.	-519.25	(0.001)
	(145.61)		(155.75)			
MODEL		6.06		13.36		22.61
		(0.000)		(0.000)		(0.000)

Table 2. Estimated regression coefficients of equations C, F and Fs, with their standard errors, F ratios and p values.

All coefficients were statistically significant. The large standard error of P indicates considerable individual differences in neutral posture. The increasing coefficients of N, L and S between the lower and the higher notes, negatively for N and positively for L and S, indicate their note-related effect on playing posture. Overall, spine length had the highest coefficients and was also significant at the second power in F and Fs. The R-square values were larger for F (0.6) and Fs (0.73) than for C (0.4), further indicating the increasing importance of anthropometry in playing the more demanding notes.

#### DISCUSSION

An analysis of the trumpeter's playing posture should regard the involvement of the whole body in sustaining the slow, controlled and forceful expiration needed to produce sound. It is the involvement of the external oblique muscles in forceful expiration (4) that triggers a kinematic chain reaction. The contraction of the obliques also tilts the pelvis posteriorly; this motion in turn decreases lumbar lordosis. The pelvic tilt also stretches the one-joint hip flexors; its motion is limited by the length of the latter. To release the restraint of the hip flexors, the knees need to be bent (5).

Our results suggest that anthropometric constraints, in addition to physiological factors, may functionally limit trumpeters' performance. Test of abdominal muscles and hip flexor strength should perhaps be included in a biomechanical profile of trumpet playing.

#### References

1. Bouhuys, A. Physiology and Musical Instruments. *Nature*. 221: 1199-1204, 1969.
2. Tucker, A. et al. Electrocardiography and Lung Function in Brass Instrument Players. *Arch. Environ. Health*. 23: 327-334, 1972.
3. Bejjani, F. et al. Standing Postures of Trumpeters. In: *Contemporary Ergonomics*. London: Francis & Taylor, 1986.
4. Draper, M. H. et al. Expiratory Pressures and Air Flow During Speech. *British Med. J.* 1837-1843, 1960.
5. Kendall, F. P.; McCreary, E. *Muscles: Testing and Function*. Baltimore: Williams & Wilkins, 3rd ed., 1983.

# INFLUENCE OF THE AMOUNT OF INFORMATION ABOUT MUSCLE PROPERTIES IN THE COST FUNCTION ON THE ESTIMATE OF INDIVIDUAL MUSCLE FORCES

Walter Herzog  
Faculty of Physical Education  
University of Calgary  
Calgary, Alberta T2N 1N4

## INTRODUCTION

Much attention has focused recently on the determination of individual muscle forces in human movements. Optimization algorithms have been used abundantly to obtain unique solutions for this inherently indeterminate problem. Most of these optimization algorithms are very similar in all aspects but one, the cost function. The differences in the cost functions can mainly be attributed to the amount of information about basic muscle characteristics which were provided in the cost functions. In this study a general nonlinear optimization algorithm was used to estimate individual muscle forces. Three cost functions containing different amounts of basic information about muscle characteristics were implemented. The purpose of this paper is to show the influence of these different cost functions on the muscle force estimates. The results obtained suggested that less information about basic muscle characteristics is needed to estimate muscle forces for slow (everyday) movements than for fast (athletic) movements.

## REVIEW AND THEORY

### Load sharing:

For a cost function  $h$  of the general form

$$\text{Minimize } h = \sum_{i=1}^n (F_i/a_i)^m \quad (1)$$

and the constraint function  $g$

$$g: M = \sum_{i=1}^n (r_i * F_i) \quad (2)$$

the load sharing of two muscles ( $i=1,2$ ) for a planar activity can be determined to be as shown in equation (3) (Haug et al. 1979)

$$F_1/F_2 = (r_1/r_2)^{1/m-1} * (a_1/a_2)^{m/m-1} \quad (3)$$

where  $F_i$  is the force exerted by the  $i$ th muscle,  $a_i$  is a function of parameters of the  $i$ th muscle,  $m$  is a real positive number,  $r_i$  is the perpendicular distance from the axis of rotation of a joint to the line of action of  $F_i$ , and  $M$  is the resultant joint moment.

For a given joint angle the ratio  $r_1/r_2$  is constant and equation (3) may be rewritten as

$$F_1 = k_1 * (a_1/a_2)^{m/m-1} * F_2 \quad (4)$$

where  $k_1$  is a positive constant.

### Muscle properties:

The active range of shortening and the maximum velocity of shortening of a muscle are dependent on the length of its fibers (Steindler 1977 and Hill 1938, respectively). For example, the fibers of the rectus femoris (RF) are much shorter than the fibers of the vastus lateralis (VL) (Alexander et al. 1975).

Therefore, during a knee extension exercise, where both these muscles shorten about the same absolute length and at about the same rate of change in length RF covers a much larger range of its active length-tension and its concentric force-velocity relationship than VL.

## METHODOLOGY

### The subject and muscle specific muscle model:

The force a muscle exerts was assumed to be a function of its activation, size, geometry, instantaneous length, and instantaneous rate of change in length. Using this assumption a muscle model was developed for the four knee extensor muscles (rectus femoris RF, vastus lateralis VL, vastus medialis VM, and vastus intermedius VI) of one male subject (Herzog 1985). This muscle model was subsequently used to calculate the maximum forces that each knee extensor muscle of that particular subject could exert under 70 different conditions of maximum effort knee extension exercises on a Cybex II dynamometer. These muscle forces, hereafter referred to as the model forces, were then used to calculate the resultant knee extension torques which were compared to the torques recorded by the Cybex dynamometer to validate the muscle model.

### Load sharing between RF and VL:

The load sharing between RF and VL was calculated using equation (4). The model force of VL was taken as input into this equation and the forces exerted by RF were obtained by treating  $a_i$  as a function of the muscle size only (case 1), as a function of muscle size, maximum muscle force, and fiber type distribution (case 2), and the whole muscle model including fiber type distribution (case 3).

The model forces and the forces obtained in cases 1, 2, and 3 were then compared to each other. Speculations about the adequacy of cases 1, 2, and 3 to predict individual muscle forces under given conditions of the knee extension exercise were made.

## RESULTS AND DISCUSSION

The differences between the resultant knee extension torques obtained using the Cybex dynamometer and the model forces were less than 12% of the maximum torque recorded for all 70 conditions of the knee extension exercise. This result suggested strongly that the model forces represented the actual maximum forces exerted by the knee extensor muscles adequately.

Three out of the 70 conditions of the knee extension exercise are depicted in Figures 1, 2, and 3. Figure 1 shows the load sharing between RF and VL for an isometric contraction executed at a knee angle of 153 degrees. RF forces obtained for cases 1, 2, and 3 are within 12% of RF model force. Similar results were obtained for other isometric trials at knee angles ranging from about 120 to 160 degrees. Assuming that the model forces are good indicators of the true muscle forces it can be argued that size

(case 1) is enough information to make accurate force predictions under these conditions.

Figure 2 shows the load sharing between VL and RF for an isometric contraction at a knee angle of 174 degrees. Case 3 yielded the only RF force that was reasonably close to RF model force. Similar results were found for other isometric knee extensions at knee angles above 170 degrees. Assuming again that RF model forces are close to the true RF forces it may be concluded that case 3 was better than case 1 or 2 in estimating the forces exerted by RF. The difference between the results in Figure 1 and 2 can be explained with the shortening that occurs in the knee extensor muscles as the knee is extended. The ability to exert force due to this shortening affects RF with its relatively short fibers much more than any of the vasti with their relatively long fibers. Comparing the model forces in Figure 1 and 2 it can be seen that VL force decreased 56%, whereas RF force decreased 94% due to the muscle shortening that occurred as the knee angle changed from 153 to 174 degrees. Case 3 was the only case which could account for this difference in decrease between RF and VL forces, because it contained information about the length-tension relationship of the muscles. Cases 1 and 2 overestimated RF model forces by a factor of five or more at knee angles above 170 degrees.

Figure 3 shows the results of a trial executed at an angular velocity of the Cybex arm of 240 deg./s and at a knee angle of 150 degrees. Only RF force predicted using case 3 was reasonably close to RF model force. Similar results were obtained for other dynamic trials at intermediate knee angles. Comparing the model forces in Figures 1 and 3 it can be observed that VL force decreased by 44% and RF force by 77% from the isometric to the dynamic trial. Since the muscle lengths for both conditions were about the same, the difference in decrease between RF and VL forces must be due to the velocity of shortening. At an angular velocity of the Cybex arm of 240 deg./s the knee extensor muscles shorten with a linear velocity of about 0.13 m/s. This corresponds to 35% and 14% of the maximum velocities of shortening for RF and VL, respectively, which, in turn, accounts approximately for the difference in muscle forces observed between the isometric and dynamic trial (Hill 1938). Information about the force-velocity characteristics of the knee extensor muscles were only contained in case 3. Cases 1 and 2 overestimated RF model forces by a factor 2-3 at these velocities of muscle shortening.

RF forces obtained in cases 1, 2, and 3 were always judged against the model forces which were assumed to be close to the true RF forces. Therefore, one may argue that the results obtained in this study are only as good as the model forces represent the true muscle forces. However, it is well accepted that muscle properties like the length-tension and force-velocity relationship exist. Furthermore, synergistic muscles are different in structure which influences these properties differently. Hence, the specific results (i.e. the muscle force magnitudes) in this study may not be absolutely accurate. However, the general results (the tendency of cases 1 and 2 to overestimate RF forces dramatically when the muscle lengths are extremely short or long or when the muscles contract dynamically) are correct.

#### FINAL COMMENTS

From the results obtained in this investigation the following speculations are made:

1. Force predictions made using optimization algorithms for muscles of similar fiber type composition and for slow movements and movements with a

small change in length of the muscles about some intermediate position (i.e. everyday movements) seem to yield adequate results using a simple muscle model that contains nothing but a measure of the size of the muscles.

2. Force predictions for fast movements covering a large range of motion (i.e. athletic movements) need a sophisticated muscle model including the basic muscle characteristics presented in this paper.

#### References

1. Alexander McN., et al. J. Hum. Movement Stud. 1:115-123, 1975.
2. Haug E.J., et al. Applied Optimal Design. John Wiley and Sons, N.Y., 1979.
3. Herzog W. Proceedings X ISB Conference, Umea, Sweden, 1985.
4. Hill A.V. Proc. Roy. Soc. Lond. 126:136-195, 1938.
5. Steindler A. Kinesiology of the Human Body. Charles C. Thomas Publisher, Springfield, IL, 1977.

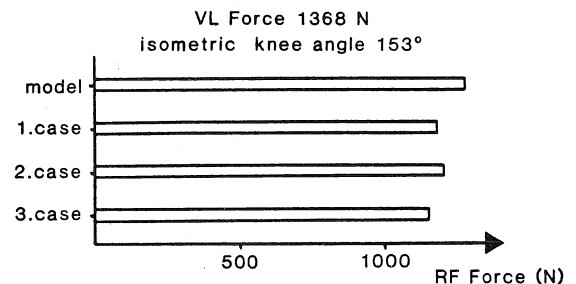


Figure 1. Load sharing between RF and VL for an isometric trial at a knee angle of 153 degrees.

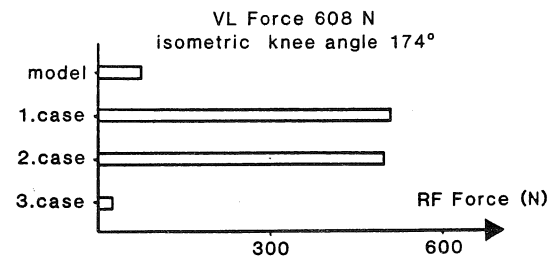


Figure 2. Load sharing between RF and VL for an isometric trial at a knee angle of 174 degrees.

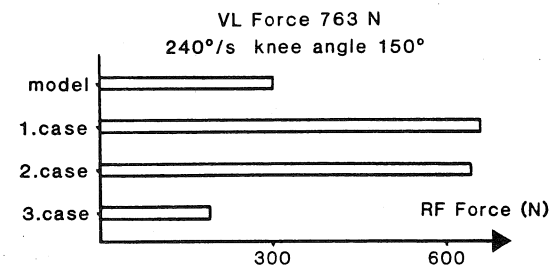


Figure 3. Load sharing between RF and VL for a dynamic trial (240 deg./s) at a knee angle of 150 degrees.

## SURFACE ELECTROMYOGRAPHY OF ILIOPSOAS

N. Evans Stüber & R. Wells

Department of Kinesiology, University of Waterloo  
Waterloo, Ontario, N2L 3G1

### Introduction

Iliopsoas muscle is a large and important hip flexor, yet electromyographic investigations of this muscle are rare because of the riskiness of using indwelling electrodes. In this paper, iliopsoas anatomy is discussed with reference to the feasibility of using surface electrodes to investigate the activity of this muscle. A suitable location for the electrodes, medial to the anterior superior iliac spine (ASIS) over the inguinal ligament, is suggested and validated. It is demonstrated that this electrode placement does not record the activity of the abdominal muscles, sartorius or rectus femoris, and does record activity which is hip flexor in nature. It is concluded that surface electromyography (EMG) can be used to investigate iliopsoas muscle using the suggested electrode placement. There is some evidence that this placement records primarily the activity of the iliacus head of iliopsoas muscle, with comparatively little influence from the psoas or vertebral head.

### Review and Theory

Iliopsoas muscle is a large strong muscle, and a major hip flexor, the only one which crosses only the hip. Yet it has rarely been investigated because it is widely accepted that surface EMG from this muscle is difficult to obtain. Basmajian [1] and Basmajian and DeLuca [2] used fine wire electrodes to record the two heads of this muscle. They describe it as a "deep and almost inaccessible muscle", and prefer the use of indwelling electrodes. Close [3] says "The necessity of internal placement of electrodes in the study of this muscle (iliacus) is obvious since there is no portion where surface electrodes may be applied over such a deep muscle."

However, the use of indwelling electrodes can be both risky and painful for the subject. The approach to psoas passes between the transverse processes of the lumbar vertebrae [1]. Vulnerable structures include the paraspinal muscles, vertebral arteries, nerve roots of the lumbar plexus, peritoneum and internal organs. The placement recommended for iliacus is in the femoral triangle [4]. Although the vascular bundle can be avoided by locating the pulse of the femoral artery, the branches of the femoral nerve are quite vulnerable. Placing

the electrodes medial to the ASIS may be less risky, but an anaesthetic is required [5] and the branches of the lumbar plexus are still in danger. For ethical reasons, the use of surface electrodes is greatly preferred.

Figure 1 shows the anatomy of iliopsoas. The two heads have a common insertion on the lesser trochanter of the femur. Iliacus originates on the iliac fossa, and psoas from the lumbar vertebrae. Both are considered to be primarily hip flexors, but they are also thought to stabilize the pelvis, and psoas may act in movements of the lumbar spine.

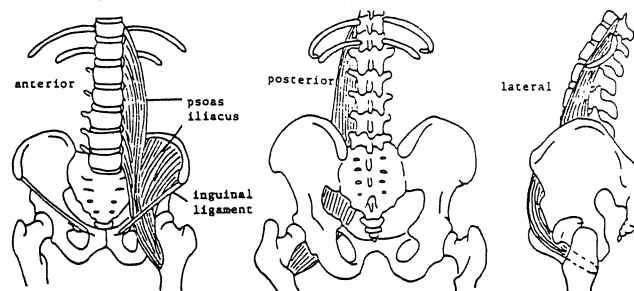


Figure 1: Anatomy of iliopsoas.

Iliopsoas passes between the inguinal ligament and the pelvic ramus, lying in a notch between the anterior inferior iliac spine and the iliopubic eminence. Iliopsoas can be palpated as it passes close to the surface just below the inguinal ligament. This can be done by flexing the hip against resistance with the hip extended, since iliopsoas will then be arched over the pelvic ramus. If the subject is thin enough, iliacus can even be followed cranially from this point to its origin on the iliac fossa, just medial to the iliac crest.

It was felt that placing the electrodes where iliopsoas can be palpated might be successful. The chief difficulty is the possibility of crosstalk, resulting from recording the activity of adjacent muscles, such as the abdominals, sartorius and rectus femoris. Pectineus on the medial side lies quite deep, is very small in relation to the other muscles being considered, and so is unlikely to cause difficulty.

Two placements will be compared in this study, both of them located over the inguinal ligament, but in one a vertical orientation (parallel to the underlying muscle fibres) is used and in the other the electrodes are oriented at an angle, parallel to the inguinal ligament. It is possible that electrode orientation may affect the amount of crosstalk.

This work was supported by NSERC grant #A2785 and the Department of Kinesiology, University of Waterloo.

### Methodology

Surface electrodes were placed over the sartorius, rectus femoris, abdominal and iliopsoas muscles (Figure 2) of six fit, healthy adult women. The EMG signals were linear enveloped and recorded on a pen recorder.

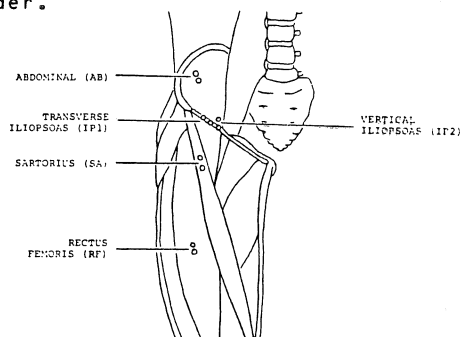


Figure 2: Placement of electrodes.

A number of manoeuvres were tried in order to determine whether crosstalk was present on any channel. Abdominal curls (raising the shoulders from the floor while lying supine) and four types of situps (with the knees bent or straight, and with the feet held down or not) were first tried. Isometric contractions were done using a system of pulleys and weights attached to cuffs about the ankle or just above the knee. Finally, a lateral trunk raise and the Valsalva Manoeuvre (expiration against a closed glottis) were performed to determine if these procedures could differentiate between the abdominal and iliopsoas channels.

### Results and Discussion

The situps and abdominal curl exercises produced activity in all muscles and so are of no use in determining whether crosstalk is present or not. The Valsalva Manoeuvre, showing both abdominal and iliopsoas activity, is also inconclusive. In order to conclude that no crosstalk is present, a case is needed where there is activity on the channel thought to be causing the crosstalk (abdominals, sartorius or rectus femoris), while the channel being tested (iliopsoas) is silent. Only then can one conclude that the iliopsoas channel is free of crosstalk.

Two such situations are shown in Figure 3. Part A shows activity on the rectus femoris and sartorius channels, while the abdominals and iliopsoas are silent. Figure 3 B demonstrates activity on the abdominal channel while all the others are inactive. Therefore one can conclude that both of the electrode placements used for iliopsoas were unaffected by crosstalk from the abdominal muscles, sartorius or rectus femoris.

The lack of iliopsoas activity in Figure 3 B is rather surprising since psoas is considered a strong lateral trunk flexor. However, it is also tendinous near its insertion, indicating that these electrode arrangements probably record iliacus without much influence from psoas. These figures also show that there was very little difference between the two iliopsoas arrangements.

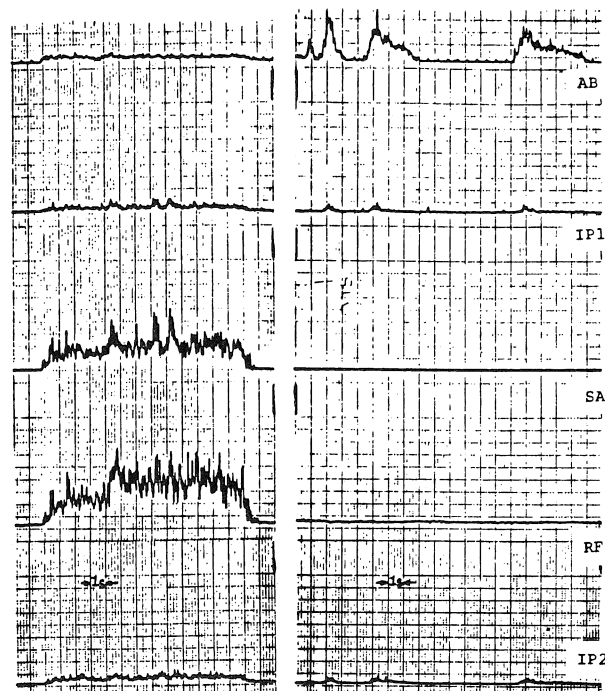


Figure 3: Demonstrating lack of crosstalk. A) 13.2 Nm of hip flexion and knee extension. B) raising the trunk laterally while lying on the left side.

### Conclusions

It is possible to record iliopsoas with surface electrodes, using the electrode placements described and tested here. Further, these placements probably record primarily iliacus, with little if any influence from psoas. The oblique placement is preferred because the electrodes are less likely to be dislodged during movement.

### References

- [1] J. V. Basmajian, Anat. Rec. 125:127-132, 1958.
- [2] J. V. Basmajian et al., Muscles Alive, Williams and Wilkins Co., Baltimore, 1985.
- [3] J. R. Close, Motor Function of the Lower Extremity, Charles C. Thomas, Springfield, pp. 125-132, 1964.
- [4] E. F. Delagi et al., Anatomic Guide for the Electromyographer, Charles C. Thomas, Springfield, pp. 176-177, 1981.
- [5] M. M. Flint, J. Amer. Phys. Ther. Assoc. 45(3):248-253, 1965.

## ISOKINETIC AND ISOMETRIC STRENGTH ANALYSIS OF HIP MUSCULATURE

T. D. Cahalan, S. H. Liu, E. Y. S. Chao  
Orthopedic Biomechanics Laboratory  
Mayo Clinic/Mayo Foundation  
Rochester, MN 55905

### INTRODUCTION

A number of studies have addressed the measurement of hip strength in healthy individuals. Jensen et al. (1971) and Olson et al. (1972), using a fairly complex device, measured hip strength isokinetically through a broad range of motion. Markhede and Grimby (1980) used a Cybex to measure isokinetic hip abduction strength at 60 degrees per second in ten relatively young subjects. None of the above mentioned studies are complete in gathering isometric and isokinetic data for a broad range of conditions in a clinically useful fashion.

Normative data are useful in determining the degree of disability, rehabilitation planning, and goal setting for patients with musculoskeletal disease. The goals of this study are: 1) develop a clinically useful method of isokinetic strength assessment for the hip musculature, 2) create a database of normal strength values at multiple isokinetic speeds for a wide variety of ages, and 3) analyze the data with respect to differences between study groups. As the testing and data analysis techniques are established, the size of the database can be increased with time to facilitate interinstitutional comparison of results and dissemination of useful information.

### METHODOLOGY

Seventy-two normal subjects were evaluated on a modified Cybex II for hip strength in three planes at multiple isokinetic speeds and isometric angles. The study sample population was divided into four groups, males under forty, males over forty, females under forty, and females over forty. The potential subjects were screened for normal pain-free range of motion and negative hip, knee, or low back pain history. The demographic data are described in Table I.

A Cybex II isokinetic dynamometer has been modified to allow adjustment of the dynamometer head to achieve proper patient positioning and stability needed for adequate hip strength testing. The torque curve recordings are smoothed electronically, and no acceleration control or gravity correction is used.

We have also designed a stabilization frame that allows a patient to stand with support when testing sagittal plane and frontal plane motion. This frame permits weight to be borne by the arms and pelvis as well as the nontested leg. This avoids full weight bearing by or lying on the nontested hip. Rotations are tested in the seated position (Figs. 1 and 2).

A modified Apple II was used to acquire, analyze, and report the Cybex data. The acquire program saves the demographic data, as well as the torque and range of motion curves. The analysis program allows selection of the torque curves to be analyzed. The report program prints six key parameters, including the peak torque of each selected curve and the average peak of all selected curves. The three highest peak torques of five to six repetitions were used for analysis.

Group data analysis was performed on a VAX 11/750. The appropriate t-test was performed within groups and between groups to identify levels of significant difference in torque production at different isokinetic velocities and isometric angles.

### RESULTS

Means and standard deviations were calculated for each sex and age grouping for each parameter. Test-retest procedures showed the data to be reproducible. Young males consistently produced the greater amounts of torque at the given velocities and angles. Older males were most commonly second, but were occasionally surpassed by young females at the faster speeds. Older females consistently produced the least amount of torque (Fig. 3).

Our torque values are similar to those reported by Markhede and Grimby (1980). The slight differences may be explained by differences in the position tested.

The torque/velocity relationship was apparent in all groups but was significantly different between the older female group and all other groups ( $p < 0.05$ ). Isometric torque at 10 degrees of flexion was greater than any flexion isokinetic torque, but at 45 degrees of flexion, isometric torque dropped to about the same level as peak torque at 90 degrees per second.

The size of the database is continually being expanded using the existing methodology.

### REFERENCES

1. Jensen RH, et al. Arch Phys Med Rehabil 52:207-215, 1971.
2. Olson VL, et al. Phys Therapy 52:149-158, 1972.
3. Markhede G, Grimby G. Scan J Rehab Med 12:169-174, 1980.

Table I. Demographic Data

	YM	OM	YF	OF
Number	18	17	21	16
Age	28 (20-39)	54 (40-81)	27 (20-39)	53 (40-64)
HT(cm)	176 ± 6	176 ± 6	167 ± 5	164 ± 5
WT(lb)	162 ± 17	177 ± 29	129 ± 13	143 ± 21



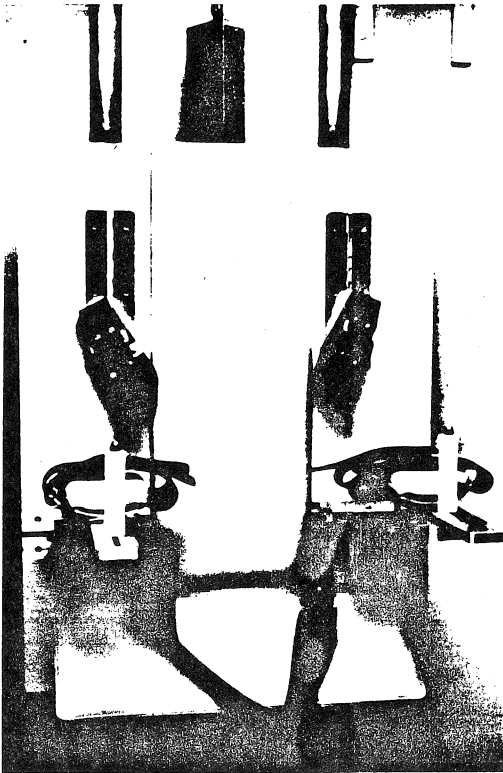


Figure 1. Stabilization frame.



Figure 2. Normal subject performing left hip flexion and extension.

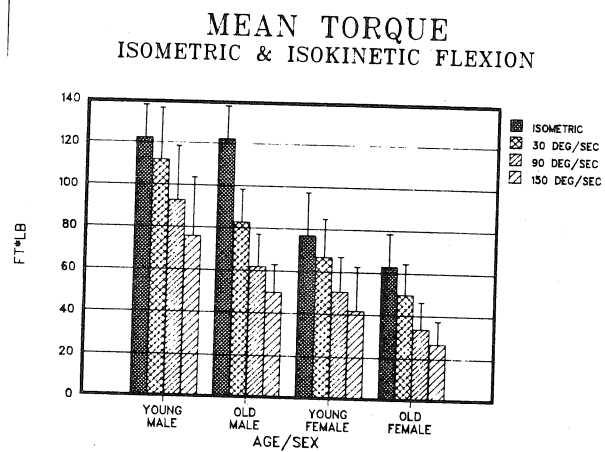


Figure 3.

A.V. Sirin and A.E. Patla  
Neural Control Laboratory  
Department of Kinesiology  
University of Waterloo  
Waterloo, Ontario, N2L 3G1

## INTRODUCTION

Muscle synergism although discussed by many researchers has not been studied experimentally in detail. This is unfortunate since rarely does one find a muscle without a functional synergist. Previous work on single joint synergism [cf. 1-3] have been either speculative or inconclusive. They have used the concept of synergistic activity to explain unexpected observations of decreased EMG activity in the muscles [cf. 1,3], drawing their conclusions from plots of electromyographic parameters AEMG, and mean power frequency (MPF) over exhaustion time.

Fibre type differences, common insertion, and the two-joint nature of two of the synergists, made the choice of the triceps surae group attractive. In addition, these muscles play an important role in activities such as locomotion. In this study, both trade-off and coactivation synergisms were hypothesized to be present and centrally regulated [1]. A complete shutdown of one muscle's neural input in favour of its synergist, reported for the jaw muscles, [3] was ruled out. The temporo-mandibular joint has more degrees of freedom, and therefore the task of sustaining a submaximal bite could be accomplished with slight movements of the jaw to relieve one muscle in favor of its synergist. In fact Clark & Carter [4], investigating under more rigid experimental conditions, failed to make the same observations as Hellsing & Lindstrom [3]. In the present study, the degree of freedom of the ankle and knee joints were restricted. The purpose of this study was then to investigate the changes in synergistic behaviour of the triceps surae muscles under fatiguing conditions.

## METHODS

Six males subjects (ages 20 to 27 years) volunteered for this study. Surface EMG were recorded from the medial and lateral heads of the gastrocnemius, (MG & LG) and soleus (SO) muscles of the right leg. The plantarflexor moment as measured via a linear variable differential transformer (LVDT 5001b). Both EMG and LVDT signals were amplified and were analog to digital converted (sampling rate - 1024Hz) on line, and stored onto floppy disks (record length = 5s).

The experiments were carried out in two sessions for each subject. At least 24 hours were allowed between successive testing sessions. For the first session the subjects were seated on the experimental bench with the knee fully extended. The right leg and upper body were immobilized through the use of velcro straps and belts. The subjects were asked to exert three maximal plantarflexor efforts at five minute intervals, each effort last approximately three seconds. The best of the three efforts (MVC) was taken and a target tension which was 50% of MVC (.5MVC) with a  $\pm 5\%$  of .5MVC band around it was displayed on a oscilloscope. The subjects were then instructed to superimpose the force tracing onto the oscilloscope target through a plantarflexor effort, and keep it there until "exhaustion". Exhaustion was defined as the point in time when the subject could

no longer maintain the force tracing within the target boundaries. During this period electromyographic activity and plantarflexor forces were collected every seven seconds for five seconds each.

In the second session the subjects were seated with the knee flexed to 120 degrees. The reduced effectiveness of the gastrocnemius muscles in this configuration was taken into account in the setting of the target tension. This was 66% of (.5MVC) or 36% and was proportional to the percent cross sectional area of the soleus within the triceps surae. The remaining procedures were identical to the previous session.

## DATA ANALYSIS

Each muscle's EMG activity was represented by the average of five one-second (AEMG) segments. This was followed by the computation of correlation coefficients of AEMG between MG/LG, MG/SO and LG/SO combinations over the entire exhaustion period, partialling out the effect of the third muscle, which were SO, LG and MG respectively. Also correlations between AEMG of SO and sum of AEMG of MG and LG and AEMG of MG with the sum of AEMG of LG and SO were calculated. These were done for each subject individually. This level of analysis was an attempt to identify long term changes in synergistic behaviour. Since a pattern of synergism is sought, the relationship between the changes in the EMG activities of two muscles should be considered separately, irrespective of what is happening to the third muscle. The partial correlation approach allows for comparison of EMG activity within each of the three muscle combinations separately.

## RESULTS AND DISCUSSION

Two forms of synergisms were identified: these are trade-off and coactivation. A trade-off between two muscles was said to have occurred when the changes in the AEMG of the muscles involved in the trade-off were negatively correlated ( $p < 0.05$ ). A trade-off would indicate that the neural input to one muscle is increasing, while the input to the other muscle is decreasing. The second form of synergism, which is coactivation was said to have taken place when the changes in the AEMG of the two muscles involved in coactivation were positively correlated ( $p < 0.05$ ).

The results of the overall partial correlations are shown in Table 1 where "+" indicates significant ( $p < 0.05$ ) coactivation, "-" indicates significant ( $p < 0.05$ ) trade-off, and a blank indicates no significant correlation. Significant partial correlations ranged between -0.726 and -0.823 for trade-off and between 0.623 and 0.984 for coactivation. Although two subjects (#5 & #6) did not show any significant correlations at the extended position, three subjects (#2, #3 & #4) showed significant trade-off in at least one of the three muscle combinations, whereas a fourth subject (#1) showed coactivation. With the knee flexed, three subjects (#1, #2 & #6) showed no significant correlation, however the other three (#3, #4 & #5) showed coactivation in at least one muscle combination, and there was one case of trade-off (#4).

Table 1: Trade-Off and Coactivation Synergism: Overall

Subj.	Knee Extended			Knee Flexed		
	MG/ LG	MG/ SO	LG/ SO	MG/ LG	MG/ SO	LG/ SO
1	+					
2		-				
3			-	+	+	
4	-	-		+	+	-
5				+		
6						

Further analysis was carried out by correlating AEMG of SO with the sum of AEMG of MG & LG and correlating AEMG of MG with the sum of AEMG of LG & SO. It was hypothesized that synergism may be manifested through a load sharing/compensation mechanism based on either fibre type or common innervation properties of the muscles. The MG and LG are known to contain greater percentage of type II fibres compared to SO, which is predominantly made up of type I fibres. Therefore, one combination selected was SO versus MG+LG. The second combination was based on that fact that LG and SO are innervated by the same branch of the posterior tibial nerve. Therefore, the second combination was MG versus LG+SO. These two choices imply different controlling strategies to minimize the effects of fatigue. The first choice suggests that the nervous system controls the activation levels across muscles to minimize fatigue in specific motor unit pools; while the second choice implies a simple control scheme based purely on a common neural drive channel.

Table 2: Synergist Patterns Based on Muscle Properties

Subj.	Knee Extended		Knee Flexed	
	SO/MG+LG	MG/LG+SO	SO/MG+LG	MG/LG+SO
1	-		+	+
2		-	+	+
3	-		-	+
4		-		+
5				+
6	-			

As can be seen from Table 2, only one subject from each knee angle did not show any changes in synergism. Findings of trade-off ( $-0.852 < r < -0.695$ ,  $p < 0.05$ ) with knee extended, and coactivation ( $0.908 < r < 0.503$ ,  $p < 0.05$ ) with knee flexed are consistent with the results shown in Table 1. Examination of the synergistic pattern of the muscle combinations between the two approaches on a subject by subject basis show that these are highly consistent with respect to the muscle combinations. A coactivation of MG and LG was found for subject 1 (Table 1) with the partial correlation approach in the extended knee position. The same subject demonstrated trade-off between SO and MG+LG activity (Table 2). Similarly, trade-off patterns for subjects 2, 3 and 4 were found to be consistent with the two approaches with the knee extended. When a comparison of the outcome of the two methods are made when the knee is flexed for comparable subjects (3, 4 & 5), the pattern of coactivation appears consistent, with perhaps the exception of subject 4. A closer examination of the results from the two methods for subject 4 show that the trade-off effect between LG and SO may have been masked by the strong coactivation exhibited between MG and LG, giving rise to a significant coactivation of MG and LG+SO combination. It is therefore not surprising to find no significant synergistic effect between SO and MG+LG combination.

When the results of Table 2 are considered on their own, several patterns become evident. The first of these is, as mentioned earlier, that all significant synergism with the knee extended are in the form of

trade-offs, whereas in the flexed position, they are in the form of coactivations. These findings along earlier results (Table 1) suggests that the type of synergistic behaviour may be dependent on the load carried by each muscle. A further observation on these results (Table 2) is that trade-off synergism is either between muscles of different fibre type (SO/MG+LG) or between muscles of different neural input (MG/LG+SO) depending on the subject, but not both. There is however, no muscle specific common pattern of trade-off synergism found in the subjects studied. The coactivation synergism on the other hand, (Table 2) appears to occur irrespective of fibre type or neural input characteristics. These latter observations make sense when one considers the presumed objectives of the two types of synergistic behaviour. Trade-off synergism is believed to be delaying exhaustion by alternately increasing and decreasing muscle activity based on either fibre type properties or neural innervation properties of muscles. Therefore, one would not expect trade-off between both SO/MG+LG, and MG/LG+SO combinations since it crosses the boundaries of these muscle properties. On the other hand, a coactivation synergism is believed to be synchronizing the muscle activity such that the load can be sustained. Therefore, under these circumstances one can expect to see coactivation in both SO/MG+LG and MG/LG+SO combinations.

EMG activity from 10 second maximum voluntary isometric plantarflexions at the extended position, recorded from six different subjects, were also analyzed for synergism. There was no significant change in the force output during these contractions [5]. These results give further support to the hypothesis of load dependency of synergism.

#### CONCLUSION

Two types of synergisms were identified: trade-off and coactivation. Partial correlation were used to quantify these type types of synergism. The manifestation of the type of synergism is postulated to be dependent on the load and muscle effectiveness as characterised by the force/length curve.

#### REFERENCES

1. Lippold, O.C.J. et al. (1960). *Ergonomics* 2:121-131.
2. Viitasalo, J.H.T. et al. (1982). *Biomechanics VIII* 271-277.
3. Hellsing, G. & Lindstrom, L. (1983). *Acta Physiol. Scand.* 118:203-207.
4. Clark, G.T. & Carter, M.C. (1985). *Arch Oral Biol.* 30:563-569.
5. Sirin, A. & Patla, A.E. (1985). *Neurosci. Abstr.* #122.7.

#### ACKNOWLEDGEMENT

Supported by a grant from NSERC (#A0070).

# THE PREDICTION OF MUSCLE FORCE USING EMG AND A MUSCLE MODEL

Scott C. White  
Dep't of Physical Education & Dance  
University of Wisconsin  
Madison, Wisconsin 53706

David A. Winter  
Dep't of Kinesiology  
University of Waterloo  
Waterloo, Ontario N2L 3G1

## Introduction

Various attempts have been made to find unique solutions to muscle forces across joints. One approach is to work backwards from the net joint moments. By grouping muscles according to function, Morrison (6) was able to 'reduce' the number of unknowns and solve for muscle forces from the joint moments. Seireg and Arvikar (11) suggested an objective criterion and solved for muscle forces using optimization. Pierrynowski (8) developed a neurophysiological model with groups of muscles being activated by spinal generators according to their ability to satisfy joint moments. Another approach is to use a measure of neural input and a deterministic muscle model to provide a forward solution. Processed EMG with models based on joint movement kinematics have been used with variable degrees of success (2,7). Joint movement based models involve the complex interaction of length, velocity and moment arm changes of a number of muscles; therefore, parameters of the model elements must be iterated or generated independent of the known properties of muscle described in the literature (2,7).

This paper proposes an EMG driven model implemented at the level of the individual muscle. A solution to selected muscle forces for the lower limb during human locomotion was generated. The model was validated by comparing joint moments calculated from the muscle forces, to equivalent moments derived from link segment mechanics.

## Theory and Methodology

Implementation of the model required kinematics and a morphological description of each muscle, as well as a representation of the neural input (EMG). The line of action and length of all muscles were modelled as elastic threads from the centroid of their origin, through constraint points where appropriate, to their tendon of insertion. After scaling these points to the subject, three dimensional cinematography was used to generate muscle lengths, velocities and moment arms every .02 seconds of the gait cycle. Each muscle was defined by its physiological cross-sectional area (PCA), fibre orientation, rest fibre length ( $l_0$ ) and fibre composition. These constants were generated from various literature sources (e.g. 12). Surface EMG was monitored for: soleus, gastrocnemius, tibialis anterior, extensor digitorum longus, short and long head of biceps femoris, medial hamstrings, vastus lateralis, vastus medialis, rectus femoris, hip flexors, gluteus maximus and medius, and adductor longus. Each signal was rectified and filtered with a single pass of a second order Butterworth low-pass filter using a cut-off frequency of 2.5 Hz (7).

The above parameters were input to a muscle model based on Hill's (1) equation describing the relationship between force and velocity for isotonic shortening of muscle. The equation:

$$(F+a)(V+b)=(F_0+a)b \quad [1]$$

was assumed to represent the mechanical response of the series elastic and contractile components

of muscle lumped together. The form of Hill's equation is defined by:

$$a/F_0 = b/V_0 \quad [2]$$

where 'a' and 'b' are the asymptotic values of force and velocity in equation 1. 'F<sub>0</sub>' designates maximum isometric force (V=0) and is dependent on the level of excitation 'E' (represented here by EMG) and muscle length 'L' (5). A regression equation defining 'F<sub>0</sub>' as a function of 'L' and 'E' was generated in vivo for each muscle using joint moment and angle information collected via slow isokinetic contractions. Instantaneous muscle lengths and moment arms were calculated from the joint angles. Muscle force was derived by first dividing the joint moment by the muscle's lever arm and then multiplying by a constant representing the muscle's PCA expressed as a ratio of the total PCA of all muscles which could contribute to the joint moment. Assuming a linear relation between EMG and force (4), individual muscle force-length-excitation equations were generated by dividing force at each muscle length by EMG ( $\mu V$ ) and expressing the relationship as a polynomial. 'F<sub>0</sub>' was then calculated using:

$$F_0 = (c_1 + c_2L + c_3L^2 + c_4L^3) * E \quad [3]$$

where 'c<sub>1</sub>-4' are regression coefficients and 'L' and 'E' are instantaneous values of muscle length and EMG measured during locomotion.

A solution to 'F' in equation 1 required values for 3 of the unknowns in equation 2. A constant of 0.5 was selected from the literature to represent the ratio a/F<sub>0</sub> (9). 'F<sub>0</sub>' is calculated from [3] allowing 'a' to be derived at each instant in time assuming 'a' changes in proportion to F<sub>0</sub> (1). A constant of 10 lo/s was calculated to be the maximum velocity (V<sub>0</sub>) for the gastrocnemius contracting isotonically under zero load conditions (2). 'V<sub>0</sub>' for each muscle modelled was then derived from their percent fast twitch content relative to gastrocnemius. Knowing 'V<sub>0</sub>', 'b' could be found from equation 2 allowing a solution to 'F' in equation 1.

For muscle lengthening the relationship for force and velocity can also be approximated by a hyperbola albeit an inverse hyperbola (5). Rearranging Hill's equation 'F' was calculated from:

$$F = (F_0 + a)b / (V - b) + 2F_0a \quad [4]$$

where all constants are defined as before with the exception of 'F' and 'V' which represent the muscle lengthening. For lengthening contractions, the ratio of equation 2 is multiplied by the constant 1.6 (5) and a boundary condition of 1.5 F<sub>0</sub> is placed on values of 'F' (3).

The model was validated by comparing measured joint moments, derived from limb kinematics and ground reaction forces, to net moments calculated from the muscle forces. Muscles not modelled during locomotion were grouped with muscles of similar function.

## Results and Discussion

A full profile of the input parameters used to predict the force output of 1 of the 14 muscles modelled

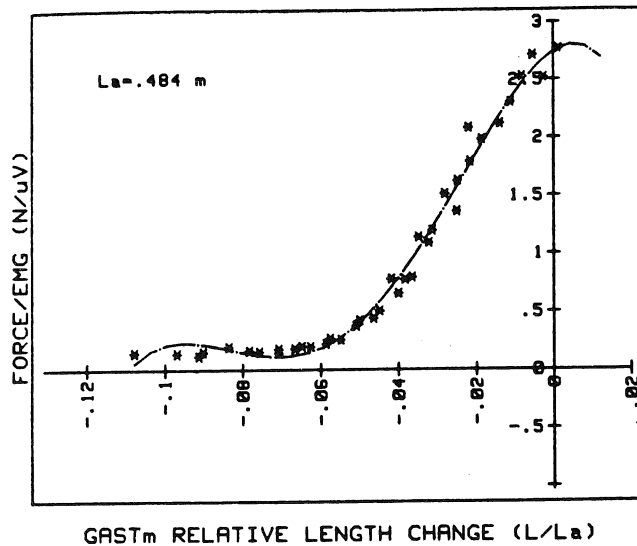


Figure 1: Force-length-excitation representation.

is presented with net joint moments in figures 1 to 3.

A third degree polynomial was required to describe the force-length-excitation relationship for gastrocnemius. Most muscles could be represented by first or second degree polynomials. Optimal length for gastrocnemius was close to its anatomical length ( $L_a$ ). The other muscles modelled did not have a similar inflection point. These results are consistent with Sale et al. (10) and support models using linear approximations of the force-length relation of muscle within a limited range (7).

The interaction of input parameters in the prediction of force is demonstrated in late stance (Figure 2). Where maximum force is recorded, the muscle is close to its optimal length and shortening slowly resulting in a peak gastrocnemius force coincident with the measured peak moment (Figure 3). From this point to toe-off EMG remains high; however, the shortened muscle length and fast concentric velocity results in a force which decreases with the measured moment. EMG is this phase is inconsistent with Hof's (2) suggestion that the plantar flexor moment continues after EMG cessation. Hof's model dealt with EMG, muscle series elasticity and the contractile component independently. This study incorporated series elasticity in the EMG processing.

Correlations between moments at the hip, knee and ankle were .89, .82 and .95. Failure to separate the series elastic and contractile components prior to calculating length and velocity changes (e.g. 2) had little effect on the temporal aspect of the predicted force curve. Absolute differences between moment curves at the ankle are small. A RMS error of 10.2 Nm is close to values calculated by Olney et al. (7) and less than the 23 Nm difference reported by Hof (2). RMS errors at the hip and knee were 11.2 and 17.1 Nm. Inspection of the input data indicated that the EMG calibration had the largest effect on the predicted force.

The results of this study demonstrates the feasibility of using the modelling approach described as a method of estimating muscle forces in locomotion.

#### References

- 1 Hill, A.V. *Proc. R. Soc. Lond.* 126:136, 1938.
- 2 Hof, A.L. *Hum. Move. Sci.* 3:119, 1984.
- 3 Joyce, G.C. et al. *J. Appl. Physiol.* 204:475, 1969.
- 4 Lippold, O.C.J. *J. Physiol.* 117:492, 1952.
- 5 Mashima, H. et al. *Jap. J. Physiol.* 22:103, 1972.
- 6 Morrison, J.B. *Biomed. Engng.* 3:164, 1968.
- 7 Olney, S.J. et al. *J. Biomech.* 18:9, 1985.
- 8 Pierrynowski, M.R. *Proc. Hum. Locom.* 11:56, 1982.

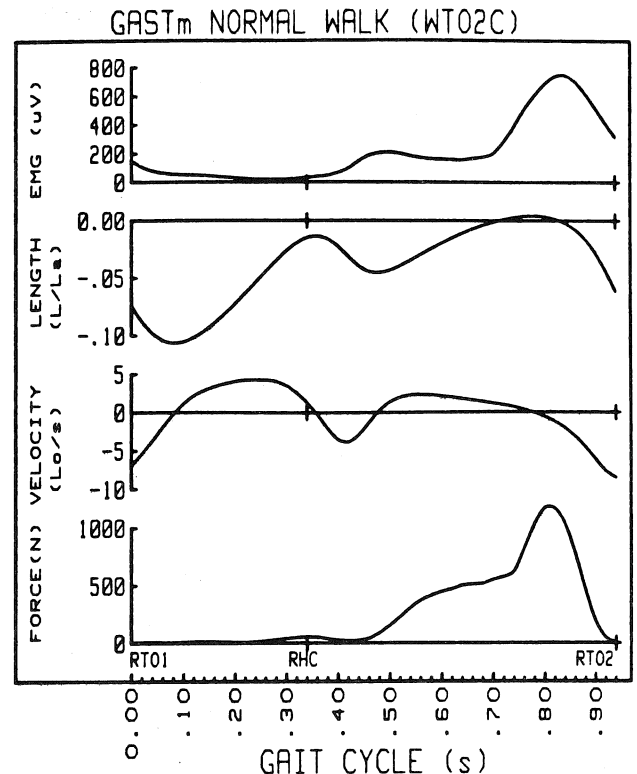


Figure 2: Input variables for prediction of force.

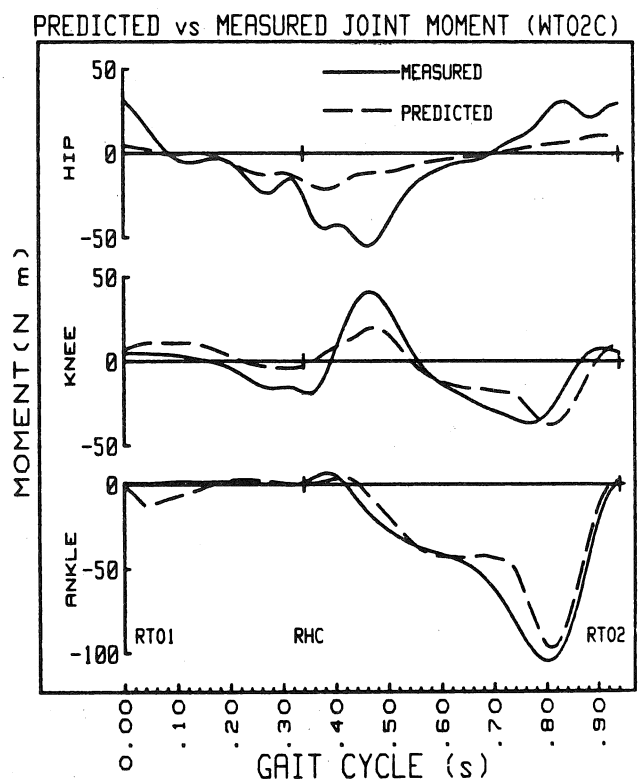


Figure 3: Comparison of joint moments.

- 9 Phillips, C.A. et al. *J. Biomech.* 13:549, 1980.
- 10 Sale, D. et al. *J. Appl. Physiol.* 52:1636, 1982.
- 11 Seireg, A. et al. *J. Biomech.* 8:89, 1975.
- 12 Wickiewicz, T.L. et al. *Cl. Orthop. & Rel. Res.* 179:275, 1983.

\* Supported by MRC (Grant MT4343)

# BIARTICULAR MUSCLES IN MULTISEGMENT LIMBS

R.H. Rozendal, G.J. van Ingen Schenau, M. Bobbert and L.H.V. van der Woude

Dept. Functional Anatomy

Interfaculty of Physical Education

Vrije Universiteit

1007 MC Amsterdam

## INTRODUCTION

In functional Anatomy form of tissues, organs or systems is related to function. The ultimate goal is explanation of the structure or morphological pattern by its function. A part of the experimental work in research is directed to the goal of explanation of the form of the human limbs. These are in conformity with or dissimilar to extremities in other species. Similarity and differences in functions can be used in explanation: comparison as a method next to experimentation.

In many species the limbs consists of three or four segments spanned by pairs of or by single biarticular muscles. Lombard's paradox about a pair of such muscles was formulated as early 1907 for Amphibian legs (6).

Biarticular muscles and their *raison d'être* in multisegment limbs are revisited in this paper.

## THEORY

Lombard's paradox stated that two biarticular muscles spanning two joints in an antagonistic fashion, could bring both joints to extension, given that at each joint the extensor muscle has the major lever arm over the flexor. This paradox assumes equal forces in both muscles and is consequently kinematic in nature.

Elftman (7) postulated that hamstring muscles in human gait could save energy in each step by transporting energy from the swinging leg to the trunk and vice versa without great changes in length. Recently Gregoire et al (2) formulated too a dynamic theory valid for at least explosive movements, like vertical jumping. In this theory the temporal sequence of the joint excursions in proximodistal order is one key element. In the hip, knee and ankle joints maximal velocity is reached consecutively. Connected to this coordinated joint excursions are e.g. the activity of monarticular knee extensors and

biarticular gastrocnemius muscles. Gregoire et al (2) stated that the latter decelerate knee extension. At the same time they transport energy to the ankle joint causing plantar flexion. The translational velocity of the centre of gravity of the body in the vertical direction continues to rise. The implication is that the diminution of vertical translational velocity by deceleration of knee extension is canceled out by an increment in translational velocity due to plantar flexion.

Speed skating was also studied (4). In this endurance sport push off is executed under two constraints. Air friction (3) and ice friction are to be kept as low as possible as performance is closely related to the power delivered to overcome these losses.

Also overhand ball throwing was studied (5).

From classic anatomy it is known that the human lower limb consists of three segments. It has a pair of biarticular (rectus femoris and hamstrings) muscles in the thigh and one in the leg (gastrocnemius). In the upper limbs also three segments do exist: upper arm, forearm and hand. It is coupled to the trunk by a moveable girdle in contrast with the lower extremity. It has three pairs of biarticular muscles: pectoralis major and latissimus dorsi; biceps and triceps brachii and the flexors and extensors of the carpus.

In both limbs the multisegmented digits are neglected in this paper as the theory will only be valid for explosive gross movements.

## RESULTS

In speed skating translational velocity of the centre of gravity of the body (cg.) with respect to the ice is achieved by knee extension. The maximal translational velocity between the upper and lower ends of the thigh (trochanter major) and leg (malleolus) is reached at 147° knee extension. Deceleration of the angular movement in the knee joint will result in a safe velocity of zero ° at full extension. At 147 ° knee angle, push off is ended by

lifting the skate from the ice, lest the ice friction will become damaging high. Hip joint extension by rotating the trunk is avoided in order to keep air friction low.

In vertical jumping the linear velocity of cg. with respect to the floor is caused by the sum of linear displacements in time due to angular rotations in hip, knee and ankle joints. In this case too, dangerous maximal extension of the knee is avoided by deceleration from the peak velocity. Deceleration starts at about  $138^{\circ}$ . Linear velocity of cg. will not diminish but is heightened by the linear velocity component due to ankle plantar flexion of  $15 \text{ rad. sec}^{-1}$  (2). The movement is started by trunk flexion in the hip joint and a knee flexion in the countermovement jump, followed by erection of the trunk while the hip is extended. Thus the vertical velocity of cg. consists of three components due to hip, knee and ankle extension.

The first and last are zero or negligible in speed skating. Only two segments are used. In the jumps three segments in the limbs are used.

Muscular works consist of power transport by rectus femoris from hip extensor activity to knee extension. The power of the monarticular knee extensors is transmitted to the ankle joint by the gastrocnemius muscles and results in plantar flexion. The three segments and the joints between them are moved by a coordinated pattern: the biarticular muscles decelerate the proximal and accelerate the distal joints they span, just at the right time.

In overhand ball throwing the sequential timing of movements of the proximodistal segments was also shown (5). Many explosive arm movements are of a pushing or pulling type in which the hand and wrist move in a prescribed path like in driving a wheelchair or in manipulating devices. Thus a constraint like that in speed skating exists. Nevertheless in the arm three free moving segments remain available: the scapula is the third free segment. All segments are spanned by an antagonistic pair of biarticular muscles.

Of these the proximal pair is very powerful.

As the human arm is adapted to the existence of the prehensile hand, the arm appears to be more versatile than the lower limb: it can be used in both directions in pulling and pushing and has also distal pairs of biarticular muscles.

Monoarticular muscles like the serratus lateralis, the rotator cuff muscles, brachialis muscle and the short heads of triceps brachii are sources of power

to transmit by the biarticular muscles in either direction: proximodistal or distoproximal.

#### DISCUSSION

In very powerful movements trunk movements will be used to initiate power production with the help of gravity or inertia. In the limb at least three segments are needed for efficient and coordinated power production. Biarticular muscles are used for decelerating dangerous joint excursions. If monoarticular muscles would perform this decelerating function by eccentric contraction much energy would be lost (2).

At the same time biarticular muscles transport power to the next joint to be activated to deliver a part of the translational velocity of the cg. or, - in the case of manipulating - the object to be moved.

In performing this function biarticular muscles can contract with a relatively low velocity yielding relatively more force, or yielding power over a range of explosive movements.

#### REFERENCES

1. Elftman, H. J. Bone Joint Surg. 48A, 363-377, 1966
2. Gregoire, L. et al. Int. J. Sports Med. 5, 301-305, 1984
3. Ingen Schenau, G.J. van J. Biomechanics 15, 449-458; 1982
4. Ingen Schenau, G.J. van et al. J. Biomechanics 18, 91 - 96; 1985.
5. Jöris, H.J.J. et al. J. Biomechanics 18, 409-414; 1985.
6. Lombard, W.P. et al. Am. J. Physiol. 20, 1-60; 1907.

# THE DEPENDENCE OF THE EMG - FORCE RELATIONSHIP ON THE MUSCLE'S MOTOR UNITS RECRUITMENT RANGE

M. Solomonow, B.-H. Zhou, R. Baratta, H. Shoji and R. D'Ambrosia  
Bioengineering Laboratory  
Department of Orthopaedic Surgery  
Louisiana State University Medical Center  
New Orleans, Louisiana 70112

## INTRODUCTION

The effect of various firing rate and recruitment control strategies on the linearity of the EMG-force relationships of a skeletal muscle was studied to provide credibility to biomechanical and gait studies utilizing EMG as a parameter representing force. The linearity of the EMG-force relationships was found to be strongly dependent on the recruitment range of the muscle. When all the motor units of a given muscle were fully recruited at near 50% of its maximal tetanic force, the EMG-force relationship is linear. The relationships become progressively nonlinear when all the motor units are recruited near 100% of its maximal tetanic force. A clear warning is issued against the indiscriminant use of EMG as representative of muscle force.

## REVIEW

The EMG-force relationship was shown to differ for various muscles. The biceps and triceps demonstrate nonlinear relationships whereas the first dorsal interosseous (FDI) demonstrates linear relationships (1-3). The biceps and triceps were shown to utilize motor unit recruitment to control most (80%-100%) of their maximal voluntary contractile (MVC) force whereas the FDI utilizes recruitment to obtain only 35% or so of its MVC force and firing rate increase to generate the remaining 65%. It could be speculated, without proof, that the control strategy used by the muscle's motor units is affecting its EMG-force relationships, or more specifically the muscle's recruitment range is directly responsible for the linearity/nonlinearity of such relationships.

## METHODS

A computer-controlled stimulator was designed and used in the experiments done on the m. gastrocnemius of three cats. The stimulator had dual-channel outputs, one controlling firing rate and the second recruitment, via stimulation of the muscle nerve (4,5). Various control strategies could be implemented to enable simultaneous increase in the firing rate and the number of active motor units according to their size (recruitment). Recruitment range varied from 40% to 100% of the maximal tetanic force of the muscle. EMG was measured with two intramuscular electrodes inserted in the muscle with hypodermic needles. Force was measured with FT-10 Grass transducer attached to the severed calcaneal tendon. EMG was band-pass filtered (20-450 Hz), full-wave rectified and smoothed with a low-pass filter to obtain its mean absolute value (MAV).

## RESULTS AND DISCUSSION

Figure 1 shows simultaneous recordings of force and its corresponding MAV (both normalized with respect to their maximal value) as a function of time, plotted with the aid of an IBM-AT (sampling rate of 50 Hz). Each value of force and its corresponding MAV value were plotted for

several force-EMG traces in which the recruitment range varied from 50% to 100% of the muscle's maximal tetanic rate (Figure 2).

Generally, the force segment generated by recruitment was linear with respect to time and to the stimulus with the exception of short initial and final segments. The initial nonlinear segment was probably due to stiction in the muscle fiber connective tissue that had to be overcome, whereas the final nonlinear segment was due to the viscoelastic component of the muscle adjusting to the new steady-state tension. The force response to the firing rate stimulus alone demonstrated saturation nonlinearity and confirming previous data (6).

As Figure 2 clearly shows, the impact of increasing recruitment range on the EMG-force relationship results in the progressive shift of the curves from quasi-linearity to nonlinearity. Although recruitment ranges of less than 40% were difficult to obtain in the m. gastrocnemius, being a fast-twitch muscle, without observing unfused force response, the data for the 50% to 100% recruitment range provide definite proof that the linearity/nonlinearity of the EMG-force relationship depends on the recruitment range of a muscle as was indirectly speculated by others (1,2).

## CONCLUSIONS

Based on the data and its analysis, the following conclusions could be made.

- A. The force generated by recruitment of motor units according to their size is linear with respect to time or stimulus.
- B. The force generated by firing rate increase alone is nonlinear with respect to time or stimulus.
- C. EMG-force relationships are dependent on the firing rate/recruitment control strategy of the muscle. Recruitment ranges of near 50% of the maximal muscle force result in linear EMG-force whereas large recruitment ranges result in nonlinear relationships.

A warning is issued against the use of EMG as direct representation of force without considering the recruitment range of the muscle under investigation and its impact on the linearity of its EMG-force relationships.

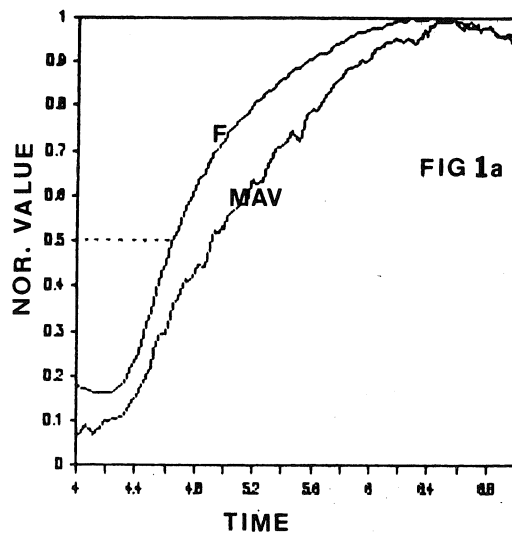
## References

1. Woods, J., and Bigland-Ritchie, B. *Am. J. Physical Med.* 62:287-299, 1983.
2. Lawrence, J., and DeLuca, C. *J. Appl. Phys.* 54: 1653-1659, 1983.

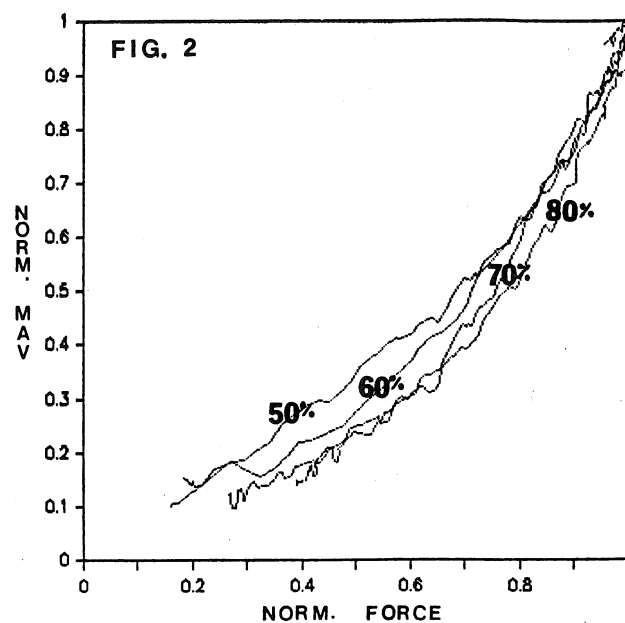
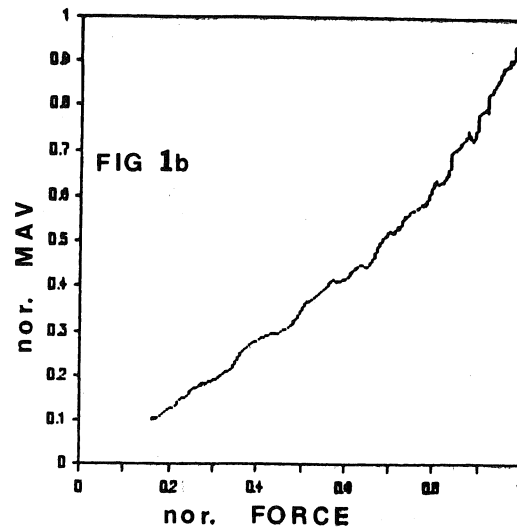


3. Solomonow, M., et al. Am. J. Phys. Med. (In press, 1986).
4. Solomonow, M. IEEE-Transactions, BME, 31:752-763, 1984.
5. Solomonow, M., et al. Proceedings of IEEE-Engineering in Medicine and Biology Society, 8, 1986.
6. Solomonow, M. Orthopedics 7:245-250, 1984.

EXP11



EXP11



# FEEDFORWARD POSTURAL CONTROL IN CHILDREN

C.L. Riach  
Physical Education and Athletics  
McMaster University  
Hamilton, Ontario  
L8S 4K1

K.C. Hayes  
Department of Physical Medicine  
and Rehabilitation  
Parkwood Hospital  
London, Ontario, N6C 5J1

## INTRODUCTION

It has been demonstrated that when a quietly standing adult quickly raises one arm forward to the horizontal position there are changes in the myoelectric activity of the postural muscles which precede the arm movement (2,3). There are also anticipatory changes in the centre of pressure of ground reaction forces (CP) prior to the arm movement (8). These changes in muscle activity and CP are made in anticipation of the disturbing forces and moments of force associated with the expected forceful arm movement. The purpose of the present study was to determine at what age children are able to anticipate postural disturbances caused by voluntary movements and to investigate the emergence of developing patterns of adjustments in CP.

## REVIEW AND THEORY

The control of dynamic balance requires a precise coordination of movement and postural adjustments as well as complex integration of the input of the three main sensory feedback systems involved in postural control: visual, vestibular and somatosensory. Very early in a child's development, neural circuits controlling the execution of such basic functions as locomotion are present at a hierarchically low level of motor control (6). In addition, preprogrammed automatic postural response synergies, triggered by feedback from the sensory systems, are present as early as 1 year 9 months, at latencies and patterns comparable to those of adults (5). To adapt these stereotyped patterns to different contexts, however, requires the adaptive functions of the later developing higher control centres (5). The ability to anticipate postural disturbances caused by self-initiated movements and the ability to coordinate postural adjustments with the movement execution may be beyond the capabilities of young children.

## METHODOLOGY

Subjects (n=32, aged 4-14 years) stood quietly on a stable force platform with feet parallel and 6 cm apart. They were asked to respond as quickly as possible to a visual stimulus. A green light signalled a forward arm raise to the horizontal position. A red light signalled a backward arm movement. The probability of each was  $p = .5$ . The subjects were given a randomly varied foreperiod (1-3 seconds) between a warning tone and the signal light. Only the forward trials were recorded and analyzed.

Force and moment of force signals from the strain gauged force platform (AMTI-OR6) were amplified (DC-1KHz) prior to A/D conversion (51 Hz) and stored in a Tektronix 4051 microcomputer. CP changes in the antero-posterior (AP) and lateral (LAT) planes were calculated, the signals filtered (10 Hz) with a Butterworth digital low pass filter (double pass) and plotted against time. The onset of movement was detected by a small uniaxial accelerometer (Endevco 7264-200) secured to the subject's wrist. The acceleration signal was conditioned and amplified, then A/D converted and plotted with the CP signals.

One full second of the four signals (force, moments and arm acceleration) was recorded; 600 msec pre-movement and 400 msec during arm movement.

## RESULTS

### Antero-posterior CP adjustments:

In the AP plane, 26 of 32 subjects (81%) demonstrated anticipatory CP adjustments. These subjects all showed the CP shifting posteriorly prior to the arm movement. When analyzed by age group, 5 of 9 subjects (4-7 years), 15 of 15 subjects (7-11 years), and 6 of 8 subjects (11-14 years) showed feedforward adjustments (AP). The feedforward patterns were present in even the youngest of the children, however, 4 of the 9 subjects (44%) in the youngest age group (4-7 years) did not show any feedforward changes (AP).

In order to test whether the CP adjustments prior to arm movement were in a constant direction, and not just random fluctuations, a sign test was used (1). A shift in CP posteriorly prior to arm movement was found statistically ( $p < .001$ ) more often than would be expected by chance.

### Lateral CP adjustments:

In the LAT plane 28 of the 32 children (87%) demonstrated the expected anticipatory changes in CP. There were two repeated patterns. One pattern (25% of subjects) showed a shift in CP directly right prior to arm movement. Other subjects (56%) demonstrated a left-right shift in CP. The CP movement to the right occurred before or just after the beginning of arm movement (Fig. 1). This left-right pattern was most common in the younger children. When analyzed by age group, all 9 subjects (4-7 years), 12 of 15 subjects (7-11 years) and 7 of 8 subjects (11-14 years) showed anticipatory adjustments.

## DISCUSSION

The feedforward patterns of change in CP were seen in the youngest of the children. In the AP plane the occurrence of feedforward changes increased with increasing age.

In the LAT plane results were quite different. The youngest children had the highest incidence of feedforward adjustments (all 9 children, 4-7 years). In addition, there was a strong preference for the left-right pattern in the youngest children. The left-right pattern of CP changes is similar to the CP pattern during gait initiation as one arm and the contralateral leg come forward (7). It is conceivable that the left-right pattern seen in such a high incidence in the young children is innate and that the young children are more reflexive (cf. 4) and stereotyped in their LAT postural responses than older children.

## CONCLUSION

In the AP plane the increasing incidence of CP changes with increasing age may be attributed to the increasing ability of children to anticipate and initiate postural adjustments and/or the ability to

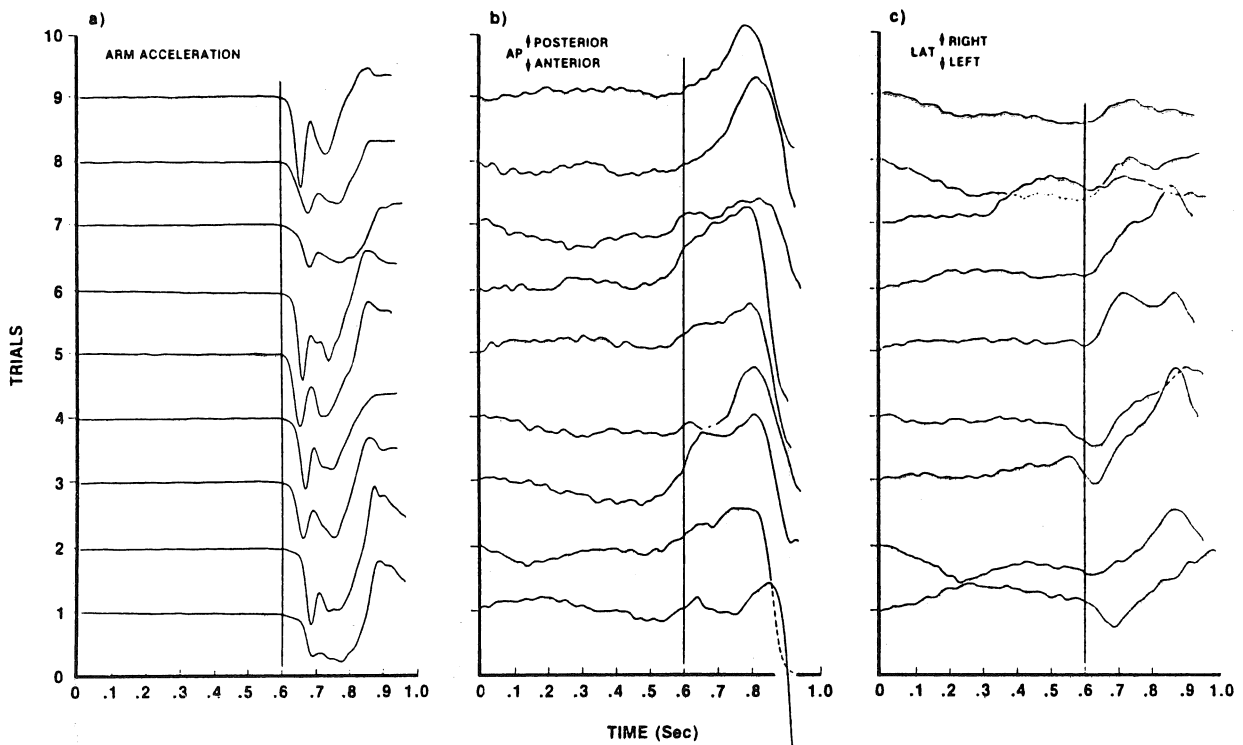


Figure 1. Nine consecutive trials of one subject (13 years)  
a) arm acceleration, b) AP-CP changes, c) LAT-CP changes.  
The vertical line indicates the beginning of arm movement.  
Note that despite the variance in CP early in each trial  
at the beginning of arm movement all 9 trials show a shift  
in CP posteriorly and most (7/9) show a shift left.

coordinate postural control with movement control.  
In the LAT plane the high incidence of the left-  
right CP pattern in the youngest of the children  
may indicate a reliance on the more stereotyped  
basic postural patterns available.

#### REFERENCES

1. Anderson, T. et al. An introduction to statistical analysis of data. Boston: Houghton Mifflin Co., 1978.
2. Belinkii, V. et al. Biophysics 12: 154-160, 1967.
3. Bouisset, S. et al. Neuroscience Letters 22: 263-270, 1981.
4. Bressan, E. et al. Human Movement Sci. 1: 155-175, 1982.
5. Forssberg, H. et al. J. of Neuroscience 2: 545-552, 1981.
6. Grillner, S. Phys. Rev. 55: 247-304, 1975.
7. Mann, R. et al. J. of Bone and Joint Surg. 232-239, 1979.
8. Riach, C. et al. I.S.B. Conference, Omea, Sweden. June, 1985.

# ELECTROMYOGRAPHIC RESPONSES OF THE LOWER LIMB MUSCULATURE IN SIMULATED POSTURAL AND LOCOMOTOR ACTIVITIES

R. Wells and N. Evans Stüber

Department of Kinesiology, University of Waterloo  
Waterloo, Ontario, Canada

## INTRODUCTION

Motion of the limbs involves compound action at two or more joints. If these joints are spanned by two-joint muscles then the patterns of activity of the musculature are not readily predictable (1). Most investigations of the functional anatomy of the limbs have concentrated upon a single joint. More recent investigations have explored processes linking several joints [Abbs et. al. (2), Nashner et. al. (3) or Winter (4)]. This paper presents some preliminary work on the changes seen in the muscle activity patterns when exerting a constant force in different directions. This simulates the loading directions found in postural control studies and in locomotion. The patterns found help to unify the findings of some of these investigators.

## METHODOLOGY

Six female subjects were placed in a side lying posture with the right leg suspended by cords. In this position the muscle activity associated with sagittal plane motion can be isolated without contamination by weight forces. The relative angles at the hip, knee and ankle were 45° and 90° of flexion and 0° (neutral) respectively. Forces exerted by the leg were measured by a six-axis force platform mounted vertically. The subjects were connected to the force platform by a Nordic ski boot and binding which allowed any combination of normal and shear forces to be applied to the force plate. Subjects received feedback on the force exerted through an oscilloscope. They were asked to generate isometric forces of equal magnitude (63N) in twelve different directions corresponding to the numerals on a clock face. The net joint moments at the ankle, knee and hip were calculated using force and joint centre coordinate information.

EMG recordings were taken from ten representative muscles of the lower limb; soleus (SOL) lateral gastrocnemius (LG), tibialis anterior (TA), biceps femoris, short head (BFSH) and long head (BFLH), vastus lateralis (VL), rectus femoris (RF), sartorius (SA), iliacus (IL) and gluteus maximus (GM). Recordings were made with 4mm IVM silver/silver chloride electrodes with skin mounted preamplifiers. The signals were amplified and linear enveloped (5Hz filter), then A/D converted and averaged over one second. Two trials were taken in each force direction.

This work was supported under NSERC Grant A2785.

The EMG amplitudes were normalized to the largest activity found for that muscle.

## RESULTS

Figure 1 shows the mean responses of the ten muscles to the loadings used. The stick figures show the ground reaction force and the direction of the muscle moment. The number beside each stick figure gives the corresponding force direction in reference to the numerals on a clock face. Table 1 displays the mean moments generated.

Table 1:

Joint moments generated at the joints (+ve extensor, -ve flexor). The ground reaction force had a constant magnitude of 63N.

Force Direction	Hip Moment	Knee Moment	Ankle Moment
6	-7	-9	-6
7	24	-28	3
8	52	-44	14
9	70	-45	19
10	72	-38	21
11	41	-13	15
12	3	13	5
1	-31	33	-4
2	-59	46	-14
3	-70	46	-20
4	-59	33	-17
5	-44	19	-14
6	-7	-9	-6

## DISCUSSION

A number of authors have suggested schemes for classifying leg function. Nashner and colleagues (3) working with platform movements during standing, experimentally identified a suspension synergy which came into action for platform movements directed caudo-cephalically and a sway synergy for platform movements directed antero-posteriorly. Movements of the platform result in changes in the ground reaction forces similar to those produced in this investigation. An upward platform motion invoked activity in rectus femoris and gastrocnemius. Direction 12 (Figure 1) shows that SOL and VL, one-joint muscles, are the prime actors in this study. For downward platform motion tibialis anterior and hamstrings were reported to have been activated. Direction 6 shows increased activity in TA, BFSH, SA and IL, mostly one-joint muscles.

When Nashner and colleagues moved the platform horizontally, activity was elicited in gastrocnemius and hamstrings for posterior

motions. This corresponds to Direction 9 where LG, SOL, BFSH, BFLH and GM responded. For anterior motions they found tibialis anterior and quadriceps activated. This corresponds to Direction 3 where the quadriceps (RF and VL) IL, TA and SA were activated. Nashner and colleagues recorded the gastrocnemius, rectus femoris and hamstrings, two-joint muscles. It can be seen that these are not representative muscles for these situations.

Roberts (5) proposed a classification of lower limb function into "prop" and "paddle" actions. Prop actions support the body and prevent collapse of the leg, and are achieved principally by one-joint musculature. Paddle actions propel the body and are accomplished by the action of two-joint muscles. The similarity to Nashner and colleagues' classification is noteworthy. His predicted dominance of one-joint muscle activity during prop activities (Directions 12 and 6) is seen but two-joint muscle activity during paddle activities (Directions 9 and 3) is not seen in this data. Paddle actions seem to result from both one-and two-joint muscle activity.

Winter (4) concentrated on the supporting function of the leg during the stance phase of gait and proposed a support moment (the sum of the extensor joint moments at the hip, knee and ankle). If this is positive then positive support results whatever the particular combination of joint moments at the joints. Directions 11, 12 and 1 are representative of the force directions encountered during the stance phase of gait. Forces directed within these limits can be produced by joint moments of moderate levels as shown in Table 1. As the force vector swings between Directions 2 and 10 one can see the trade off between the knee and hip moment and

the activities of VL, RF and BF as described by Winter. It is noteworthy that for Directions 11, 12 and 1 (those representative of gait), the support moment reflects the supporting function of the leg. This does not seem to hold for the other Directions.

## CONCLUSIONS

The results found here concur with those of Nashner et al. (3) even though they measured rapid reflex responses while the present work studied voluntary isometric contractions. Roberts' prediction (5) of one-joint muscle activity during prop actions was supported, but paddle actions were found to involve both one- and two-joint muscles. This work also supports that of Winter (4) since positive support moments were found for those directions which are comparable to the stance phase of gait. The trade-off between the activities of different muscles which he predicted based on joint moments is also apparent in the EMG data. Therefore this study serves to support, link and unify the highly diverse work of these researchers.

## REFERENCES

- (1) Kumamoto, M. et al, Biomechanics IX-A: 324-329, 1985.
- (2) Abbs, J. et. al., J. Motor Behav. 15: 195-231, 1984.
- (3) Nashner, L.M., et. al. Exp. Brain Res. 36: 463-476, 1979.
- (4) Winter, D.A., J. Biomech. 13: 923-927, 1980.
- (5) Roberts, T.D.M., Nature, 230: 499-501, 1971.

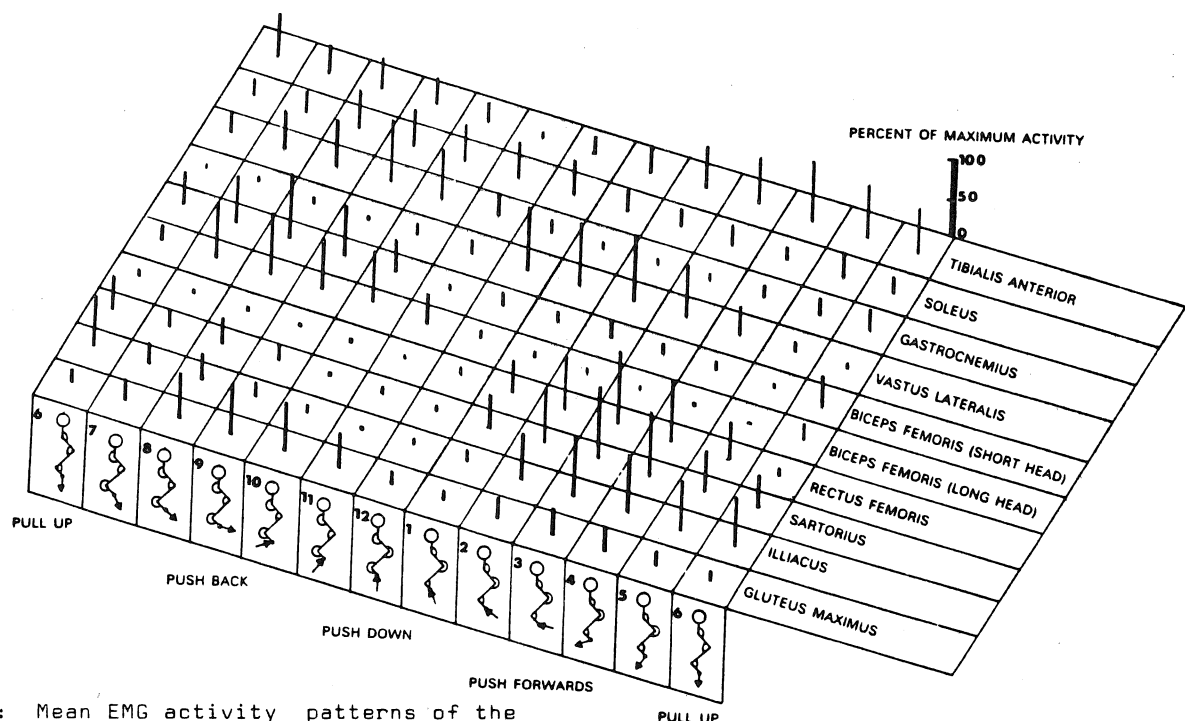


Figure 1: Mean EMG activity patterns of the leg musculature to produce a constant magnitude force with different directions.

K. Schneider, R.F. Zernicke, R.A. Schmidt, and T.J. Hart  
 Department of Kinesiology  
 University of California  
 Los Angeles, CA. 90024

## INTRODUCTION

Studies on planning and controlling motions of the human arm are mainly experiments in which pointing or reaching tasks are performed with the hand or in which human arm trajectories and robotic manipulations are compared or mathematical models used to simulate optimal hand paths. Most of these results are based on observations of restricted arm movements and agree with each other only in part, as Atkeson and Hollerbach (1) pointed out recently. They ask for more studies on "natural" unrestrained arm movements. Kinematic invariances frequently provide the only basis for postulating mechanisms and processes of motor control. In neuromotor control and especially in motor learning, very few investigations report on limb intersegmental dynamics. In the present study, a planar rigid-body model was used to analyze changes in intersegmental dynamics during learning to perform an unrestrained rapid arm movement. The goal of the task was to minimize movement time. The results indicated that throughout learning, subjects increasingly took advantage of the passive dynamical characteristics of the moving limb. This resulted in greater inertial joint moment components causing appropriate accelerations, which increased segment velocities and decreased movement time. Subjects self-structured the movement and although a basic joint moment profile developed during learning, moments scaled differently within each of the movement parts.

## REVIEW AND THEORY

Results obtained for restricted arm movements in a horizontal plane (2,3,4,5) suggest a planning of the hand trajectory in the Cartesian handspace. Dynamical results indicate the significance of joint interaction moments such as inertial moments, and the scaling of a basic moment profile in order to increase movement speed. Therefore, several researchers (6,7) suggest a hierarchical movement plan with three levels: (a) at the object level the task command is translated into a trajectory, (b) at the joint level the trajectory is transformed into the coordination control of multiple joints and, (c) at the actuator level the joint movements are caused by appropriate muscular activity. The researchers hypothesize that a movement is planned at the object level rather than the joint or muscle level, and a fixation of a specific profile occurs on the higher level and a determination of the movement parameters occurs on the lower level. Practice strategies are seen as learning of the basic moment profiles during slow motions and increasing the speed by scaling those moments. The complexity of the control mechanism is reduced by (a) coupling the shoulder-elbow movement and decoupling the wrist movement (7) and (b) minimizing the jerk-cost to get a smoother movement (5,8). Simulations under jerk-cost minimization conditions describe the hand trajectories adequately (2), and this criterion is suggested as an organizing principle (5). A reduction of the complexity of the dynamical parameters for the movement's control to a few

key features is also indicated by Bernstein (9). In addition, he hypothesizes that a system increasingly takes advantage of its passive dynamical characteristics in order to create the most effective movement. Although some of the results mentioned above apparently confirm Bernstein's first concept, nevertheless his hypotheses have to be tested by further experiments.

## METHODOLOGY

Four subjects performed movements with their left arm in a vertical sagittal plane between two targets. The left hand had to be moved from a lower target to an upper one and back in a single motion. During the upward and downward phase the hand had to go around a barrier, but otherwise the movement was unrestrained. No instruction was given to the subjects about the hand's path. The goal of the task was to minimize movement time. The number of learning trials was 100. Subjects (male; age =  $25.01 \pm 4.50$  years) were right-handed and untrained regarding this task. Throughout the learning, arm movements during selected trials were recorded by high-speed cinematography (number of filmed trials = 12). The limb model consisted of three segments (upper arm, forearm, hand), and the equations of motion were obtained by the method of inverse dynamics (10). The parameters for the model segments (length, mass, center of gravity, moment of inertia) were individually determined by anthropometric measurements for each subject using an anthropomorphic model of the human body (11). The arm movements were calculated in three dimensions by comparing the filmed and anthropometrically measured limb lengths and used for a spatial kinematical analysis as well as a planar analysis of the intersegmental dynamics during the learning.

## RESULTS AND DISCUSSION

The results indicated that the movement was self-structured by subjects as a sequence of movement parts and each of the parts was improved at different rates of learning. The three movement parts included: (a) the motion from the beginning until the hand entered the top target (upward part), (b) from entering to leaving the top target (reversing part), and (c) from leaving the top target until the end of the motion (downward part). The greatest relative and absolute decrease in movement time occurred during the reversing part which required a greater degree of both speed and accuracy. The mean movement time for the last trial (as percentage of the first trial) was:  $42.4 \pm 7.8\%$  for the reversing part versus  $79.2 \pm 12.0\%$  for the upward,  $65.3 \pm 11.9\%$  for the downward part and  $63.9 \pm 7.6\%$  for the total movement. During learning kinematical results showed that, except for a contraction of the trajectories during the reversing part, the spatial path of the hand remained relatively stable, but the velocity and acceleration vectors underwent significant changes. At the inflection points of the movement (e.g., going around the barrier, entering and leaving the target) subjects

learned to become faster by accelerating and decelerating more effectively. During learning the jerk-cost decreased, but considering the significant decreases in movement time the change in jerk-cost may not necessarily have been connected to an increased smoothness of the motion. A basic joint moment profile was observed throughout learning, however, joint moments scaled differently within each of the three movement parts. Dynamical interactions between muscular and inertial moments became more effective during learning, especially at the shoulder, where subjects made increasing use of a flexor inertial upper arm moment to counterbalance the shoulder extensor muscle moment. The interactive effect was most prominent at the reversal of the movement, where the results indicated that the behavior changed from a "static" reversal which separated the whole movement into two independent parts to a "dynamic" reversal which combined the upward and downward motion most effectively and rapidly.

### CONCLUSIONS

Apparently subjects self-structured the movement and although a basic joint moment profile was observed throughout learning, moments scaled differently within each of the movement parts. Therefore a uniform scaling did not appear to be adequate for this unrestrained and rather complex motor task. Dynamical interactions between muscular and inertial moments became more effective during learning, confirming Bernstein's (9) hypothesis that the system increasingly takes advantage of its passive dynamical characteristics in order to become most effective. During learning the jerk-cost decreased, but considering the significant decreases in movement time the change in jerk-cost may not necessarily have been connected to an increased smoothness of the motion. Therefore, the jerk-cost appeared to be an inappropriate optimization criterion in this unrestrained and complex motor task. The data from our study emphasize the importance of incorporating intersegmental dynamics into investigations of the mechanisms of neuromotor control of limb movements, especially during motor learning.

### References

1. Atkeson, C.G. et al. J. Neurosci. 5(9): 2318-2330, 1985.
2. Flash, T. et al. Soc. Neurosci. Abstr. 8: 282, 1982.
3. Lacquaniti, F. et al. Brain Res. 252: 394-397, 1982.
4. Morasso, P. Biol. Cybern. 48: 187-194, 1983.
5. Hogan, N. J. Neurosci. 4(11): 2745-2754, 1984.
6. Hollerbach, J.M. Trends NeuroSci. 5: 189-192, 1982.
7. Lacquaniti, F. et al. J. Neurosci. 2(4): 399-408, 1982.
8. Nelson, W.L. Biol. Cybern. 46: 135-147, 1983.
9. Bernstein, N. The Co-ordination and Regulation of Movements. Oxford 1967.
10. Hoy, M.G. et al. J. Biomech. in press.
11. Hatze, H. J. Biomech. 13: 833-843, 1980.

Aftab E. Patla  
Neural Control Laboratory  
Department of Kinesiology  
University of Waterloo  
Waterloo, Ontario, N2L 3G1

## INTRODUCTION

Feedforward postural adjustments associated with voluntary movements have been shown to occur in mammals such as cats (cf. 1) and in man (2-4). These anticipatory responses provide stability so that the task at hand can be completed successfully. Until recently, the postural set had been studied while the animal was stationary: a relatively clean experimental paradigm. To date, only one study has examined these anticipatory adjustments during treadmill locomotion when the subjects were asked to pull or push an arm lever in response to a tone (5). Holding a rigid handle while walking can alter the muscle activity patterns and response strategies to perturbation. The purpose of this study was to examine the postural response when the subjects are asked to raise their arm quickly and forcefully in response to a light cue occurring at different phases of the step cycle.

## METHODOLOGY

The subjects (N=6) walked at their natural, self-paced speed on the treadmill. The light cue, placed at eye level and triggered by a heel strike signal, was activated unexpectedly at three different points in the step cycle: heel strike (HS), late stance (two thirds of the time between heel strike and toe-off) (LS), and early swing (one fifth of the time between toe-off and heel strike) (ESw). Responses while standing (St) were also included as control. Rectified and low pass filtered (10 Hz, 4th order Butterworth, zero lag) myoelectric signals from the right anterior deltoid, long head of biceps femoris (BF) and footswitch signals from both limbs were collected to study the response. From each trial record a normal cycle was subtracted from the perturbed cycle to provide a response. Five of these responses for each condition were ensemble averaged. An interactive program provided the latency of the response. The latency values are summarized in Figs. 1 and 2. The magnitude of the responses in both muscles were determined by taking the area under the response curve for 50 ms, after the onset of their activity. The changes in the durations of the normal and perturbed strides, stance and swing phase for both limbs were determined from the footswitch signals (Table 1).

## RESULTS AND DISCUSSION

The latency values for the anterior deltoid (Fig. 1) represent reaction time. A one way ANOVA showed no significant effect of condition. Thus subjects initiated their arm movements at the same time; irrespective of their posture. This is in contrast to the results found by Cordo and Nashner (4). They found that the reaction times to an arm pull were greater when the subjects support surface was rotated, and attributed this increase to the increased requirement for postural stabilization. It is therefore surprising to find no increase in reaction time during walking, a rather complex task demanding greater postural control. Researchers studying dual task execution would suggest that locomotion is a robust task

requiring no attention (cf. 6).

Fig. 1: Latencies from the stimulus to the onset of Anterior Deltoid activity. Values shown are means and  $\pm 1$  S.D.

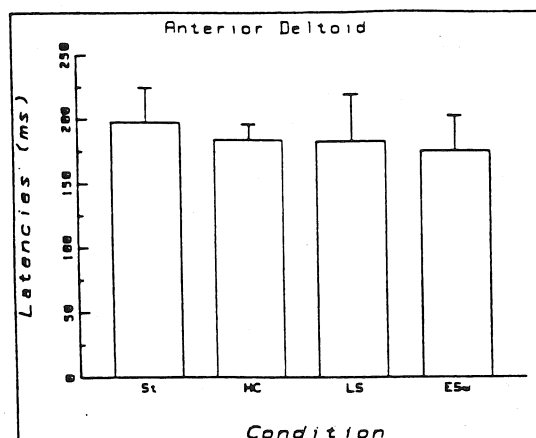
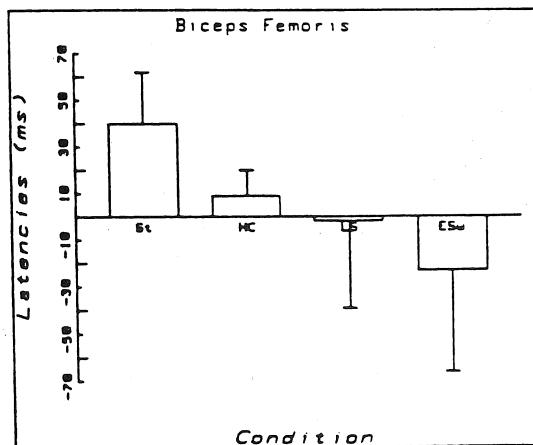


Fig. 2: Latencies from the onset of Anterior Deltoid Activity to the onset of Biceps Femoris activity. Positive values indicate onset before AD activity.



The question that arises is whether the adaptations during walking are similar in organization to those found in static condition. The latencies of the biceps femoris (Figure 2) answer this question, at least partially. The biceps femoris is one muscle that has been shown to be consistently activated prior to arm movement while the subjects are standing (2,3). In this study, a one way ANOVA showed a significant effect of condition on the biceps femoris latency ( $F(5, 3) = 4.248, p < .02$ ). A posthoc analysis by the method of Scheffe revealed that the ESw condition was significantly different from the St condition ( $p < .05$ ). In the St condition, the earlier activation of BF is in agreement with the earlier results. As the



results show, the onset of BF activated is modulated during the step cycle, such that in the ESw condition it is no longer anticipatory. Because of intersubject variability, the HS and LS conditions were not significantly different from the St condition. When individual subject results were examined, in the HS condition all but one subject showed anticipatory BF activity. In the LS condition the results were more variable; only three subjects showed anticipatory responses. The greater variability in responses during the transition phase is similar to those found in other perturbation studies [cf.7].

The magnitude of the responses in both the focal muscle (AD) and the postural muscle (BF) were analysed. A one way ANOVA of the AD response showed a significant effect of the phase of the step cycle ( $F(5,3) = 4.16, p < .03$ ). A posteriori analysis by the method of Scheffe revealed that AD response in the ESw condition was smaller than the HS condition. In contrast, the magnitude of the BF response showed no significant modulation during the step cycle. Unlike the responses to unexpected perturbation where only the gain of the response was modulated [7], the postural adaptation only show changes in the latencies (Fig. 2).

Table 1: Significant changes (\*,  $p < .05$ ) in the temporal data.

Condition	Ipsilateral			Contralateral		
	Stride	Stance	Swing	Stride	Stance	Swing
Heel Strike	*	*	-	-	-	-
Late Stance	-	-	-	*	*	-
Early Swing	*	-	*	-	-	-

Although the task of walking was maintained by the subjects, the locomotor cycle during the perturbation was altered. There were behavioural changes (Table 1) associated with the postural adjustments. When the light cue was activated at HS, the ipsilateral stance phase was shortened. At heel strike, the contralateral limb is in the late part of stance phase [8]. An accelerated weight transfer on the ipsilateral side for greater stability could explain the observed reduction in stance phase. In LS, the contralateral stance phase was shortened. During normal gait, at LS the contralateral limb is just about to make ground contact [8]. By the time the subject responds (~200 ms) the ipsilateral limb is near toe-off and the contralateral limb is in the stance phase [8]. Thus, in this case, for better stability, an accelerated weight transfer on the contralateral side could cause the reduced stance phase. When the light cue was presented in the swing phase, the ipsilateral swing phase was shortened. Enhanced BF response creates a braking action at the knee joint, and thus enhances the subjects stability by providing a double support phase sooner [8].

To summarize, the latency of the postural response to voluntary arm raise during locomotion is modulated. Although the voluntary perturbation were different, the phase dependent modulation was also found by Nashner and Forssberg [5]. The results of this study show that the responses may not always be anticipatory in nature, but are adapted to provide improved stability to carry out the task. Rather than categorizing responses to perturbations as feedforward or feedback induced, this study suggests that it may be more appropriate to treat them as functional adaptations.

#### REFERENCES

1. Massion, J. & Gahery, J. (1979). In Progress in Brain Research. 50: 219-226.
2. Bouisset, S. & Zatzara, M. (1981). Neurosci. Lett.

22: 263-270.

3. Lee, W.A. (1980). J. Motor Behav. 12: 185-196.
4. Cordo, P.J. & Nashner, L.M. (1982). J. Neurophys. 47: 287-302.
5. Nashner, L.M. & Forssberg, H. (1986). J. Neurophys.
6. Heuer, H. & Wing, A.M. (1984). In Psychology of Human Movement. 183-213.
7. Belanger, M. & Patla, A.E. (1984). Neurosci. Lett. 49: 291-295.
8. Winter, D.A. (1983). J. Motor Behav. 15: 302-330.

#### ACKNOWLEDGEMENTS

This work was supported by a grant from the National Science and Engineering Research Council of Canada. The author gratefully acknowledges the assistance of Marc Belanger.

## QUANTITATIVE ANATOMY OF TRUNK MUSCLES

DUMAS, G.A., Mech. Eng., Queen's University, Kingston, Canada  
 POULIN, M.J., Phys.Ed., Laval University, Quebec, Canada  
 ROY, B., Phys.Ed., Laval University, Quebec, Canada  
 GAGNON, M., Phys.Ed., University of Montreal, Montreal, Canada  
 JOVANOVIC, M., Anatomy, Laval University, Quebec, Canada

### INTRODUCTION

Load is one factor that may contribute to low back pain. In order to evaluate load on the lower lumbar spine, it is necessary to know the position and orientation of lines of action of trunk muscles with respect to it. This paper presents a method to obtain lines of action of nine trunk muscles and their moment arm lengths. Each muscle is represented as one or several either linear or curvilinear lines of action. The results obtained for one specimen are reported.

### REVIEW AND THEORY

Few attempts have been made to quantify the anatomy of trunk muscles. Rab<sup>1</sup> et al determined the successive cross-sections of seven trunk muscles. They also calculated the force developed by each muscle from the cross-section in order to compute the moments acting at the centre of the lumbar discs. However, because of the assumptions made in the evaluation of forces these results cannot be directly used. The method presented in this paper is intended to provide quantitative anatomical data on trunk muscles that can be used in modelling the loads on the lumbar spine.

Figure 1

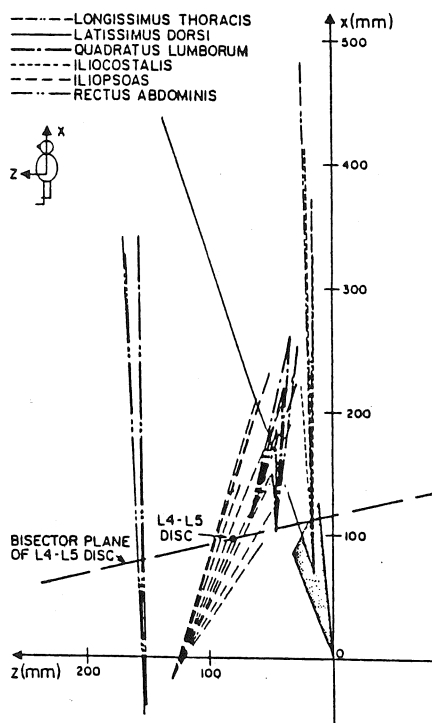
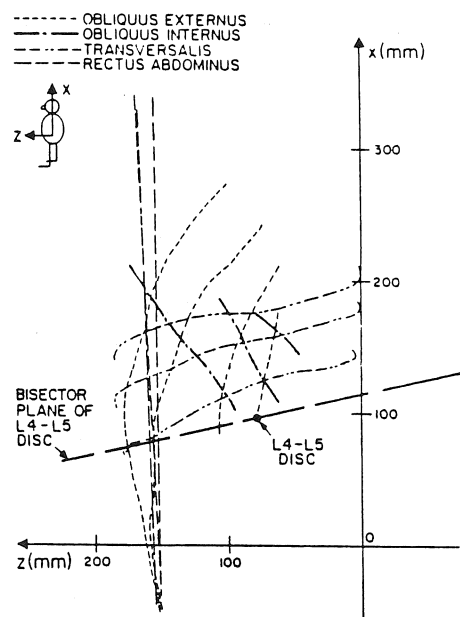


Figure 2



### METHODOLOGY

The nine muscles studied are: latissimus dorsi, ilio-costalis, longissimus thoracis, rectus abdominis, obliquus externus and internus, transversalis abdominis, quadratus lumborum and ilio-psyas. For each muscle, the origin and insertion points were localized and lines of action joining these points were defined (Figures 1 and 2). The origin of the latissimus dorsi, ilio-costalis and longissimus thoracis muscles was assumed to be the geometric centre of three points at the ends of the common insertion, located on the spinous processes of L3 and S3, and on the crest of the ilium. For the obliqui and transversalis muscles, curvilinear lines of action were assumed and points were taken along their lengths. Origin and insertion points and points along the length were digitized on embalmed cadavers. The dissection proceeded by removal of successive layers on the front and back faces of the specimen and each muscle was digitized using a 3-D digitizer built by Res Tech. The components of the unit force vector and the unit moment vector about the centre of the L4-L5 disc (according to Jensen's<sup>2</sup> definition) were calculated for each line of action. A reference frame related to the disc was used for these calculations: axis  $Ox$  is perpendicular to the bisector plane of the disc and oriented positively towards the head; axis  $Oy$  is perpendicular to the sagittal plane and oriented positively to the right;  $Oz$  completes the frame.

## RESULTS

Measurements were completed for one male, 39-year old embalmed specimen. The lines of action are plotted in Figures 1 (back muscles) and 2 (abdominal muscles). Components of unit force vectors and unit moment vectors are reported in Table 1.

## DISCUSSION

From Table 1, it can be seen that the highest component of the unit moment vector is generally related to the main expected contribution of the muscle. However, the contribution to other moments can also be important.

Not all lines of action of the quadratus lumborum and obliquus internus muscles intersect the bisector plane of the L4-L5 disc for this specimen

(Figures 1 and 2). This is due to the position of the crest of the ilium with respect to L4 and can be expected to vary among specimens. The lines of action of the transversalis muscle are nearly parallel to the bisector plane of the L4-L5 disc and therefore cannot contribute to flexion-extension or lateral bending moments.

The appropriateness of using a number of lines of action for each muscle was confirmed because variations were found in the associated moments. Two exceptions to this were the ilio-costalis and longissimus thoracis muscles where a single line representation would have sufficed.

## References

1. Rab, G.T. et al. Orthop. Clinics of North Am. 8: 193-199, 1977.
2. Jensen, R.H. et al. J. Biomech. 8: 103-110, 1975.

Table 1

MUSCLE	UNIT FORCE VECTOR			MOMENT PER UNIT FORCE (Nm/N)		
	F <sub>x</sub>	F <sub>y</sub>	F <sub>z</sub>	M <sub>x</sub>	M <sub>y</sub>	M <sub>z</sub>
LATISSIMUS DORSI	0.935	0.334	0.118	-21.0	46.4	35.2
OBLIQUUS EXTERNUS						
TO CREST OF ILIUM FROM						
COSTA IX	0.892	-0.424	-0.156	45.1	-86.8	21.3
COSTA X	0.827	-0.446	-0.342	59.0	-64.9	58.0
COSTA XI	0.839	-0.078	-0.539	64.6	-35.0	95.4
COSTA XII	0.906	-0.003	-0.423	46.8	-8.3	100.2
OBLIQUUS INTERNUS						
TO CREST OF ILIUM FROM						
COSTA X	*	*	*	*	*	*
COSTA XI	*	*	*	*	*	*
COSTA XII	*	*	*	*	*	*
RECTUS ABDOMINIS						
XIPHOID APPENDIX TO CREST OF OS PUBIS (EXTERNAL SIDE)	-0.975	0.044	0.220	-1.0	-74.5	-19.4
COSTAL CARTILAGE OF COSTA VI (EXTERNAL SIDE)	-0.977	0.108	0.182	+6.6	-79.3	-11.6
OF COSTA VI (INTERNAL SIDE)	-0.983	0.033	0.182	+4.0	-79.6	6.9
COSTA VI (EXTERNAL SIDE)	-0.969	0.186	0.163	+19.6	-80.4	24.7
ILIO-COSTALIS LUMBORUM						
CENTROID OF COMMON ORIGIN TO						
COSTA XII	0.948	-0.291	-0.125	-13.1	57.	33.7
COSTA IX	0.951	-0.237	-0.199	-8.4	60.2	31.6
COSTA VII	0.970	-0.151	-0.199	-3.9	60.9	28.5
LONGISSIMUS THORACIS						
CENTROID OF COMMON ORIGIN TO						
COSTA XII	0.969	-0.150	-0.198	-3.6	61.2	28.4
COSTA VIII	0.970	-0.120	-0.213	-1.7	61.8	27.2
COSTA IV	0.977	-0.078	-0.196	0.2	61.6	25.7
QUADRATUS LUMBORUM						
INTERNAL LIP OF CREST OF ILIUM						
EXTERNAL SIDE TO COSTA XII	*	*	*	*	*	*
INTERNAL SIDE TO COSTA XII	-0.935	0.101	-0.342	20.5	28.2	48.
EXTERNAL SIDE TO TRANSVERSE PROCESS OF L4	*	*	*	*	*	*
INTERNAL SIDE TO TRANSVERSE PROCESS OF L3	*	*	*	*	*	*
EXTERNAL SIDE TO TRANSVERSE PROCESS OF L2	*	*	*	*	*	*
INTERNAL SIDE TO TRANSVERSE PROCESS OF L1	*	*	*	*	*	*
INTERNAL SIDE TO TRANSVERSE PROCESS OF L4	-0.974	0.129	-0.187	13.4	28.7	49.9
INTERNAL SIDE TO TRANSVERSE PROCESS OF L3	-0.972	0.012	-0.237	12.6	28.8	50.2
INTERNAL SIDE TO TRANSVERSE PROCESS OF L2	-0.955	0.066	-0.289	16.9	28.6	49.2
INTERNAL SIDE TO TRANSVERSE PROCESS OF L1	-0.948	0.101	-0.302	18.6	28.4	48.7
ILIO-PSOAS						
TO COMMON COURSE MARK FROM						
L4 - L5 disc	0.785	-0.078	0.614	-24.	2.	-30.9
L3 - L4 disc	0.839	-0.056	0.543	-22.2	13.6	-35.7
L2 - L3 disc	0.852	-0.049	0.521	-21.8	17.0	-37.2
L1 - L2 disc	0.861	-0.059	0.506	-20.1	19.3	-38.5
T12 - L1 disc	0.851	-0.068	0.521	-20.1	17.	-35.1
TO COMMON COURSE MARK FROM						
L5	*	*	*	*	*	*
L4	0.721	-0.024	0.693	-32.2	-11.3	-33.1
L3	0.769	-0.014	0.639	-30.5	-1.7	-36.7
L2	0.783	-0.007	0.623	-30.2	1.1	-38.0
L1	0.811	-0.078	0.579	-22.4	7.7	-32.3
TRANSVERSALIS						
SUPERIOR LINE	*	*	*	*	*	*
MEDIAN LINE	*	*	*	*	*	*
INFERIOR LINE	0.137	-0.926	-0.352	100.2	-13.6	3.2

\* THIS LINE OF ACTION DOES NOT INTERSECT THE BISECTOR PLANE OF THE DISC.

# CORRELATION OF OBJECTIVE MEASURES OF TRUNK MOTION AND MUSCLE FUNCTION WITH LOW BACK DISABILITY RATINGS

John Triano, MA, DC  
Patient Research Center  
National College  
Lombard, Ill. 60187

A.B. Schultz, PhD  
Mechanical Engineering  
University of Michigan  
Ann Arbor, Mi. 48109

## INTRODUCTION

The present study was undertaken to examine relations among some objective and subjective measures of low-back-related disability. Objective measures of ranges of trunk motions, intrasubject ratios of lumbar trunk muscle voluntary strengths in attempted extension to those in attempted flexion, and of the presence or absence of the flexion-relaxation phenomenon in the back muscles were obtained in a group of 41 low-back-pain patients and in 7 pain-free control subjects. Subjective measures of disability were obtained from Oswestry patient questionnaires; and the objective and subjective measures were compared.

The Oswestry disability score related significantly ( $p < .01$ ) to the presence of relaxation in back muscles while fully flexed. Similarly, mean extensor/flexor trunk strength ratios were inversely related to the disability score ( $p < .05$ ). Range of trunk mobility was meaningfully reduced ( $p < .01$ ) in patients with higher disability scores. Despite loss of motion, a large enough excursion was observed to predict presence of back muscle relaxation in all but three patients. These findings imply that, under conditions similar to those described here, myoelectric signal levels, trunk strength ratios, and ranges of trunk motion may be used as objective indicators of low-back-pain disability.

## REVIEW AND THEORY

Intrasubject trunk strength ratios in low back pain patients reported (1,2). McNeill, et al, found healthy control subjects to have a mean ratio of voluntary strength in trunk extension to that in trunk flexion of 1.37, while low back pain patients had a mean ratio of 0.90. Sixteen male patients needing hospitalization for low back pain, to have a mean ratio of 0.62.

The flexion-relaxation phenomenon refers to the diminishment of myoelectric activity in the back muscles upon substantial forward bending of the trunk while standing. Schultz, et al (3) reported readily-detectable flexion-relaxation even upon only 40 degrees of lumbar trunk flexion in healthy subjects. In two of the earlier reports (4,5) on the phenomenon, found no relaxation of back muscle myoelectric activity upon flexion in patients with low back pain. These reports did not describe whether partial absences of the flexion-relaxation phenomenon were observed.

There are number of methods for subjective evaluation of disability due to low back pain (6,7,8,9). The Oswestry questionnaire is simple to administer, internally consistent, and has a high test-retest reliability. Ranking of responses to ten questions with respect to limitations of routine daily activities imposed by low back pain permits calculation of a subjective 'disability' score for comparison with other measures.

## METHODS

Tests were performed on 19 males and 23 females 22 to 59 years of age. Forty-one of these complained of low back pain with or without leg pain, and seven were volunteer control subjects. The Oswestry Disability Questionnaire was completed by each individual to provide a subjective rating of limitation in performance of daily activities. Location of pain recorded to

categorize their discomfort as being in the low back, leg, or combined low back and leg pain.

The range of trunk motion in standing flexion and extension was measured by inclinometer in each subject without aggravation of pain. The subjects then performed six other tasks: stand relaxed; stand with trunk flexed maximally; and exert maximal isometric strengths against resistance from the upright position, in both attempted trunk flexion, and trunk extension.

During performance of the standing flexion range of motion task and latter six tasks, trunk muscle myoelectric activity was picked up by four pairs of bipolar surface electrodes. Two pairs were placed bilaterally, over the erector spinae muscles and over the rectus abdominus muscles. Rectified and integrated myoelectric signals were used to quantify muscle action.

Subjects stood in a comfortable position within a testing frame. The pelvis was strapped to a posteriorly-placed support and knee flexion hindered by a strap. The subject then attempted to bend the trunk against the resistance of a fixed load cell in both flexion and extension. Subjects were coached to ensure maximal force production, but instructed to cease exertion if too painful. Intra-individual trunk muscle strength ratios were determined by dividing the force developed during attempted extension by that in attempted flexion.

Patients were grouped for analysis according to the presence or absence of flexion-relaxation upon trunk bending; that is, near silence of the myoelectric signals in the back muscles. This analysis compared Oswestry scores, strength ratios and motion ranges among these three groups.

## RESULTS

Twenty-three of the 41 patients with complaints of low back or leg pain and all seven of the control subjects exhibited normal flexion-relaxation; that is, myoelectric activities in their back muscles substantially diminished upon full trunk flexion. In the remaining 13 patients, flexion-relaxation was absent. (Table 1.)

Control and relaxation-present subjects showed three separate phases of back muscle activity; while bending forward, while fully-flexed and while rising to the upright. Relaxation-absence was readily identified by persistence of marked myoelectric activity during full flexion. Relaxation-absent subjects showed an unequal response in paraspinal activity at full flexion. Larger myoelectric signals were found on the painful side in two-thirds of these subjects.

Oswestry disability scores related significantly to the presence of relaxation. Relaxation-absent subjects had a mean score of 15.7, while relaxation-present subjects had a mean score of 5.76 ( $p < .001$ ). Findings as to trunk strength ratios were similar. The relaxation-absent group had a mean ratio of 0.74, the relaxation-present group had a mean ratio of 1.07, and the healthy controls had a mean ratio of 1.35. Statistically, all three of the relaxation-present/relaxation-absent/control pair differences were significant ( $p < .05$ ).

Grouping of subjects by pain distribution is shown in Table 2. Mean values for Oswestry and extension/flexion ratio tend to be more severe for leg complaints, the low back, or low back and leg complaints. Owing to the small number of subjects with this category of complaint and the high intersubject variability, the results are not statistically significant.

Controls had a mean trunk extension of 33 degrees and a mean trunk flexion of 109 degrees (Table 3). Relaxation-present

subjects had a mean extension of 29 and a mean flexion of 102 degrees. Relaxation-absent subjects were noticeably less mobile. Mean extension was 21 degrees while mean flexion was 71 degrees. Relaxation-absent /relaxation-present and relaxation-absent/control differences were significant ( $p < .01$ ).

#### DISCUSSION

Presence or absence of flexion-relaxation in the paraspinal lumbar muscles, the extensor/flexor strength ratio and the range of trunk motion corresponded approximately to the Oswestry score. Several reasons might be given to explain the absence of flexion-relaxation. First, relaxation of myoelectric activity during trunk flexion is dependent upon the amount of flexion. Schultz, et al (1955) found relaxation to begin at 40 degrees of flexion. A subject might voluntarily constrain flexion to a range insufficient to produce relaxation. Review of the inclinometer measurements showed that was not the case in our study. While relaxation-absent subjects had smaller ranges of both extension and flexion compared to controls and relaxation-present subjects, all subjects flexed their trunks beyond 40 degrees. Second, muscle contraction may persist beyond 40 degrees of flexion as a volitional or reflexive reaction to pain. Despite instructions to cease bending at the onset of substantial pain, pain was sometimes reported during the performance.

Flexion-relaxation presence implies that the structural loads are being transmitted primarily by the ligamentous and articular passive tissues of the spine. Persistent activity, reflecting persistent muscle contractions, may serve to transmit loads through muscles rather than through injured spinal ligamentous tissues in an effort to avoid increased pain.

Attempted extension/flexion trunk muscle strength ratios also appeared to be sensitive to the degree of disability. As Oswestry scores increased, the strength ratio mean values monotonically decreased ( $r = -.32$ ). Rarely did the presence of substantial pain associate with an extension/flexion strength ratio as large as those in control subjects. In three cases, ratio values were within one standard deviation of the control mean. Above an Oswestry score of 12 only one subject had an extension/flexion ratio greater than 1.2.

#### References

1. McGill R, et al : Spine 5: 529-533, 1975.
2. Addison R, Schultz A: Spine 5: 535-544, 1980.
3. Schultz AB, et al : J Orthop Res 3(2): 135-197, 1985.
4. Golting JB: Postgraduate Medical Journal 28: 401-406, 1952.
5. Lloyd R, Silver P: J Physiol 122: 154-232, 1955.
6. Leiman TR, et al : Spine 8: 300-315, 1983.
7. Fairbank JC, et al: Physiotherapy 65(3): 271-273, 1983.
8. Mansford A, et al: Spine 1: 127-134, 1976.
9. Roland M, Morris R: Spine 8: 141-150, 1983.

Table 1.

	WHILE BENDING	FULLY- FLEXED	WHILE RISING
Relaxation- absent	52(23)	48(34)	81(51)
Relaxation- present	41(16)	7(8)	98(33)
Control	30(13)	2(4)	82(33)

Myoelectric activity of erector spinae muscles for all three phases of the flexion event expressed in microvolts.

Table 2.

Pain Site	Oswestry Score	Trunk Strength Ratio	n
Low back	10.5 (9.0)	1.0 (.40)	28
Leg	16.3 (11.6)	.83 (.24)	8
LB & Leg	10.4 (8.8)	1.02 (.30)	5

Oswestry scores and trunk strength ratios for subjects grouped by site of complaint. Parentheses indicate standard deviation.

Table 3.

	CONTROL	RELAXATION PRESENT	RELAXATION ABSENT
Extension	33(8)	28(8)	20(7)
Flexion	109(12)	101(22)	71(27)

Range of motion in degrees.

# EFFECTS OF CHANGE IN INTRADISCAL FLUID CONTENT ON MECHANICAL RESPONSE OF A LUMBAR MOTION SEGMENT IN COMPRESSION AND EXTENSION

A. SHIRAZI-ADL, G. DROUIN  
Department of Mechanical Engineering  
Ecole Polytechnique de Montréal  
Montreal, Quebec, Canada, H3C 3A7

## INTRODUCTION

Previous analytical and experimental studies have indicated that disc pressure plays a significant role in the mechanical response of a lumbar motion segment when subjected to different loadings (1-6). An alteration in the magnitude of the intradiscal pressure (or intradiscal volume) is bound to affect the overall response as well as the states of stress and strain in the various elements of the segment. Such conditions are expected to take place in the events that the nucleus material is dissolved or removed, and that a fluid injection or loss occurs. The purpose of the present work is the analytical determination of the mechanical effects of change in volume of the intradiscal fluid on the response of a lumbar motion segment when subjected to compression alone and combined with extension. In this paper, both an increase and a decrease in the volume of the intradiscal fluid are considered.

## METHOD

The analysis utilizes a general three dimensional finite element program which has been previously used for the study of the segment under compression, sagittal plane moments and axial torque (3-5). The details of the finite element model of the lumbar L2-3 joint including the posterior elements and the analytic formulation have been reported elsewhere (4). For the sake of the present study, formulation of the solid-fluid interaction has been modified to account for an induced change in the volume or pressure of the cavity which is filled with an inviscid fluid and enclosed by a solid. The previous nonlinear contact problem has also been modified to yield the magnitude and direction of the contact forces generated during the articulation of the facets. The axial forces transmitted through the disc itself are evaluated by means of employing stiff vertical links supporting the lower vertebral body.

The loadings considered in the present paper consist of the axial compression acting alone and in combination with the extension moment. These loads are initially increased by incremental steps reaching maximum values of 1000 N in compression and 12 N-m in extension. The analysis is then followed by considering for a loss of or gain in the nucleus material reaching incrementally to a maximum value of about 0.9 cc or 15% of its initial volume occurring while the applied loads remain constant.

## RESULTS AND DISCUSSION

The predicted variations of the percentage changes in the average axial displacement and in the intradiscal pressure with the relative change in the nucleus volume under a constant axial force of 1000 N are shown in Figure 1. As expected, the intradiscal pressure is seen to rise as the fluid volume increases and to drop as it decreases. The rate of change in the pressure is noticed to be larger in the former than in the latter case. A similar variation in the

disc pressure is computed when an extension moment of 12 N-m is also present. Variation of the change in the average axial displacement (as a percentage of its initial value of 0.77 mm) with the change in fluid volume is seen to be contrary to that of the pressure. This is due to the effect of the change in the fluid volume on the disc pressure and hence on the disc axial stiffness. However, the effect of the change in nucleus volume on the segmental sagittal rotation is found to be small (<15%).

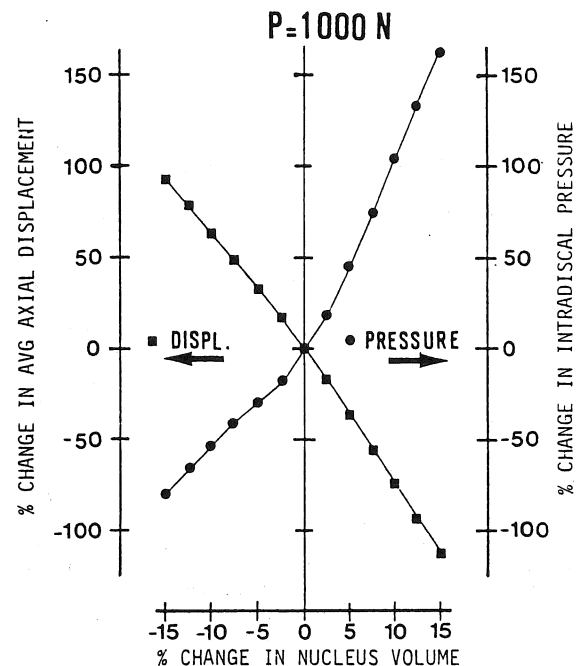


Fig. 1. Variation of the predicted % changes in average axial displacement and in intradiscal pressure with % change in nucleus content under  $P = 1000$  N.

Figure 2 shows the predicted variations of the maximum tensile strains in the disc fibres and annulus bulk (in the radial direction) with the relative change in the nucleus volume under constant loads of 1000 N compression and 12 N-m extension. These maximum strains are found to occur in the disc fibres mainly at the anterior location in the innermost layer and in the annulus bulk at the posterior location in the outermost layer. Reduction in the fluid volume and hence disc pressure tends to have a decreasing effect on the tensile strains in the disc fibres while an increasing effect on the radial tensile strains in the annulus bulk.

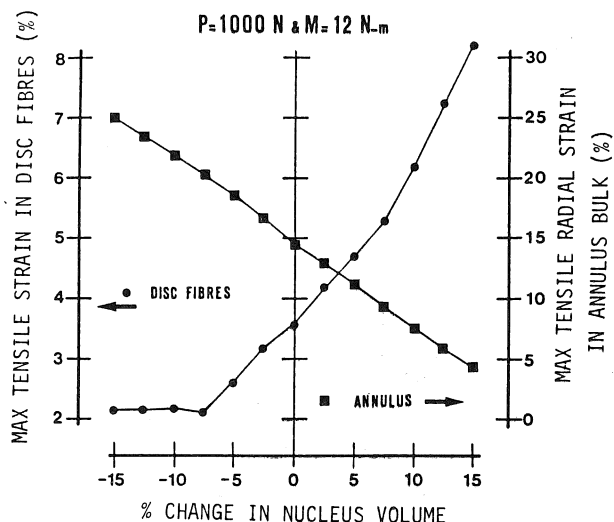


Fig. 2. Variation of the predicted maximum tensile strains in the disc fibres and in the annulus bulk (at radial direction) with % change in nucleus content under  $P = 1000$  N and  $M = 12$  N-m.

The forces are transferred from the upper vertebra to the lower one via the vertebral body and the disc, articulation at both facets and the capsular ligaments. The remaining posterior elements for the loadings considered in this study remain unstressed. Figures 3 and 4 show the predicted variations of the axial forces carried by the disc, articular surfaces of both facets, and the capsular ligaments with the relative change in the fluid volume under compression with and without extension respectively. The axial forces in these figures are expressed as a percentage of the externally applied compression of 1000 N. Figure 3 shows that, under an axial compression of 1000 N, the disc carries a significant portion of the compression and that the remaining compression is transmitted through the articular surfaces while the capsular ligaments remain unstressed. Moreover, loss of nucleus volume tends to reduce the share of the disc while to increase that of the facet articulation. Comparison of the results shown in Figures 3 and 4 clearly indicates that the facet joints carry a significant share of the axial force in the presence of a 12 N-m extension moment (nearly 4.0 degrees extension rotation). Furthermore, the effects of the change in the fluid volume on the axial forces carried by the disc and the facet joints become more pronounced when the extension moment is added to the compression force.

#### CONCLUSIONS

The present study predicts that: 1) A change in the nucleus pressure is directly associated with a change in the fluid volume. 2) There is a significant increase or decrease in the disc axial stiffness as the fluid volume increases or decreases respectively. 3) The rates of change in the disc pressure and the axial displacement are larger when the fluid volume increases than when it decreases. 4) An increase in the fluid volume increases the maximum tensile strains in the disc fibres and reduces them in the annulus bulk in the radial direction. Opposite trends are found when the fluid volume decreases. 5) The axial contact forces developed during articulation of the facets increase noticeably when the disc loses its fluid and/or when the extension moment is present.

6) Under compression alone, the capsular ligaments do not carry any portion of the external force even if the fluid content changes. However, in the presence of fluid loss and extension moment, they carry a fair percentage of the compressive force. 7) The effects of the change in the fluid content on the axial forces carried by the disc, articular surfaces, and capsular ligaments become more pronounced when extension moment is added to the compression force.

**Acknowledgement:** The research work is supported by NSERC (Canada).

#### References:

1. Andersson, G.B.J., et al. *J. Biomech.* 12: 453-458, 1979.
2. Panjabi, M.M., et al. *Spine* 9: 707-713, 1984.
3. Shirazi-Adl, A., et al. *Spine* 9: 120-134, 1984.
4. Shirazi-Adl, A., et al. *J. Biomech.*, in press.
5. Shirazi-Adl, A., et al. *Spine*, in press.
6. Spencer, D.L., et al. *Spine* 10: 555-561, 1985.

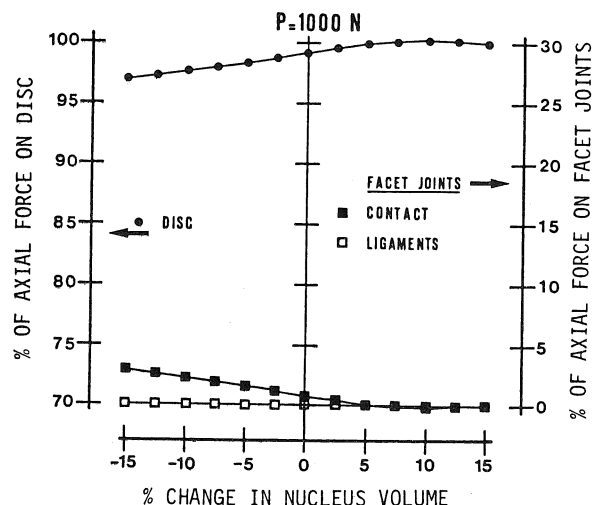


Fig. 3. Variation of the predicted axial forces taken by the disc and by the facet joints (as a % of applied axial force) with % change in nucleus content under  $P = 1000$  N.

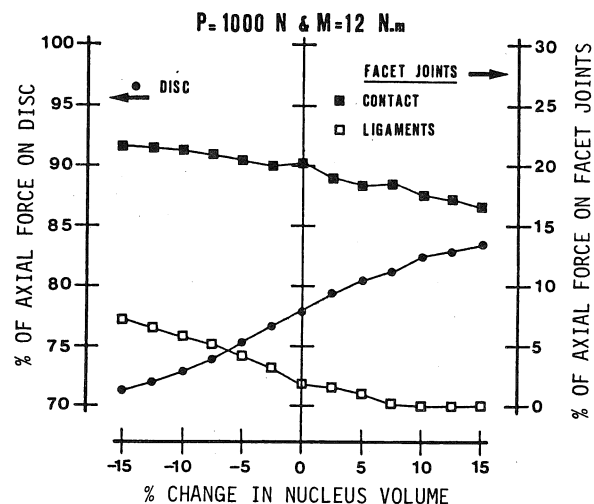


Fig. 4. Variation of the predicted axial forces taken by the disc and by the facet joints (as a % of applied axial force) with % change in nucleus content under  $P = 1000$  N and  $M = 12$  N-m.

# FAILURE OF INTRA-ABDOMINAL PRESSURIZATION TO REDUCE ERECTOR SPINAE LOADS DURING LIFTING TASKS

M. H. Krag, K. B. Byrne, L. G. Gilbertson, and L. D. Haugh  
Vermont Rehabilitation Engineering Center  
The University of Vermont, Burlington, Vermont 05405

## INTRODUCTION

Abdominal pressurization by tensing the trunk muscles has long been hypothesized to produce a trunk extension moment, reducing erector spinae tension and disc/vertebral body compression (1,2). Although this concept is the rationale for widely-used low back pain treatment regimens, only one recent study done in this laboratory has tested the hypothesis directly (3).

## METHODS

Ten healthy, male subjects (ages 20-35) performed isometric, isotonic trunk extension efforts at 33%, 66%, and 90% of each subject's maximum voluntary effort, in both an upright (0°) and flexed (45°) posture. The following measurements were recorded: effort, right and left erector spinae surface EMG at L3, and intra-abdominal pressure (IAP, via nasogastric tube). Three different pressurization modes were used: natural or "uncoached", increased (maximum valsalva maneuver), and decreased (relaxed, slow inspiration or expiration to maintain an open glottis). Two different pressure modes were performed for five seconds each during a single, constant 10 second trunk extension effort. Various pairs of pressure modes were used for each posture and effort level. A calibration curve of effort vs. EMG was recorded for each subject and posture before the experiment.

The data were recorded onto FM tape. The tape channels were later fed into an IBM PC/XT computer at 50 Hz using an A/D converter. The two EMG channels were processed using an analog RMS/DC converter prior to data acquisition. A three-second constant force segment was then visually selected from each of the two five-second segments of each 10 second effort. Mean effort, EMG, and IAP were obtained by rectifying and integrating over each three-second segment. The right and left EMG were then averaged. In order to combine the results across subjects, the EMG's (in volts) were converted to percent maximum voluntary effort units (%MVE) using the calibration curves for each subject.

## RESULTS AND DISCUSSION

Consistent with previous reports, an approximately linear relationship between %MVE and EMG was found during uncoached extension efforts. A similar relationship was found between %MVE and IAP. However, when IAP is deliberately altered, a different conclusion must be considered. Figure 1 presents the change in EMG vs. change in IAP for both relaxed and valsalva pressures relative to the uncoached mode, for all subjects at all effort levels and postures. Points on the left side of the Y-axis represent tests in which the volunteers attempted to relax their abdominal muscles, thus reducing their IAP below uncoached levels. Points on the right side of the graph represent tests in which the volunteers attempted to increase their IAP above uncoached levels. Because not all the subjects were able to produce

relaxed pressures below that of their uncoached pressures, somewhat more than half of all the data points are to the right of the Y-axis. A linear regression of the data has been plotted on the graph, as well as a 90% confidence band for the position of that linear regression line.

Table 1 presents the mean and standard deviations of the slopes of the linear regression lines for each effort level and posture separately, and for the regression line of the combined data that are shown in Figure 1. A 95% confidence limit for each parameter of the regressions is also included. Note that the slopes of the lines at all effort levels and postures are very close to zero.

## CONCLUSIONS

1. During isometric, isotonic extension efforts using a natural or "uncoached" IAP mode, increases in effort do result in increases in both EMG and IAP, as previously reported.
2. Contrary to widespread belief, deliberate changes (either increase or decrease) in IAP during constant trunk extension effort do not result in significant changes in erector spinae EMG, and thus do not produce significant reduction in back muscle tension.
3. Further testing of low back pain subjects and the role, if any, of lumbosacral support is in progress.

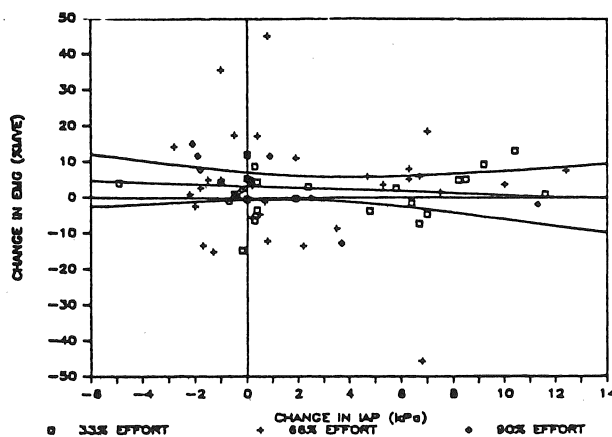


Figure 1. Change in EMG vs. change in IAP for all postures and effort levels.



Table 1

95% Confidence Limits of Slope and Intercept  
of Linear Regression Lines for Change in IAP  
vs. Change in EMG for Each Posture and Effort Level

Posture	Effort	Slope	95% Conf.	Intercept	95% Conf.
UPRIGHT	33%	0.24	±0.61	1.41	±3.05
UPRIGHT	66%	0.08	±1.71	0.59	±2.44
UPRIGHT	90%	-2.10	±14.85	8.24	±2.20
FLEXED	33%	0.03	±1.84	0.37	±3.55
FLEXED	66%	-1.23	±3.69	9.39	±13.78
FLEXED	90%	-0.85	±4.55	2.53	±27.39
ALL POINTS		-0.25	±0.74	3.20	±3.26

#### References

1. Bartelink DL. (1957) The role of abdominal pressure in relieving the pressure on the lumbar intra-vertebral discs. J. Bone Joint Surg. 39B:718-25.
2. Morris JM, Lucas DB, & Bresler B. (1961) Role of the trunk in stability of the spine. J. Bone Joint Surg. 43A:327-51.
3. Krag MH, Gilbertson L, & Pope MH. (1985) Intra-abdominal and intra-thoracic pressure effects upon load-bearing of the spine. Orthopedic Research Society 31st Annual Meeting, Las Vegas NV.

#### Acknowledgement

This research was supported by a grant from the National Institute of Handicapped Research, U.S. Dept of Education (#G008303001-03) and by Camp International, Inc.

MH Pope\*, DG Wilder\*, L Jorneus+, H Broman\*\*\*, M Svensson\*\*\*, G Andersson\*\*\*\*

\*Orthopaedics & Rehabilitation, Given Bldg., University of Vermont, Burlington, VT 05405 USA; \*\*Ort. Kir. 1, Sahlgrenska Sjukhuset, Goteborg, Sweden; +Chalmers Technical University, Goteborg, Sweden; ++Department of Orthopaedics, Rush Presbyterian - St. Luke's Hospital, Chicago, Illinois USA

## INTRODUCTION

Low back pain and degenerative diseases of the spine have been shown by many studies to occur more frequently amongst vehicle drivers than in representative control groups (5,7,8,10,12,13,15,20). Thus, there has been great interest in measuring the transmission of vibrations through the human body.

## REVIEW AND THEORY

The majority of these studies have utilized accelerometers at the head and at the seat surface so as to establish the mechanical response of the system (3,4,17,24). Usually accelerations at either a helmet or a bitebar are measured and related to input at the seat to give the transmissibility (transfer function). These studies give valuable information about the overall response of the subject, but only indirect information about the response of various segments of interest, for example between the seat and the pelvis, and between the pelvis and different parts of the lumbar spine. For these reasons, there have been a limited number of attempts to measure vibration directly at the regions of interest. Much of the literature regarding the response to vibration is contradictory. Some different results can be attributed to different experimental techniques, but not all. Some workers report considerable differences in biodynamic response between human subjects under the same experimental conditions (9,11,24). In addition, even similar experimental conditions have produced different results (2,6). An attempt has been made to resolve some of these contradictions by investigating the relative response as measured by transducers mounted to the body surface compared to those rigidly attached to the skeleton (18). The present study is a comprehensive investigation of the response to the spine to both impact and sinusoidal excitation, looking at both the overall and regional responses of the system.

## METHODOLOGY

The sinusoidal apparatus is a resonating system consisting of two parallel wooden beams, simply supported, that can vibrate (16). The spinal impact apparatus consists of a platform suspended by eight rubber springs (designed for use as spring lines when docking boats) and guided by two linear bearings. Ten subjects (five males, five females) were evaluated for their seated mechanical response using the two different methods described above. Anthropometric data were obtained for each subject at the time of the test. The subjects were aged between 18 and 45, weighed between 65 and 90 kg, and were free of low back pain and other health problems. Two different postures were maintained by the seated subjects. The mechanical response was determined by recording the measured acceleration versus time at both the seat and at a bite bar held in the subject's teeth. Transfer functions could then be determined for each subject. The sinusoidal excitation device was used to expose

subjects to both postures and vibrations of  $1 \text{ m/s}^2$  at discrete frequencies, from 2 to 14 Hz. Fifteen seconds of data were recorded at each of the vibration exposures. The vibrator was adjusted to produce the discrete vibrations by adjusting the input displacement and frequency at an eccentric displacement drive and by adjusting the end support locations of wooden beams on which the seat was placed. Two series of tests were run using the spinal impactor. In each series, the two postures (erect and relaxed) were studied. In the second series, the subjects listened to light music via lightweight headphones in order that they have no aural cue as to the release of the impact mechanism. Ten repeats were recorded in each of the two postures.

## RESULTS

In each comparison, the response is always similar. Between the impact and sinusoidal methods, it was a consistent finding that, in the 2-4 Hz region in the erect postures, the magnitude of the vibration response exceeds that of the impact response. Also, in each of the vibration and impact magnitude comparisons (in the 2-4 Hz region), the relaxed posture exhibits a greater magnitude than the erect posture. In the 4-8 Hz region, the vibration magnitude is greater than the impact response. Conversely, the impact response exceeds the vibration response in the phase spectrum of the 4-8 Hz region for the erect posture and for the phase spectra in the 8-16 Hz region, for the relaxed posture. Posture has a more consistent effect. Excepting the magnitude spectrum in the 2-4 Hz region, the erect posture response was always greater than the relaxed posture response for both the magnitude and phase spectra in all of the 2-4 Hz, 4-8 Hz, and 8-16 Hz regions.

## DISCUSSION

There are considerable advantages in the impact method. The method provides rapid testing over a large frequency range; the method could be made portable; it is easy to use and it is straightforward to change test variables, such as posture, muscular contraction and seat characteristics. In this paper, we have validated the impact method by comparing the results with sinusoidal excitation.

## CONCLUSION

An impact apparatus has been tested and proved to be useful in the study of mechanical responses of the seated subject. The response has been compared to that of sinusoidal excitation. Certain differences in response are attributed to the role of the musculature. Further work is indicated.

## ACKNOWLEDGEMENT

The authors wish to acknowledge the support of the Swedish Work Environment Fund and the National Institute of Handicapped Research (U.S. Department of Education).

## References

- 1 Adams, MA et al., *Spine* 10(6): 524-531, 1985.
- 2 Broderson, AB, et al., ASME Publ. No. 71-WA/BHF-8 (AMRL-TR-71-67), 1971.
- 3 Coermann, RR, *Human Factors* 4:227-253, 1962.
- 4 Dieckmann, D, *Int Z Ang Physiol Arbeitsphysiol* 16:519-564, 1957.
- 5 Dupuis, H et al, Max Plank Inst, Bad Kreuznach, Heft A 72/2, 1972.
- 6 Edwards, RG et al, *J. Biomech.* 9:55-61, 1976.
- 7 Frymoyer, JW et al, *Spine* 5:419-423, 1980.
- 8 Frymoyer, JW et al, *J. Bone Joint Surg.* 65A(2):213-218, 1983.
- 9 Garg, DP et al, *IEEE Transactions on Systems, Man, and Cybernetics*, Vol. SMC-6:102-112, 1976.
- 10 Gearhart, JR, *Aviat. Space Environ. Med.* 49:253-256, 1978.
- 11 Griffin, MJ et al, *AGARD Conf. Proc. No. 253*, p. A28-1 to A28-18, 1979.
- 12 Gruber, GJ et al, US DHEW (NIOSH) Contract No. HSM-00-72-047, 1974.
- 13 Heide, R et al, *Z. ges. Hyg.* 24:153-159, 1978.
- 14 ISO 2631-1978 (E), International Organization for Standardization, Ref. no. ISO 2631-1978 (E).
- 15 Kelsey, JL et al, *Am J. Epid* 102:63-73, 1975.
- 16 Panjabi, MM et al, In proceedings: 30th Orthop Res Soc, Atlanta, 7-9 Feb 1984, pp 205.
- 17 Pope, MH et al, Meeting Brit Orth Assoc and Inst Mech Eng, U.K., 1980.
- 18 Pope, MH et al, Accepted by *J. Biomech.*, 1985.
- 19 Quandieu, P et al, *J. Biomech.* 15:985-1006, 1982.
- 20 Rosegger, R et al, *Arch. Landtechn.* 2:3-65, 1960.
- 21 Sandover, J, *Spine* 8:652-658, 1984.
- 22 Schulte-Wintrop, HC et al, *AGARD-CP-255*, 1978.
- 23 Slonim, AR, *ARML - TR-81-153*, 1983.
- 24 Wilder, DG et al, *Spine* 7: 243-254, 1982.
- 25 Wilder, DG, University Microfilms International, Ann Arbor, MI, 1986.
- 26 Zagorski, J et al, *Acta Physiol Pol* 27(4):347-354, 1976.

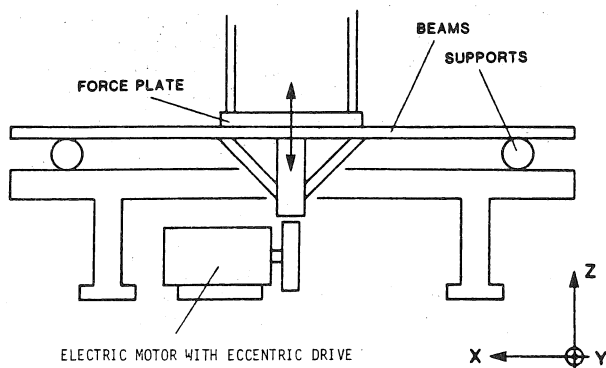


Figure 1. Vibration apparatus

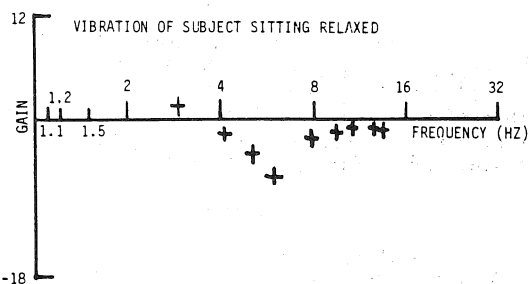


Figure 3. Response of a seated subject to discrete vibrations.

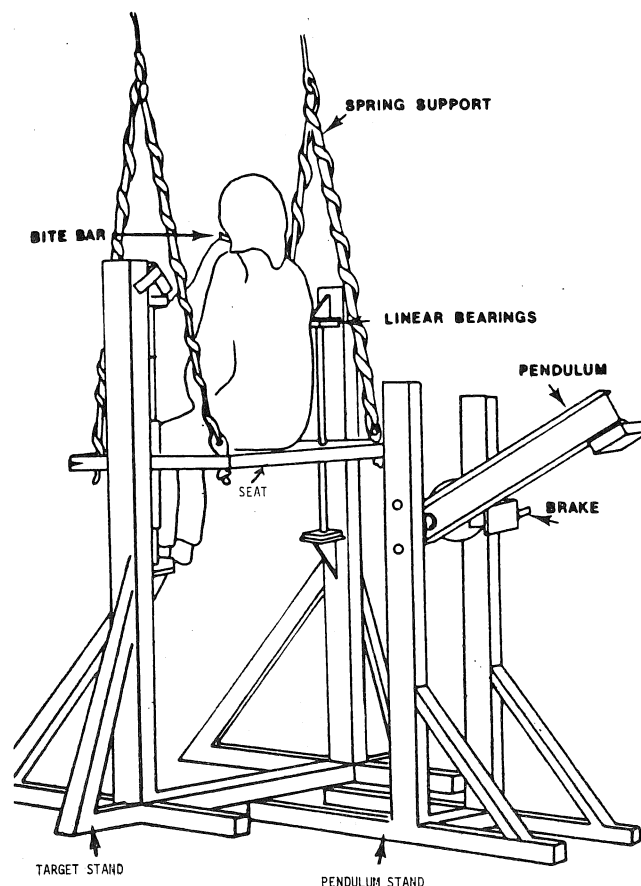


Figure 2. Impact apparatus

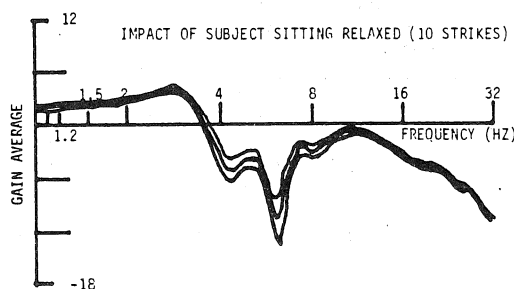


Figure 4. Response of a seated subject to impact.

# ENERGY TRANSFERS IN THE SPINAL ENGINE

S.A. Gracovetsky and S. Iacono  
Concordia University and Diagnostics Research Inc.  
Montreal, Quebec, Canada

## INTRODUCTION

The most common and repetitive voluntary movement performed by humans is gait. While biomechanical analyses of gait traditionally begin with a systematic measurement of limb motion, a problem arises when all data are combined in order to explain the mechanism that makes us walk. Various patterns invariable with walking speeds have been identified and discussed, although little explanation for the origins of these traits is given.(1)

The purpose of this paper is to examine an earlier hypothesis that the spine is the basic engine for human locomotion in which it is suggested that the spine drives the pelvis, and the legs follow the spinal motion. One can show through mathematical analyses that the power variation incurred by the transfer of spinal energy to the pelvis is markedly similar to the variations of power at the hip described by others during their analyses of leg motion.

## REVIEW AND THEORY

According to the current theories of bipedal locomotion, the legs do all the work. Cavagna et al. (2) proposed that mechanical components account for up to 50% of the energy used, although no direct evidence has been supplied. Others have evaluated this storage in the elastic deformation of material to be about 25%. In all of these studies, no provisions have been made for a possible spinal contribution towards the energy transfer occurring between segments, although it can be calculated that the very large posterior ligamentous system should be able to store an amount of energy comparable to the potential energy variation of the centre of gravity at each cycle. (3)

We have reservations in accepting many previous models, as we see that the motion of the pelvis, spine and shoulders cannot be hampered without disturbing the locomotive process. For example, gait modifications have been noted to be prevalent in persons with fused spines. Vertical displacement of the centre of gravity of the body becomes incomprehensible. Why not flex the knees more to clear the ground rather than lift the entire trunk? Newton's law of motion encourages the smoothest possible trajectory for the centre of gravity. There must be some clear evolutionary advantages to such strong interactions with Earth's gravitational field.

From a philosophical point of view, only with great difficulty do we think of the trunk, arms and head as "passive" elements in the locomotion process. It would be a waste of muscular mass not to use them in some essential way instead of having to drag them about while walking or running.

It is this desire to explore the essentials of vertebrate locomotion that led us to propose a somewhat unconventional theory of locomotion.(4)

We proposed that the spine is the essential component in vertebrate locomotion, and proceeded to analyse the kinds of spinal motion that will manoeuvre an animal in its environment. We supported the idea that the primitive lateral flexion of the spine, inherited from our piscatory ancestors, had to be complemented by the acquisition of flexion-extension in order to permit the quadruped to gallop.

As early as 1903, Lovett demonstrated that a flexible rod, already bent in one plane, will induce an axial torque when simultaneously flexed in a different plane. (5) This fundamental property has been exploited by the human spine. The combination of lateral flexion and flexion-extension of the spine, together with spinal lordosis, has been experimentally demonstrated to generate an axial torque that can be estimated as sufficient to drive the pelvis. (4) Once the pelvis is driven, one can argue that the legs will follow.

Admittedly, the evidence presented above is insufficient. This paper will develop further arguments to support the theory.

## METHODOLOGY

The mathematical model used in this analysis is limited to the dynamic response of an intervertebral joint made up of the disc and two adjacent vertebrae. The motion of this physical system during locomotion during locomotion has been derived from the experiments of Thurston and Harris.(6) Differential equations, characterizing the relation between joint motion and the forces necessary to induce the motion, and modelling of the forces and inertia acting upon the L<sub>4</sub> joint can be derived from the work of Cappozzo and many others. (6,8)

We fed the experimentally-determined inertial forces and displacements into the differential equations describing the system response. By expressing the conservation of energy during all phases of joint motion, we calculated the instantaneous power flowing through the joint during all sequences of gait, for walking speeds varying from 1 m/sec to 2.16 m/sec.

The axial torque  $T_{joax}$  that an intervertebral joint can resist in the static case when axially rotated is a function of the axial compression applied to the joint.(8) The relative contribution of the facet and disc to the static torque strength is shown in Figure 1.

In the dynamic case, because of the visco-elastic properties of the annulus,  $T_{joax}$  must be a function of the angular displacement, its rate of change and axial compression (Figure 2). The dynamic case can be derived by assuming that the ability of the facets to oppose  $T_{joax}$  does not depend on  $d\phi/dt$ , but solely on compression and axial displacement  $\phi$ . This assumption also implies that the axis of rotation will not move into the canal.(9)

During locomotion, the total torque present at the joint is a sum of  $T_{joax}$  and the torque necessary to overcome the force of inertia. The torque at the joint caused by inertia has been analysed by Cappozzo.(7) Hence, it is possible to calculate the instantaneous torque once the displacement of the joint is known. Thurston and Harris collected this information in an earlier study.(6)

## RESULTS AND DISCUSSION

Having calculated the instantaneous torque necessary for the motion of the joint in the sagittal, transverse and horizontal planes, the respective energies can be calculated by integrations.

As the walking sequence progresses, the spine flexes/extends, bends laterally, and induces an axial torque. (5) The corresponding torques and levels of energy can be shown to obey the following relation (within 3% accuracy):

$$E_{sag} = E_{lat} = E_{ax}$$

That is to say, the energy spent in sagittal motion is recovered during lateral and axial motion. This suggests the actual losses are, indeed, very small, and the system is nearly perfect from the point of view of energy conservation.

It also suggests that energy is transferred and converted from potential to kinetic. This energy is then used to force the spine to bend laterally, which in turn induces the axial rotation required to rotate the pelvis during walking. It seems reasonable to assume that the human body tries to minimize energy losses.

However, there is no known published data on axial, lateral and sagittal displacements measured simultaneously with the forces and couples at the joints on one individual. We calculated the various torques from the results derived from the experiments of Cappozzo, Thurston and Harris, Winter and others. Thus, our calculations may be of qualitative value only.

The actual power needed to produce the required torques in all three planes of motion can also be derived and is shown in Figure 5. As expected from the equal energy transfer relations above, the power requirement is exactly the same in all three planes. Winter showed the correlation between the power at the hips and at the  $L_4$  level during walking. (1,10)

Figure 3 illustrates the striking similarity between our calculated power patterns and the one measured by Winter. The difference in scale can be explained by the fact that most of the energy flows through the soft tissue (fascia, supraspinous and interspinous ligaments) surrounding the spine. How this is precisely achieved is now under investigation. Note that the power measured at the hips by Winter peaks after the power delivered by the spine at the  $L_4$  level. The above conclusion supports the idea that the legs follow the pelvic motion, and not the reverse, as commonly believed.

It should be noted, however, that the analysis leading to this conclusion is dependent upon experiments conducted under artificial conditions.(8) Proper experiments will have to be carried out to analyse the response of the intervertebral joint under more physiological conditions.

### CONCLUSION

The calculated shape of the power pulses driving the pelvis is very close to the shape of the power pulses available at the hip joint as measured by Winter. Moreover, it can be shown mathematically that the peak of the energy pulses calculated at the  $L_4$  level occur 20-50 milliseconds before those appearing at the hips, as measured by others.

This small period of lead time is significant in that it supports the concept of spinal motion being ahead of leg motion during gait. Hence, the pelvis is driven by the spine, and not, as commonly assumed, by the lower extremities.

### REFERENCES

1. Winter DA: Biomechanical motor patterns in normal walking. J Motor Behavior 15:302-330, 1983
2. Cavagna G, et al.: The mechanics of sprint running. J Phys 217:709-721, 1971
3. Ralston HJ, et al.: Energetics of human walking. Advances in Behavioural Biology 18:77-98, 1976
4. Gracovetsky SA: An hypothesis for the role of the spine in human locomotion: a challenge to current thinking. J Biomed Eng 7:205-216, 1985
5. Lovett AW: A contribution to the study of the mechanics of the spine. Am J Anat 2:457-462, 1903
6. Thurston AJ, Harris JD: Normal kinematics of the lumbar spine and pelvis. Spine 8:199-205, 1983
7. Cappozzo A: The forces and couples in the human trunk during level walking. J Biomech 16:265-277, 1983
8. Farfan HF: Mechanical disorders of the lumbar spine. Philadelphia, PA, Lea and Febiger, 1973, pp. 112-133
9. Shirazi-Adl SA, et al.: Stress analysis of a lumbar motion segment in axial torque alone and combined with compression. Proc 12th Ann Mtg Inter.Soc. Stud. Lum. Spine, Sydney, Australia, April 1985
10. Winter DA: Kinematic patterns in human gait: variability and compensating effects. Hum Movem Soc 3:51-76, 1984.

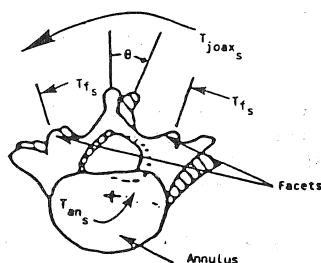


Figure 1. Distribution of torques in the static case. See also Table 1.

Type	$T_{joax_s}^m$ (N.m.)	$T_{an_s}^m$ (N.m.)	$2 \cdot T_s^m$ (N.m.)
Intact I.V. joint CA = 0	84.2	61.0	23.2
Intact I.V. CA = $1.38 \cdot 10^5$	106.2	58.7	47.5
Intact I.V. CA = $2.1 \cdot 10^5$	115.2	39.5	75.7

Table 1. Torque strength of I.V. joint components under varying axial compression (CA in Pascals).

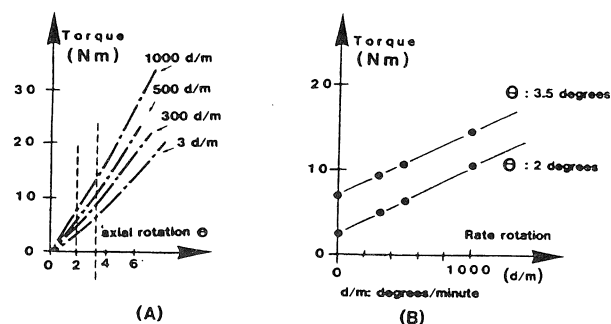


Figure 2. Figure A is re-drawn from Farfan (8). For each value of the axial rotation angle  $\theta$ , we measured the corresponding torque for a given rate of change  $d\theta/dt$ . This is shown in Figure B. The equation fitting the data points is:

$$T(\text{Nm}) = A \frac{d\theta}{dt} + B\theta ; \text{ with } A = .37, B = 1.72 \text{ (angle } \theta \text{ in degrees)}$$

This particular series of experiments shows that for an axial rotation of  $\theta = 3.5$  degrees, the quasi-static torque strength of the joint is 6 Nm. This is not representative of the average response of the joint which, it is suggested, is 150 inches/lb or 20 Nm. (8) To accommodate these claims, we rescaled the parameters A and B to the values of A = 1.2 and B = 5.7.

It is important to realize that no one knows how the joint is loaded *in vivo*. Hence, the Farfan experiments are necessarily arbitrary, and probably represent an unphysiological type of loading. Since we could not find any other source of data to substantiate these experiments, we decided to use the values of A = 1.2 and B = 5.7, bearing in mind that the calculation that would be made with them might be of qualitative value only, until other experimental evidence becomes available.

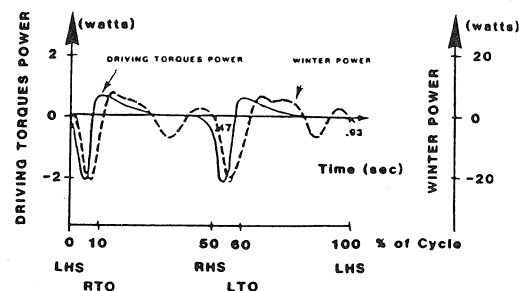


Figure 3. Superposition of the Winter and  $L_4$  power curves. Note the scale difference between the two torques.

## JOINT SURFACE GEOMETRY AND ESTIMATION OF JOINT FORCES.

Ian A.F. Stokes

Department of Orthopaedics and Rehabilitation  
University of Vermont  
Burlington, VT 05405

Estimation of joint forces is a cardinal problem in musculoskeletal biomechanics. The usual method is to measure externally applied forces and moments, position data for the skeleton and other anatomical components, moment arms for muscles and ligaments, and to write six equilibrium equations (for force, and torques in a 3 axis system). This method is applied both to the complete kinematic analysis of a force system, and to the quasi-static case which is common in biomechanics. Usually there are more than six unknowns in the equations, so assumptions are made (a) about the line of action and the joint force and (b) about the distribution of muscle and ligament forces around the joint. This paper concentrates on the first assumption which enables equations of moment equilibrium to be simplified, since the unknown joint force has no moment about a point on its own line of action.

1392 papers published in the Journal of Biomechanics between Jan 1969 and Dec 1986 were reviewed. Of these, 54 were concerned with estimation or evaluation of articular forces and/or moments of muscles about joints. Among these 54 papers, three types of assumption about the line of action of the joint force were made. Eleven used observations of the area of contact between joint surfaces to define a point on the line of action of the joint force. Eleven assumed that the joint forces passed through a point on the axis of rotation (or center of rotation for planar motion) and used this as a point about which to consider moment equilibrium. Two papers used this point and the further constraint of having the joint force pass through the joint contact area. One of these papers considered errors introduced by uncertainty about these points. Seventeen assumed that the joint force passed through some fixed geometric feature (normally the center of curvature of an articular surface). One paper made this assumption and also constrained the line of action of the joint force to pass through the contact area. In 6 cases an assumption was not made or not evident. Two papers showed how the principle

of virtual work could be used to find moment arms of muscles by measuring tendon length/joint angle relationships. In another study, a region of zero moment due to external and muscle forces was found and related to the anatomic features of the knee joint. One study of the shoulder investigated whether the joint center of rotation lay on the line of the joint force.

Two papers addressed the question of what differences in the calculated joint forces would be produced by adopting either the joint center of curvature or the experimentally determined axis of rotation of the temporomandibular joint (TMJ) as a point about which to consider moment equilibrium. In the TMJ joint (which is relatively unconstrained) the axis of rotation could become quite remote from the joint itself.

Is it valid to assume that the joint force has zero moment about the center of rotation? Under conditions of zero friction (an accepted assumption in synovial joints) the joint force is perpendicular to the joint surface. In a concave/convex non-congruent joint, there is initially a single point of contact which is located in the common tangential plane between the surfaces. Subsequently, as the force increases, the area of contact increases, but the common tangent assumption remains reasonable. The line of action of the joint force resultant then acts on a perpendicular to the common tangent, through the center of pressure.

For planar motion in the joint, the relative motion at the cartilage surface is either rolling about a point of contact or gliding on the common tangential plane, or a combination of both. In both cases, the axis of rotation transects the perpendicular to the common tangent plane. The point of intersection is the center of rotation for planar motion. Thus, in the absence of friction, it is correct to assume that the joint force has no torque about the center of rotation, under both static and dynamic conditions, providing the center of rotation is controlled by contact at joint surfaces with inelastic cartilage.

The axis or center of rotation is, however, notoriously difficult to measure experimentally. Joint laxity can make its position quite variable, so it is not certain that the center of rotation found in one experiment can be applied directly to estimating forces under different experimental conditions. An alternative approach is to use information about the joint surface geometry. If the center of pressure in the contact area were known, then the line of action would be defined. If only the joint surface geometry is known, then the constraints on the line of action of the force are known.

A two dimensional, sagittal plane model\* of the metatarsophalangeal joints of the toes was used as an illustrate example. Lateral photographs of the metatarsal heads showed that their profile could be represented by two circular arcs. The magnitude and center of pressure of the external force on the toes was measured during walking. The motion of the foot was recorded by cine-photography in synchrony with the force recordings. The toes were assumed to be in equilibrium under the influence of the external force, a flexor tendon force and the joint force. The three forces intersected at a point.

time. With two points on the line of action of the joint force now known, the unknowns (joint force and tendon force magnitudes) could be determined.

It is proposed that in many cases, joint force estimation can be done more easily and accurately by using joint surface shape measurements rather than measurements of the center of rotation.

**\*Reference:** Stokes IAF, Hutton WC Stott JRR.

J.Anat 129:579-590 1979.

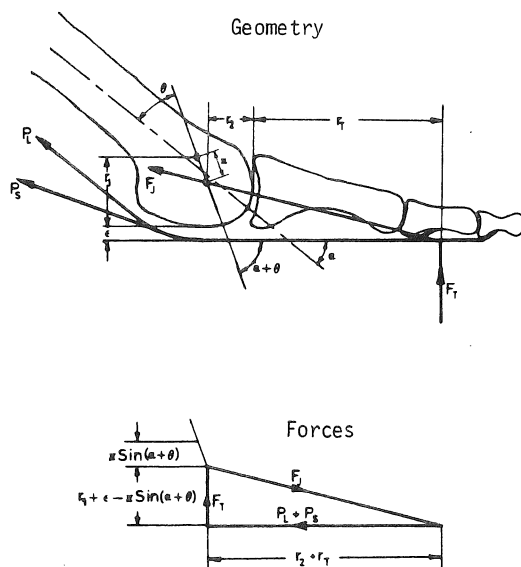


**Figure 1** Planar model of forces at the toe joints.

The line of action of the joint force was then determined by finding which of the two circular arcs could generate a radial line meeting this intersection point. Since the angle made by the metatarsals with the toes changes during the stance phase of walking, each circular arc articulated with the phalanx at some

# SIMULATION OF KNEE JOINT MECHANICS IN TWO DIMENSIONS

G.T. Yamaguchi, M.G. Hoy, and F.E. Zajac

Design Division, Mechanical Engineering Department, Stanford University, Stanford, CA 94305  
and Rehabilitation R & D Center, Palo Alto Veterans Administration Medical Center

## INTRODUCTION

Lower extremity musculoskeletal computer models of mammalian movement require modeling the joints. In typical simulations of human gait, posture and jumping, the knee joint is treated as a pin joint. Yet, it is known that the knee acts in a much more complicated fashion [1-7]. Some models developed, therefore, take some of these factors into account [7]. Unfortunately, most of these models are unsuitable for real-time whole-body dynamic simulations of motion since they require excessive computation. This paper describes a model composed of simple mechanical elements that simulates the kinematics of the joint and yet remains computationally fast. To date, this model has been valuable in describing the effects of quadriceps tendon orientation on the calculated moment arm for flexion angles less than 90 degrees.

## REVIEW AND THEORY

Several studies have indicated that the patella acts as more than a simple spacing device to increase the moment arm of the quadriceps. The finding that the contact surface forms a narrow band across the posterior side of the patella [1] supports the idea that the patella operates as a levering device. Grood, *et al.* [2], utilized this notion to determine curves of the effective moment arm of the quadriceps force versus knee flexion angle. The effective moment arm of the quadriceps is the ratio of the patellar ligament force to the quadriceps tendon force, multiplied by the moment arm distance of the patellar tendon to the axis of rotation of the tibiofemoral joint. They found that the effective moment arm rose sharply from about 2.0 cm at full extension, reached a peak of 3.5 to 4.4 cm at about 20 to 25 degrees, and fell rapidly to less than 2.0 cm as flexion further increased. They also found that small variations in the direction of the applied quadriceps force had negligible effect. Van Eijden, *et al.*, recently reported such directional changes in the quadriceps force as the knee is flexed [6].

One difficulty in using the effective moment arm curves of Grood, *et al.* [2] in computer models, is that at flexions higher than 60 degrees, the moment arm has decreased to values so small that it is difficult to reconcile with dynamometer test results. Often reported moment arm curves [4,5] appear to be more reasonable, even though the relatively inaccurate method of Reuleaux was used to determine the instantaneous centers of 2-D joint rotation (ICR) and the moment arm length.

## METHODOLOGY

A simple 2-D model of the knee joint may be constructed as in Figure 1. An ellipse of semi-major axis dimensions of 2.0 and 2.5 cm is used to approximate the sagittal-plane projection of the articular surfaces of the femur. The open circle, P, denotes the center of this ellipse while the star, C, is used to indicate the position of the center of joint rotation for an incremental rotation angle. Picking a pathway of discrete "instant centers" is done in such a way as to define a rolling and sliding motion of the ellipse across an imaginary horizontal surface (first rolling, then progressively more sliding) thought to mimic the motion of a ligament-constrained femur flexing with respect to a fixed tibia.

The patella is modeled as a rectangle 3.2 cm long by 1.0 cm thick. The front surface of the rectangle is the patellar axis, joining the lines of action of the quadriceps force and the patellar ligament force. The patellar ligament is assumed to be an inextensible string fixed at its lower end. Also, since the geometric forms representing the femur and the patella are assumed to be rigid, the line of action of the quadriceps force is constrained to remain outside of either body. Thus, the model is a frictionless, single-degree-of-freedom cam follower joined by inextensible strings.

The elements are configured according to reported data [6] and a single point of contact established. The quadriceps force angle is prescribed by either: a bilinear approximation to the reported data (Fig. 2), or a direction parallel to the femoral axis. Given the applied quadriceps force and the starting values for the vertical angles subtended by the quadriceps ( $\theta + \epsilon$ ), patella ( $\alpha$ ), and patellar ligament ( $\beta$ ), the force transmitted to the patellar ligament is calculated by balancing the nonlinear force and moment equilibrium equations using Newton-Raphson iteration. Knowledge of this force and the perpendicular distance to the ICR yields the effective moment arm.  $\beta$ , of course, is a function of  $\alpha$  given that the string representing the patellar ligament is taut and inextensible. The effective moment arm is calculated for each knee flexion angle and its associated cam position (Fig. 3).

## RESULTS AND DISCUSSION

Comparison of the moment arm curves corresponding to the two quadriceps force angle curves shows a difference as flexion proceeds beyond 60 degrees. Pulling on the quadriceps at an angle parallel to the femoral axis results in a constantly falling effective moment arm curve, until the string ("tendon") begins to touch the cam ("condyle") surface. Decreasing the angle ( $\delta$ ) with flexion tends to affect the static force/moment balance, yielding a larger effective moment arm at high angles of flexion. Very little change is detected for flexions less than 60 degrees. Thus, it is important to control the quadriceps force angle during experimental measurements at the knee, especially at flexion angles in the range of 60 to 90 degrees.

For flexions greater than 65 degrees the change in quadriceps force angle with flexion could be due to a turning of the tendon around the femoral condyles [6]. Yet, others report no contact between the trochlea and the tendinous band of the quadriceps below 80 degrees with no significant transmission of transverse force below 90 degrees [1,3]. Therefore, we assume that the relative position of the patella alone determines the force angle for flexions less than 80 to 90 degrees; beyond this the orientation of the force exerted on the patella is influenced by the presence of the femoral condyles. As the curves measured by Grood, *et al.*, fall well below those of other researchers beyond 30 degrees of flexion, it is possible that the rapid decline in Grood, *et al.*'s curves might result from the nearly constant force angle provided by the cable/Instron linear actuator arrangement.

We use a different ICR pathway than is commonly measured [4,5] to obtain a realistic rolling/sliding motion of the "femoral" cam. Usually measurements of the ICR are performed using the method of Reuleaux. The accuracy of this approach decreases as successive images are taken at finer flexion increments. As



the difficulty of measurement is further hampered by the three-dimensional motions of the actual joint, we propose modeling as an alternative method to determine realistic, 2-D representations of the ICR pathway.

## References

1. Goodfellow, J., *et al.* J. Bone and Joint Surg. 58:287-290, 1976.
2. Grood, E. S., *et al.* J. Bone and Joint Surg. 66:725-734, 1984.
3. Hungerford, D. S., *et al.*, Clin. Orth. and Related Res. 144:9-15, 1979.
4. Lindahl, O., *et al.* Acta Orthop. Scandinavica 38:226-234, 1967.
5. Smidt, G. L., J. Biomech., 6:79-92, 1973.
6. Van Eijden, T. M. G. J., *et al.* J. Biomech. 18:803-809, 1985.
7. Wismans, J. S., *et al.* J. Biomech. 13:677-686, 1980.

This work was supported by NIH grant NS 17662 and the Veterans Administration.

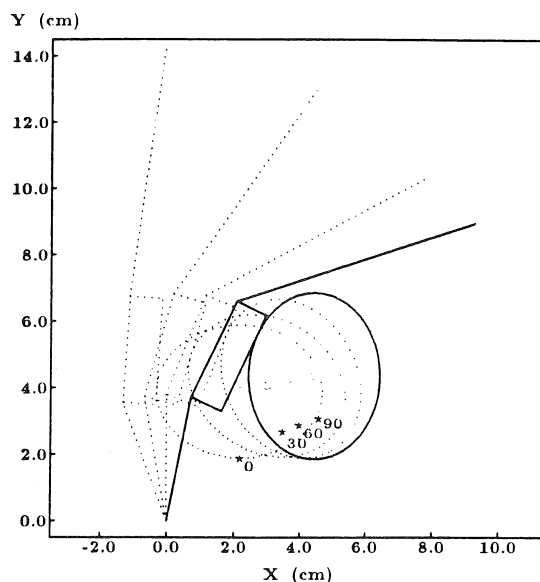


Figure 2. Motion sequence for a variable quadriceps force/femoral axis angle.

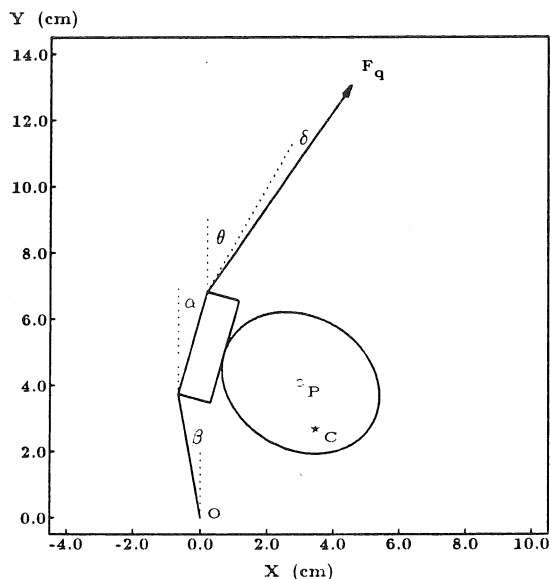


Figure 1. Angular definitions for the 2-D model.  $\theta$  is the knee flexion angle with respect to a fixed tibia;  $\delta$  is the angle of the applied quadriceps force with the femoral axis.

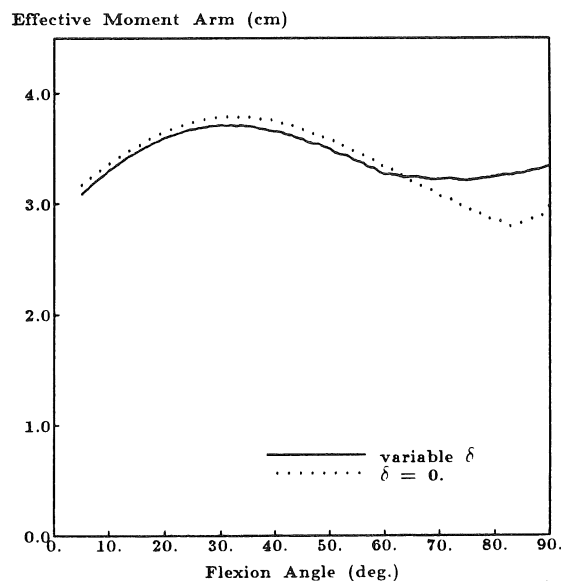


Figure 3. Effective extensor moment arms calculated for the motion sequences of Figure 2.

# PRESSURE DISTRIBUTION ON ARTICULAR SURFACE:

--Application to Muscle Force Determination and Joint Stability Evaluation--

S. Himeno, K. N. An, H. Tsumura, and E. Y. S. Chao  
Orthopedic Biomechanics Laboratory  
Mayo Clinic/Mayo Foundation  
Rochester, MN 55905

## INTRODUCTION

Precise knowledge of pressure distribution in joints is not only a prerequisite for determination of stresses in articular cartilage but might also be the determining factor that influences the distribution of muscle force under synergistic and antagonistic conditions. The concept of joint pressure distribution and its application were discussed extensively by Pauwels (1963) by considering a simple, hinged elbow joint. In our study reported here, a generalized method to solve the joint pressure distribution problem is developed based on the minimum strain energy principle. An analytic and numeric model is formulated by using the rigid body spring method of Kawai and Takeuchi (1977, 1978). The results are first verified by comparison with those of Pauwels for the special case of a hinge joint. The effects of size of the articular surface and location of the resultant joint force on pressure distribution are examined. Its implication to the distribution of force on multiple synergistic and antagonistic muscles is then discussed with consideration of its relationship to joint stability.

## METHOD

In establishing the analytic and numeric model for joint pressure determination, the shapes of articular surfaces are either mathematically or numerically described. The rigid body spring model is then formulated by considering the rigid body to be in equilibrium with external loading. Reaction forces between adjacent bodies are produced by the spring system distributed over the possible contact surface of the two adjacent bodies. Displacements, normal and tangential to the articular surface, can be described as functions of the displacement of the centroid of the body. Strain energy due to relative displacement of the spring system can then be formulated in the quadratic function of the displacement vectors of the centroid of adjacent rigid bodies. By applying Castigliano's theorem, the stiffness equation can be obtained by differentiating strain energy with respect to displacement of centroids of adjacent rigid bodies. A system of equations is obtained for solving centroid displacement of rigid bodies. Displacement and force in the spring system are then determined which gives the pressure on articular surfaces. Furthermore, the "attempted displacement" of the centroid of rigid bodies is also obtained. The direction of "attempted displacement" corresponds well with the direction of maximum pressure and could be a useful parameter in describing joint stability.

## RESULTS

Two problems are considered in this study. First, the model is applied to the special case of a hinge joint. The effects of available articular surfaces, as represented by angle  $\psi$ ; the location of resultant joint force,  $R$ , as represented by angle  $\theta$  on the peak pressure,  $P_m$ ; and the direction,  $\phi$ , of "attempted displacement,"  $U$ ; are illustrated in Figs. 1a, 1b, respectively.

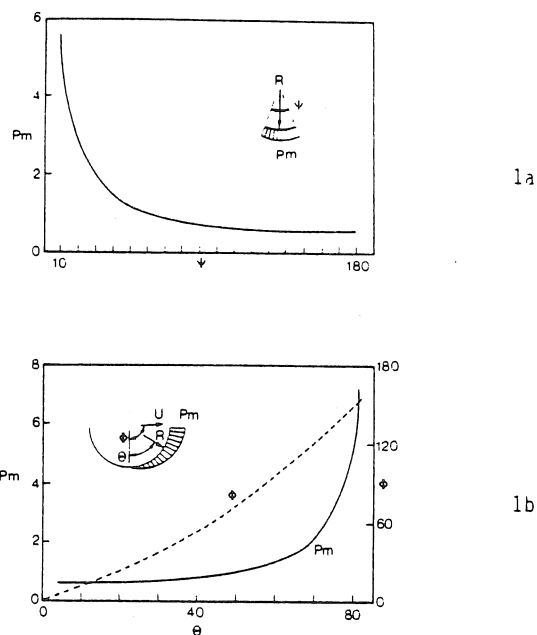


Fig. 1 Peak pressure on articular surface and direction of "attempted displacement" of articulating bodies are related to available contact surface, enclosing angle,  $\psi$ , (1a); and location,  $\theta$ , of the resultant joint force on the hemispheric articular surface (1b).

In the second problem, the effect of muscle force distribution on joint pressure is analyzed. For given lines of action of the flexor,  $F_f$ , and extensor,  $F_e$ , on each side of the elbow joint, there are infinite possibilities of force distributions among these two muscles in resisting loads,  $P$ , applied on the forearm.

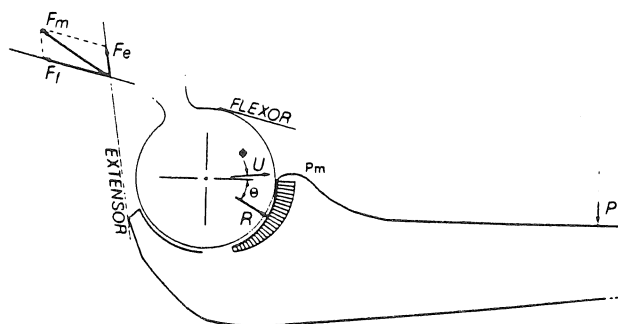


Fig. 2a Distribution of muscle force influences the magnitude and direction of resultant force on the elbow joint.

Resultant joint force,  $R$ , locations on the articular surface,  $\theta$ , as functions of the ratio of extensor force to flexor force are calculated (Fig. 2b). Furthermore, the associated direction of "attempted displacement,"  $\phi$ , and peak joint pressure,  $P_m$ , as functions of relative involvement of antagonistic muscles are illustrated (Fig. 2c).

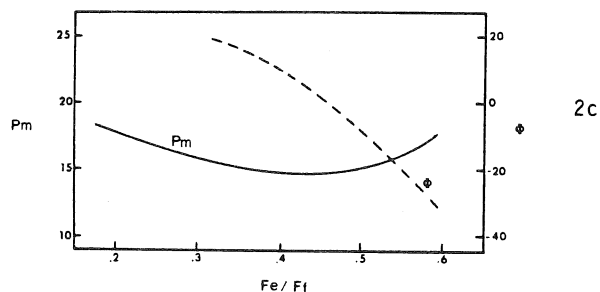
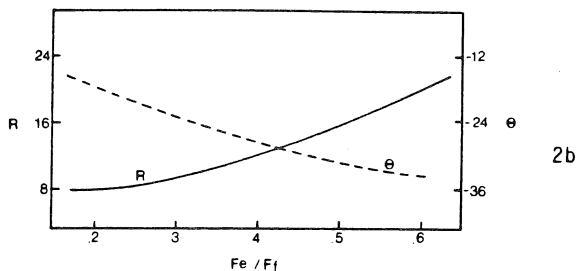


Fig. 2b,2c For the given loading condition in Fig. 2a, resultant joint force increased with increasing involvement of extensor muscle (2b). Peak articular pressure and "attempted displacement" of the humerus are also effected by involvement of extensor muscle (2c).

#### DISCUSSION

It is clearly illustrated that, if the resultant joint force is centrally located on the articular surface, the pressure distribution will be most uniform. The "attempted displacement" will be close to the direction of the resultant force. The peak pressure decreases with the increase of available contact area. However, when the resultant joint force moves away from the center of possible contact area, the peak pressure increases. In addition, the direction of "attempted displacement" moves away from the direction of the resultant joint force and toward the rim of the surface of joint contact. It is our hypothesis that, for a given loading condition, various muscle force distributions could lead the joint to: a) a stable condition, when both the resultant joint force and "attempted displacement" are within the arc of contact area; b) a subluxation condition, i.e., resultant joint force within but "attempted displacement" outside the articular

surface; or c) a dislocated condition, when the resultant joint force and "attempted displacement" are outside the articular surface (Fig. 3).

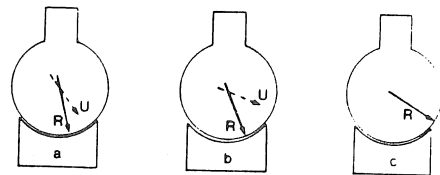


Fig. 3 Based on the relationship of the directions of resultant joint force,  $R$ , and "attempted displacement,"  $U$ , of the articulating body, loading on the joint could lead to a) stable, b) subluxation, c) dislocation conditions.

Usually, resultant joint force is minimal when there is no involvement of antagonist muscle, and it progressively increases with the addition of antagonist activity. However, for the given configuration in the example, contraction of an antagonist muscle may favor the peak pressure and "attempted displacement." This is because the line of action of resultant muscle force is modified by adding antagonists, thus bringing the resultant joint force more toward the center of the contact surface.

#### SUMMARY

A generalized method has been developed to determine the joint contact pressure of any shape of articular surface and loading condition. The implication of this study, that joint pressure distribution and direction of "attempted displacement" might have a significant influence on muscle force distribution and joint stability, are discussed.

#### REFERENCES

1. Pauwels, F: Biomechanics of locomotor apparatus, Springer-Verlag, 1980.
2. Kawai, T et al.: "A New Element in Discrete Analysis of Plane Strain Problems." Seisan Kenkyu, Vol. 29, 1977, pp. 204-207.
3. Kawai, T: "New Discrete Models and their Application to Seismic Response Analysis of Structures." Nuclear Engineering and Design, Vol. 48, 1978, pp. 207-229.

#### ACKNOWLEDGEMENT

This study is supported in part by NIH grant AM 26287.

R. Shiavi, H. Borra, M. Frazer and T. Limbird

Departments of Electrical and Biomedical Engineering  
and Orthopaedics and Rehabilitation  
Vanderbilt University  
Nashville, Tennessee 37235

## INTRODUCTION

Knee stability relies upon muscle action as well as ligamentous integrity. The anterior cruciate ligament (ACL) is a key supporting structure in the tibio-femoral joint. Along with its posterior cruciate counterpart (PCL), the two ligaments are responsible for maintaining the roll-and-slide characteristics of the joint. ACL deficiency is a potentially crippling condition, -- defeating normal joint rolling and gliding, with subsequent destruction of the menisci [1]. The primary function of the ACL is to check anterior displacement of the tibial plateau from the head of the femur. The ACL is more or less attached to the posterior side of the femoral condyles while the opposite end is attached to the tibia in the anterior aspect of the tibial plateau. The PCL may be thought of as being attached in an opposite manner, so as to prevent posterior displacement. Since the two ligaments cross each other obliquely, with the ACL on the medial side, loss of the ACL can lead to excessive medial rotation [2]. Normally, the ACL and PCL will twist on each other and consequently limit medial rotation of the knee.

Electromyographic (EMG) signals of five major muscles about the knee have been recorded from both normal and anterior cruciate ligament deficient individuals. Between group comparisons of the EMG linear envelopes reveal differences in the number of peaks and the relative time of peak phasing in walking and pivoting. Since laxity is controllable with muscle activity, comparison of the muscular synergy patterns between groups may uncover the functional deficits and compensatory muscle contractions and mechanisms. Close evaluation of the results may lead to new therapeutic goals and reconsideration surgical procedures.

## METHODOLOGY

All participants selected are between 18 and 40 years of age and all patients have clinical or surgical documentation of ACL deficiency. These include the standard drawer tests and pivot shift maneuver. The normal and patients groups consisted of 10 and 7 individuals, respectively. The participants are asked to perform two functional tasks at free and fast speeds on a 12 meter walkway. These tasks are walking straight and pivoting at 90 degrees about the injured or control leg. The EMG signals are acquired with bipolar surface electrodes placed over the bellies of the gastrocnemius (GS), vastus lateralis (VL), biceps femoris (BF), rectus femoris (RF), and semitendinosus (ST) muscles. The signals are sent to our acquisition computer via a telemetry pack. Before the signals are digitized, they are band-pass filtered from 40-400 Hz, full-wave rectified and integrated over 12.5 msec. Since stride time varies from stride to stride, the data set must be normalized to a standard number of points. Our lab employs the LaGrange interpolator to achieve this normalization [3][4]. The final form of the data is a linear envelope of the EMG signal from each muscle. EMG envelopes from individual strides are then averaged together to

produce the ensemble averaged signal used in making comparisons. In addition to the envelopes, the foot-contact patterns of both feet are recorded. The patterns help the analyst to define the different phases of the gait. Values are assigned to different regions of the feet. The heel is given a value of 2; the 5th metatarsal contact equals 4; 1st metatarsal equals 8; and the big toe has a value of 1. For example, when the heel strikes the floor at 0% time, the foot-contact value is 2; when the 5th metatarsal makes contact, a value of 4 is added to the current value. Therefore, if the heel and 5th metatarsal are touching the floor the net value is 6. The contact patterns of ipsilateral and contralateral feet are shown at the bottom of figures 1 and 2.

One must take into account that this is not a periodic process. Unlike walking, in which the individual strides may be viewed as epochs, the EMG record cannot be considered as continuous through 100% of the stride time. That is, it would be erroneous to extrapolate through 100% of the stride time and back through 0%, -- although it is acceptable with walking. The number of cutting maneuvers averaged per patient is from four to six.

## RESULTS AND DISCUSSION

The results from all of the tasks reveal moderate to major changes in the activity in a majority of the muscles. The results presented here are taken from the casual 90 degree cutting maneuver. Figures 1 and 2 illustrate three of the five EMG envelopes and their respective foot-contact patterns taken from the normal and the patient population during this maneuver. During this task, the patients have a more intense activity in the thigh throughout midstance. This may be seen in the RF record between 0 and 35%. The vastus lateralis (not shown) has increased activity also. Additionally, there is a remarkable shift in the peak activity of the ST; and a new peak of activity in the GS in the initial mid-stance stage that is considerably greater than the normal activity.

The vastus lateralis and rectus femoris act as stabilizers during the loading stage (0 to 10%). There increased activity is devoted to keeping the ipsilateral knee extend while the leg takes on more weight, as the contralateral leg is being lifted from the floor. The patient group seems to be using these muscles in excess, so as to stabilize the tibia under the femur, throughout the cutting phase (10 to 35%). The patients seem to be using the RF, VL, and GS muscles more, so as to stabilize the knee. Parallel studies of these patients indicate extreme lateral rotation in normal walking and cutting. Increased activity of the ST throughout the cut may serve to limit rotation, during an intentional maneuver requiring lateral rotation. Since loss of the anterior cruciate tends to increase medial rotation, and medial rotation is certainly not present in the cut, this increased activity in the ST may be present to restrain anterior displacement of the tibia. However, another mechanism seems just as likely. The ACL, by virtue of its constant length, pulls the medial

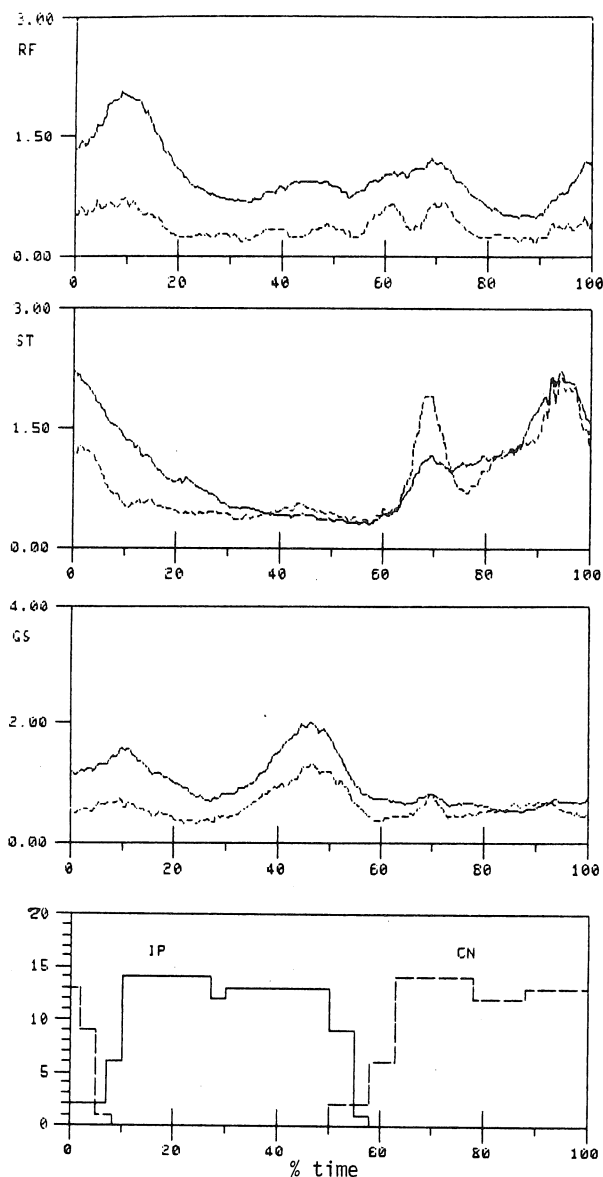


Figure 1. EMG envelopes of normal group average in solid, standard deviation is dashed with ipsi and contralateral patterns.

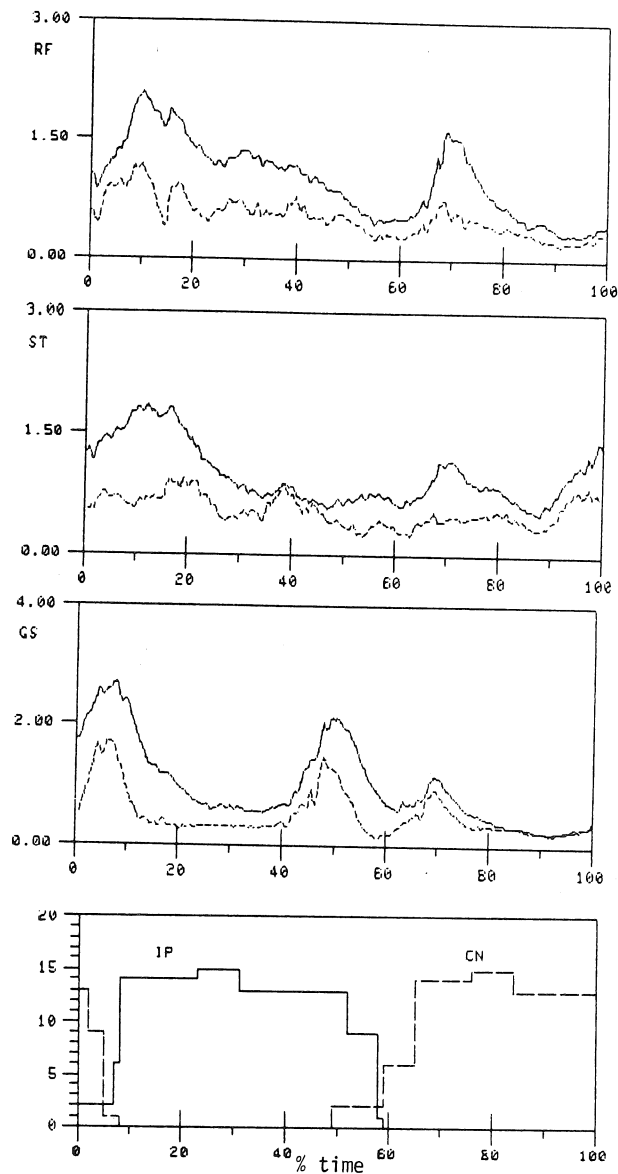


Figure 2. EMG envelopes of patient group average in solid, standard deviation is dashed with ipsi and contralateral patterns.

femoral condyle forward as the knee is flexed [2][5]. In the absence of the ACL, increased ST activity may serve to effect the same procedure by retracting the medial aspect of the tibial plateau. Note that the ST peak is definitely within the stride interval where axial rotation of the knee the greatest. In normal population, activity of the ST is on a definite decline throughout the cutting procedure. The ACL is performing its normal function; acting as a static line connected to the femur, to pull the femoral condyle forward during peak flexion of the pivot.

#### References

1. Noyes, F., et al., J. Bone Joint Surg., 61A:154-162, 1983.
2. Kaphdiji, I., et al., The Physiology of the Joints. Vol II, E & S Livingston Co., 1970.
3. Shiavi, R., et al., Med. & Biol. Eng. & Comput., 21:573-578, 1983.
4. Schafer, R., et al., Proc IEEE, 61:692-702, June, 1973.
5. Shoemaker, S., et al., J. Bone Joint Surg., 64A:208-216, 1982.

## THE EFFECT OF DEGREES OF FREEDOM ON VARUS-VALGUS KNEE LAXITY

J.M. Hollis, M.A. Gomez, M. Inoue, E.M. Burleson and S.L-Y. Woo  
Division of Orthopaedics and Rehabilitation M-030  
University of California, San Diego, and  
San Diego Veterans Administration Medical Center, La Jolla, California

### INTRODUCTION

In recent years, the contribution of ligaments and other periarticular structures on knee motion has been objectively evaluated. In particular, several studies on varus-valgus (V-V) knee rotation using a variety of testing devices and procedures have been performed. Markolf, et al<sup>1</sup>, using a device which allowed the application of a load (manually) to the distal tibia, reported that sectioning both cruciate ligaments showed no appreciable increases in V-V laxity. Mains, et al<sup>2</sup> evaluated the "abduction laxity" of the knee joint by employing a device which applied a force to the distal tibia and allowed tibial rotation. These authors reported that when the anterior cruciate ligament (ACL) was sectioned, the abduction laxity increased only 1°. Whereas, when the medial collateral ligament (MCL) was sectioned, laxity increased by 4.7°. Piziali, et al<sup>3</sup> measured the moment for V-V rotation of the knee about a fixed axis of rotation for intact knees vs. knees with only the cruciates. The moment was reduced 72% in varus and 82% in valgus in the specimens with intact cruciates. Recently, Grood, et al<sup>4</sup> found that the MCL was the primary restraint in limiting the valgus joint opening, and the cruciates had only a small secondary effect. The study showed a reduction in the restraining moment of 78% for MCL cutting, and 13% for ACL and PCL sectioning. Note that in their study, the testing applied a force to the distal tibia and allowed no tibial rotation or anterior-posterior (A-P) translation.

The aforementioned studies, in general, were designed to emulate the manual laxity test used clinically. However, it appears that physiological knee motion has less restraints. It is our hypothesis that the restrictions to joint motion present in any testing may have a significant effect on the results obtained. Therefore, the objectives of this study are: 1) to design a device which would allow V-V knee laxity testing with five degrees of freedom (DOF), 2) to compare the effect of limited DOF (i.e. three) on the V-V laxity to the case of five DOF, and 3) to determine the effects of DOF on the relative contribution of ligaments (MCL and ACL) on the V-V knee.

### METHODOLOGY

In order to simulate clinical V-V laxity tests of the knee, a device was designed based on a four-point bending test (Fig. 1). Canine knee joints with an intact capsule and normal ligaments were used. Three threaded stainless steel pins, 6.5 mm in diameter were inserted sagittally through the tibia and femur. A fourth pin was placed coronally through the proximal end of the femur. The two tibial pins were fixed inside two axial rotary bearings to avoid limiting axial tibial rotation. The proximal bearing was fixed to a frame attached to linear bearings so that A-P translation was allowed.

This frame was attached to two support blocks containing two small (V-V) rotary bearings. Motion in the proximal-distal (P-D) direction can occur through the use of linear bearings (on four parallel longitudinal support bars). The pin through the distal femur was supported by a similar block/linear bearing arrangement. Equal loads were applied to the outer tibial and femoral rotary bearings which were placed 6 cm from each of the inner bearings. This applied load created a constant bending moment across the knee joint. The moment was perpendicular to the axis of the MCL. The V-V rotation was measured by two rotary variable differential transformers attached to the inner V-V rotary bearings and rotation vs. applied moment was plotted on an X-Y recorder.

For the five DOF experiment, A-P, P-D, medial-lateral translation, V-V and tibial axis rotation were allowed. In the three DOF experiment, A-P translation and tibial axis rotation were restricted.

Five pairs of canine knees were tested. All muscle and other tissues were removed leaving the joint capsule and all ligaments intact. The femur and tibia were drilled and the pins inserted into the bone, and the knee was mounted on the testing device at 90° of flexion (the device is designed to accommodate all knee flexion angles), with the MCL perpendicular to the axis of applied moment. The knee was preconditioned for 10 cycles between -0.6 and +0.6 N-m, and the V-V angle vs. moment with hysteresis loops, were recorded. The knee was then returned to its neutral position (defined by V-V angulation halfway between the positions at which the hysteresis loop crossed the zero load). At this point, the tibial rotation and A-P translation were restrained (3 DOF) and the knee was again tested. The V-V angle vs. moment curves were recorded. The specimen was again returned to its neutral position. For five knees, the ACL was surgically sectioned, and in the remaining five knees, the MCL was sectioned. The five pairs of legs were randomly assigned to the two groups. The knee was tested as before, but with 3 DOF first, and then 5 DOF. The V-V laxity was defined as the V-V joint rotation between  $\pm 0.6$  N-m.

### RESULTS

The differences in V-V laxity for the intact canine knees between 3 and 5 DOF are shown in Fig. 2. It can be seen that with 5 DOF the knee laxity in V-V rotation is over three times higher than with the knee restricted to 3 DOF ( $p < 0.005$ ). The effect of MCL or ACL cutting on V-V laxity was shown in Fig. 3. When plotted in terms of increased valgus laxity (referenced to the original neutral position), the difference between the 3 DOF tests and the 5 DOF tests when either the ACL or the MCL was cut was dramatic. When the MCL was cut, the laxity increased an average of 179% in the 3 DOF tests, but increased only 21% in the 5 DOF test. This is in contrast to that observed when the ACL was cut. The V-V laxity increased only 10%

in the 3 DOF tests, but increased 136% in the 5 DOF tests.

## DISCUSSION

The present study clearly demonstrates that restraints by the testing apparatus can greatly reduce the V-V knee laxity. In this respect, the reported data on V-V laxity may be too low, possibly due to limited axial tibial rotation and A-P translation. The contribution of the ACL in restraining V-V motion is highly dependent upon these two degrees of freedom. Therefore, investigation of various ligament deficiencies on the V-V knee stability must take into account the restraints imposed on the joint during testing. It is felt that the newly designed device which permits five DOF can be used to evaluate true V-V knee motion and has inspired additional studies on the knee at different angles of flexion.

## References

1. Markolf, K.L., et al. JBJS, 58A (5):583-592, 1976.
2. Mains, D.B., et al. Am. J. Sports Med. 5(4):144-152, 1977.
3. Piziali, R.L., et al. J. Biomech. Eng. 102:277-283, 1980.
4. Grood, E.S., et al. JBJS, 63A(8):1257-1269, 1981.

## Acknowledgments

Support from the RR&D of the Veterans Administration, NIH Grant AM14918, and the M. & D. Coutts Institute for Joint Reconstruction and Research is gratefully acknowledged.

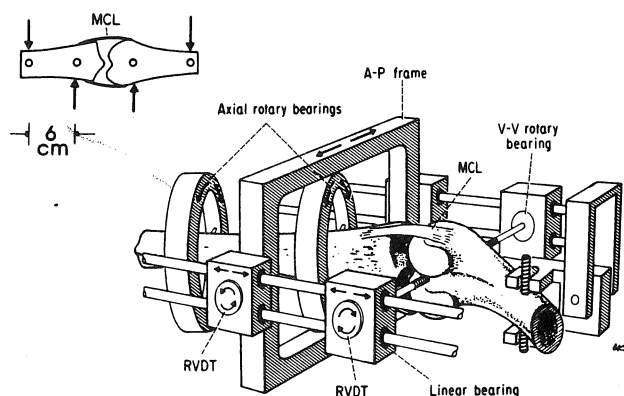


Fig. 1 - Varus-Valgus laxity testing device which allows up to five degrees of freedom.

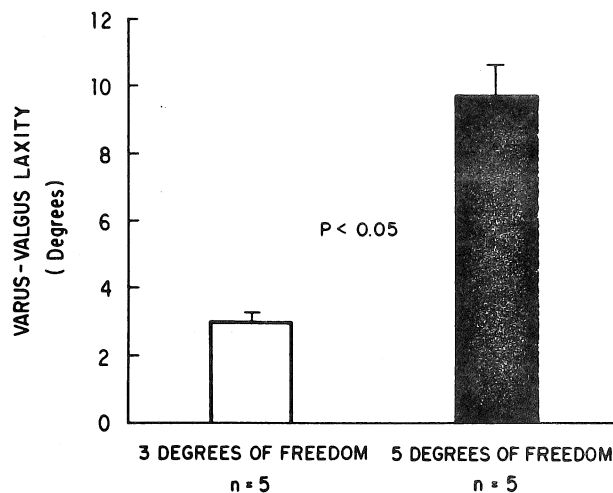


Fig. 2 - Varus-valgus canine knee laxity vs. number of degrees of freedom of testing device.

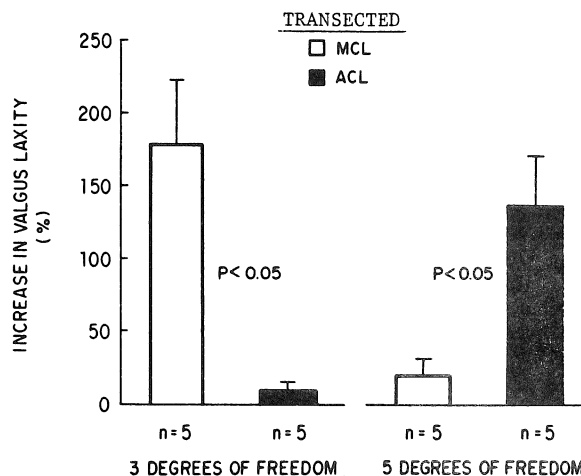


Fig. 3 - Increase in valgus laxity vs. number of degrees of freedom for canine knees with ACL or MCL transected.

# A TWO DIMENSIONAL ANALYSIS OF THE CONTRIBUTION OF THE ABDOMINAL MUSCLES TO TRUNK FLEXION

D.J. Morton and J.G. Reid  
School of Physical and Health Education  
Queen's University  
Kingston, Ontario, K7L 3N6

## INTRODUCTION

Maximal static forces exerted by the abdominal muscles during full supine trunk flexion were calculated from a two dimensional vectorial representation of the human trunk. Biomechanical models require further information regarding the force output and the geometry of the trunk flexor musculature. This study quantifies the relative static force contributions of external oblique, rectus abdominis, and internal oblique to maximal trunk flexion.

The data were collected from five male and two female cadavers (75  $\pm$  10.2 years). The results indicate that the mean force contributions of external oblique, rectus abdominis, and internal oblique were 48, 28, and 24% respectively.

## REVIEW AND THEORY

Mathematical modelling of the trunk musculature has been difficult because of the limited information available on the structural orientation and cross-sectional areas of these muscles. Many earlier attempts at modelling ignored the internally generated muscle forces by regarding the spine as a passive engineering structure acted upon by an external load (2), while others have calculated these forces using linear programming techniques (8).

Force data have been obtained indirectly from anatomical illustrations (8) and from displacement data (9). Others have obtained the data directly from cadavers by taking serial cross-sections (4,5).

Rab, et.al (5) modelled the forces acting on the lumbar spine using a serial cross-section approach modified from Jenson and Davy (4). Based on information collected from two cadavers, percentage force contributions for trunk flexors and extensors were presented. External oblique (EO), rectus abdominis (RA) and internal oblique (IO) contributions were 34%, 36% and 30% for cadaver one, and 30%, 40% and 30%, for cadaver two, respectively. No information about the muscle areas, fibre angles or muscle moment arms was presented. In addition, the cross-sectional area was calculated from the anatomical cross-sections and expressed as an average value. Dostal and Andrews (3) suggested that a possible disadvantage of using this approach may be the inability of transverse cross-sections to accurately define irregularly shaped muscles.

Recently, Reid and Costigan (7) predicted the force contribution of RA to trunk flexion by measuring its physiological cross-sectional area from data collected from MRI scans of live subjects. The predicted values were compared with peak static strength

scores obtained during isometric testing. Their results indicated that the predicted RA muscle force can only account for 40% of the torque measured during maximal trunk flexion.

The purpose of the present study was to determine the geometry of the three trunk flexor muscles and to predict the relative contributions of these muscles based on their physiological cross-sectional areas.

## METHOD

The data were collected from five male and two female cadavers with a mean age of 75 years (range : 60 - 88). Measurements were made from the fibres of IO originating from the anterior two-thirds of the iliac crest and from the individual digitations of EO (EO2 to EO7).

Embedded markers were placed along the muscle fibres of EO and IO. A string connecting origin to insertion was assumed to be the line of pull (3). The angle of insertion of these muscles was measured from the linea alba to the muscle line of pull. The average angles for EO and IO are presented in table 1.

Physiological cross-sections were obtained for EO, RA, and IO by slicing the fibres perpendicular to their long axes at the level of the muscle belly. For EO, each separate digitation (EO2 - EO7) was sectioned while the fibre orientation of IO determined how it was to be sectioned. Sections from the first and fourth segments were obtained from RA. All cross-sections were wetted, mounted, photographed and subsequently digitized in order to determine the muscle areas (table 2).

Having collected the geometrical data, each muscle was represented by several two dimensional resultant force vectors. These were then resolved into vector components. The component of interest was that which acted along the midline of the body and contributed to trunk flexion.

The assumption for this study was that all three abdominal muscles have equivalent moment arms. For this to be accepted the three abdominal muscles must be considered to have components that act along a common vector (linea alba).

The value used in this study for force per unit area (force constant) was 50 N/cm<sup>2</sup>. The flexion force components of RA, EO, and IO were calculated as follows:

$$\text{Area} * \text{Force Constant} * \cos x$$

where  $x$  is the muscle angle. The sum of these flexion components represented the total force generated by the abdominal muscles. Relative contributions were obtained



for each muscle by dividing the individual forces by the total force.

## RESULTS AND DISCUSSION

Rectus abdominis has been considered to be the predominant muscle involved in active trunk flexion. The data indicate the role of the RA in trunk flexion is less than that of the obliques. For each cadaver examined, EO had consistently higher relative force contributions supplying, on average, 48% of the predicted muscle force. RA and IO each exerted 28% and 24%, of the total force, respectively (table 3). In comparison, Rab et al. (5), in a three dimensional analysis of the muscles affecting the lumbar spine, found average contributions of 32, 38, and 30 %, for EO, RA, and IO, respectively.

In this two-dimensional analysis of the abdominal muscles, the force contribution for RA was about 10 % less than the values obtained from young male adult subjects used by Reid and Costigan (7) and from the cadavers studied by Rab et al. (5). The average IO value was 6 % less than that found by Rab, et al. (5). In contrast, the EO was calculated to exert 16 % more force during maximal trunk flexion.

The greater percentage force estimate for EO may have been due to the limitations of the two dimensional model used in this study. Because EO has component vectors in all three anatomical planes, calculated force values for trunk flexion may have been overestimated. The age of the cadavers used in this study ( $75 \pm 10.2$ ) should also be considered, primarily when analyzing the muscle areas.

The mean total area for RA in this study was 6 cm<sup>2</sup>, compared with values for live subjects of 10.5 cm<sup>2</sup> (age =  $54.6 \pm 15$  yrs) (6) and 15.1 cm<sup>2</sup> for younger subjects (age =  $21.2 \pm 1.7$ ) (7). This apparent decline in muscle area with age is consistent with the data of Aniansson et al. (1) who found a decrement in strength between the ages of 70 and 75. The effect of this decreased strength on muscle cross-sectional area or, more specifically, on the relative size of the abdominal muscles, is presently unknown. In addition, the muscle area data obtained from this study may be less than data reported in the above studies because of possible differences in fluid content between cadaveric and live muscle.

## CONCLUSIONS

Within the limitations of this study, the percent contribution of EO, RA, and IO to trunk flexion can be calculated using a simple two-dimensional model of the human trunk. The relative contributions obtained from this model are least effected by variation in the measurements of the muscle angles. This suggests that reliable cross-sectional area data should be obtained from subjects within a wide range of ages in order to increase the accuracy of existing trunk models.

This simple model indicates that the RA muscle contributes 28% of the maximum trunk flexion force. The remainder of the force was generated by the obliques (48% by EO, 24% by IO).

Table 1. Mean angle of insertion of EO, IO, and RA measured from the linea alba to the muscle line of pull

Subject	Mean muscle angles [degrees]			
	EO2-6	EO7	RA	IO
1	39.2	0	0	125.5
2	38.1	0	0	135.4
3	39.4	0	0	118.3
4	43.8	0	0	143.3
5	41.8	0	0	141.2
6	48.1	0	0	135.5
7	40.6	0	0	131.5
mean	41.5			133.1
SD	3.4			8.8

0 = parallel to linea alba

Table 2. The unilateral cross-sectional area of the three abdominal muscles.

Subject	Cross-sectional area [cm <sup>2</sup> ]			
	EO2-6	EO7	RA	IO
1	5.21	2.07	2.31	4.44
2	4.64	1.42	2.23	2.65
3	3.17	0.67	1.62	2.14
4	1.82	0.64	2.27	2.70
5	8.36	1.02	3.26	5.39
6	8.80	2.76	5.19	3.26
7	4.77	0.77	4.00	5.26
mean	5.25	1.34	2.98	3.69
SD	2.55	0.81	1.25	1.33

Table 3. The relative contribution of EO, RA, and IO to trunk flexion.

Subjects	EO	RA	IO
1	55.8	20.8	23.4
2	55.3	24.4	20.3
3	53.7	27.4	18.9
4	30.8	35.9	33.1
5	49.9	21.8	28.3
6	55.3	32.8	11.9
7	36.9	33.3	29.8
Mean	48.2	28.1	23.7
SD	10.1	6.0	7.3

## REFERENCES

1. Aniansson, A., et al. Scand. J. Rehab. Med. suppl. 9:92-102, 1983.
2. Belytschko, T.B., et al. J. Biomech. 6:361-371, 1973.
3. Dostal, W.F. and Andrews, J.G. J. Biomech. 14 (110):803-12, 1981.
4. Jenson, R.H. and Davy, D.T. J. Biomech. 8:103-110, 1975.
5. Rab, G.T., et al. Orth. Clin. N. Amer. 8(1): 193-199, 1977.
6. Reid, J.G. and Costigan, P.A. J. Orth. Sport. Phys. Ther. 69(5):278-80, 1985.
7. Reid, J.G. and Costigan, P.A. in press, 1986.
8. Schultz, A.B. et al. J. Bone Joint Surg. 64A (5):713-20, 1982.
9. Yettram, A.L. and Jackman, M.J. J. Biomed. Eng. 4:118-24, 1982.

# A COMPARISON OF ACTUAL INTERNAL DISPLACEMENTS OF HUMAN SPINAL MOTION SEGMENTS PRODUCED BY IN VITRO LOADING AND FINITE ELEMENT MODEL PREDICTIONS

M. H. Krag, R. Seroussi, D. G. Wilder, K. B. Byrne and I. Trauschn  
Vermont Rehabilitation Engineering Center  
The University of Vermont, Burlington, Vermont 05405

## INTRODUCTION

The mechanical properties of intervertebral discs have been extensively tested, and a number of mathematical models have been devised (2,3). These have included modeling of the internal displacements of discs under loading, even though no experimental data have been previously available to directly validate these predictions. We present here data describing these internal displacements, which may be used to verify or refute the predictions of many finite element models (FEMs) of internal disc deformation that are now in use. To provide a context for interpretation of these data, they are compared to a linear, elastic, isotropic, finite element model.

## METHODS

The lower vertebral body of each of 11 motion segments was rigidly fixed to a loading frame. Seven metallic markers (0.84 mm x 1-2 mm) were placed in each disc. The markers were injected one at a time, using a 22 gauge 3.5 inch hypodermic needle that had been inserted from front to back approximately along the midplane of the disc. A sagittal plane x-ray was obtained before and after application of a flexion-compression load. As shown in Figure 1, the disc markers were labelled as follows: lower vertebral bodies markers (1 and 2), interior markers (3 through 9), upper vertebral markers (10 and 11). The displacements of the seven interior marker points and the upper vertebral body points were measured relative to the lower vertebral body markers using an x-y digitizer.

A two-dimensional planar stress finite element model (linear, elastic, isotropic, material with Poisson's ratio of 0.25, using 20 triangular elements) was used to predict marker point displacements for each specimen separately. The lower and upper vertebral body displacements served as boundary conditions. Predictions at the marker point locations were linearly interpolated from the FEM nodes.

## RESULTS

Figure 1 shows a sagittal plane view of a representative disc specimen. The solid lines show the experimental displacements of each marker. The dashed lines present the displacements predicted by the finite element model.

The displacements of equivalent markers were averaged across all discs. The results are plotted in Figure 2a showing the up-down (UD) and in Figure 2b showing the anterior-posterior (AP) components. For the UD component, good agreement can be seen between the experimental data and the FEM predictions (no significant differences according to a matched pair t-test). However, for the AP component, the experimental displacements are significantly different than those predicted. The anterior surface marker 3 moves more anteriorly, whereas internal markers 5, 6 and 7 move more posteriorly than the FEM predictions (all matched pair differences significant

at the  $p < 0.01$  level). In addition, the central internal markers 5, 6 and 7 have very similar motions, both in direction and in the amount of displacement. These motion patterns are also illustrated by the example in Figure 1.

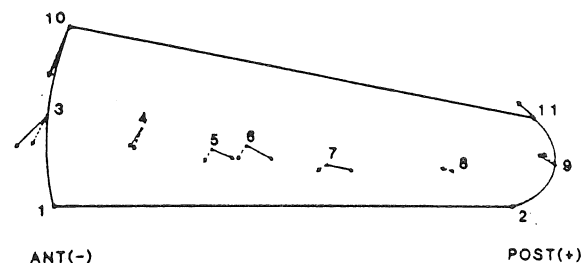


Figure 1. Sagittal plane view of internal displacements of a representative disc. Experimental data are indicated by solid lines, model predictions by broken lines.

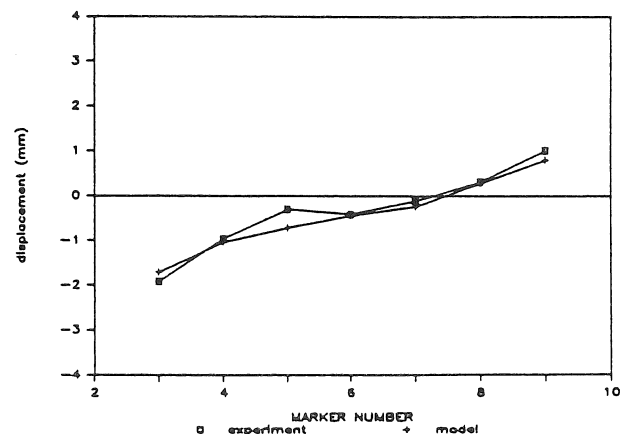


Figure 2a. Average marker displacement in the up-down direction.

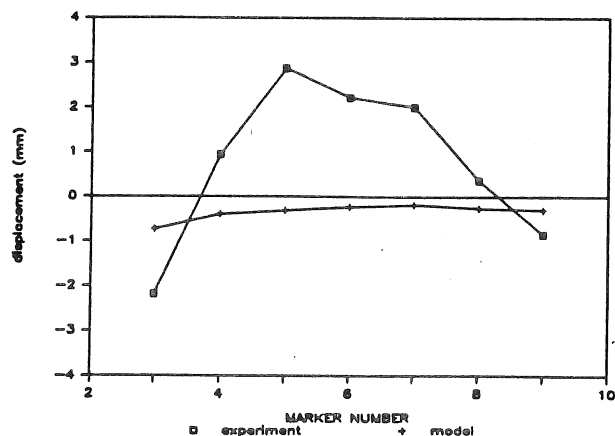


Figure 2b. Average marker displacement in the anterior-posterior direction.

### CONCLUSIONS

1. Empirical data describing the internal displacements of the intervertebral disc under a flexion-compression load are described here for the first time.
2. These data agree closely with the predictions for a linear elastic isotropic material in the up-down direction, but are significantly different in the anterior-posterior direction.
3. The method presented here provides new opportunities to validate existing disc mathematical models.

### References

1. Krag M, Wilder DG, and Pope MH. (1983) Internal strain and nuclear movements of the intervertebral disc. Annual Meeting of the Int'l. Soc. for the Study of the Lumbar Spine, Cambridge, U.K.
2. Simon, BR, Wu JS, Evans JH, and Kazarian LE. (1984) Poroelastic structural models for human spinal motion segments. 8th Annual American Society of Biomechanics Meeting, Tucson, AZ.
3. Spilker RL, Dargirda DM, and Schultz AB. (1984) Mechanical response of a simple finite element model of the intervertebral disc under complex loading. J. of Biomechanics, 17:103-112.

D.G. Wilder\*, R.E. Seroussi\*, J. Dimnet\*\*, M.H. Pope\*

\* Orthopaedics & Rehabilitation, Given Bldg., University of Vermont, Burlington, VT 05405 USA

\*\* Ecole Centrale de Lyon, Lyon, France

## INTRODUCTION

The objective of this study was to correlate mechanical changes occurring in the intervertebral motion segment due to exposure to seated-posture loading environments (e.g., seated factory or office work, or car and truck drivers) with epidemiologic data showing an increased incidence of herniated nucleus pulposus in seated humans in static or vibration environments (3,5). The results of this study help elucidate the mechanical factors involved in the production of low back pain in humans working in a seated environment.

## REVIEW AND THEORY

The lumbar spine motion segment is at risk for long-term, mechanical derangement (12,13) as long as it is exposed to environments which: 1) increase its disc pressure (10) and 2) increase its flexibility (9,11), while: 3) decreasing its resistance to large rotations, 4) stressing the posterior aspect of the disc (6,7) and 5) repetitively loading it in the form of static or dynamic load environments (1,2,8,14). These conditions are found in sustained sitting in factories, offices, homes, and vehicles.

## METHODOLOGY

A systematic study was conducted to assess the effects of the parameters of loading rate and load exposure history upon the mechanical response of forty lumbar motion segments free to move in six degrees of freedom (figure 1). Changes in mechanical properties (main and coupled compliance characteristics (figure 2) and the segment's balance point location) were assessed before and after cyclic or static load exposures via translation-load and rotation-load tests at three different loading rates.

Load exposure history consisted of loading the lumbar motion segments as they would be while sitting for one hour in either a static environment (office or factory seat) or a conservative vibration environment (car or truck driving). After the one-hour load exposure, the segments were subjected to a rapid, flexion-compression overload event to simulate a person catching a falling load.

## RESULTS

One hour load exposures produced significant changes in the mechanical characteristics of the segments. Further mechanical property changes were observed following the overload event.

Motion segments tested at various load rates exhibited coupled viscoelastic mechanical responses.

During testing, some specimens exhibited a behavior suggestive of a buckling response. The segments exhibited a sudden large rotation in both flexion and lateral bend (up to physiologic limits). This response occurred more often in the cyclically loaded L2-3 motion segments (figures 3 and 4). The postero-lateral region of the disc may be at risk during such sudden combined rotations.

## DISCUSSION

A method and an apparatus have been developed and tested which allow the testing of the main and coupled motion, compliance and viscoelastic response of a spinal motion segment to pure axial compression loading applied at or away from the specimen's balance point. For the first time there has been shown a mechanical cause and effect response of the isolated vertebral motion segment to a known load history including: a simulated, one-hour, seated load exposure to the conservative vibration accelerations of the International Standards Organization (4), eight-hour "Fatigue, Decreased Proficiency" limit at the 5 hertz frequency. There were significant changes in the segment's coupled motion and compliance characteristics as a result of static or cyclic seated loading simulations.

## CONCLUSIONS

Segments tested have shown sensitivity to load rate, load vector (magnitude and orientation), and load history.

## ACKNOWLEDGEMENT

The authors would like to thank the NIOSH Small Grants program and IRSST for the funding to conduct this work.

## References

1. Adams, MA et al., *Spine* 10(6): 524-531, 1985.
2. Brown et al, *J. Bone & Joint Surg.*, 39-A: 1135-1164, 1957.
3. Frymoyer, JW et al, *J. Bone Joint Surg.* 65A(2):213-218, 1983.
4. ISO 2631-1978 (E), International Organization for Standardization, Ref. no. ISO 2631-1978 (E).
5. Kelsey, JL et al, *Am J.Epid* 102:63-73, 1975.
6. Keegan, JJ, *J. Bone & Joint Surg.*, 35-A:589-603, 1953.
7. Krag et al, *Intl. Soc'y Study Lumbar Spine*, Cambridge, 5-9 April 1983.
8. Liu et al, *Intl. Soc'y Study Lumbar Spine*, Cambridge, 5-9 April 1983.
9. Panjabi et al, *Ortho Clinics North America*, 8:181-192, 1977.
10. Schultz et al, *J. Bone & Joint Surg*, 64-A:713-720, 1982.
11. Schultz et al, *ASME J. Biomechanical Engineering*, 101:46-52, 1979.
12. Weisman, G et al, *Am. J. Sports Medicine*, 8:24-30, 1980.
13. Wilder, DG, *University Microfilms International*, Ann Arbor, MI, 1986.
14. Wilder, DG et al, 10th NE Bioengineering Conf, IEEE cat# 82CH1747-5, pp 9-11, 15-16 March 1982, Dartmouth College, Hanover.

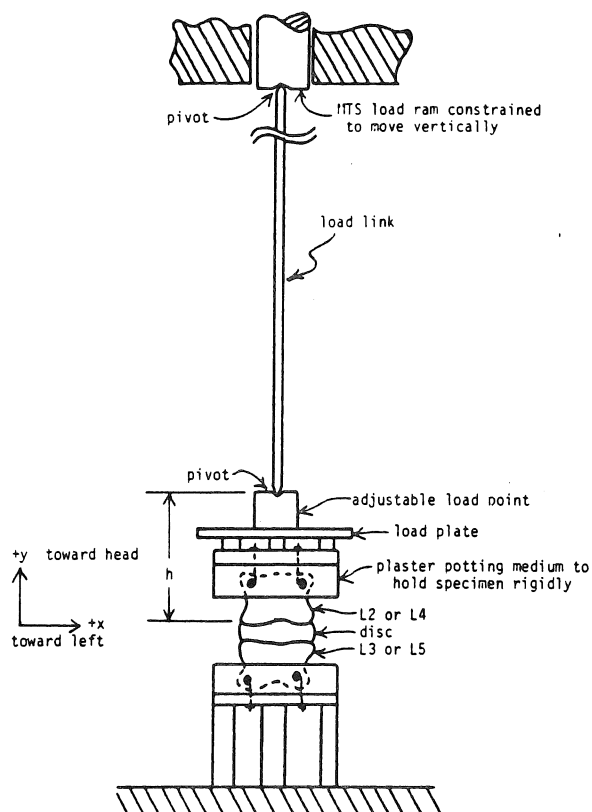


Figure 1. Loading scheme of motion segment in motion sensor. The value "h" varies with the specimen used.

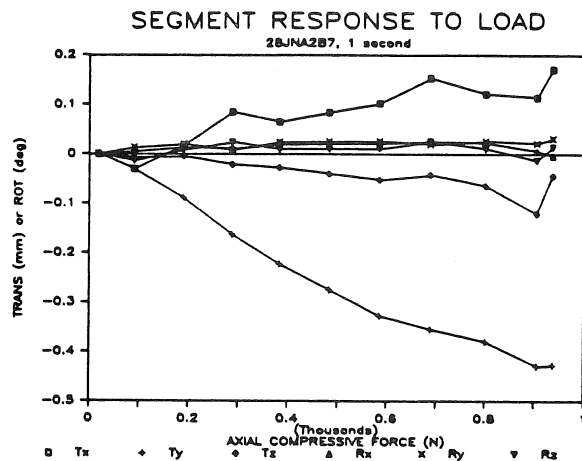


Figure 2. Typical translation and rotation responses of a motion segment (L2-3) to a compressive load applied at the original balance point. Where the slopes ("m" in mm/N or deg/N) and correlation coefficients ("r") of the linear regressions (of the data less than 1 mm or 1°) through each of the response curves are as follows:

$$\begin{aligned} T_x: (m = -.00018, r = -.91); R_x: (m = 0.0, r = -.12); \\ T_y: (m = .00048, r = .99); R_y: (m = -.00002, r = -.74); \\ T_z: (m = .00009, r = .84); R_z: (m = -.00001, r = -.17). \end{aligned}$$

Note also the negligible rotations resulting from vertical load applied at the balance point.

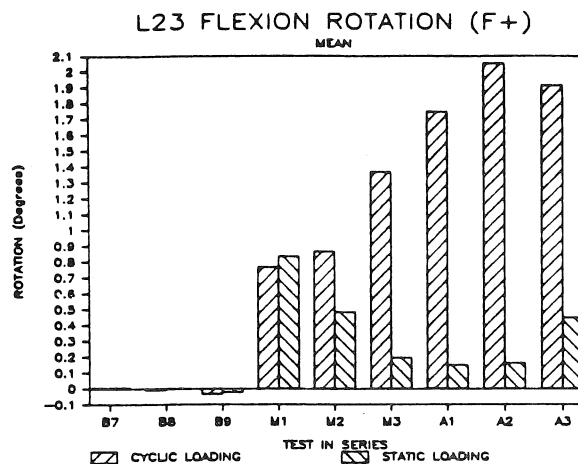


Figure 3. Histogram of the means of the L2-3  $R_x$ : flexion rotations including those exceeding 1°, due to static and cyclic load exposures, where: B7-9 are the tests at 3 different loading rates, prior to a 1-hour load exposure; M1-3 are the tests at 3 different loading rates after the 1-hour load exposure; A1-3 are the tests at 3 different loading rates after the 1-second overload event.

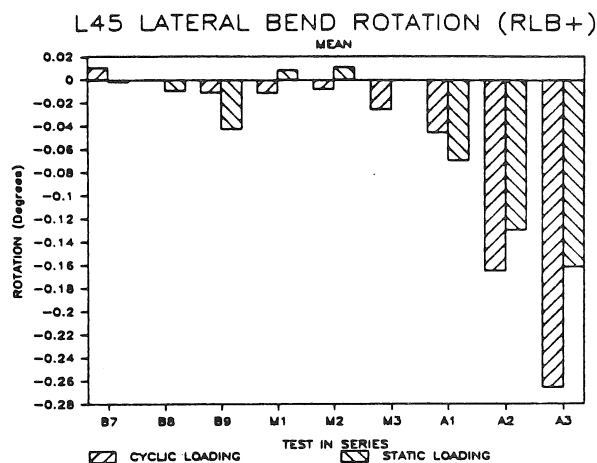


Figure 4. Histogram of the means of the L4-5  $R_z$ : lateral bend rotations including those exceeding 1°, due to static and cyclic load exposures, where: B7-9 are the tests at 3 different loading rates, prior to a 1-hour load exposure; M1-3 are the tests at 3 different loading rates after the 1-hour load exposure; A1-3 are the tests at 3 different loading rates after the 1-second overload event.

# PARAVERTEBRAL MUSCLE RECRUITMENT IN LATERAL SPINE CURVES

J.A.A. Miller, A.B. Schultz.  
Department of Mechanical Engineering,  
University of Michigan,  
Ann Arbor, MI 48109-2125, U.S.A.

H. Steen, I. Bjerkreim,  
Biomechanics Laboratory,  
Sophies Minde Orthopaedic Hospital,  
University of Oslo, Norway.

## INTRODUCTION

We are not aware of previous studies aimed at quantifying how selectively, in terms of numbers of vertebral levels and side-to-side differences, the paravertebral muscles can ordinarily be recruited in the healthy human in familiar postural tasks. In this study intramuscular electrodes were used to record unilaterally from the paravertebral muscles of healthy subjects while they performed a number of carefully-controlled, standardised postural tasks involving spine curvatures in the frontal plane.

## REVIEW AND THEORY

Idiopathic scoliosis is a lateral and torsional deformity of the spine which often progresses during the adolescent growth spurt. The factors which make the curvature(s) progress are not well understood. However, a number of theoretical studies have shown that the neural strategies used to recruit the muscles of the spine or trunk may play a major role in dictating whether a curve will progress. To improve our understanding of which muscles are normally recruited to equilibrate a laterally-curved spine, we performed a quantitative electromyographic (EMG) study of paravertebral muscle recruitment patterns in healthy subjects performing standardized tests.

## METHODS

Five healthy adults (four females and one male) between the ages of 24 and 41 years were studied. Bipolar intramuscular wire electrodes were inserted to the depth of the lamina 2 and 4 cm to the right of the midline at the T1, T6, T11 and L3 levels. EMG signals from the eight electrode pairs were amplified, rectified and low-pass filtered (50 ms) in the usual manner. Subjects stood with the pelvis firmly restrained in a test frame. To estimate spine lateral curvatures, LED markers were glued to the skin on the midline at the four selected vertebral levels. An optoelectronic (SELSPOT) system enabled the lateral positions of the LED markers to be read to the nearest 1.5mm. All signals were recorded on an FM tape recorder for later analysis of average values over each 5 second test period.

For EMG normalization purposes, subjects performed 100% efforts in isometric trunk extension and attempted lateral bending to each side. Subjects performed five tests to each side: each position was held

isometrically for at least 5 seconds. Standardized neutral head and AP trunk inclinations were used to minimize myoelectric variability. In the "lateral flexion" test subjects held T1 offset 5, 10 then 20 cm from the midline. In the "lateral curve" test subjects formed a maximal lateral curve. In the "tangent curve" test, subjects translated Head, T1 and shoulders 5 cm, then 10 cm laterally from the midline. In the "double curve" test subjects used a 2 cm buildup under one foot to assist them in forming a single curve to each side while T1 remained over S1. In the last test investigated the interaction of spine lateral curves with a pelvic tilt. Subjects stood with a fixed lateral pelvic tilt and with the spine and head oriented at right angles to a line joining the iliac crests: the pelvis and spine were first held such that T1 lay offset +10cm from a vertical reference line through the center of the sacrum. EMG and spine configuration readings were then taken as T1 was moved 5, 0 and -5 cm from the vertical reference line.

Since only right-side EMG signals were recorded, left-side EMG values were estimated by assuming symmetry, i.e. setting them equal to right-side EMG results for a given test directed in the opposite direction. For each left-directed test, differences in averaged left (L) and right (R) EMG signal amplitudes at each spine level were compared using the ratio D, where  $D = 2(L-R)/(L+R)$ . A two-sided t test was used to test the null hypothesis that  $D=0$ . Results were analysed both in terms of absolute (cited here) and normalized EMG values; the latter did not significantly reduce scatter.

## RESULTS & DISCUSSION

In general, EMG values in these activities rarely exceeded 20% of maximum values, while quiescent values in relaxed standing averaged from 1 to 5% of maximum values. The results show that paravertebral muscle activity at medial and lateral electrode sites can typically differ by 10 to 20%. In contrast, twenty-fold differences were observed between electrodes spaced four to six vertebrae apart. Thus localised unilateral recruitment over this number of vertebral levels appears possible. This is of interest because, to prevent scoliosis progression, muscles may be required to contract unilaterally only over the length of a curve convexity, which may extend only five or six vertebral levels. Table 1 shows predicted average side-to-side differences in some left-directed tests; a positive value of 1.0 indicates that

right-side EMG was 100% greater than the averaged activity for both sides. In general, the study shows that each curve type

had its own characteristic muscle recruitment pattern depending mostly, but not always, on the offset of the superincumbent body mass.

Table 1. Mean(sd) value of ratio D in three tests.

Level	L. Lat. Flex.		L. Tangent		L. Curve
	5cm	10cm	5cm	10cm	
T1	.41(.9)	.44(1.1)	.76(.7)**	.78(.8)●	.81(1.1)
T6	.70(.9)	.74(.7)	1.78(.2)**	1.58(.7)*	.12(1.3)
T11	.82(1.2)	.45(1.2)**	1.72(.2)**	1.82(.2)*	.14(1.2)*
L3	.95(.9)●	1.36(.3)	.94(1.2)	.58(1.1)	1.20(0.4)*

●:P=0.075; \*:P 0.05; \*\*:P 0.01

## The Analytical Measurement of Vertebral Rotation

VJ Raso and DL Hill

Biomechanics Laboratory  
Glenrose Rehabilitation Hospital  
Edmonton, Alberta, T5G 0B7

JB McIvor and GG Russell

Division of Orthopaedic Surgery  
University Hospital  
Edmonton, Alberta, T5G 2B7

### INTRODUCTION

The relation between scoliosis and the cosmetic deformity in Idiopathic Scoliosis is poorly understood. Recently, the significance of vertebral rotation in the pathomechanics of scoliosis has come under close scrutiny. Our own research is aimed at a complete geometrical description of the spinal and cosmetic deformity. A means of assessing vertebral rotation and its contribution to the deformity is fundamentally important to both the understanding and the clinical treatment of this deformity. As part of our studies, we undertook a review and an evaluation of methods used to measure vertebral rotation.

### THE ASSESSMENT OF VERTEBRAL ROTATION

#### A) Empirical Methods

There are a number of methods that can be used for the qualitative evaluation of rotation. Cobb (1948) described a method which depended upon the relative location of the base of the spinous process with respect to the midline and the lateral margin of the vertebral body. Nash and Moe (1969) studied the relative merits of using such a system, based on the spinous process, as compared to one based on the pedicle shadows. They radiographed spinal segments from the upper thoracic, thoracic and lumbar regions with various degrees of rotation. The migration of the convex side pedicle across the vertebral body was used as a measure of rotation. They concluded that this method was easier than Cobb's method to use and more reliable over a greater range of values.

Mehta (1973) described a method based on three anatomical landmarks: the convex side pedicle, the convex side transverse process and the convex side intervertebral foramen. She developed guidelines, based on the image of these landmarks, to be used to determine vertebral rotation. Mehta concluded that although the method is only approximate it's measurement intervals compared favourably, 15° versus 25°, to Nash and Moe and has the advantage of being able to monitor rotation through 90°.

Perdriolle and Vidal (1985) used a 'torsion meter' to measure the degree of rotation. This template used the location of the convex side pedicle relative to the lateral borders of the body. Apical rotation and the relative rotation of the two vertebrae about the superior neutral vertebra were used in an algorithm to predict curve progression.

Benson et al (1976) studied the reliability of pedicle shadow methods for measuring vertebral rotation and concluded that such methods are significantly affected by pedicle morphology and vertebral tilt which may introduce an uncertainty of 50% in the measurement. Conversely, Drerup (1984) concluded that pedicle shadow methods are

reliable and independent of lateral tilt and spinal flexion or extension when used to determine local vertebral rotation. They also proposed a simple correction factor for the Nash-Moe method.

#### B) Analytical Methods

Although empirical methods may be sufficient to determine the relative degree of rotation, they are not sufficiently precise to be useful in understanding the pathomechanics of scoliosis. For this reason investigators have attempted to define analytical techniques for measuring vertebral rotation.

Fait and Janovec (1970) proposed a similar method to that of Nash and Moe. They measured the distance between the lateral margin of the convex side pedicle and the lateral margin of the body as well as the waist diameter of the body. The ratio of these distances was taken as a measure of vertebral rotation and termed the f-factor. The outline of the convex side pedicle was used because they found that the concave side pedicle shadow disappeared with slight rotation. They presented an equation to describe the relation between vertebral rotation and the f-factor and found that it was reliable,  $\pm 3^\circ$ , up to a maximum of  $40^\circ$ .

Drerup (1984) studied 150 axial radiographs of vertebral specimens to determine the geometrical considerations that define rotation. He found that the ratio of the distance from the centre of the body to the medial margin of the pedicle, r/d, is approximately 0.6. A trigonometric function was developed based on this ratio and the distances between the medial edges of the pedicles and the body centroid. Drerup determined the accuracy to be  $\pm 5^\circ$ .

Bunnell (1984) presented a technique, similar to Cobb's method, for measuring vertebral rotation based on the relative location of the base of the spinous with respect to the lateral margins of the body. Measurements were made on radiographs, taken at  $5^\circ$  intervals up to  $30^\circ$ . Linear regression analysis was used to define the relation between these measurements and vertebral rotation. The error was found to be  $3^\circ$  on measurements made up to  $30^\circ$  of vertebral rotation.

Koreska (1985) developed a method which was based on the relative displacement of contralateral pedicle shadows as compared to the width of the vertebral endplate.

There are certainly other techniques available that can be used to determine vertebral rotation. These generally involve more extensive procedures. Matteri et al, and Pearcy and Whittle describe methods based on biplane radiography. Aaro et al (1981) used computer tomography to establish vertebral rotation.



## METHODOLOGY

A study was designed to evaluate the reliability of 3 analytical methods: Drerup, Bunnell, and Koreska, that can be used to quantify vertebral rotation. The study was limited to methods that did not require more radiographic procedures than were presently used.

A device was developed that provided an arbitrary degree of rotation. A single vertebra was mounted on this device. The vertebra was rotated, at 5° intervals from -20° to +20°, as well as at ±45°, and ±30°. A thoracic and a lumbar vertebra were tested with 3 radiographs obtained at each increment. This provided 78 views in total.

These radiographs were randomly assigned to an orthopedic surgeon, a orthopedic resident and a computer engineer. This provided 3 levels of expertise: expert, intermediate and novice. Each persons marked on the radiograph the 8 points necessary to determine vertebral rotation by each of the 3 methods. The observers was asked to comment, subjectively, on the reliability of selecting points, and hence on the method, with which he felt most confident.

The correlation coefficients and the mean errors were determined for the different methods as used by the 3 observers. The data was subjected to a linear regression analysis to determine the slope, ideally = 1, and the intercept, ideally = 0.

## RESULTS AND DISCUSSION

The correlation coefficients,  $r$ , between the actual degree of rotation and that calculated by Drerup's method, Koreska and Bunnell were 0.80, 0.90 and 0.76 respectively. The mean differences ( $\pm 1$  Std. Dev.) were  $0.6 \pm 12^\circ$ ,  $-2.5 \pm 12^\circ$ , and  $-4.4 \pm 15^\circ$ . These are not significantly different. The correlation coefficient varied from 0.63 to 0.98 for the different methods as used by persons with different levels of expertise. By chance, the expert received most of the trials with large rotations and this significantly affected his overall result. The mean errors varied from  $-1 \pm 4^\circ$  to  $-6 \pm 15^\circ$ .

The data were then divided between thoracic and lumbar vertebrae. The best result by the novice was obtained by using Koreska's method; with errors in the lumbar and thoracic spine of  $0 \pm 2^\circ$  and  $-3 \pm 5^\circ$ , respectively. The errors with the other methods varied from  $2 \pm 5^\circ$  to  $-6 \pm 10^\circ$ . The results by the intermediate observer varied from  $0 \pm 8^\circ$  to  $-11 \pm 18^\circ$  for the lumbar spine and from  $3 \pm 14$  to  $-7 \pm 11$  for the thoracic spine. For the expert the respective variation was  $-2 \pm 2^\circ$  to  $2 \pm 19$  for the lumbar segment and  $-3 \pm 9$  to  $-7 \pm 27^\circ$  for the thoracic segment.

A linear regression analysis of the calculated data against the actual data provided the following 3 regression equation:

$$a) \text{ Drerup: } Vr = 0 + 0.5 * Vr_a, \quad F_{1,70}=123$$

$$b) \text{ Koreska: } Vr = -2 + 1.0 * Vr_a, \quad F_{1,75}=317$$

$$c) \text{ Bunnell: } Vr = -4 + 0.6 * Vr_a, \quad F_{1,71}=94,$$

where  $Vr_a$  is the actual rotation present.

The data for rotations less than 30° were analyzed. Overall,  $r$  varied from 0.86, for Drerup's method to 0.97 for Bunnell's method. For novice,  $r$  varied from 0.90, using Drerup's method in the thoracic region to 0.98 for Bunnell's method in the lumbar region. For the intermediate observer,  $r$  varied from 0.73, using Drerup's method in the thoracic region to 0.99 for Bunnell's method in the thoracic region. There was insufficient data to analysis the results for the expert.

A linear regression analysis of the data for rotations less than 30° provided the following 3 regression equation:

$$a) \text{ Drerup: } Vr = -1 + 0.7 * Vr_a, \quad F_{1,52}=365$$

$$b) \text{ Koreska: } Vr = -2 + 1.1 * Vr_a, \quad F_{1,52}=365$$

$$c) \text{ Bunnell: } Vr = -1 + 1.0 * Vr_a, \quad F_{1,52}=761$$

The subjective impression of the observers was that in most cases the spinous process and the margins vertebral body, and hence Bunnell's method, were the most reliable points. None of the methods were felt to be reliable beyond 30° of rotation.

## References

- 1) Cobb JR. Outline For The Study of Scoliosis. American Academy of Orthopaedic Surgeons, Instructional Course Lectures, 5:261-275, 1948.
- 2) Nash CL et al. A Study of Vertebral Rotation. J Bone Jt Surg. 51A:223-229, 1969.
- 3) Mehta MH. Radiographics Estimation of Vertebral Rotation in Scoliosis. J Bone Jt Surg. 55B:513-520, 1973.
- 4) Perdriolle R et al. Thoracic Idiopathic Scoliosis Curve Evolution and Prognosis. Spine, 10:785-791, 1985.
- 5) Benson DR et al. Roentgenographic Evaluation of Vertebral Rotation. J Bone Jt Surg. 58A:1125-1129, 1976.
- 6) Drerup B. Principles of Measurement of Vertebral Rotation From Frontal Projections of the Pedicles. J Biomech. 17:923-935, 1984.
- 7) Fait M et al. Establishing of the Rotation Angle in the Vertebra. Scripta Medica, 43:207-215, 1970.
- 8) Drerup B. Improvements in Measuring Vertebral Rotation from the Projections of the Pedicles. J Biomech. 18:369-378, 1984.
- 9) Bunnell WP. Vertebral Rotation - A Simple Method of Measurement on Routine Radiographs. Ortho Trans. 9:114, 1985.
- 10) Monji J et al. Analysis of Spine Rotation - A New Accurate Method for Clinical Use. Spine (in press).
- 11) Matteri RE et al. A Biplane Radiographic Method of Determining Vertebral Rotation in Postmortem Specimens. Clin Ortho Rel Res. 116:95-98, 1976.
- 12) Pearcy MJ et al. Movements of the Lumbar Spine Measured by Three-Dimensional X-ray Analysis. J Biomech Eng. 4:107-112, 1982.
- 13) Aaro S et al. Estimation of Vertebral Rotation and the Spinal and Rib Cage Deformity in Scoliosis by Computer Tomography. Spine, 6:460-467, 1981.

# ESTIMATIONS OF FORCE AND MOMENT GENERATING CAPACITY OF TRUNK MUSCULATURE FROM CT SCAN MEASURES

S.M. McGill<sup>1</sup>, R.W. Norman<sup>1</sup> and N. Patt<sup>2</sup>

<sup>1</sup>Occupational Biomechanics Laboratories  
Department of Kinesiology  
University of Waterloo  
Waterloo, Ontario, N2L 3G1

<sup>2</sup>Department of Diagnostic Imaging  
St. Michael's Hospital  
Toronto, Ontario, M5B 1W8

## INTRODUCTION

Mathematical modelling of the spinal musculo-skeletal system is a potentially powerful, non-invasive method for the study of phenomena such as low back injury mechanisms and human manual load handling techniques. However, currently available models have been of limited utility because the accuracy of the predictions of sizes of forces and muscle force-time patterns has been questionable (1,2,3). The radiologic technique of computerized tomographic scanning (CT scans) has enabled the improved determination of muscle geometry, such as cross-sectional areas and moment arm lengths, on relatively large samples of active living subjects.

The purpose of this study was to measure muscle cross-sectional areas and mechanical moment arm lengths of healthy men utilizing the technique of CT scanning. These variables are essential determinants in the accurate modelling and prediction of muscle moments and resultant forces on vertebral components involved in the maintaining of static positions and in generating body segment movement.

## REVIEW AND THEORY

Until very recently, information on muscle anthropometry was obtained from tedious dissections of cadavers for use in models of the lumbar spine (1,4,5). While preserved specimens are essential for some aspects of anatomical work, the musculature bulk can be quite different when compared to young, healthy active individuals. State of the art CT scanners possess high image resolution to provide a very detailed view of tissue sections. Tissues such as muscle sheaths are easily distinguished for accurate area quantification.

## METHODOLOGY

**Subjects.** The 13 human subjects in this study (age  $\bar{X}$ =40.5 S.D.=11.9 yr; height  $\bar{X}$ =173.8 S.D.=5.9 cm; weight  $\bar{X}$ =89.1 S.D.=11.7 kg) were referred to the diagnostic imaging department of a hospital for various suspected injury and disease. Criteria for selection were that they be male, ambulant, active and relatively healthy overall. The transverse scans were taken through the level of the L4/L5 disc, with the gantry of the scanner set to the plane of the disc. The musculature was in a relaxed state.

**Data Reduction.** Thirty-five mm slides were made of the developed CT films and projected onto a tablet where perimeters of muscles, disc, peritoneum and total section areas were scribed using a polar planimeter (>95% accurate). The planimeter readings were then adjusted to the scaled grid provided on each scan.

Some muscle fibres do not run perpendicular to the anatomical transverse scan slice. Physiologic areas, needed for force estimation were obtained by correcting for fibre angles:

$$A_{io} \text{ \& } A_{eo} = (1+.25)(A_u \times \cos 45^\circ) \quad (1)$$

$$A_m = (A_{te}) (.1855) \quad (2)$$

$$A_s = (A_{te} - A_m) (\cos 30^\circ) \quad (3)$$

$$A_{ta} = (W_{ta}) (11) \quad (4)$$

where  $A_{io}$  &  $A_{eo}$ : internal and external oblique area (cm<sup>2</sup>)

$A_u$ : uncorrected anatomical area (cm<sup>2</sup>)

$A_{te}$ : total erector area (cm<sup>2</sup>)

$A_m$ : multifidus area (cm<sup>2</sup>)

$A_s$ : sacrospinalis area (cm<sup>2</sup>)

$A_{ta}$ : transverse abdominis area (cm<sup>2</sup>)

$W_{ta}$ : transverse abdominis width (cm)

Approximately one-quarter of the abdominal obliques were not observed within the scan-slice placement. This was accounted for in equation 1. The coefficients in equations 2 and 3 were derived from the work of Langenberg (6). Equation 4 assumes the average "height" of the transverse abdominis to be 11 cm. Muscle moment potential was estimated from the anterior-posterior distance from the disc centroid to the "middle" fibre of the muscle.

## RESULTS

Physiological muscle areas (corrected from anatomic areas) for both sides of the body are summarized in Table 1, along with a percentage of the total physiologic muscle area. Moment arm lengths appear in Table 2. The estimated potential of the musculature to produce force and moments, assuming various force producing potentials, are shown in Table 3.

## DISCUSSION

The results of this study indicate disparities in the areas calculated and utilized in models by other research groups. The subjects of this study were certainly younger and heavier than those of most cadaver studies. For example, the psoas group is twice the area of that quoted by Eycleshymer and Shoemaker (7) and used by Farfan (1). The uncorrected erector area was 142% of the values quoted in another CT scan study by Reid and Costigan (8). The abdominal wall was quite similar to those of other research groups although the rectus abdominis was found to be larger in this study.

The muscle forces predicted in Table 3 are not for the entire muscle but only that position that can be observed in an L4/L5 slice. For example, the work of Langenberg (6) suggests that the actual sacrospinalis area may approach 2<sup>1</sup>/<sub>2</sub> times that seen at the L4/L5 level. It is interesting that the moment provided by the erector area seen within the scan plane is in the range of those quoted by Farfan (1) for the entire extensor musculature. Powerful extensors, not observed at the L4/L5 level, such as sacrospinalis

laminae to L5, L2 and L1, iliocostalis lumborum, longissimus thoracis and other extensors such as quadratus lumborum and latissimus dorsi must be considered for estimating the total extensor capacity. Once these muscles are considered, the prediction of 420 Nm (4) and measurement of 490 Nm (9) being produced almost entirely by extensor musculature, becomes feasible.

Prediction of muscle areas, using linear regression, from the simple variables of subject height and weight was not supported by the data of the 13 subjects of this study. Only the areas of psoas and internal oblique yielded a statistically significant multiple R with height and weight but the  $r^2$  values were only .65 and .63, respectively.

Muscle data derived from living, working individuals using the technique of CT scan radiography, describes both larger muscle areas and larger moment producing potential than previously reported.

#### References

1. Farfan, H.F. Mechanical Disorders of the Low Back. Lea and Febiger, 1973.
2. Gracovetsky, S., et al. SPINE 6:249-262, 1981.
3. Schultz, A.B., et al., J. Bone Jt. Surg. 64-A: 713-720, 1982.
4. Morris, J.M., et al., J. Bone Jt. Surg. 43-A: 327-351, 1961.
5. Rab, G.T., et al., Orthop. Clin. N. Am. 8:193-199, 1977.
6. Langenberg, W., Z. Anat. Entwickl. 132:158-190, 1970.
7. Eycleshymer, A.C., and Shoemaker, D.M. A Cross Section Anatomy. Appleton Co., 1911.
8. Reid, J.G., and Costigan, P.A., J. Orthop. Sports Phys. Ther. 6:278-280, 1985.
9. Troup, J.D.G., and Chapman, A.E., J. Biomech. 2:49-62, 1969.

TABLE 1. Areas observed in CT scans. Muscle areas are corrected for fibre angle and division of erector mass (physiologic area).

		Average area [cm <sup>2</sup> ]		Area as a % of total m. area	
		$\bar{X}$	S.D.	$\bar{X}$	S.D.
Sacrospinalis	R	15.3	2.6	11.6	1.5
	L	16.5	2.5	12.6	2.1
Multifidus	R	4.0	0.7	3.1	0.4
	L	4.3	0.7	3.3	0.5
Rectus Abdominis	R	8.3	3.0	6.6	2.5
	L	7.5	2.0	6.1	2.0
External Oblique	R	8.8	2.7	6.7	2.0
	L	10.0	2.7	7.6	1.6
Internal Oblique	R	7.7	2.1	5.9	1.5
	L	8.5	2.5	6.6	1.6
Transverse Abdom.	R	2.9	1.3	2.2	0.7
	L	2.9	1.3	2.2	0.7
Psoas	R	17.2	3.7	13.0	1.8
	L	18.0	4.2	13.6	2.0
Disc Area		19.0	2.4		
Peritoneal Cavity		144.4	66.7		
Total Area		647.1	152.0		

TABLE 2. Distance (cm) or moment arm (M.A.) from disc centroid to middle fibre within a muscle (right side of body). Negative values correspond to a moment arm posterior to the disc centroid.

	Lateral $\bar{X}$	M.A. S.D.	Ant. $\bar{X}$	Post. M.A. S.D.
Erector Area	3.26	.36	-5.90	.52
Erector Common Tendon	1.98	.35	-8.49	.68
Rectus Abdominis	4.35	1.31	10.28	2.07
External Oblique	13.83	1.03	4.63	1.68
Internal Oblique	11.57	1.30	5.77	1.47
Psoas	4.88	.36	.58	.40

TABLE 3. Muscle forces and the flexion-extension moment (Nm) of each muscle assuming various values of force producing potential.

Muscle Force (N)	Force Producing Potential (N/cm <sup>2</sup> )			
	30	50	70	90
Psoas	540	900	1260	1620
Erector Area	1350	2250	3150	4050
External Oblique	280	470	658	846
Internal Oblique	243	405	567	729
Rectus Abdominis	237	395	553	711
Muscle Moment (Nm)				
Psoas	6	10	14	18
Erector Area	80	113	186	239
External Oblique	26	43	61	78
Internal Oblique	28	47	65	84
Rectus Abdominis	49	81	114	146

Note: These values are calculated from the muscle area seen in a transverse slice at the L4/L5 level. For example, the erector area may be more than 3 times that seen at L4/L5.

# OBJECTIVE DETERMINATION OF TRUNK MUSCLE DIMENSIONS USING ULTRASOUND: IMPLICATIONS FOR LOW BACK PAIN RESEARCH

M. H. Krag, L. Miller, K. B. Byrne, L. G. Gilbertson, G. B. Johnson  
The Vermont Rehabilitation Engineering Center  
The University of Vermont, Burlington, Vermont 05405

## INTRODUCTION

Quantitative descriptions of muscle size and location are important issues in spine biomechanics. However, until recently, there have been major limitations in the techniques available to determine these muscle dimensions *in vivo*. For example, studies have shown that circumference measurements of the thigh are poor indicators of changes in quadriceps muscle bulk, even if allowances are made for skinfold thickness (1,2,3). Muscle biopsies, in addition to being invasive, have limited usefulness because major assumptions must be made concerning the number of fibers in the muscle and the extent to which biopsies of tiny areas can indicate changes in whole muscles (4). Cadavaric muscle dimensions may be distorted during specimen preparation and have not been correlated with live subjects. CT scans are accurate, but involve significant irradiation. Indirect methods such as trunk strength or EMG may be used, but must be correlated with muscle dimensions. In contrast, ultrasonic scanning has developed sufficiently to allow widespread use in defining cross-sectional views of many internal body structures, including muscles. Presented here is the first study of the error of measurement reproducibility of ultrasound scans of the trunk muscles.

## METHODS

Ten healthy, adult males had transverse ultrasonic scans of the trunk extensor and flexor muscles taken at the L3 (third lumbar vertebra) level, using a Picker #80LDI ultrasonic scanner with a 5 MHz transducer (focal zone of 3-5 cm). Sagittal scans of the extensor muscles were taken at various distances (0.0, 1.0, 2.0, 3.0, 3.5 cm) from the midline. Duplicate scans were taken 10-15 minutes later, with subject positioning and machine set-up repeated.

Next, an 8x10 photo-enlargement was made of each scan. Local coordinates were then established using anatomical landmarks on the scans. Significant anatomical features were traced manually from the photo-enlargements of the transverse scans, and from the sagittal extensor scans taken at 3.0 cm off the midline (the latter provided the best delineation of the extensor muscles). The transverse scans of the trunk extensors did not provide enough detail to be useful. One tracing of a photo was done at a time, repeatedly selecting a photo at random from the entire pool of photos, until each had been traced three times. The various muscle dimensions were measured using an x-y digitizer for the areas and a millimeter ruler for the lengths and widths.

The following dimensions were used: length, width, and area for the rectus abdominis (RA); width and area of the external oblique (EO), internal oblique (IO), and transversus abdominis (TA); and width of the oblique group (OG = EO, IO, TA + thickness of the fasci between them). On the sagittal scans, depth of the spinous process (SP) from the skin surface was measured at the L1-L4 levels. All anthropometric data are scaled to life size.

In order to determine the error in the observer's ability to digitize the information, one set of measurements of the dimensions on each tracing was done at a time, repeatedly selecting a tracing at random from the entire pool of tracings, until each muscle dimension had been measured twice. This means that across all subjects and time points, a total of 120 measurements were made of each dimension. From this data, various extrapolations were made using the repeated-measures analysis of variance test in order to examine the how the error of measurement reproducibility changes as the number of subjects, time points, tracings per scan, and measurements per tracing are varied.

## RESULTS

The first two columns of Table 1 present the means and standard deviations of all muscle dimensions across all 120 measurements. The analysis presented in the other columns of Table 1 indicates the amount of relative change in the various muscle dimensions needed between two time points in order for that change to be statistically significant. The difference detection threshold has been chosen at the 95% confidence level. The various columns present the expected errors for sample groups of 1, 10, and 50 subjects; one or two time points; and one or four measurements per tracing of the photo-enlarged ultrasound scans. Both one-tailed and two-tailed analyses have been included for the columns for multiple subjects.

Further analysis indicates that approximately 16% of the variability in measurement is due to errors between scans taken 10-15 minutes apart, 74% is due to errors in the manual tracing of the photo-enlargements, and 10% is due to errors in taking measurements from the tracings with the ruler or x-y digitizer.

## DISCUSSION

While inter-individual variation is relatively large, as expected, reproducibility error is acceptably small for certain important dimensions, especially erector spinae depth, oblique group width and rectus abdominis length. As expected, increasing the number of measurements per scan and the size of the sample improves measurement reliability. Our results show that ultrasound can provide reliable, non-invasive measurements of trunk muscles using standard clinical scanners and reasonably small groups of subjects. Further research is currently underway in our laboratory to determine the correlation between CT scans and ultrasound scans of the trunk muscles, and examine the effects of exercise and lumbosacral corsets on trunk muscle dimensions.

Table 1.

## REPRODUCIBILITY ERRORS OF ULTRASOUND TRUNK MUSCLE SCANS

# of Subjects	1	1	10	10	10	10	50	50
# of Time Points	1	1	2	2	2	2	2	2
# Scans/Time Point	1	1	1	1	1	1	1	1
# Tracings/Scan	1	4	1	1	4	4	4	4
# Meas./Trace	1	4	1	1	4	4	4	4
1 or 2 tailed analysis	-	-	1	2	1	2	1	2

Dimension	Mean	S.D.	<-----Reproducibility Error----->									
RA LENGTH	7.4	0.9	16%	8%	12%	13%	6%	7%	3%	3%		
RA WIDTH	1.3	0.4	23%	14%	23%	25%	9%	10%	4%	4%		
RA AREA	7.6	2.5	30%	20%	23%	26%	15%	16%	7%	7%		
EO WIDTH	0.9	0.2	22%	12%	17%	18%	8%	9%	4%	4%		
EO AREA	4.1	1.4	30%	19%	22%	24%	14%	15%	6%	7%		
IO WIDTH	1.2	0.2	33%	14%	25%	27%	10%	11%	4%	5%		
IO AREA	6.0	1.0	17%	12%	12%	14%	9%	10%	4%	4%		
TA WIDTH	0.4	0.1	50%	28%	37%	41%	22%	24%	10%	11%		
TA AREA	1.6	0.5	50%	32%	37%	41%	23%	25%	10%	11%		
OG WIDTH	3.2	0.5	13%	7%	9%	10%	5%	6%	2%	3%		
SP DEPTH AT L1	3.0	0.4	13%	7%	10%	11%	5%	6%	2%	3%		
SP DEPTH AT L2	3.2	0.5	13%	8%	9%	10%	6%	6%	3%	3%		
SP DEPTH AT L3	3.4	0.5	18%	9%	13%	14%	7%	7%	3%	3%		
SP DEPTH AT L4	3.5	0.5	17%	8%	13%	14%	6%	6%	3%	3%		

Note 1: Means and S.D.'s in cm. or cm<sup>2</sup>

Note 2: Means and S.D.'s are for all 120 measurements (i.e. 10 subjects x 2 time points x 3 tracings per photo-enlargement of each scan x 2 measurements for each tracing).

## REFERENCES

1. Ingemann-Hansen T and Halkjaer-Kristensen J: Lean and fat component of the human thigh: The effects of immobilization in plaster and subsequent physical training. Scand. J. Rehab. Med. 9:67-72, 1977.
2. Kirwan JR, Byron MA, Winfield J, Altman DG, and Gumpel JM: Circumferential measurements in the assessment of synovitis of the knee. Rheum. and Rehab. 18:78-84, 1979.
3. Nicholas JJ, Taylor FH, Buckingham RB and Ottonello D: Measurement of circumferences of the knee with ordinary tape measure. Ann. Rheum. Dis. 35:282-284, 1976.
4. Young A, Hughes J, Russell P, Parker MJ, Nichols PJR: Measurement of quadriceps muscle wasting by ultrasonography. Rheum. and Rehab. 19:141-148, 1980.
5. Ferrucci JT: Body ultrasonography. New Eng. J. Med. 300: 590-602, 1979.

## Acknowledgement

This work was supported by a grant from the National Institute of Handicapped Research, U.S. Dept. of Education (#G008303001-03).

M. Parnianpour, L. Pavlidis, F.J. Bejjani, M. Nordin

Occupational and Industrial Orthopaedic Center,  
The Hospital for Joint Diseases Orthopaedic Institute,  
New York University,  
Program in Ergonomics and Occupational Biomechanics,  
New York, New York, U.S.A.

## INTRODUCTION

In previous studies, the authors demonstrated the existence of a high inverse correlation between knee and back forces during sagittal lifting (1). A highly significant correlation was also found between the anthropometric measurements and the minimal and maximal values of the knee and back joint reaction forces. The effects of load height and weight on the total force on the body were also analyzed (2). Based on these results, and in order to individualize and optimize lifting technique, the Lifting Stress Calculator, a microprocessor based device, was designed (3).

Other studies stressed the importance of the load horizontal distance from the heel during lifting (4,5).

The purpose of this paper is to investigate the effect of the various load parameters on the knee and lumbar spine during lifting, adding the horizontal load distance as a variable to the previous model (2). This new model is evaluated, using data taken from actual test subjects.

## REVIEW AND THEORY

It is a two-dimensional static model of symmetric sagittal bimanual lifting, based on trigonometry and anthropometry (2). It represents the projection in the sagittal plane of the mechanical axes of the spine and the dominant upper and lower limbs of an individual. This position corresponds to the phase when the load is just about to leave the ground. Using free-body analysis, equations for JB and JK, the L4-L5 and tibio-femoral joint reaction forces respectively, were derived.

## METHODOLOGY

The anthropometric data were collected, using an anthropometric tape, from 53 subjects, 27 males and 26 females (Table).

	Number	Age (years) Mean (SD)	Weight (kg) Mean (SD)	Height (m) Mean (SD)
Females	26	21.92 (8.92)	57.25 (7.91)	1.60 (0.06)
Males	27	25.11 (8.26)	79.56 (11.88)	1.77 (0.08)
Total	53	23.55 (8.66)	68.62 (15.28)	1.69 (0.11)

Table. Demographic distribution of the sample, with mean ( $\pm$  Standard deviation) age, weight and height.

A computer program was written to solve the equations previously derived. The program was run several times for each subject, varying one load parameter and keeping the other two constant. The values used for these parameters were ratios of the relevant anthropometric measurements of the subject, in an attempt to individualize the results. The horizontal distance of the load, D, was varied from 1/60 to 1/3 of the trunk length, b, by increments of b/20, while the load height, H, was kept constant at 1/3 of e (distance between the knuckles and the ground, when standing upright); and the load weight, P, was kept constant at 1/5 of the subject's weight, W. Then H was varied from 1/57 to 1/3 of e, by increments of e/19, while D was kept constant at b/3 and P at W/5. P was then varied from 1/90 to 1/5 of W, by increments of W/18, while D was kept constant at b/3 and H at e/3.

For each of these load conditions, all possible lifting positions, according to the model, were considered and the related JB and JK forces computed. Minimum JB and JK, with their corresponding back and knee flexion angles, were then obtained for each of the load conditions, and normalized over body weight for each subject:  $JBm/W$  and  $JKm/W$ . Averages and standard deviations of these ratios were then tabulated and plotted graphically as a function of each of the three load parameters (Figures 1 and 2).

## RESULTS

1. As seen in Figures 1A and 2A, increase in load height did not affect much the minimum knee force, while the minimum back force decreased slowly in the beginning then rapidly. Both knee and back angles, corresponding to those forces, decreased with increasing load height.
2. Increase in load weight, as seen in Figures 1B and 2B, was followed by a rather rapid increase in the minimum back force and a very slow increase in the minimum knee force. The back angle, corresponding to this minimum back force remained unchanged; while the knee angle, corresponding to the minimum knee force, increased slowly.
3. When the horizontal load distance increased, both the minimum back force and its corresponding back angle increased (Figure 1C). However, the minimum knee force and its corresponding knee angle followed different irregular trends (Figure 2C).

## DISCUSSION

As expected, the overall magnitude of minimum forces was larger for the back (2-4W) than the knee (0.5-2.5W). The larger standard deviations of the former suggest a more significant role of individual anthropometry in minimizing back forces, as compared to knee forces. The latter seems to be mostly dependent on the load distance from the body.

At last, back and knee flexion angles did not always follow the same trends as the corresponding forces. This suggests that standard biomechanical computations are not sufficient to predict the optimal lifting posture for a given individual.

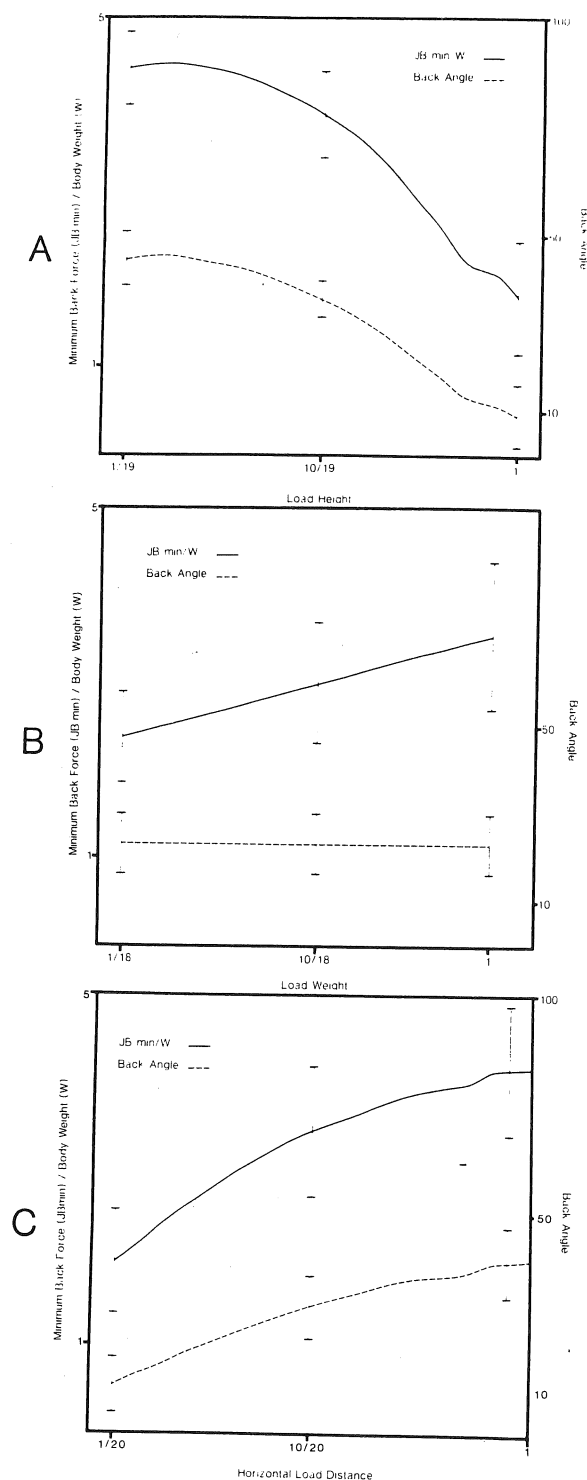


Figure 1. Average ( $\pm$  Standard deviation) normalized minimum back (L4-L5) joint reaction force and corresponding back flexion angle, as a function of load height (A); load weight (B); and load horizontal distance (C).

#### References

1. Bejjani, F.J.; Gross, C.M.; and Pugh, J.W.: Stress relationship between the knee and the back. Proceedings of the International Society for the Lumbar Spine, Cambridge, U.K., 1983.
2. Bejjani, F.J.; Gross, C.M.; and Pugh, J.W.: Model for static lifting: Relationship of loads on the spine and the knee. J. Biomechanics 17(4): 281-286, 1984.

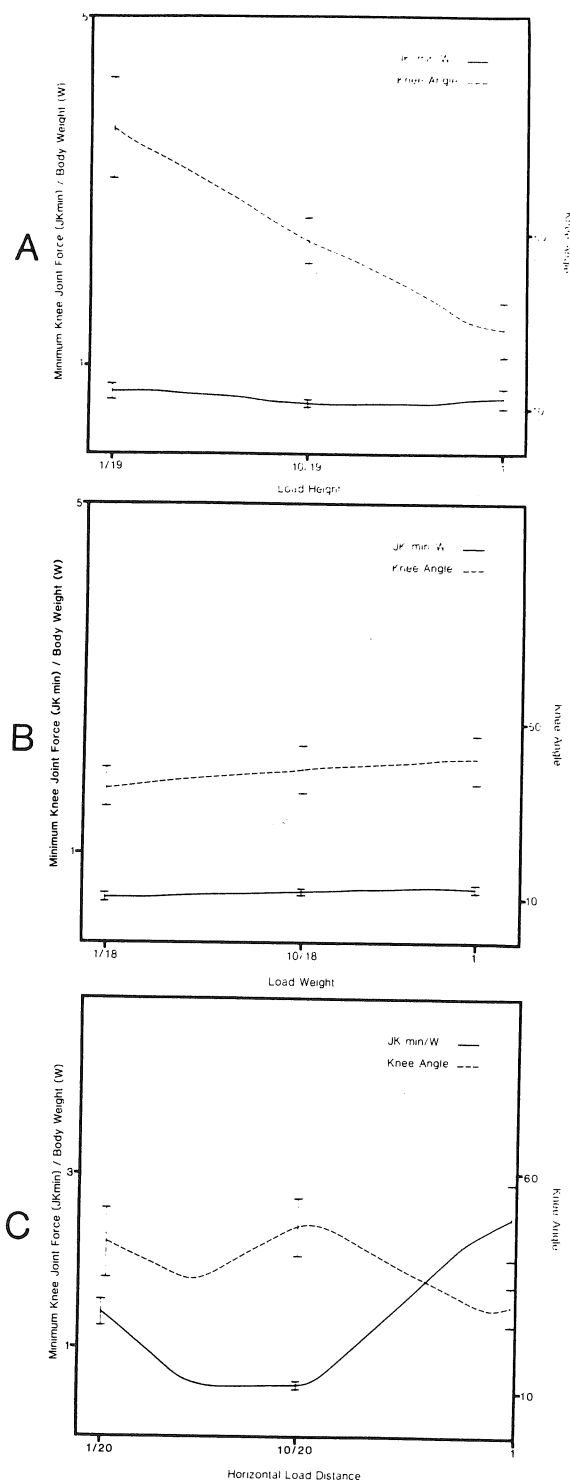


Figure 2. Average ( $\pm$  Standard deviation) normalized minimum knee (tibio-femoral) joint reaction force and corresponding knee flexion angle, as a function of load height (A); weight (B); and horizontal distance (C).

3. Bejjani, F.J.; Josephson, K.A.; Thornton, Jr., R.B.: The Lifting Stress Calculator. J. Biomed. Eng. 6: 219-222, 1984.
4. Parnianpour, M.; Bejjani, F.J.; Pavlidis, L.; Bejjani, N.: The Lifting Stress Calculator. Study of various lifting parameters in 53 subjects. In: Trends in Ergonomics/Human Factors III, North-Holland, 1986.
5. Bendix, T. and Eid, S.E.: The distance between the load and the body with three bimanual lifting techniques. Appl. Ergonomics 14:185-192, 1983.

# THE USE OF TRUNK MUSCLE ELECTROMYOGRAPHY TO HELP VALIDATE A SIMPLE PHYSICAL MODEL FOR LIFTING TASKS

R. E. Seroussi, M. H. Pope  
Department of Orthopaedics & Rehabilitation  
The University of Vermont, Burlington, VT 05405

## INTRODUCTION

We present a simple out-of-sagittal plane physical model of the spine to quantify the relationship between moments in the frontal and sagittal planes, generated by a lifting task, versus the electromyographic (EMG) activity of right and left trunk muscle groups. As a validation procedure, we collect lifting moment data and surface EMG of the erector spinae and external oblique muscles for 10 males performing a grid of frontal and sagittal plane tasks. As expected, we obtain high correlation ( $r^2 > .95$ ) between: 1) the sagittal plane moment versus right plus left erector spinae EMG and 2) the frontal plane moment versus right minus left erector spinae EMG. This simple model gives insight into the function of the spine and the trunk muscles when performing lifting tasks.

## REVIEW AND THEORY

Andersson et al. (1) explored lifting moments in the sagittal and frontal planes versus predicted force in the erector spinae and external oblique muscles. They obtained good correlation of erector spinae predicted force and measured EMG, but did not measure the external oblique muscles or attempt a systematic model validation. Schultz et al. (2) used linear programming techniques for a much more complex model to predict muscle forces and the reaction force on the spine.

We hypothesize that the functional dependence between erector spinae muscle activity and the applied moments about the spine due to lifting is as follows:

$$M_s = f(\text{RES} + \text{LES}) \quad (1)$$

$$M_f = g(\text{RES} - \text{LES}) \quad (2)$$

where RES and LES are the RMS EMG activity of the left and right erector spinae muscles,  $M_s$  and  $M_f$  are the applied sagittal and frontal plane moments about the spine, and  $f$ ,  $g$  are general monotonic functions. The physical justification for equations (1) and (2) in terms of muscle forces counteracting applied loads, comes from the balance of moments equations for the simple model in Figure 1.

To test the validity of equations (1) and (2), we measure erector spinae EMG activity and the applied moments about the spine for a set of lifting tasks. For these tests, we also obtain left and right (LEO, REO) external oblique EMG activity, but do not try to incorporate these muscles into our simple model. However, we present the REO and LEO data to offer a qualitative picture of the stabilizing effect of the external oblique muscles for large frontal plane moments.

## METHODOLOGY

We collected surface EMG and lifting moment data for 10 standing males performing a grid of 28 frontal and sagittal plane lifting tasks. For these

tests, we measured EMG for the left and right erector spinae and for the left and right external oblique muscles. At each of four constant sagittal plane moment arms (20, 25, 30, 35 cm), the subject held a weight of 75 Newtons (7.6 kg mass) in seven positions across the frontal plane. From the mid-sagittal plane these seven positions, each representing a different frontal plane moment arm, were -30, -20, -10, 0, 10, 20, 30 cm. We also measure EMG for an unloaded standing posture. At each static position, raw EMG signals from the four muscle groups were clocked into an A/D converter controlled by a microcomputer. A digital RMS-to-DC algorithm was developed for processing raw EMG. EMG data for each subject at each position were normalized and averaged across all subjects.

## RESULTS AND DISCUSSION

The EMG signals from the right and left erector spinae muscles varied with moments in both the frontal and sagittal planes. This is shown in Figure 2, where the EMG signals are plotted against the frontal plane moment arm, with the sagittal plane moment arm as a parameter. Figure 3 shows that the sum of the right and left erector spinae EMG signals at each position depended only on the sagittal plane moment ( $r^2 = .96$ ) and not on the frontal plane moment ( $r^2 < .004$ ). Figure 4 shows that their difference depended only on the frontal plane moment ( $r^2 = .95$ ) and not on the sagittal plane moment ( $r^2 < .004$ ), confirming the hypotheses.

As shown in Figure 5, agonist external oblique muscle activity was quiescent until a threshold frontal plane moment arm of 15 cm, beyond which it rises sharply to stabilize the spine.

## References

1. Andersson, G.B.J. et al. (1980) *J. Biomech.* 13, 513-520.
2. Schultz, A. et al. (1983) *J. Orthop. Res.* 1, 77-91.

Figure 1. Out-of-sagittal plane physical model.

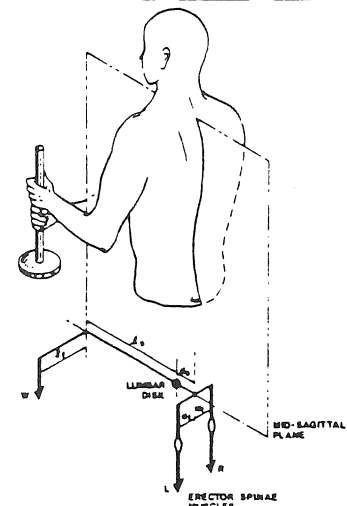




Figure 2. Normalized RMS EMG activity for erector spinae muscles, average of 10 subjects.

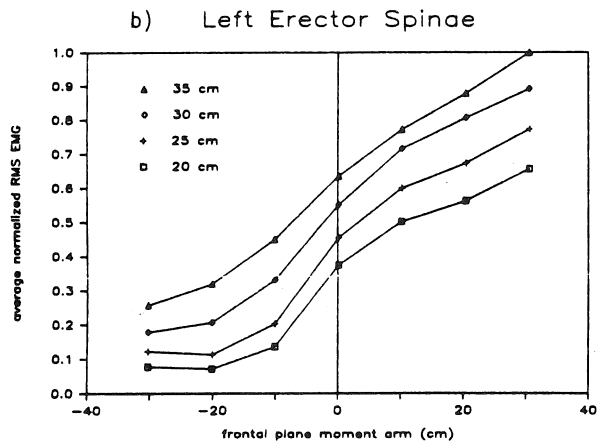
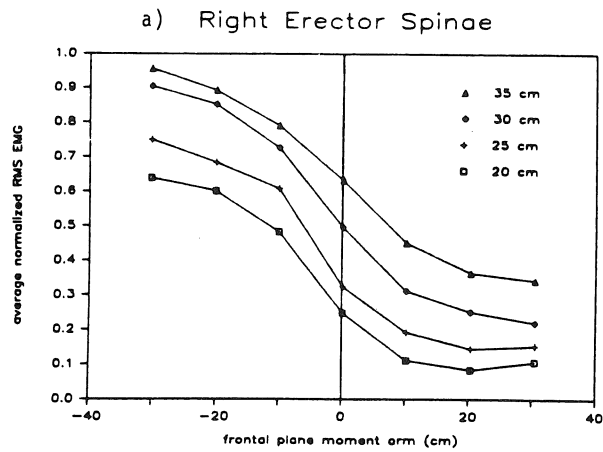


Figure 3. Sum of erector spinae EMG.

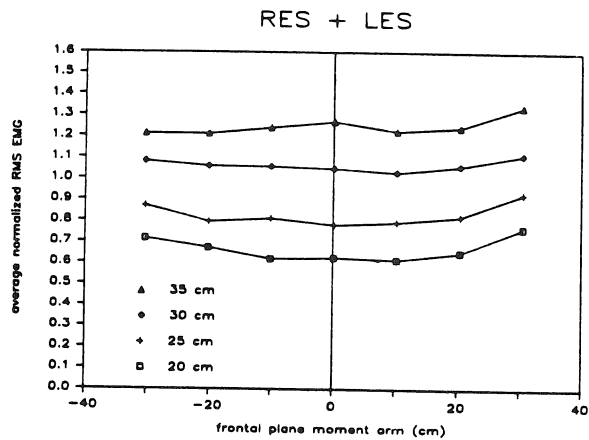


Figure 4. Difference of erector spinae EMG.

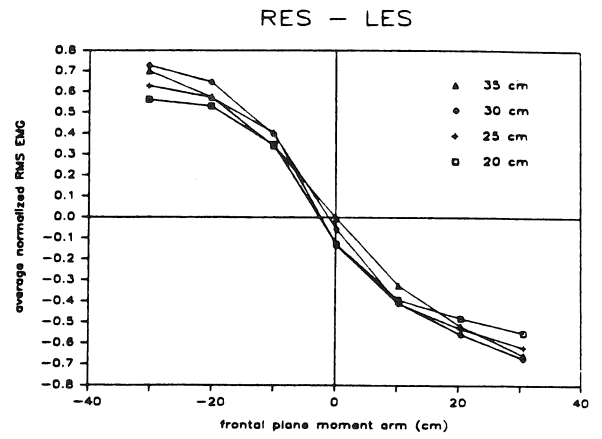
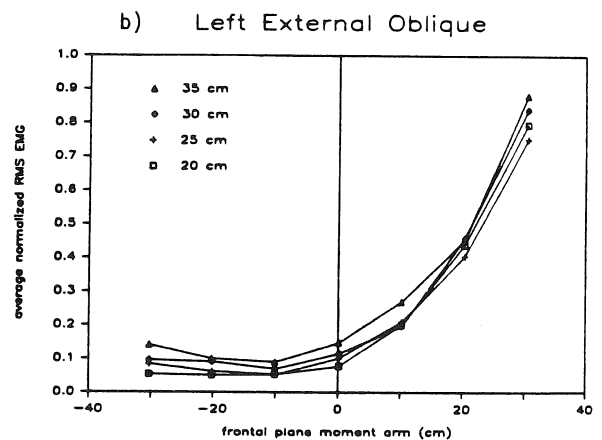
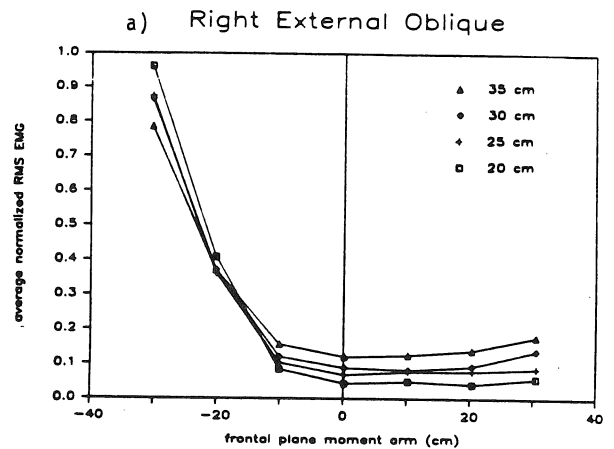


Figure 5. Normalized RMS EMG activity for external oblique muscles, average of 10 subjects.



H. VAILLANCOURT, G. DROUIN and G. MCINTYRE  
 Department of Mechanical Engineering, Ecole Polytechnique of Montreal,  
 P.O. Box 6079, Station "A", Montreal, Canada, H3C 3A7.

## INTRODUCTION

The cancellous bone is largely responsible for the mechanical behavior of the human vertebra. Although it is a composite structure consisting of trabeculae surrounded by marrow, it has been often modeled as a continuous medium. Because of the interest in understanding bone behavior, a model of the cancellous bone of a human lumbar vertebra has been developed. The present model only take into account the bony structure. The interaction of the bone marrow is not included.

The external loading on the spine creates a complex mechanical loading on the disk and the vertebral plates. The cortical (cortex of the vertebra) and the cancellous bone are physically arranged to support that loading. Large finite element models are used to study the effects of this loading. However a better understanding of cancellous bone behavior is essential to obtain more accurate results. To achieve this, the physical arrangement of the trabeculae should be taken into account. In the present model, cancellous bone is modeled as an assembly of struts rigidly connected.

## REVIEW AND THEORY

Traditionally, the cancellous bone has been modeled as a continuous isotropic medium. More recently, an approach based on the structure of the cancellous bone has been used in finite element modeling. Williams (1) drew the exact outline of the structure in a 2-D plane section, made a mesh with the surface obtained and assumed a constant thickness. This provides a very specialized model. Pugh (2) used plates to create a generalized structural model of the cancellous bone of the femur. Real geometrical parameters had to be changed to obtain realistic behavior of the model. Beaupre (3) made an analogy between the structure of the cancellous bone and an open-celled foam. He modeled the "cells" of the cancellous bone with a fine mesh. It permits to analyse the stresses in the trabeculae.

It is well known that the pattern of the cancellous bone changes from one bone to another. Because the aim was to reproduce the mechanical behavior of the cancellous bone of the human lumbar vertebra, data related to that particular bone was sought. Oxnard (4) observed that it has a generally orthogonal pattern. Whitehouse (5) used the scanning microscope to measure the mean length and size of its trabeculae. Kafka (6) analysed the effect of the marrow on the mechanical behavior of the vertebra. He found that in static loading, except for high magnitude loads, the marrow has negligible effect.

## METHODOLOGY

From the observations of these reseachers and ours, an idealised 3-D model made of bony struts was created. This model is suitable for every human lumbar vertebrae because some variable geometrical parameters allow to change the density of the bone.

Enlarged photographs of sections through the vertebrae were made. Sections in the longitudinal axis of the vertebral column gave us the mean length of the vertical trabeculae, that is 1 mm. From sections parallel to the coronal plane, it was found that each cell has a mean number of sides of 5. From the number of those cells per unit area, the length of horizontal trabeculae was calculated and that is between .75 and 1 mm. Those results are in good agreement with Whitehouse's results (5). The model showed on figure 1 was created where the axis 3 is perpendicular to the coronal plane. The trabeculae are modeled as struts that are rigidly connected. To implement the observed pentagon geometry, hexagons were used because they can easily be assembled and each hexagon was divided in two thus creating the desired pentagon geometry.

The vertical trabeculae are not exactly perpendicular to the coronal plane. So, the orientation of vertical struts that are joining each plane of pentagons is at an angle with axis 3. Models have been created with different angle. Two of them are included in this paper: model #1 refers to the small angle while model #2 refers to the larger angle.

Finite element method was used to simulate mechanical compression tests. Displacements were imposed at the nodes in three (3) orthogonal directions and they were processed by static condensation. The aim is to obtain the macroscopic mechanical orthogonal properties of the cancellous bone. The sum of the forces (computed by finite element method) on each side of the cube are divided by the area in order to have the stress. Three (3) cases of imposed displacements gives the following system :

$$\begin{bmatrix} a_{11} & a_{12} & a_{13} \\ a_{21} & a_{22} & a_{23} \\ a_{31} & a_{32} & a_{33} \end{bmatrix} \times \begin{bmatrix} S_{11} & S_{12} & S_{13} \\ S_{21} & S_{22} & S_{23} \\ S_{31} & S_{32} & S_{33} \end{bmatrix} = \begin{bmatrix} e_{11} & e_{12} & e_{13} \\ e_{21} & e_{22} & e_{23} \\ e_{31} & e_{32} & e_{33} \end{bmatrix}$$

where,  $S_{ij}$  : Stress (Mpa)

$e_{ij}$  : Deformation ( $10^{-6}$  m/m)

$a_{ik}$  : terms of the compliance matrix

$i, k$  : refer to the axis

$j$  : refers to the imposed displacements test number

$$a_{11} = 1/E_1$$

$$a_{22} = 1/E_2$$

$$a_{33} = 1/E_3$$

$$a_{12} = \nu_{21}/E_2 = a_{21} = \nu_{12}/E_1$$

$$a_{13} = \nu_{31}/E_3 = a_{31} = \nu_{13}/E_1$$

$$a_{23} = \nu_{32}/E_3 = a_{32} = \nu_{23}/E_2$$

where,  $E_i$  : Elastic modulus

$\nu_{ij}$  : Poisson ratio

$i, j$  : refer to the axis

The solution of this system gives the compliance matrix which contains the macroscopic mechanical properties of a cube of cancellous bone. This matrix is always symmetric.

## RESULTS

Rather than trying to obtain absolute value of the mechanical properties of the cancellous bone, the emphasis of the exercise was to study the sensitivity of the model to the following parameters:

- length of the vertical struts (Lvs)  
(in fact, this length is the distance between two planes of pentagons)
- length of the horizontal struts (Lhs) or number of cells per unit area
- modulus of elasticity of the bony struts (E)
- radius of the bony struts (R)
- vertical angle (model #1 or model #2)

Typical results of the study are presented in table 1. It also includes a comparison with Williams' results which were measured on dried and degreased cancellous bone from tibia. Since reported results were characterized by three models, struts-struts, plates-plates and plates-struts, the comparison is made only with struts-struts.

Figure 2. shows one of the graph obtained. It presents the sensitivity of model #2 ( $E_1$ ,  $E_2$  and  $E_3$ ) to the length of horizontal struts, where  $E=15$  GPa,  $R=50$   $\mu$ m and  $Lvs=.75$  mm.

## DISCUSSION

This simple model was run on an IBM AT with 640 K core memory. The size of the computer dictated a maximum number of nodes and required to introduce the argument of symmetry. The fact that only one quarter of the cube was modeled may create errors.

Table 1. shows that the results are comparable to those of Williams, especially the model #2 with  $Lvs=.75$  mm,  $Lhs=.877$  mm,  $E=15$  GPa and  $R=50$   $\mu$ m. Poisson ratios vary slightly. From the graph (fig. 2), it appears that  $E_3$  is the most sensitive elastic modulus to horizontal length since it decreases threefold while  $E_1$  and  $E_2$  decrease twofold when the horizontal length is doubled.

From anatomical data, our model can provide rapidly macroscopic orthogonal mechanical properties that could be used in a larger finite element of a spinal unit. This simple model could be a base for further investigations in vertebral cancellous bone modeling. It also could be a useful tool for studying the mechanical behavior of each strut, especially if buckling and fracture of trabeculae are included.

In the future, the vertical angle will be fixed to the one with which the model behaves most nearly like real cancellous bone.

## CONCLUSION

A 3-D generalized model for the cancellous bone of a human lumbar vertebra has been created. This model only takes into account the bony structure and is based principally on anatomical data easily measured.

Model #	Lvs mm	Lhs mm	E GPa	R $\mu$ m	$E_1$ MPa	$E_2$ MPa	$E_3$ MPa	$E_2/E_1$	$E_3/E_2$	$E_3/E_1$	$\nu_{12}$	$\nu_{21}$	$\nu_{13}$	$\nu_{31}$	$\nu_{23}$	$\nu_{32}$
1	.75	.877	15	50	24.8	40.7	164	1.64	4.02	6.60	.619	1.015	.004	.029	.005	.021
1	.75	.877	20	50	33.1	54.3	218	1.64	4.02	6.60	.619	1.015	.004	.029	.005	.021
1	1.00	.877	15	50	18.4	30.3	177	1.65	5.84	9.63	.618	1.019	.003	.026	.003	.019
1	1.00	1.013	15	50	14.6	24.6	128	1.69	5.18	8.74	.620	1.047	.004	.032	.004	.020
2	.75	.877	15	50	26.4	43.1	122	1.63	2.82	4.60	.614	1.001	.016	.076	.009	.025
2	.75	1.013	15	50	20.8	34.8	81.3	1.67	2.34	3.91	.619	1.035	.019	.076	.009	.020
2	.75	1.013	15	75	64.9	99.3	188	1.53	1.89	2.89	.601	.918	.022	.064	.014	.026
2	1.00	1.013	15	50	15.3	25.7	99.8	1.68	3.89	6.53	.619	1.040	.013	.084	.006	.024
Mechanical tests, Williams					33.3 $\pm 17.9$	40.9 $\pm 20.4$	128 $\pm 44$									

Table 1. Macroscopic mechanical properties obtained from compression of the finite element model for the cancellous bone of a human lumbar vertebra.

Compression, simulated by the finite element method, proved that the model can reproduce the behavior of the cancellous bone.

## References

- Williams, J.L. et al., J. Biomech. Eng., 104: 50-56, 1982
- Pugh, J.W. et al., J. Biomech., 6:657-670, 1973
- Beaupre, G.S. et al. J. Biomech. Eng., 107:249-256 1985
- Oxnard, C.E. The Physiologist, 25:Suppl., 1982
- Whitehouse, W.J., J. Microscopy, 101:153-168, 1974
- Kafka, V. Biorheology, 20: 789-793, 1983

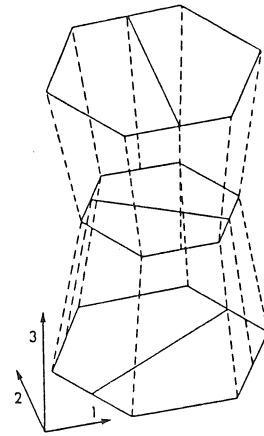


Figure 1. A structural model for the cancellous bone of a human lumbar vertebra. (Model #1)  
Axis #1 and #2 are in the coronal plane and axis #3 is perpendicular to this plane.

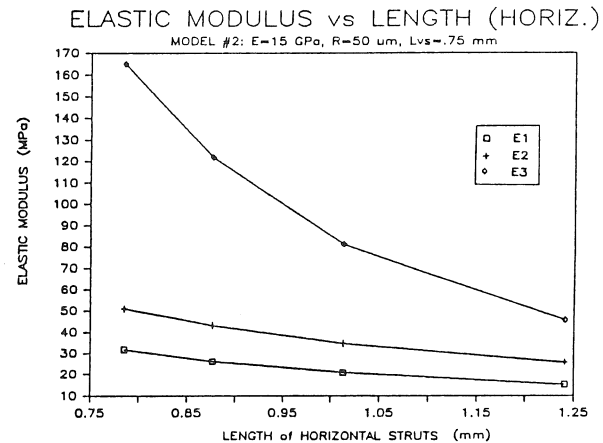


Figure 2. Sensitivity of elastic modulus of model #2 to the length of horizontal struts.

# THE SOFT TISSUE SYSTEM AT THE HEEL REGION OF THE FOOT: ITS MECHANICAL BEHAVIOR AND FUNCTION

Steven E. Robbins, M.D. Adel Hanna, Ph.D. (eng.)

Human Performance Group  
Concordia University Civil Engineering Department  
1455 de Maisonneuve Blvd. West, Montreal, Quebec, H3G 1M8

## INTRODUCTION

The soft tissue system at the heel pad was examined using a modified penetrometer. This system was found to have properties that do not allow for significant shock absorption while running, but it is very sophisticated in its capability of preventing injury of local foot structures local insult when walking and running barefoot. This knowledge leads to running shoe design considerations.

## REVIEW AND THEORY

In 1949, Kuhns (1) presented his often quoted manuscript concerning elastic adipose tissue. Since that time, there has been little change in the knowledge of the behavior of this tissue at the heel pad location. Light (2) suspected that a shock wave was produced by the heel pad bottoming. This suggests a shock absorbing capability of the soft tissue system of the heel pad (STSHP). Cavanaugh, a luminary in the field of biomechanics of locomotion, states that the function of the STSHP in running is as yet unknown (3).

From gross examination, one can observe the ability of the STSHP to deflect without failure on loading. This is the essential element of a shock absorbent system (fig 1).

In running, when the load is equivalent to approximately 2.5 times one's body weight, useful shock absorbency requires the deflection of the STSHP over a significant part of this range of the loading. Systems that deflect over an extremely narrow segment of the load range, would be of insignificant value for shock absorbency while running (fig. 1).

Although there is no doubt that these tissues deflect on loading, there has been no investigation determining whether the STSHP deflects over a sufficient range to be a useful shock absorber when running. This is the subject of this report.

## METHODOLOGY

The STSHP is a layered system consisting of integumental membrane (epidermis, dermis and subdermal connective tissue), and a layer of specialized elastic adipose tissue. A means was needed to examine the system.

An existing instrument, a penetrometer, is a tool that is used commonly in geotechnical investigations. The device consists of a spring loaded housing and shaft. A calibrated scale is provided on the housing for control of the load which is applied to the shaft. This device

demonstrated a high level of repeatability ( $\pm 0.1$  kg. for load;  $\pm 0.5$  mm. for penetration) as one would expect from a device of this construction. The specific instrument used in this experiment had a 9 kg. full scale deflection.

This device was modified. A collar (33 mm. O.D., 25 mm. I.D.) was added to the shaft so that it could slide down the shaft with a minimum of resistance. Removable ends made of steel balls were designed to slide onto the shaft, by attaching a tubular sleeve to the ball (fig. 2). With these modifications, the depth of deflection of the soft tissue system could be measured by obtaining the distance from the most distal aspect of the ball end, and the rim of the collar (fig 3). For this experiment, two ends using balls of 10 mm. and 23 mm. were used. The smaller ball was the smallest size that subjects could tolerate without significant pain at the high load range. The larger ball was the largest diameter that could fit into the collar of the penetrometer. The right foot was examined in all subjects at a heel pad location. This point was located by measuring 4 cm. anterior of the most posterior part of the Achilles attachment, and a line bisecting the heel area in the medial-lateral plane.

This modified penetrometer was used to measure the force-deflection relationships of the STSHP in 17 volunteers using both penetrometer ends in all subjects.

## RESULTS

With the 1 cm. end on the penetrometer, 87.5% of the maximum deflection was obtained at the lowest load of 1.8 kg. (fig. 4, fig 5). The depth of deflection then plateaued, reaching a maximum mean depth of about 14 mm. which is identical to the thickness of the fat pad as measured from autopsy examination (4).

With the 23 mm. end on the penetrometer, 85% of the maximum deflection was reached at the lowest load of 1.8 kg. The depth of deflection surprisingly plateaued at average maximum depth of 10.5 mm.; a level greatly less than the 14 mm. obtained with the smaller end. (fig. 4, fig. 5)

By extrapolative calculation, the deflection by a flat surface would be 7 mm. with 95% deflection at a load of 9 kg. (fig 4, Fig. 5). Overall standard deviation for the population tested, respecting load levels, was 1.29 mm.

## DISCUSSION

It is clear from the data presented, that the STSHP deflects to its maximum over

a very limited range of load. This type of system does not have characteristics which allow for significant shock absorbent function in the load range experienced in running (fig. 1). Knowing this, what is the function of this very complicated multilayer system?

There can be little doubt that man has evolved in the barefoot state. This system has very attractive properties for protection from small rigid objects when barefoot. Small pointed objects would have little chance of penetrating the integumental membrane because the STSHP deflects with relatively low loading. Small objects would thus be contained within the void created by the deflection, with the major component of the load sustained on the larger surrounding area of the heelpad.

When making contact with increasingly large objects, penetration of the membrane is less likely. The STSHP acts as a load distributing system under these circumstances, avoiding localized load to the calcaneus. This is very sophisticated mechanical behavior indeed.

The STSHP must be considered as mainly a system for local protection rather than

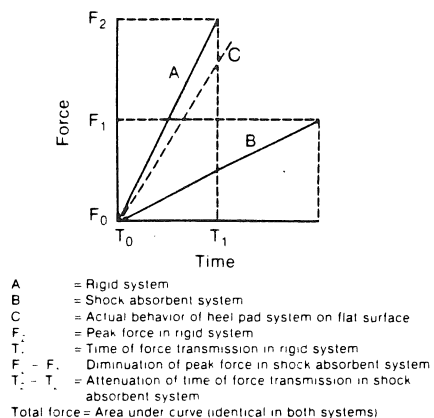


Figure 1.

#### USE OF THE PENETROMETER

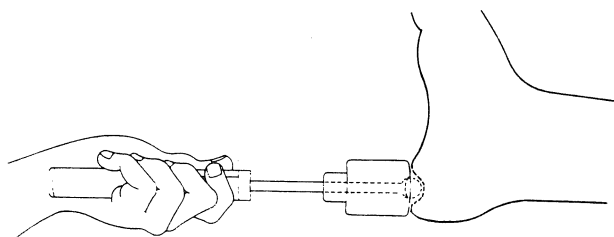


Figure 2.

#### PENETROMETER

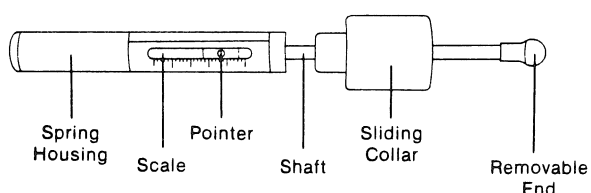


Figure 3.

shock absorbency. The authors believe that a system that deflects easily to contain, thus accommodate surface irregularities, as the STSHP, would have a distinct advantage over current running shoes when running over natural (irregular) surfaces. This is consistent with the unusual success barefoot runners have had on natural surfaces. The authors are interested in running shoe designs that incorporate a more yielding outsole than is currently used in running footwear.

#### REFERENCES

- 1) Kuhns, J.G.: Changes in elastic adipose tissue. J. Bone Joint Surg. 31A:541-547, 1949.
- 2) Light L.H. et al: Skeletal transients on heel strike in normal walking with different footwear. J. Biomech. 13:477-480, 1980.
- 3) Cavanaugh, P.R.: The Running Shoe Book, Anderson World Inc., Mountain View Cal., 1980.
- 4) Robbins S.E., Hanna A.M.: Plantar sensory integration of natural human locomotory biomechanics. Submitted for publication. J. Biomech.

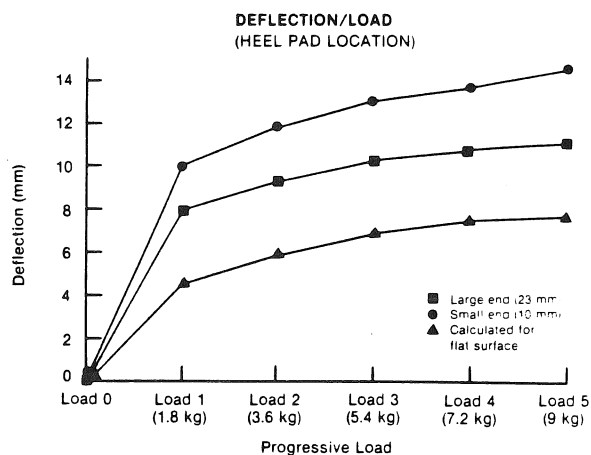


Figure 4.

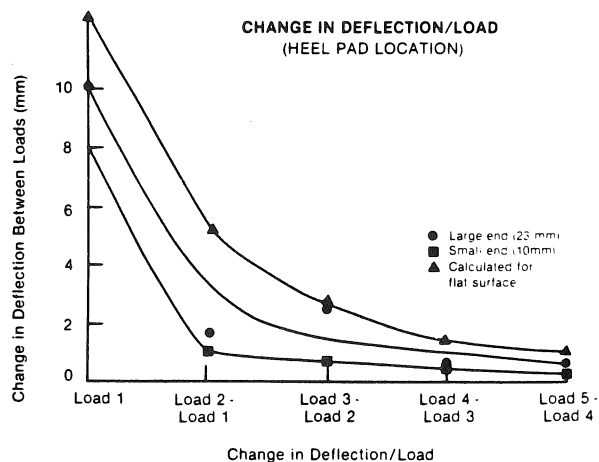


Figure 5.

J.L. Ku, S.A. Goldstein, K.W. Choi, S. Stein, L. Degnore, L.S. Matthews

The Biomechanics, Trauma and Sports Medicine Laboratory, Section of Orthopaedic Surgery and the Bioengineering Program, University of Michigan, Ann Arbor, MI 48109

The mechanical properties of trabecular bone tissue have long been an issue of debate. Though many studies have been conducted to determine structural moduli of trabecular bone as a continuum solid, few have investigated the actual trabecular material properties. The purpose of this study was to design a method to experimentally determine a range of moduli for trabecular bone tissue, and compare it to the modulus of cortical bone found by the same method.

Bone specimens were extracted from human cadaveric long bones ranging in age from 21-60 years. From each long bone, trabecular specimens were taken from the metaphysis, and cortical specimens from the diaphysis. Using a low speed isomet saw, rectangular paralleloiped cortical specimens of dimensions: 70-150u X 70-150u X 2 mm were produced. Osteon direction was noted and both longitudinal and transverse sections were made. All trabecular specimens were produced on a specially designed mini-milling machine while observed through a stereomicroscope. By using a series of miniature mill bits, homogeneous and continuous paralleloiped trabecular specimens having the same dimensions as described above were made. A series of cortical specimens were also machined in this manner.

All specimens were photographed under a microscope using a 10 power objective. The cross-sectional properties were determined by digitizing slides of specimen base and height, and correcting each measurement for the magnification factor.

A Lietz microscope was converted to a testing apparatus by attaching a stepper motor to the fine focus adjustment, a load cell and specimen support to the microscope stage and a 160u wide load head to the base of the body tube. An LVDT was used to measure displacement. Each specimen was placed across the supports, leaving a bending length=1.04 mm. The load head contacted each specimen at L/2. Observations during each test were made through a stereomicroscope and recorded. Data was acquired directly using an A/D converter and a Tektronix 4054 computer. Linear regressions were performed on the slope of the load-deflection curve. Using the equation:  $y = PL^3/48EI$ , the modulus was calculated.

There was no significant difference in the cortical specimen moduli due to different preparation techniques. Modulus values for longitudinal cortical specimens ranged from 1-17 GPa. Modulus values for trabecular specimens ranged from .3-6 GPa. Modulus values for transverse cortical specimens ranged from .5-2.0 GPa.

The preliminary results from cortical bone tests agree with the results of Ascenzi et al (1) in which tensile tests of portions of longitudinally sectioned osteons were performed. In their study,

the moduli of wet osteons, ranged from 1.0-12 GPa. This comparison serves to validate our apparatus and mechanical test. The trabecular specimens displayed an average modulus which was on the same order of magnitude as cortical specimens, possibly one half the value. It is expected that the large variance in moduli for all specimens may be attributed to the specimen's degree of calcification, and ultrastructural characteristics. Therefore, these factors are being evaluated in further studies. This test may prove valuable in determining material property changes occurring in bone affected by age, metabolic and degenerative disease.

#### References

1. Ascenzi & Bonucci, Anat. Rec., 158:375, 1967.



N. CHARBONNEAU, G. DROUIN, G. DUMAS  
Mechanical Engineering department  
Ecole Polytechnique, C.P. 6079 Succ. A  
Montreal, Quebec, H3C 3A7

C.H. RIVARD  
Orthopaedical Experimental Biomechanics  
Ste-Justine Hospital, 3175 Côte Ste-Catherine, suite 8222  
Montreal, Quebec, H3T 1C5

## INTRODUCTION

A common surgical procedure for severe idiopathic scoliosis is the implantation of Harrington rods and bone fusion. In the early stage of the evolution of the arthrodesis, the mechanical load is almost totally supported by the rod. The healing of the bone progressively restores rigidity to the spine allowing it to reassume its upholding role thus freeing the rod of its load. The aim is to evaluate in vivo the stress imposed in the rod in order to deduce the progression of the fusion and determine the necessity and duration of post-operative restraint. This project is a feasibility study of a long term implantable system on a dog.

The measuring system consists of strain gages placed on the rod. A lengthy procedure of several coating of the gages isolate them from the biological fluid and the same time assume the short term biocompatibility of the system. Instrumented Harrington rods are implanted on dogs for a 4 months period. Transcutaneous wires are connected to external instrumentation and data are saved, processed and analysed on an IBM Pc. During the implantation period, the gages are measuring the forces induced in the rod.

## REVIEW AND THEORY

Considering that the correction force is applied through the hooks, there will be compression and bending stresses induced in the Harrington rod when implanted (figure 1): A simple analysis of this system indicates that for this loading, the bending stress is larger than the compression stress. Nachemson (1) in the "pressductor system", considered only the compression.

In 1982, Quintin et al. (2) built a system that measures the bending and compression forces, the bending moment and determine the position of the neutral axis on Harrington rod. They placed 120 ohms strain gages on the smooth part of the rod 90° apart, and the signal was obtained using transcutaneous wires. They also built a metallic capsule to cover the gages for mechanical protection.

## METHODOLOGY

From previous observations in this paper, there is advantages in measuring the bending deformation and the compression. The experimental device should allow for these measurements. The design of the system was also inspired from Quintin's work (2). The design is using four 350 ohms strains gages in order to have a more sensitive system.

Following a correct procedure for the implantation of the Harrington rod, the upper hook is locked as near as possible to the smooth part of the rod. Therefore, we can neglect the part with ratchets and considere the rod as uniform. The point where the deformation is the largest is located half way on the smooth part of the rod. Following this assumption,

the system consists of four strain gages placed longitudinally half way on the smooth part of the rod, 90° from each other around the circumference (figure 2).

Each gage is connected to its own Wheatstone bridge by a three wire circuit (3). This arrangement will minimize the effect of the long transcutaneous wires. The output of the Wheatstone bridge is amplified and saved on an IBM Pc by a data acquisition program.

Following this technic, the equations used to analyse the rod are:

$$\text{compression force: } F = (\pi r^2 E / 4) (\epsilon_1 + \epsilon_2 + \epsilon_3 + \epsilon_4)$$

$$\text{compression stress: } \sigma_c = F/A \text{ and } A = \pi r^2$$

$$\text{bending moment: } M = (\pi r^3 E / 8) \sqrt{(\epsilon_1 - \epsilon_3) + (\epsilon_2 - \epsilon_4)}$$

$$\text{bending stress: } \sigma_b = M/I \text{ and } I = \pi d^4 / 64$$

$$\text{neutral axis: } \tan \alpha = (\epsilon_1 - \epsilon_3) / (\epsilon_2 - \epsilon_4)$$

where  $\epsilon_i$  represent the deformation reading of the gage i.

The 3 wire copper cables, are covered by a silver shield and a coat of PVC. The connection between the gages and the wires is protected by a drop of PMMA. The impermeability and biocompatibility are ensured by one coat of nitril rubber, another of acrylic and one of flexible polyurethane. A PVC capsule provides mechanical protection. Each rod is then put into a 2M saline solution for 2 weeks. Each day the resistance of the gages is measured to make sure that the system is well sealed by the coating.

The rod is then mounted on a tensile machine and connected to the acquisition system. A calibration resistor is placed in parallel with a branch adjacent to the strain gage in the Wheatstone bridge, in order to calibrate the acquisition system so that the input voltage and the amplification factor do not need to be measured. Compression force is applied to the hooks in a manner similar to the in vivo loading. This procedure permits to calibrate each gage and verify its linearity. Once the rod is implanted, the adjustment of the zero is done with a small device built with four 350 ohms resistors.

The instrumented Harrington rods are implanted on normal dogs for a 4 months period without arthrodesis (figure 3). The position of each gage is carefully noted. The transcutaneous wires are attached to a connector that can be easily hook-up to the acquisition system. In immediat post-operation, the dog's trunk is put into plaster in order to prevent the dislocation of the rod, the transcutaneous wires and connector. Data are collected each 1 or 2 days in the earlier post-operative period. After 1 or 2 weeks the frequence of measurement is then reduced.

## RESULTS

Data from 4 dogs has been analysed. Each movement of the dog is noted and, in each case, the results are processed and graphs are plotted using Lotus 123



program for IBM Pc (figure 4).

Knowing the position of each gage, the correlation between the readings and the movements of the dog can be shown. Figure 4 shows a example of data taken when the dog was turning thus inducing lateral flexion in his spine and so in the rod. The median and lateral strain gages showed opposite signals, one in tension and the other in compression. They also showed greater signal than the anterior and posterior gages due to the fact that the total deformation in this direction is the sum of the compression and flexion deformation.

#### DISCUSSION

The results obtained proved the mechanical reliability of the system. Four dogs have been instrumented as described above, but only one has kept the rod for over 4 months. In the other cases, the problems were not due to the system itself, but to utilisation of animals for the experiment. Indeed, dogs have not tolerate wearing cast and having transcutaneous wires. They managed to destroyed the external parts of the system (wires and connector). The coating and the encapsulation were efficient for over 4 months. However, observation made after withdrawal of a rod implanted for 2 1/2 months, showed that the flexible polyurethane has a tendency to become brittle. This has not affected the reliability of the system up to now, but it may if implanted for a longer period. Therefore, more testing has to be done replacing the polyurethane by silicone rubber (Silastic) often used in similar situations.

Figure 1. Loading mode of the Harrington rod.  
F=compression force on hooks  
e=eccentricity  
L=length between the 2 hooks  
v=deflection

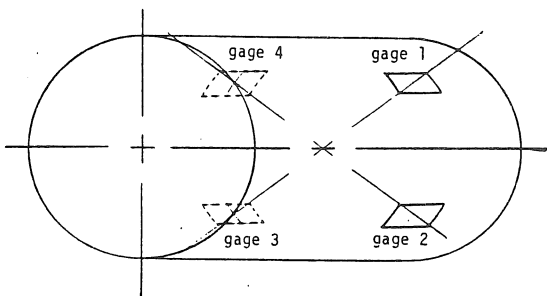
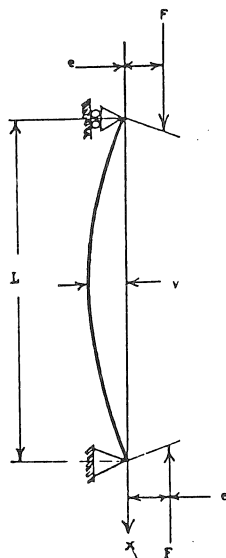


Figure 2. Layout of the gages on the Harrington rod. Four 350 ohms strain gages.

The nexts steps of this project will consist on the utilisation of a telemetric device that could be implanted with the system and transmit the strains by radio waves to an external receiver. This will eliminate the inconvenience of the transcutaneous wires thus protect the system from the dog's anger and eliminate risks of infection.

#### CONCLUSION

The monitoring system describe before, shows good results and met our objectives. The project feasibility is now established. The nexts steps (change in the coating and the telemetric device) will improve this system.

#### References:

1. NACHEMSON A. & al.: J.B.J.S.,53-A: 445-465, april 1971.
2. QUINTIN J. & al.: Belgica, 48(4): 688-709 1982.
3. AVRIL J. & al.: Encyclopédie d'analyse des contraintes. Micromesures editor, France, 1983, p.314.



Figure 3. Harrington rod implantation on a dog. The PVC capsule provides mechanical protection. The readings are performed by transcutaneous wires.

#### CHIEN #2, POST-OP; LATERAL FLEXION

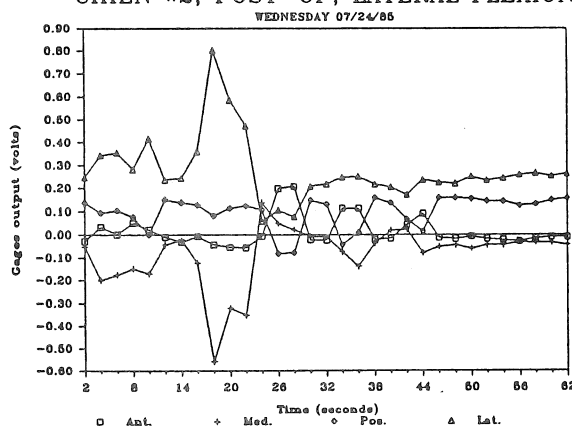


Figure 4. Strain gages readings at the time of lateral flexion on the right side. The rod is on the right side of the spine. The (+) sign is for compression. The (-) sign is for tension.

C. Krettek, N. Haas  
Trauma Departement  
Hannover Medical School  
Konstanty-Gutschow Str. 8  
D-3000 Hannover 61, FRG

L. Gotzen  
Trauma Departement  
Phillips-Universität Marburg  
Baldinger Straße  
D-3550 Marburg, FRG

## INTRODUCTION

Many experiments have been performed to improve the intramedullary nailing - inaugurated by KÜNTSCHER (3) and perfected by the AO (4). But among the numerous devices which have been designed, only the fluted and the interlocking nail were introduced successfully in clinical work (1,2). To enlarge the applications of intramedullary fixation in the femur with its large differences in shape and solidity at different levels, a new nailing device has been developed.

## MATERIAL AND METHODS

In the upper third, the nail is constructed as a fluted tubular rod with twelve sharp edged longitudinal ribs (Fig. 1). This part is connected with two long leaves forming a split tubular rod, which can be opened by a mechanism in the upper third of the nail. The configuration and expanding mechanism of the nail ensure a good fitting of the implant in almost every segment of the femur (Fig. 2). In the proximal part, stability is guaranteed by the rib profile of the nail head and the two leaves pressing against the inner cortical wall. In the distal part, the nail gets a firm grip at the divergent bone by the spreaded laminae. A special mechanism allows disconnection of the two leaves which makes the extraction easily possible, even in the presence of callus or granulation tissue.

On cadaver femora with transverse osteotomies in the middle or distal third, biomechanical experiments were performed in order to analyse the bending and torque stability. The proximal fragment was horizontally fixed into a jig. The free distal fragment was subjected to bending loads, acting in sagittal and frontal plane. The bending forces  $F_B$  causing the bending moment were continuously measured and plotted against the electrically recorded displacement of the unfixed distal fragment. The bending moment  $M_B$  was calculated from the bending force  $F_B$  and the lever arm  $l$ . The deflection angle  $\beta$  was calculated from the displacement  $s$  of the unfixed distal fragment in a defined distance  $a$  from the osteotomy gap as  $\beta = 180^\circ \cdot s / 3.14 \cdot a$ . Stress diagrams were set up, indicating on the ordinate the bending moment  $M_B$  and on the abscissa the deflection angle  $\beta$ . In a modified experimental setting torque stability was tested. The arrangement provided torque without disturbing bending moment. The moment of torque  $M_T$  was calculated from the force of torque  $F_T$  and the lever arm  $k$ . The angle of torque  $\varphi$  was calculated from the displacement  $t$  and the distance  $b$  from the axis of torque as  $\varphi = 180^\circ \cdot t / 3.14 \cdot b$ . Stress diagrams were set up indicating on the ordinate the moment of torque  $M_T$  and on the abscissa the angle of torque.

## RESULTS AND DISCUSSION

When bending load was applied in the frontal plane, the highest stability was achieved for the midshaft osteotomies, but still in the distal osteotomies,

this nail provides an effective stabilization (Fig. 3). When the bending load was applied in the sagittal plane (Fig. 4), the gapping of the osteotomies was less than in the frontal plane. The displacements in bending experiments were reversible. In torque experiments this nail shows excellent stability for both, middle and distal osteotomies. As in bending experiments the deformations are reversible (Fig. 5).

The satisfying experimental data encouraged us to introduce this system into clinical work. Femoral fractures of different types and levels were successfully stabilized with this nail. Nail extraction in some cases is already done with an interval up to 27 month after osteosynthesis. The easy and save use of the 'unlock-mechanism' enabled nail extractions without problems (Fig. 6).

## CONCLUSIONS

Because of the good biomechanical properties and the easy handling, this nail seems to enlarge the possibilities of application of intramedullary nailing in the femur.

## References

1. Aginsky J. et al. Injury 11:190-196, 1980.
2. Klemm K. et al. Unfallheilkunde 75:568-575, 1972.
3. Küntscher G. Langenbecks Arch. Klin. Chir. 2:443-455, 1940.
4. Müller M.E. et al. Manual der Osteosynthese. Springer Berlin, 1977.

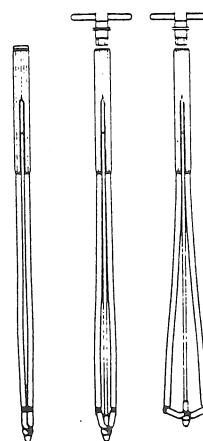


Fig. 1 The nail with spreading instrument.



Fig. 2 Transversely osteotomized human bone preparation with implant. Good fitting in almost every segment of the femur.

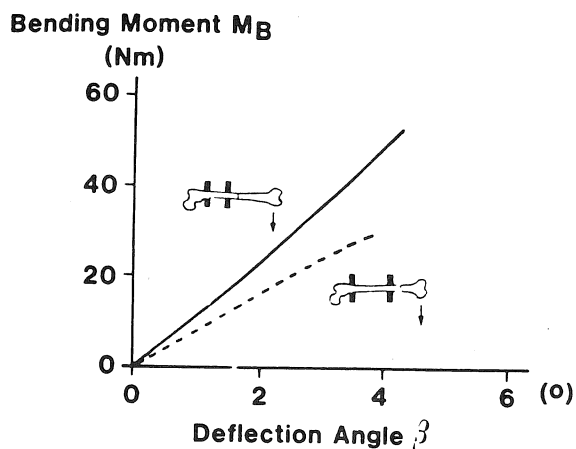


Fig. 3 Mean of bending stability when the bending moment was acting in frontal plane (solid lines: midshaft osteotomies, dashed lines: distal osteotomies).

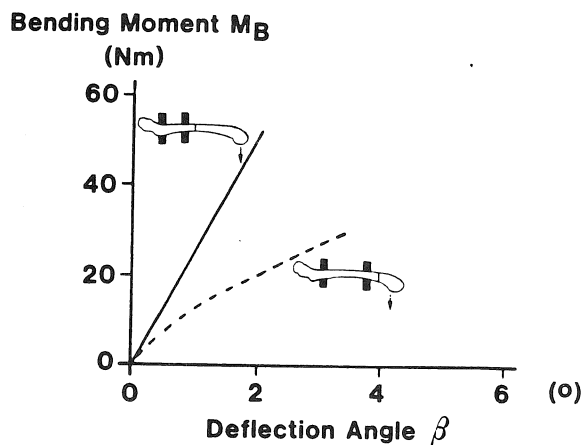


Fig. 4 Mean of bending stability when bending moment was acting in sagittal plane (solid lines: midshaft osteotomies, dashed lines: distal osteotomies).

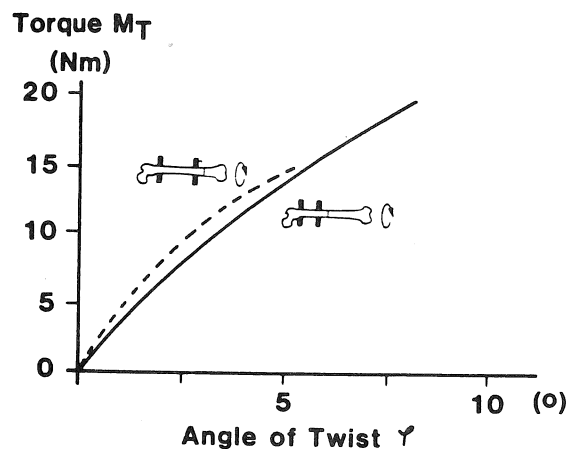


Fig. 5 Mean of torque stability (solid lines: midshaft osteotomies, dashed lines: distal osteotomies).



Fig. 6 A 29 year old multiple injured female patient with a closed femur fracture stabilized with this new intramedullary nailing device. Implantation and fracture healing without complications. Easy nail extraction 24 month after stabilization.

# MATHEMATICAL MODELS FOR PREDICTING BONE DENSITY FROM STRESS HISTORY

D.R. Carter, D.P. Fyhrie, and R.T. Whalen

Mechanical Engineering Department  
Stanford University, Stanford, CA and  
Rehabilitation Research and Development Center  
Veterans Administration Medical Center, Palo Alto, CA

## INTRODUCTION

It is well recognized that a relationship exists between the severity of mechanical loading to which the skeleton is exposed during daily activities and the mass and strength of the bones. Large, heavy individuals who are physically active tend to have denser and stronger bones than frail, sedentary individuals. In addition to the density variations which occur among bones of different people, there are also complicated distributions of bone apparent density within bones of specific individuals. The general patterns of trabecular orientations and distributions of apparent density are similar for each of the bones. The magnitude of apparent density at specific locations within the bones, however, are quite different as are the apparent densities of bone at the same site in bones of different people. Most researchers agree that the variations of apparent density within specific bones and among bones of different individuals are influenced by the loading histories to which the bone tissue is exposed. In this study, we develop mathematical approaches to relate bone apparent density to local mechanical loading histories.

## REVIEW AND THEORY

Previous investigators who have tried to explain the trabecular orientation and distribution of trabecular bone apparent density within a bone have considered a single "typical" loading condition to which the body is exposed on a repetitive basis. Such a loading condition creates a complicated stress distribution within the trabecular bone which correlates with trabecular morphology. Most have explicitly or implicitly assumed that bone apparent density distributions within a bone are optimized with respect to some measure of the local ultimate strength. That is, it is assumed that the ratio of stress to ultimate strength (stress ratio) is the same throughout the entire region of cancellous bone. Trabecular bone alignment has been shown to correspond to principle stress directions and consequently reduces the apparent density required to achieve a specific stress ratio.

Studies which consider a single load application have proved to be very useful. However, a better understanding of these relationships requires a more complete consideration of the nature of intermittent, repeated loading of bone during daily activities. We assume that some relatively stable (homeostatic) situation exists between bone stress and local bone density. That is, the daily activity levels of the individual have been consistent for long enough that the skeleton is not experiencing significant bone loss or gain. Our goal is then to determine the relationship between the stress history and the current trabecular bone apparent density at a specific site.

In this study, we introduce three new approaches which account for the daily tissue

loading history to predict bone apparent density. These methods incorporate measures of either (1) an "effective" stress; (2) bone fatigue damage; and (3) tissue strain energy density, and consider the number of loading cycles which are applied in different activities. The approaches introduced in this study may be convenient methods for representing the density of energy which is dissipated over the period of an "average" day and predicting the effect of that energy in maintaining the local bone apparent density.

## METHODOLOGY AND RESULTS

### Effective Stress Approach

The regulation of bone apparent density can conceivably be affected by many different mechanical factors including the cyclic stress (or strain) magnitudes, strain rates during loading, and the number of loading cycles. Because of the nature of normal activity and exercise patterns, the loading strain rates tend to correlate with the magnitudes of the imposed stresses. As a first approximation we will assume that the most important parameters to consider are the magnitudes of the cyclic stresses and the number of applied loading cycles. We will further assume that the daily activities can be decomposed into histograms of load histories which consist of  $i$  discrete loading conditions which are each associated with  $n_i$  cycles of load applications per day. For example,  $i = 1$  may represent the activity of single-limb-stance during walking with  $n_1 = 5,000$  cycles. The activity of getting out of a chair may be represented by  $i = 2$ ,  $n_2 = 37$  cycles. We assume that the severity of the loading state created during each  $i$ th load pattern can be expressed as a single scalar "effective stress" parameter,  $\bar{\sigma}_i$ , which indicates the "magnitude" of the cyclic stress tensor for a certain theory of failure (or in our case, remodeling theory). One way that the effective stress,  $\bar{\sigma}_i$ , is used is to compare it to the effective stress for failure,  $\bar{\sigma}_{ult}$ .

The stimulus needed to maintain the local bone apparent density is a function of the stress magnitudes and loading cycles as well as the current apparent density. In a homeostatic situation, we will assume that the daily stimulus to maintain a certain bone mass is related by a linear superposition of the stimuli created by each  $i$ th loading conditions. To calculate the stimulus in each  $i$ th loading condition, we do not know at this point the relative importance of cyclic stress magnitude and the number of loading cycles. We thus assume that a region of bone which is experiencing neither a net loss or gain of bone apparent density will be exposed to a constant daily stimulus  $\bar{S}$  that can be expressed as

$$\bar{S}_{day} = \sum_i n_i (\bar{\sigma}_i / \bar{\sigma}_{ult})^m, \quad (1)$$

where  $m$  is a constant. The value of  $m$  is a weighting factor for the relative importance of stress ratio and loading cycles. If  $m = 1$ , stress

magnitude and the number of cycles are equally important. Increasing values of  $m$  indicate increasing dependence of the stimulus on the activities which are associated with high loading cycles.

If we assume that (1) the bone strength is proportional to the apparent density squared and (2) the bone maintenance stimulus is constant everywhere, the local bone apparent density is given as

$$\rho \propto [\sum n_i \bar{\sigma}_i^m]^{1/2m} \quad (2)$$

where  $m$  is an arbitrary constant whose value is yet to be determined.

Notice that in the case of a single typical load analysis of previous investigators, Equation (2) degenerates to

$$\rho \propto \bar{\sigma}^{1/2} \quad (3)$$

This is the same results as derived using the static strength optimization principle (1).

#### Fatigue Damage Approach

The fatigue damage approach assumes that the daily damage accumulated in trabecular bone is constant throughout the bone structure. The local apparent density has, therefore, been established to ensure that the safety margin for fatigue fracture is equal at all locations.

The number of cycles to failure ( $N$ ) for bone tissue exposed to a cyclic stress range,  $\Delta\bar{\sigma}_i$ , can be approximated by the relationship:

$$N = A \left( \frac{\Delta\bar{\sigma}}{\bar{\sigma}_{ult}} \right)^{-b} \quad (4)$$

where  $A$ ,  $b$  = experimentally determined constants.

To extend this relationship to trabecular bone, we employ the finding that  $\bar{\sigma}_{ult}$  is proportional to the square of the apparent density.

If the daily fatigue damage fraction is constant at all locations then

$$\rho \propto [\sum n_i \Delta\bar{\sigma}_i^b]^{1/2b} \quad (5)$$

where  $b$ , determined from *in vitro* testing, is between 5 and 18 for different loading conditions.

#### Strain Energy Approach

Cancellous bone consists of both mineralized bone marrow spaces. The volume fraction,  $v$ , is the ratio of bone volume to total bulk volume. In a continuum model of bone, the apparent stiffness matrix (or apparent elastic moduli) are approximately proportional to the cube of the apparent density (2). The strain energy density,  $U$ , is in reality an "apparent" strain energy density and is calculated as:

$$U = \frac{1}{2} \bar{\sigma}^T S(\rho, \theta) \bar{\sigma} \quad (6)$$

where  $\bar{\sigma}$  = apparent stress,  $S$  = apparent compliance matrix,  $\rho$  = apparent density,  $\theta$  = orientation of material directions relative to principle stress directions. All of the strain energy is, however, stored in the mineralized bone tissue. Therefore the "true" strain energy density in the bone tissue is much greater than the "apparent" strain energy density calculated using the continuum model. To better reflect the energy stored in the mineralized bone tissue, we introduce the parameter:

$$U_b = U/v \quad (7)$$

where  $U_b$  = average true bone tissue strain energy density.

The true density of mineralized bone can be considered, in the first approximation, as a constant. Therefore

$$U_b \propto U/\rho \quad (8)$$

Following a loading history approach comparable to that used in the previous section, we assume that the daily stimulus to maintain bone mass,  $\bar{S}$ , is given by

$$\bar{S} \propto \sum \frac{n_i (U_b)_i^k}{\text{day}} \quad (9)$$

or

$$\bar{S} \propto \frac{1}{\rho^k} \sum \frac{n_i U_i^k}{\text{day}} \quad (10)$$

If we again assume that the bone maintenance stimulus is constant everywhere, the local bone apparent density is given as

$$\rho \propto [\sum n_i U_i^k]^{1/k} \quad (11)$$

We have previously (1) introduced the concept of an energy stress,  $\sigma_{\text{energy}}$ , where

$$\sigma_{\text{energy}}^2 = 2 E_{\text{ave}} U \quad (12)$$

and  $E_{\text{ave}}$  is the average elastic modulus. Using this relationship, and the finding that the elastic moduli are proportional to the cube of the apparent density, we find:

$$\rho \propto [\sum n_i \sigma_{\text{energy}_i}^{2k}]^{1/4k} \quad (13)$$

where  $k$  is an arbitrary constant.

#### **CONCLUSIONS**

The fatigue damage approach to predicting apparent density is a special case of the more general, effective stress approach. Although both methods result in the same mathematical form, the power exponent,  $m$ , in the stress approach is an arbitrary constant whose value is yet to be determined. In the fatigue damage approach the power exponent,  $b$ , has been shown in *in vitro* test to have a value between 5 and 18 for different loading conditions.

The strain energy approach differs in philosophy from the other two approaches in that it attempts to consider the stimulus at the level of the mineralized tissue ( $U_b$ ) rather than using only the continuum model representations of stress and energy. If one assumes that the continuum model effective stress  $\bar{\sigma}$  is the energy stress  $\sigma_{\text{energy}}$ , however, the energy approach results in exactly the same prediction for apparent density as the stress approach.

#### References

1. Fyhrie DP, and Carter DR, Trans. ORS 10:377, 1985
2. Carter DR, and Hayes WC, J. Bone Joint Surg. 59:954-962, 1977
3. Carter DR, and Caler WE, J. Orthop. Res. 3:84-90, 1985

Supported by the Veterans Administration, and NIH grants AM32377 and AM01163 (RCDA). We thank William Caler and Prof. Charles Steele for their advice and assistance.

# SCALING OF LONG BONE FRACTURE STRENGTH WITH ANIMAL MASS

Frank Selker and Dennis Carter  
Department of Mechanical Engineering  
Stanford University

## INTRODUCTION

The geometry of long bones is important to their structural function. It is the shape of bones, together with bone tissue properties, that determines their mechanical behavior under *in vivo* loading. In order to understand the stresses for which bones have evolved, and the demands placed on bones during normal and traumatic loadings, it is helpful to understand how bone geometry and strength scale across the very wide range of animal sizes. Most long bone fractures are the result of bending and/or torsional loading. To allometrically relate bone torsional and bending strength to animal mass  $M$ , we define the bone strength index  $S_b = J/dl$  where  $J$  is midshaft cross-section polar moment of inertia,  $d$  is external diameter, and  $l$  is length. If bones and animals scaled geometrically one would expect  $S_b \propto M^{2/3}$ . In this study, long bone geometric parameters were measured for 12 species of the order Artiodactyles. The relationships determined for length and diameter are similar to those reported by previous investigators ( $l \propto d^{2/3}$ , and  $l \propto M^{1/4}$ ). For the Artiodactyles studied, we found that  $S_b \propto M^{.76-.89}$ . Data previously collected by Biewener (1) on a wide range of mammals (non-Artiodactyles) showed different scaling relationships between length, diameter, and animal mass ( $l \propto d^{.89}$ ,  $l \propto M^{.31}$ ). However, analysis of his data suggest similar scaling of the torsional and bending strength index,  $S_b \propto M^{.77}$ . It therefore appears that, in spite of differences in scaling of length and external diameter, the bending and torsional strength of animals scale similarly across a broad range of animal sizes.

## REVIEW

The chemical composition of bone tissue is similar among all mammals. Small variations in microstructure or composition can result in changes in strength or stiffness up to a factor of two, however these changes are subtle when compared with the order-of-magnitude changes observed in studies of allometric scaling. The primary factor in the scaling of bone strength with increasing animal size is therefore geometry, rather than material properties.

A substantial amount of data has been collected pertaining to the scaling of the length and external diameters of bones. McMahon (2) measured these dimensions of bones for a variety of Ungulates and found that, in general  $l \propto d^{.67}$ . Alexander (3) took similar measurements and found that  $l \propto M^{.26}$  and  $d \propto M^{.34}$ , giving  $l \propto d^{.76}$ . Alexander (4) also took measurements on a wide variety of mammals, and found that in general  $l \propto M^{.35}$  and  $d \propto M^{.34}$ , giving  $l \propto d^{.97}$ . Thus, bone diameter scales nearly proportionally with length for a wide range of animals and sizes, while bones become increasingly stout with increasing size among many Ungulates. Because most large animals are Ungulates, and most small animals are not, the distinguishing feature between these groups may be size, rather than phylogeny. Biewener (5) measured midshaft cross-section areal properties of a variety of bones and found that the second moment of inertia,  $I$ , for bending in the antero-posterior plane scaled  $I \propto M^{1.43}$ .

## THEORY

A long bone is a hollow, irregular, curved structural beam. In life, these structural members are exposed to axial, bending, and torsional loading. It can be shown, based on simple relationships implied by geometric scaling, that for bones which scale geometrically  $F \propto M^{2/3}$ , where  $F$  is the force to fracture a bone. This result is independent of whether the bone is loaded axially, in bending, or in torsion.

It is extremely rare that a long bone will be fractured in a living animal as the result of a pure axial load. Most fractures are primarily due to stresses created by bending and torsion. Therefore, the single geometric parameter which best serves as an indicator for bone

strength is  $S_b = J/dl$  (or, comparably  $I/dl$ ). In this presentation we will refer to  $S_b$  as the "bone strength index".

## METHODOLOGY

Bone geometry data were collected from 93 dry bones, from 12 species of the order Artiodactyle. The bones vary in length by a factor of 5.3, representing an approximate range of animal mass of 30 to 700 Kg. Femora, tibiae, humeri, radii and ulnae were measured. All bones were selected for fused epiphyseal plates, to assure bones were from mature animals.

Images of the bone cross-sections at midshaft were made with a Computer Aided Tomography (CAT) X-ray scanner. The CAT scans were digitized, and the cross-sectional area and moments were calculated by computer (repeatable to 2 percent for area, 3.5 percent for polar moments). Calculated values were corrected for small systematic errors associated with image edge location and contrast.

Only two of the animals were weighed at the time of death. To estimate animal mass for the remaining animals we had to rely on estimates taken from the literature. Animal masses typically vary greatly between individuals, so the averages of documented ranges were used. This introduces unavoidable imprecision and scatter in the data.

## RESULTS

The data collected in this study is summarized in Table 1. In developing allometric relationships for bones, one finds that if a few fundamental relationships can be estimated, many others can be derived. One danger inherent in such a technique is that small errors in the empirically established fundamental relationships can cause larger errors in the derived relationships, and thus misinterpretations of the data. It is therefore prudent to directly examine several of the relationships which can be established with the data and check for consistency of interpretation. This is the approach taken in the present study. We arbitrarily have chosen three fundamental relationships: 1),  $d$  vs  $M$ ; 2)  $l$  vs  $d$ ; and 3)  $J$  vs  $A$ . Based on these allometric relationships we have derived the implied relationships of several other variables.

These inferred relationships, together with the empirical values for each variable and bone element, are shown in Table 2. The allometric exponents were calculated using least-squared linear regressions of the log transformations of the variables. The values of the exponents, and their 95 percent confidence intervals, are given in Table 2. Because of the considerable scatter in the data, we can reasonably approximate the empirical values of the fundamental relations with simple fractions within the range of values for different bone elements. These fractional approximations were then used to calculate expected exponents for the other relations (Table 2). In nearly all cases the predicted exponents are within the 95 percent confidence intervals of the empirical data.

## DISCUSSION

For the group of Artiodactyles considered in this investigation, we have found the data consistent with the hypothesis that long bone diameter,  $d$  and cross-section fracture resistance,  $J/d$ , scale in geometric similarity with animal mass,  $M$  (Table 2). The bone lengths,  $l$ , however, become proportionally shorter with increasing animal mass. Consequently,  $J/d$  is approximately proportional to  $l^4$  rather than  $l^3$  as expected in pure geometric similarity. The increasing stoutness of these bones with increasing animal size reduces the magnitude of bending and torsional moments created in the diaphysis when the bone is loaded. As a result, the bone fracture index,  $S_b$ , is approximately proportional to  $M^{3/4}$  rather than  $M^{2/3}$  as would be expected with geometrically similar scaling (Fig. 1).

As shown in Table 2, the relation between the polar moment of inertia and the area of the cross sections was found to be  $J \propto A^{1.96 \pm .08}$  (Fig. 2). An exponent of less than 2 indicates that the bone walls thicken with increasing bone size, and an exponent of greater than 2 indicates that bone walls become thinner. An exponent of 2 indicates geometric scaling of the cross section, which is consistent with this data. Biewener (5) published data on the cross-sectional bending moment,  $I$ , and the cross-sectional area,  $A$ , for a variety of non-Artiodactyle animals. From his tabulated data, we calculated that for the group of animals considered  $I \propto A^{1.88 \pm .07}$ . It therefore appears that the ratio of bone thickness to diameter ( $t/d$ ) increased with increasing animal mass, unlike the Artiodactyle bones considered in the present study.

Biewener also found that the second moment of inertia was proportional to  $m^{1.43}$ . However, geometric similarity would have  $I \propto M^{1.33}$ . In a later study of 32 species, from 4 orders, Biewener reported that  $I \propto M^{0.31}$  and  $d \propto M^{0.35}$  (1). If one assumes that in these bones too  $I \propto M^{1.43}$ , one would calculate that  $S_b \propto M^{0.77}$ . This scaling is similar to that found for Artiodactyle bones of the present study, although the relative scaling of  $I$ ,  $d$ , and  $I$  with body mass is different. One must be wary, however, of combining data from two different studies to calculate the value of  $S_b$  for non-artiodactyles. Further comprehensive studies of bone scaling among non-Artiodactyles are necessary to verify this consistency of scaling of  $S_b$ .

## REFERENCES

- 1) Biewener, A.A. *J. Exp. Bio.* 105:147-171 (1983).
- 2) McMahon, T. *Am. Natur.* 109(969):547-563 (1975).
- 3) Alexander, R.McN. *J.Zool., Lond.* 183:125-146 (1977).
- 4) Alexander, R.McN. et al. *J.Zool., Lond.* 189:305-314 (1979).
- 5) Biewener, A.A. *J. Exp. Biol.* 98:289-301 (1982).

Table 1

### Bone Geometry Data, Order Artiodactyle

Family	Genus and Species	Bone	Animal			
			Length cm	Diam. cm	Mass Kg	J cm <sup>4</sup>
Bovidae	Boselaphus B.	tibia	33.8	3.06	200	5.50
		radius/ulna	35.4	2.84		4.54
		humerus	25.8	3.38		5.23
		femur	32.6	3.08		4.88
	Kobus	humerus	21.5	2.56	<270	3.35
		tibia	30.5	2.48		3.59
		femur	26.8	2.48		3.67
	Antilocapra americana (m)	femur	22.7	1.86	36-60	1.54
		humerus	19.0	2.12		1.93
		radius/ulna	25.3	1.62		1.51
	Gazelle thompsoni	tibia	26.7	1.88		1.95
		radius/ulna	22.0	1.44	14-75	1.28
		tibia	25.3	1.78		2.02
	Damaliscus hunteri	humerus	15.0	1.76		1.64
		femur	19.6	1.78		1.76
		tibia	33.2	2.96	114-136	5.07
		radius/ulna	31.4	2.46		3.43
Cervidae	Odocoileus	humerus	24.3	2.96		4.33
		femur	31.8	2.94		4.51
	hemionus	tibia	30.3	2.70	48-145	2.94
		humerus	25.4	2.88		3.35
		tibia	34.6	2.54		3.50
	Cervus (m)	femur	22.5	2.04	100-250	2.01
		tibia	24.4	2.06		1.94
		axis (f)	18.0	2.08		2.11
	Cervus elaphus	humerus	35.6	3.34	100-250	4.82
		(canadensis) (f)	39.3	3.30		5.68
		tibia	31.2	3.04	100-250	4.03
	Cervus elaphus (nannodes) (f)	femur	26.7	3.14		4.23
		humerus	35.1	3.02		4.70
		tibia	26.5	1.88	48-145	1.84
	Odocoileus hemionus	humerus	19.3	1.92		1.38
		columbianus (f)	23.1	1.88		1.59
Giraffidae	Giraffa camelopardalis (f)	radius/ulna	80.5	5.56	550-1800	16.97
		femur	46.4	5.34		12.84
Camelidae	Camelus bactrianus (f)	tibia	40.3	4.56	450-690	10.82
		humerus	37.4	5.78		15.93
		femur	46.8	4.54		11.72
		radius/ulna	44.5	4.86		13.01

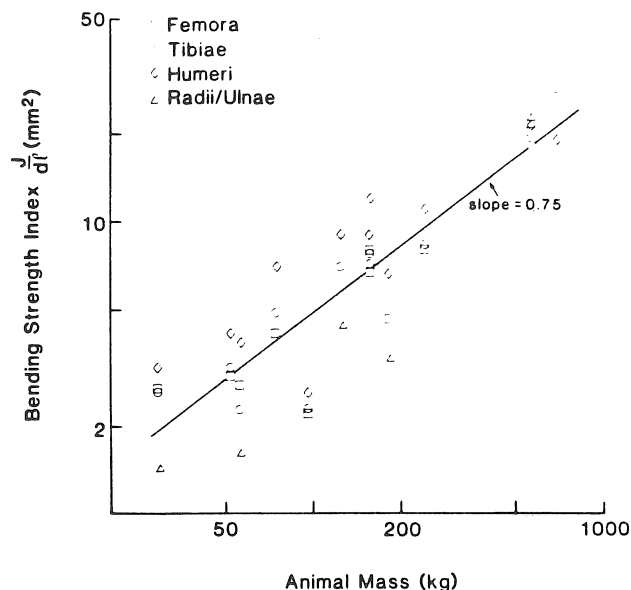


Figure 1

"Bone Strength Index" ( $J/dI$ ) plotted against Animal Mass on log-log scales. Empirical values for regression slopes vary between .76 to .89. Line with slope of .75 shown for comparison.

Table 2

### Allometric Relationships for Artiodactyle Bones

Allometric Relation $\alpha \propto \beta^x$	Empirical Exponent ( $\pm 95$ percent interval)				Approx. Exponent
	Femura	Tibiae	Humeri	radii/ulnae	
$d \propto M^x$	0.34 (.10)	0.32 (.11)	0.37 (.13)	0.41 (.09)	$\frac{1}{3}$
$I \propto d^x$	0.78 (.09)	0.56 (.16)	0.73 (.12)	0.80 (.24)	$\frac{3}{4}$
$J \propto A^x$	1.96 (.18)	2.00 (.17)	1.97 (.16)	2.01 (.03)	2
$I \propto M^x$	0.27 (.07)	0.18 (.08)	0.28 (.09)	0.32 (.13)	$\frac{1}{4}$
$\frac{J}{d} \propto M^x$	1.03 (.29)	0.94 (.33)	1.12 (.42)	1.21 (.27)	1
$\frac{J}{d} \propto I^x$	3.71 (.51)	4.59 (1.3)	3.87 (.83)	3.34 (.93)	4
$A \propto M^x$	0.70 (.20)	0.62 (.24)	0.74 (.30)	0.81 (.19)	$\frac{2}{3}$
$\frac{J}{dI} \propto M^x$	0.76 (.23)	0.76 (.28)	0.84 (.34)	0.89 (.19)	$\frac{3}{4}$
$\frac{J}{dI} \propto A^x$	1.09 (.08)	1.20 (.13)	1.14 (.03)	1.08 (.10)	$\frac{9}{8}$

# SCALING OF LONG BONE TORSION STRENGTH DURING GROWTH

T.S. Keller  
Biomechanics Lab  
V.A. Medical Center  
Nashville, TN 37203

D.R. Carter  
Engr. Design Division  
Stanford University  
Stanford, CA 94305

J.A. Main  
Mechanical and Materials Engr.  
Vanderbilt University  
Nashville, TN 37235

A.M. Strauss

D.M. Spengler  
Dept. of Orthop. and Rehab.  
Vanderbilt University MCN  
Nashville, TN 37232

## INTRODUCTION

During locomotion long bones are subjected to bending and torsion moments resulting from forces exerted by muscles across joints. Bending and/or torsional loads are responsible for most fractures, and the torsional strength of long bones has been shown to be allometrically ( $y=ax^b$ ) related to animal mass (1). In this study, a bone strength index  $S_B$  is formulated for immature mammals in a manner similar to that derived previously in scaling studies of mature animals (2). Long bone geometric and structural properties are measured for two species of mammals, rats and monkeys, and the relationships between  $S_B$  and animal mass is determined. The analysis indicates that torsional strength scales across a broad range of sizes in maturing animals. Maturing animals appear to use both geometric scaling strategies and material property modulations to achieve appropriate bone strength as body mass increases during growth.

## REVIEW AND THEORY

Consider the forces exerted about the knee joint by the quadriceps and hamstring muscles. For a beam with a circular cross section which exhibits little ductility prior to fracture, the torsional strength is given by:

$$\tau \propto TD/J \quad (1)$$

where T=ultimate torque  
D=bone diameter  
J=polar moment of area.

Equation 1 can be written in terms of the force F required to cause fracture:

$$F \propto J/(LD) \quad (2)$$

where L=bone length. One would predict a relationship between the magnitude of forces required to fracture a bone and the mass M of the animal, since the bones of large animals must withstand greater forces. If we assume that  $F \propto M^b$ , then equation 2 becomes

$$M^b \propto J/(LD) \quad (3)$$

where b is a power coefficient. In a mature animal  $\tau$  is constant (or nearly so) and equation 3 simplifies to

$$S_B \propto M^b \quad (4)$$

where we have defined  $S_B = J/(LD)$  as the bone strength index. In this case  $S_B$  is a function of geometry only. In growing animals, however,  $\tau$  increases allometrically with animal mass. Hence, the primary variable which best serves as an indicator for bone strength in maturing animals is

$S_B = T/L$ , the latter obtained by substituting for  $\tau$  in equation 3. Both T and L are readily measurable quantities.

It should be emphasized that the above analysis assumes that the bone material is homogeneous with a linear stress distribution throughout the cross section. Due to the material maturation and remodelling in the cortex during growth, this assumption is incorrect. The values calculated for  $\tau$  are thus "effective" strength values for the non-homogeneous bone and will henceforth be designated as  $\tau^*$ .

## METHODOLOGY

Body mass (M) and femoral bone length (L) were measured in 41 male rats ranging in age from 3-44 weeks (0.04-0.68 Kg) and 5 male and 15 female monkeys (P.C. Anubis and M. Nemestrina) ranging from 1-650 weeks (0.3-12.8 Kg). Nominal maturation ages are 17 weeks for the rats and 312 weeks for the monkeys. Bone length was determined as the distance from the greater trochanter to the distal medial condyle using dial calipers. A twisting moment to failure was applied to the left femur with a Burstein-Frankel torsion testing machine (3) and the torsional moment and angular deformation were recorded on a digital storage oscilloscope.

The right femora were utilized for histomorphometry. Photographs of 60 micrometer mid-diaphysis cross sections were digitized and a Fortran program SLICE (4) was used to determine areal and areal inertial properties: cross-sectional area (A), polar moment of area (J), major diameter (D2), and minor diameter (D1). An average diameter  $D = (D1 + D2)/2$  was also computed.

## RESULTS AND DISCUSSION

Tables I and II summarize the allometric relationships (geometry and strength indices) determined for rat and monkey femora, respectively. Linear and exponential regressions did not yield as good a fit as determined by the coefficient of determination ( $R^2$ ) and the F-test. In general, the exponents obtained for geometric relations for the monkey were greater than those obtained for the rat.

The bone strength index  $S_B$  is plotted as a function of animal mass for both rats and monkeys in Figure 1. The exponent obtained for the geometric strength index  $J/(LD)$  of the monkey femora as a function of growth was 50 percent greater than that obtained for the rat femora. An analysis of co-variance indicated that this difference was statistically significant at the  $P < 0.05$  level. Total strength  $T/L$  increased at a lower rate for monkey femora in comparison to rat femora during growth, although this difference was not significant. When the  $T/L$  exponent of the rat femora was averaged with the  $T/L$  exponent of the monkey femora an exponent  $b = 0.93$  was obtained indicating that bone strength relative to body mass



may decrease slightly during maturation for these animal groups.

An effective material strength  $\tau^*$  can also be computed by dividing the total strength contribution  $T/L$  by the geometric strength contribution  $J/(LD)$ . Based upon the exponents obtained for  $T/L$  versus  $M$  and  $J/(LD)$  versus  $M$  (see Tables I and II), exponents of 0.49 and 0.17 are estimated for rat and monkey effective material strength, respectively. The material changes computed (see Fig. 1) indicate that the rat modulates bone material approximately 3 times faster in order to achieve appropriate bone strength during growth. Hence, in the rat material changes dominate, whereas in the monkey geometric changes dominate in modulating bone strength during growth.

TABLE I. Allometric relations for the rat

Relation	Exponent (b)	Correlation Coefficient	95% Confid. Interval
Dl vs M	0.19	0.88	$0.15 < b < 0.22$
L vs D	1.34	0.87	$1.10 < b < 1.58$
J vs A	1.61	0.98	$1.50 < b < 1.71$
J vs L	2.99	0.96	$2.69 < b < 3.29$
$J/(LD)$ vs M	0.47	0.93	$0.41 < b < 0.53$
$T/L$ vs M	0.96	0.93	$0.83 < b < 1.09$
$\tau^*$ vs M	0.50	0.77	$0.36 < b < 0.63$

TABLE II. Allometric relations for the monkey

Relation	Exponent (b)	Correlation Coefficient	95% Confid. Interval
D vs M	0.37	0.98	$0.34 < b < 0.41$
L vs D	1.07	0.99	$0.98 < b < 1.16$
J vs A	1.96	0.99	$1.90 < b < 2.02$
J vs L	3.72	0.96	$3.05 < b < 4.39$
$J/(LD)$ vs M	0.72	0.95	$0.58 < b < 0.86$
$T/L$ vs M	0.89	0.93	$0.71 < b < 1.07$
$\tau^*$ vs M	-0.08	-0.27	not signif.

#### CONCLUSIONS

In growing animals, both geometric and material properties are regulated in order to maintain an optimal bone strength. In rapidly growing animals the material changes dominate, whereas in slower growing animals geometric changes dominate. Analysis of the fracture strength due to torsional loading of immature rat and monkey femora indicated that the torsional strengths scale across a broad range of animals in spite of differences in scaling of geometry. The bone strength index  $S_p = T/L$  appears to be a common scaling factor by which growing animals modulate bone strength, and an exponent  $b = 0.93$  was obtained. The latter indicates that bone strength relative to body mass may slightly decrease with maturation.

#### References

1. Keller, T.S., et al. JOR, in press.
2. Selker, F. and Carter, D.R. Submitted NACOB, 1986.
3. Burstein, et al. J. Biomech. 4:155-158, 1971.
4. Nagurka, et al. J. Biomech. 13:59-64, 1980.

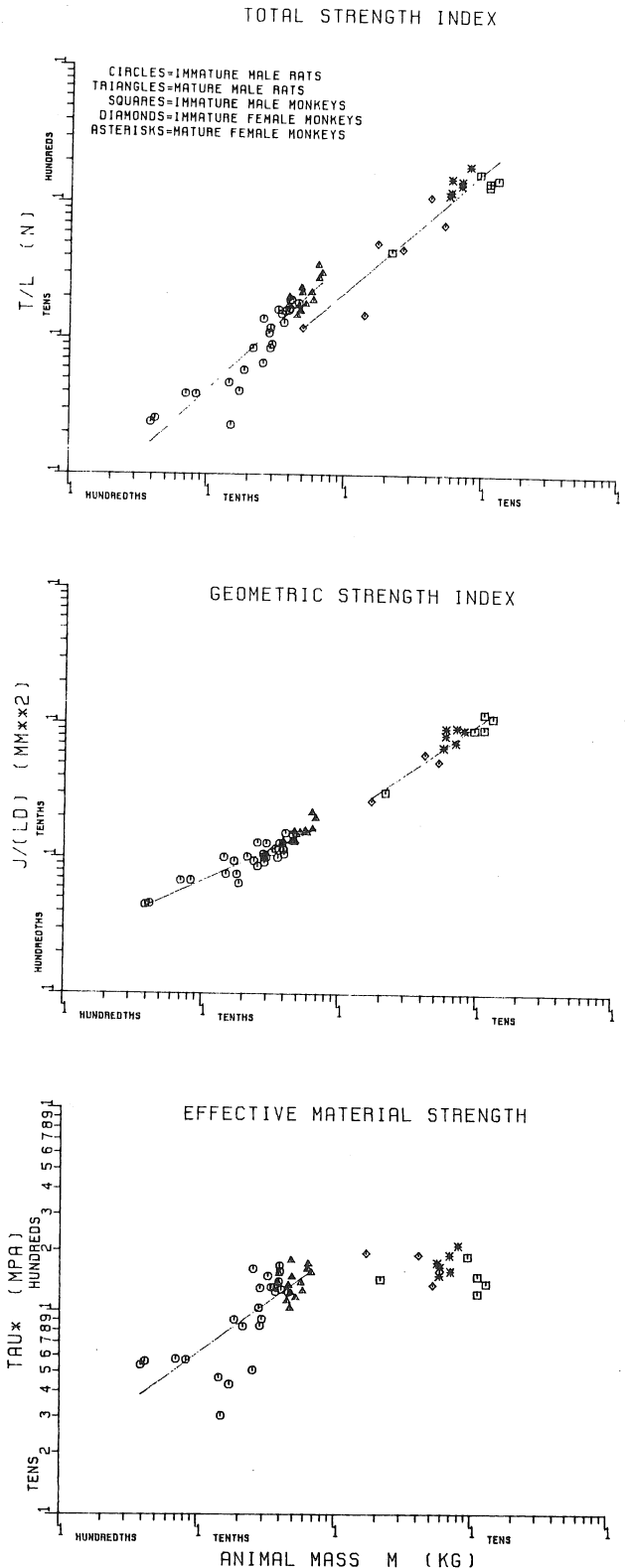


Figure 1. Log-log plots of the total strength index, geometric strength index, and effective material strength as a function of animal mass. Exponents (b) and correlation coefficients are given in Tables I and II for the rat and monkey, respectively.

# THE ROLE OF COLLAGEN CROSSLINKS IN THE AGE RELATED CHANGES IN MECHANICAL PROPERTIES OF PIG DIGITAL TENDONS

Robert E. Shadwick  
Agricultural and Food Research Council, Bristol, U.K. and  
Department of Biology,  
University of Calgary,  
Calgary, Alberta, T2N 1N4.

## INTRODUCTION

Tendons are stiff, resilient biological springs which are important as elastic energy storage elements in terrestrial locomotion. Tendon mechanical properties arise from a linear array of crosslinked collagen fibres. The relationship between collagen crosslinking, fibre structure and mechanical properties of tendons is not clearly understood. This paper reports findings from a preliminary study of the mechanical, morphological and crosslink characteristics of the digital extensor and flexor tendons of pigs. The results show that at birth the flexor and extensor tendons have identical properties. With growth and aging the strength, stiffness, resilience and elastic energy storage capacity increase substantially, concomitant with increases in fibril diameter and more extensive crosslinking. All these changes are more marked in the flexor, which is the major load bearing tendon, compared to the extensors. These results suggest that the mechanical properties of digital tendons are altered with aging and functional requirements by changes in the internal structure and the collagen crosslinking.

## REVIEW AND THEORY

A wide range of values has been reported for the tensile strength and stiffness of mammalian tendons, suggesting that there are species, tissue or age specific differences in the mechanical properties of collagen fibres. Comparisons of digital tendons in humans and pigs have shown substantial differences between the mechanical properties of antagonistic flexor and extensor tendons (1, 2). Changes in mechanical properties have also been observed with aging and with exercise (3, 4). A primary determinant of the tensile mechanical properties of tendons is covalent crosslinks which join adjacent collagen molecules into stable macromolecular structures. The crosslinks formed in new tissue are reducible bifunctional structures which are transformed with aging to non-reducible polyfunctional 'mature' forms (5). Morphological studies have shown that the distribution of collagen fibril diameters changes with growth and aging in tendons. Parry et al. (6) suggested a positive correlation between tensile strength and the mass-average diameter of the collagen fibrils. They postulated that an increase in the fibril diameter should be paralleled by an increase in the density of intra-fibrillar crosslinks, and thus an increase in tensile strength. The study reported here is an attempt to test this hypothesis.

## METHODOLOGY

In this study, the digital flexor and extensor tendons of the front limb of domestic pigs were used. Tensile mechanical properties were measured *in vitro* using an Instron Materials Testing Machine, and a video dimension analyser according to the procedure of Woo et al. (2). Collagen fibril diameters were measured from electron micrograph negatives using a Wild filar eyepiece micrometer on an M5 stereo

microscope. Collagen crosslink characteristics were assessed in two ways. First, reducible crosslink structures were labelled by reduction with  $\text{NaB}^3\text{H}_4$ , fractionated from tissue hydrolysates by ion exchange chromatography and detected by liquid scintillation counting, according to (7). Second, the relative abundance of non-reducible mature crosslinks was determined by analysing peptide maps of cyanogen bromide (CNBr) cleaved collagen molecules, according to (8). This method allows comparisons among samples of the the extent of lateral polyfunctional inter-molecular crosslinking.

## RESULTS AND DISCUSSION

Table I. Mechanical properties of digital tendons

Age	birth	4 month	
Tendon	*E & F	E	F
Elastic Modulus (Pa)	$2 \times 10^8$	$1 \times 10^9$	$2 \times 10^9$
Yield Strain	0.15	0.05	>0.10
Tensile Strength (Pa)	$1.8 \times 10^7$	$3 \times 10^7$	$>6 \times 10^7$
Resilience	70%	80%	92%
Maximum Stored Energy (Joules/Kg)	400	680	3000

\* E=extensor; F=flexor

The results of tensile tests on pig digital tendons are shown in Table I. At birth the flexor and extensor have identical mechanical properties, with relatively high extensibility and low strength and elastic modulus (i.e. stiffness). At 4 months both tendons show greatly improved mechanical properties, becoming stronger and stiffer than at birth. These changes are more marked in the flexor than in the extensor. The flexor has a large elastic energy storage capacity, and its high resilience (i.e energy recovered/energy stored) make it a much more effective biological spring than the extensor.

Table II compares the collagen fibril diameters in the tendons at three ages. At birth flexor and extensor have identical unimodal distributions of fibril diameters, averaging 55 nm in both cases. With growth the fibrils increase and their diameters become bimodally distributed. At 4 months the flexor has predominantly large diameter fibrils (peak B) averaging 132 nm, while the extensor has mostly small diameter fibrils (peak A) averaging 97 nm. With further aging the fibril diameters increase, such that by 40 months the flexor is composed of two groups of large fibrils averaging 158 and 270 nm in diameter. By contrast, the 40 month extensor has fibril diameters which are only slightly larger than those at 4 months.

Table II. Collagen fibril diameter in digital tendons.

Age	birth	4 month		40 month	
Tendon	*E & F	E	F	E	F
Mean Diameter	55	97	70	79	158
Peak A (nm)					
Mean Diameter		140	132	181	270
Peak B (nm)					
% fibrils in A	100	68	39	63	53
% fibrils in B		32	61	37	47
% area in A	100	41	16	21	29
% area in B		59	84	79	71

\* E=extensor, F=flexor

When the load-bearing cross-sectional area of the collagen fibrils is considered, the differences between the two tendons are more striking. At 4 and 40 months the majority of the fibril cross-sectional area in the flexor is represented by large rather than small fibrils, while in the comparable extensor the fibril cross-sections are relatively small. According to Parry's hypothesis, the strength and stiffness of a large diameter collagen fibril should be greater than the equivalent mass of small diameter fibrils, because of greater internal crosslinking density. The mechanical and morphologic data from the pig tendons supports this hypothesis.

Table III \*Relative abundance of reducible crosslinks.

Age	Extensor	Flexor
birth	1885	2030
4 month	1038	1023
40 month	206	102

\* cpm <sup>3</sup>H per mg collagen dry weight

The abundance of reducible collagen crosslinks in digital tendons at different ages are compared in Table III. At birth flexor and extensor have virtually identical levels of reducible crosslinks. Since these are only intermediate structures which eventually convert to non-reducible forms *in vivo*, the reducible crosslinks typically decrease with age (7). This decrease is taken to be an indication of the accumulation of the 'mature' polyfunctional crosslinks. In the pig tendons the reducible crosslinks decrease substantially at 4 and 40 months, with the greatest change occurring in the flexor. This suggests that the crosslink maturation is accelerated in this high load bearing tendon compared to the extensor.

CNBr cleavage liberates characteristic peptide fragments from the  $\alpha 1$  and  $\alpha 2$  chains of collagen molecules. The reducible bifunctional crosslinks are located in a peptide designated  $\alpha 1\text{CNBr-6}$  (5). With maturation this crosslink forms a further link with another  $\alpha 1\text{CNBr-6}$  in an adjacent layer of collagen molecule, to make extensive lateral crosslinks throughout the fibril (5). Analysis of CNBr peptides by electrophoresis shows that with age the amount of monomer  $\alpha 1\text{CNBr-6}$  decreases as mature crosslinks form, concomitant with a decrease in reducible crosslinks, because polymers of  $\alpha 1\text{CNBr-6}$  are formed (8).

Table IV. Relative extent of crosslink maturation indicated by the ratio of  $\alpha 1\text{CNBr-6}:\alpha 1\text{CNBr-3}$ .

Age	Extensor	Flexor
birth	1.0	1.1
4 month	1.2	0.8
40 month	0.7	0.1

Comparison of the quantity of monomer  $\alpha 1\text{CNBr-6}$  to a non-crosslinked peptide,  $\alpha 1\text{CNBr-3}$ , gives an indication of the relative extent of crosslink maturation in different samples. Table IV shows that crosslink maturation proceeds with age as expected (decrease in  $\alpha 1\text{CNBr-6}:\alpha 1\text{CNBr-3}$  ratio), and that this occurs more dramatically in the flexor than in the extensor, as did the decrease in reducible crosslinks. These changes indicate that the flexor was more extensively stabilized by lateral intermolecular crosslinks than the extensor at 4 and 40 months. These results fully support Parry's hypothesis on the relationship between fibril size, crosslinking and mechanical properties.

## CONCLUSIONS

1. At birth digital flexor and extensor tendons of the pig have identical mechanical properties, collagen fibril diameters and crosslink characteristics.
2. With growth and aging the stiffness, strength and elastic energy storage capacity of the tendons increase. Fibril diameters increase and collagen crosslinking becomes more extensive.
3. All these changes are more pronounced in the digital flexor than in the digital extensor.
4. The digital flexor appears to adapt to the role as the major load and impact resisting tendon in the foot by changes in the internal structure and crosslinking of the constituent collagen molecules.

## References

1. Benedict, J.V., et al. J. Biomech. 1:53-63, 1968.
2. Woo, S.L-Y., et al. J. Biomech. Engng. 103:51-56, 1981.
3. Kastelic, J. and E. Baer, S.E.B Symposium XXXIV: 397-436, 1980.
4. Woo, S.L-Y., et al. Connec. Tiss. Res. 7:177-183, 1980.
5. Light, N.D. and A.J. Bailey, in Biology of Collagen A. Viidik and J. Vuust eds. Academic Press, N.Y. 15-38, 1980.
6. Parry, D.A.D. et al. Proc R. Soc. Lond. B 203: 305-321, 1978.
7. Robins, S. et al. Biochem J. 131:771-780, 1973.
8. Light, N.D. and A.J. Bailey, FEBS Letts. 97:183-188, 1979.

Z. Ladin

Biomedical Engineering Department, Boston University, Boston, MA 02215

## INTRODUCTION

Optoelectronic position measurement systems are widely used to study the biomechanics of human movement. The calibration and performance analysis of such systems are based on the measurement of known static geometries (Whittle (5), Thurston (4)). Since the position information is used to calculate time derivatives (velocity and acceleration), there is a clear need to develop a method to calibrate the dynamic performance of position measurement systems. This paper presents a methodology to achieve this goal. It describes an electromechanical system that produces pure sine-wave motion, and a data-processing package which together provide the dynamic performance characterization of the position measurement system in the frequency range of 1-11 Hz. Preliminary results that illustrate the role of the cutoff frequencies of the low-pass filter, used to obtain acceleration estimates are presented.

## METHODOLOGY

The electro-mechanical device which was used in the experiment is shown in Fig. 1. It contains a DC motor that drives a steel shaft to which an aluminum arm and a belt pulley were connected. An off-centered bearing was inserted into the arm, and a second steel shaft was inserted into the bearing. The two shafts were connected by a timing belt, driving the two belt pulleys. The main aspect of this design is the angular rotation of the second shaft without a change in its orientation (e.g. if a vertical arm is attached to the second shaft, it is going to remain vertical while its center describes a circle). This kind of movement produces a pure sine-wave motion in an inertial reference system which is attached to the laboratory.

The pure sine-wave spacial motion produces pure temporal sine-wave velocities and accelerations. Hence, by changing the rotational velocity of the electrical motor, the frequency of oscillations changes. As the second shaft rotates at a constant radius, its velocity changes linearly with the frequency of oscillations, while its acceleration is proportional to the square of the oscillation frequency. Hence, a controlled study of the acceleration estimates and measurements in a given frequency range is possible. This represents for the first time a methodological approach for studying the overall dynamic performance of a position measurement system. Such an approach complements the static characterization of such a system, which yields the spacial resolution.

The position measurements were done using the TRACK III system in the Laboratory for Biomechanics and Human Rehabilitation Engineering at M.I.T.. TRACK III (based on the Selspot-I optoelectronic system) monitored the spacial positions of infrared LED's (Light Emitting Diodes), which were attached to the second shaft. An Entran accelerometer fixed to the second shaft was used to measure the acceleration. Synchronous readings of the position and acceleration were done using two PDP 11/60 mini-computers at a sampling rate of 315 Hz. A spectrum analyzer has been used to perform an on-line frequency decomposition of the accelerometer signal. A total of 38

experiments which were roughly 0.5 Hz apart in the frequency range of 1-11 Hz have been performed. The experiments were one or two seconds long, and the time domain traces of the acceleration measurements by the accelerometer and the position measurements by TRACK III were stored for later processing.

The quantitative analysis of the acceleration estimates by TRACK III is based on trying to fit a sine-wave function to the time domain traces. The function which has been chosen was  $A_0 + A_1 \cos(\omega t + \phi)$ , where  $A_0$  is the offset,  $A_1$  is the amplitude,  $\omega$  is the frequency and  $\phi$  is the phase angle. An algorithm based on the Fast Fourier Transform of the time-domain traces was used to calculate the values of  $A_0$ ,  $A_1$ ,  $\omega$ , and  $\phi$  which resulted in the best fit between the above function and the acceleration traces.

The knowledge of the basic frequency of oscillations (from the spectrum analyzer information) and the radial position of the second shaft (see Fig. 1) enabled us to calculate the expected value of the acceleration at that frequency. Hence, a three-way comparison was possible between the accelerometer measurements, TRACK III estimates and the theoretically predicted acceleration values. Such a procedure fully characterizes the dynamic performance of TRACK III over the frequency range covered in the experiment.

The data analysis presented above determines the capability of the position measurement system to extract basic kinematic information (the acceleration amplitude of a pure sine-wave). A second question that directly relates to it is how noisy the processed information is. The answer to this question could result in the determination of the noise level that is introduced by the data processing. This question was especially intriguing as TRACK III performs an elaborate process of noise rejection, low-pass filtering and differentiation to derive velocity and acceleration estimates from the position measurements. The basic steps in this process have been published by Antonsson et al (1).

The noise characterization was based on the calculation of the variance in the acceleration estimates by TRACK III:

$$V = \frac{1}{N} \sum_{i=1}^N (a_{ei} - a_{fi})^2 - \left[ \frac{1}{N} \sum_{i=1}^N (a_{ei} - a_{fi}) \right]^2$$

where  $V$  is the variance,  $N$  is the number of data points in a given experiment,  $a_{ei}$  is the instantaneous estimated acceleration by TRACK III,  $a_{fi}$  is the instantaneous value of the 'best fit' function described above. As the square root of the variance is the standard deviation, a signal to noise ratio can be obtained by dividing the amplitude of the 'best-fit' function by the standard deviation. Thus, a characterization of the noise in the acceleration estimates over the given frequency range was obtained.

## RESULTS AND DISCUSSION

The first question that needs to be addressed concerns the kinematic performance of the electromechanical system. In other words, how pure is the sine-wave generated by such a system. In order to address this question a spectrum analyzer was used to perform an on-line spectral decomposition of the accelerometer signal. As theory dictates that the signal amplitude goes up with the square of the frequency, we expected to see an improvement in the signal to noise ratio (SNR) as the frequency increased. The spectrum analyzer data verified this expectation: The signal to noise ratio was about 10 at the frequency of 1.1 Hz and reached a value of 100 at 2.5 Hz. The SNR had values of 100 or higher for frequencies up to 12 Hz. At that frequency, mechanical vibrations were visually noticeable and recorded by the spectrum analyzer. Based on the results described above, the frequency range of 1-11 Hz was chosen for analysis.

Figures 2 and 3 demonstrate the dramatic effect of the filtering process on the quality of the acceleration estimates. The values of the cutoff frequencies were 100 Hz for the position data and 60 Hz for the derivatives in one case (100/60), and 20 Hz for the position and the time derivatives for the second case (20/20). Fig. 2 shows that the 100/60 filter failed to extract the primary oscillation for frequencies below 3 Hz. The 20/20 filter failed only once (at the frequency of 2.5 Hz). The figure shows a general trend of improvement (i.e. a decrease in the relative error) with increasing frequency.

Fig. 3 shows the signal to noise ratio obtained for the same filters. Even though there are occasional peaks larger than 10, the average value of the 20/20 filter is about 10. There is a monotonic improvement of the SNR for the 100/60 filter, reaching values of about 6 at the highest frequency. It is interesting to note that the 20/20 filter shows a slight decrease in the values of the SNR at the highest frequencies, probably reflecting the slight attenuation of the signal due to the filter (whose cutoff frequency is about twice the nominal signal frequency).

The figures below illustrate the nature of the dynamic characterization that can be obtained using the experimental approach described in this paper. Such an approach enables to quantify the effects of different components in the data processing chain (filters, differentiators, etc.), and thus complement the analysis and optimization done on synthesized data (Cappozo et al (2)), and comparisons of accelerometry and position measurement systems (Pezzack et al (3)).

### ACKNOWLEDGEMENT

The author thanks Mr. Bill Messner and Professor Woodie Flowers for their help in the execution of this study. Partial support by Whitaker Fellowship and NSF Grant No. ECS8023193.

### REFERENCES

1. Antonsson, E.K., et al. Advances in Bio-engineering, ASME, 51, 1979.
2. Cappozo, A. et al. J. Biomech. 16: 767-776, 1983.
3. Pezzack, J.C. et al. J. Biomech. 10: 377-382, 1977.
4. Thurston, A.J. J. Biomed. Eng. 4: 129-132, 1982
5. Whittle, M.W. J. Biomech. 15: 185-186, 1982.

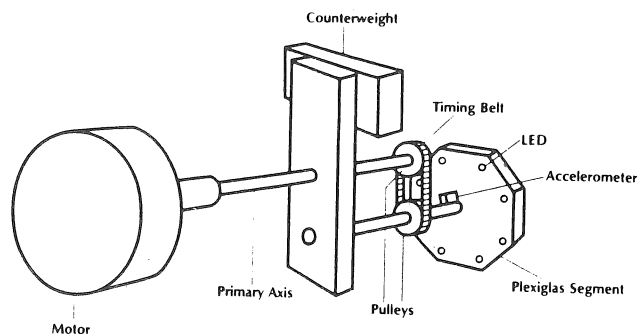


Fig. 1 - The electromechanical system

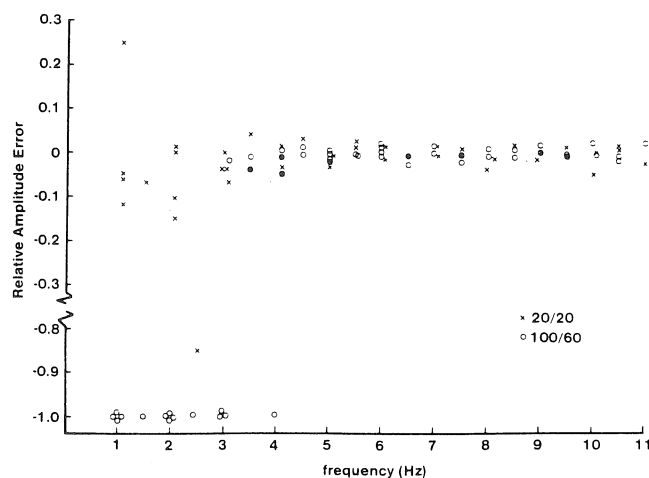


Fig. 2 - The effect of filtering on the relative amplitude error

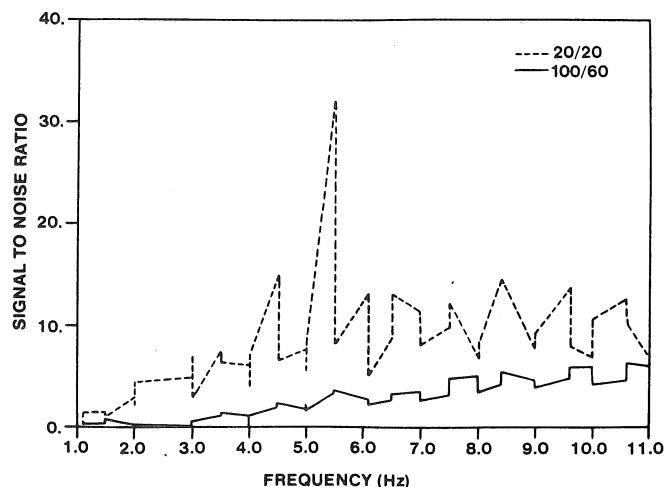


Fig. 3 - The effect of filtering on the signal to noise ratio

L. McCarthy, J. Frank, J. Brown and S. Maki  
Department of Kinesiology  
University of Waterloo  
Waterloo, Ontario, N2L 3G1

## INTRODUCTION

The development of postural control in children involves the adaptation of automatic postural responses to environmental conditions and to the demands of voluntary motor activity. Developmental research to date has focused primarily on postural control processes which serve to maintain stance, particularly during support surface perturbation. Automatic postural adjustments to correct body sway were present and directionally appropriate in children as young as 18 and 15 months of age (3,6). Such postural reactions were found to be of increased latency and duration in children below the age of 7½ years.

In adults, potentially destabilizing movements have been shown to be preceded by the activation of postural muscles. Such activity in the postural muscles in advance of activity in the task-defined (focal) muscle has been well documented (1,5,2). The purpose of the present study was to determine whether pre-movement postural activity would be evidenced in children; and to examine the temporal-spatial characteristics of the postural-focal muscle activity with respect to age. Electromyographic (EMG) procedures were used to measure the onset times of postural and focal muscles during a reaction time shoulder flexion, in children between the ages 7-13.

The work of Sweigard (1974) indicates that trained dancers have acquired fine control over their postural musculature, facilitating balance during destabilizing extremity movement. It was of further interest in this study to determine whether children in dance training might thus exhibit postural responses characteristics different from their peers resulting in improved reaction times.

## METHODOLOGY

Thirteen girls aged 7-13 participated as subjects. Six of the subjects were obtained from the Carousel Dance Centre, University of Waterloo, and had been training in dance from the age of 6. Two adults, one an advanced dancer, between the ages 20-24 were also tested.

Following presentation of a warning light (variable foreperiod) and tone signal, subjects were required to release a button positioned at their side, and to hit a foam target bar in front of them at shoulder height. The response tone was initiated with a four bank interval timer which was wired in series with the response button and target bar. The response tone, button release and target contact were indicated by voltage changes recorded on channel one of the data record (Fig. 1). Ten reaction time shoulder flexions were performed.

To record postural and focal muscle activity, a pair of silver-silver chloride surface electrodes was placed over the following muscles: tibialis anterior; lateral gastrocnemius, biceps femoris and anterior deltoid. Amplified EMG input was full wave rectified, low pass filtered (4th order butterworth filter, 10 ms. time constant), A/D converted at 100 Hz on the Watscope data acquisition system and stored on floppy disc by an IBM PC computer.

## RESULTS AND DISCUSSION

Reaction times, movement times, and onset times of postural (TA, LG, BF) and focal (AD) muscles were determined from the CRT using an interactive digitizing program on the IBM PC computer. The components of the reaction time response are summarized in Tables I and II. See table for abbreviations.

It can be seen in Table I that P-F latency, the time between the onset of first postural muscle activity, and that of the focal muscle, did not change systematically between the ages 7-13. Response components observed in adults indicate that the mature response may be characterized by reduced P-F latencies and reduced reaction times. These characteristics were evident in the two oldest dance students (age = 12-13 years) displaying the shortest P-F latencies and fastest reaction times among subjects.

As in previous research on anticipatory postural responses in adults (1,2,4,5), postural muscle onset preceded AD onset in all trials for all non-dance children (age = 7-13) and younger dance students (age = 7-10). In contrast, postural muscle onset followed or was coincident with AD onset on more than 50% of the trials performed by the oldest dance students.

In conditions where adult subjects have been aided with additional postural support, reaction times have been reported to be significantly reduced (2). Conversely, increased postural requirements have been shown to delay the activation of the focal muscles (4). The oldest dance students may thus possess greater stability in the standing position, such that postural activity is minimized, and reaction time performance is improved.

The precise activation order of postural muscles was extremely variable across all ages in both dancers and non-dancers. This was the case for both within and between subjects (see Table II). This can likely be accounted for by the necessity of integrating the activation pattern into the ongoing control of body sway as the subjects waited to respond.

For all non-dance children and younger dance students the most prevalent postural pattern was TA followed by BF. This can be explained by TA activating first to counter balance the backward displacement of the body by torques generated at the shoulder. Subsequently, BF was activated to extend the hip and counter balance the final forward displacement of the centre of gravity as the arm was held in front of the body. LG was activated with or slightly following TA, but before BF onset.

The older dance students displayed an activation order in the postural muscles of BF followed by TA and finally LG. BF and TA were activated in the same order for both adults, however no activation of LG was observed.

The patterns of postural activity observed differ from those which have been shown to occur prior to reaction time displacements of a stiff handle (2,8). Gastrocnemius - hamstrings and tibialis anterior - quadriceps have been identified as synergist pairs activated, in relatively fixed sequences, in advance of the pull and push focal movements. The present

authors propose that postural activity will occur in the musculature that is optimally suited for stabilization with respect to the designated task and to the current state of equilibrium.

#### REFERENCES

1. Belen'kii, V.Y.E. et al. Biophysics. 12: no. 1, 135-141, 1967.
2. Cordo, P.J. et al. Journal of Neurophysiology. 47: no. 2, 287-302, 1982.
3. Forssberg, H. et al. Journal of Neuroscience. 2: no. 5, 545-552, 1982.
4. Friedli, W.G. et al. Journal of Neurology, Neurosurgery and Psychiatry. 47:611-622, 1984.
5. Lee, W.A. Journal of Motor Behavior. 17: no. 2, 131-147, 1985.
6. Shumway-Cook, A. et al. Journal of Motor Behavior. 17: no. 2, 131-147, 1985.
7. Sweigard, L.E. Human Movement Potential: Its Ideokinetic Facilitation. New York: Dodd, Mead, and Company, 1975.
8. Woollacott, M.H. et al. Exp. Brain Res. 55:263-271, 1984.

Table I Response Component Latencies (ms.) Across Subjects

Age	RT	MT	P-F Latency
	$\bar{X}$ (sd)	$\bar{X}$ (sd)	Median (range)
7	460 (90)	260 (20)	140 (200)
7	700 (140)	310 (30)	130 (240)
8	390 (50)	270 (20)	90 (220)
*8	590 (50)	290 (30)	130 (160)
9	530 (60)	280 (20)	105 (100)
*9	370 (50)	230 (40)	170 (150)
10	480 (50)	260 (10)	130 (150)
*10	290 (30)	270 (20)	60 (60)
*10	360 (60)	290 (50)	100 (270)
12	430 (40)	290 (20)	150 (240)
12	310 (40)	270 (30)	110 (100)
*12	230 (20)	200 (10)	20 (40)
*13	260 (40)	180 (8)	-10 (110)
Adult	340 (40)	280 (20)	45 (120)
*Adult	260 (30)	240 (20)	30 (40)

Note: Subjects marked with \* are in dance training. RT = reaction time, MT = movement time; P-F latency = postural-focal latency.

Table II Mean Onset Times (ms.) of Postural and Focal Muscles Across Subjects

Age	TA	LG	BF	AD
	$\bar{X}$ (sd)	$\bar{X}$ (sd)	$\bar{X}$ (sd)	$\bar{X}$ (sd)
7	280 (90)	440 (190)	430 (180)	410 (80)
7	440 (120)	410 (140)	600 (150)	610 (140)
8	210 (30)	280 (160)	280 (50)	300 (60)
*8	400 (80)	420 (80)	440 (60)	540 (70)
9	320 (30)	380 (90)	560 (240)	440 (50)
*9	140 (20)	140 (30)	210 (60)	290 (50)
10	280 (30)	300 (40)	370 (60)	390 (70)
*10	170 (20)	310 (30)	220 (50)	230 (20)
*10	190 (110)	220 (130)	240 (70)	280 (70)
12	240 (120)	280 (230)	340 (50)	340 (60)
12	160 (40)	320 (50)	160 (80)	260 (40)
*12	150 (30)	240 (40)	140 (20)	140 (20)
*13	180 (20)	200 (70)	150 (30)	140 (30)
Adult	210 (50)	--	240 (40)	240 (30)
*Adult	150 (20)	--	160 (30)	180 (30)

Note: Subjects marked with \* are in dance training. TA = tibialis anterior; LG = lateral gastrocnemius; BF = biceps femoris; AD = anterior deltoid

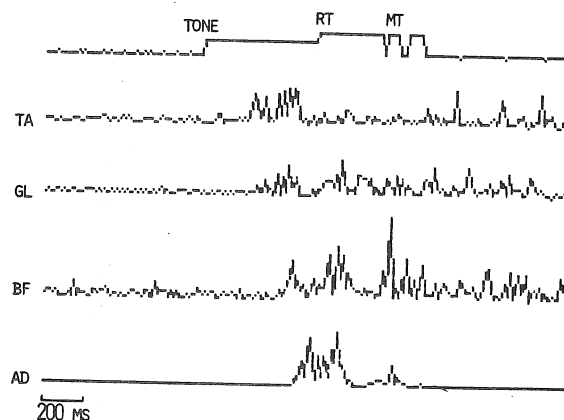


Fig. 1 Typical onset pattern of postural and focal muscles observed in 9 year old.

MOBILITY OF HALO-VEST ON THORAX: COMPARATIVE  
BIOMECHANICS OF 7 CURRENT AND 1 EXPERIMENTAL  
VEST DESIGN

Department of Orthopaedics and Rehabilitation  
The University of Vermont, Burlington, VT  
05405

Martin H. Krag and Bruce D. Beynnon

### INTRODUCTION

The halo vest is a type of cervical orthosis (orthosis device which stabilizes a particular body region) which consists of 1) a metal ring ("halo") attached to the skull by means of "skull pins" placed through the skin and embedded in the calvarium, 2) a "vest" (typically made of semi-rigid plastic, partially reinforced by metal components) surrounding and contacting the upper torso, and 3) rigid uprights (typically 2, 3 or 4 metal rods or bars) connecting the halo to the vest in a manner allowing adjustment of the location of the halo relative to vest. Application of the halo-vest is usually considered to maximize the stability, (through minimization of loads, and corresponding displacements), of a particular region of concern within the cervical spine. Current halo vest systems provide required stability to varying degrees, but all do so with a weak link, poor vest attachment to thorax. Koch, et al. (1978) reported an average of 1/3 normal cervical spine flexion extension motion existed in subjects wearing the halo vest, recognizing the vest to require careful fitting to sternum and upper thoracic spine. In addition to the above mentioned study clinical experience has made us recognize the inadequacy of currently available vests and motivated us to design and develop a new one. To biomechanically evaluate our experimental vest, and compare it to commercially available systems, a study was designed to quantify vest motion on thorax.

### REVIEW AND THEORY

The goal in clinical application of a halo vest is usually considered to be minimization of motion between head and thorax (2). It is probably more useful, however, to consider minimization to be that of load (forces and moments) acting upon some particular location of concern within the cervical spine, (e.g., site of fracture, tumor, ligamentous laxity) for which the halo vest is being applied. There are two possible sources of load transmission between head and thorax for a subject using current halo vest systems. Firstly, loads generated by muscles acting at a distance from the neck may be transmitted to the local site of interest by the halo vest itself, acting as a force transmission linkage. For example, if the shoulder, in moving relative to the thorax, is able to push against the vest this will transmit loads through the uprights to the head and subsequently to the cervical spine. Similarly, if the upper abdomen is able to push against the lower part of the vest (such as during the movement of sitting up), similar undesired load transmission will occur. Finally, if there is a large amount of friction between the posterior surface of the back half of the vest and some supporting surface (chair back or bed mattress) then body movement within the chair or bed will also allow undesired loads to be produced across the cervical spine. Secondly, gravity can produce local

load transmission across the cervical spine. Since the halo is rigidly connected to the skull, the weight of the entire halo vest assembly or some portion of it may be transmitted across the cervical spine if the vest fails to acquire proper attachment to thorax. This has been shown to occur clinically through strain gauge instrumentation of halo uprights. Decreasing the weight of the halo vest will decrease the gravity-induced loads. Additionally, reduction of the trunk surface area which the vest covers would make the vest more comfortable to wear.

Recognizing that current vests are the weak link in minimization of load transmission, an experimental one has been developed which grips thorax at the regions of low relative mobility, only partially used by currently available vests. These regions are the posterior thoracic interscapular area, ribs along the midaxillary line, and sternum. Corresponding to these regions the experimental vest uses a sternal plate rigidly connected, without thoracic contact, to lateral midaxillary pads, which are strapped to a posterior thoracic interscapular plate. The sternal and thoracic plates are rigidly linked with a bilateral yoke which runs over the shoulder, avoiding shoulder girdle contact. Figures 1 and 2 are the conceptual design diagrams.

### METHODS

To evaluate the mobility of vest on thorax 7 current commercial and four experimental vests were worn one at a time by each of 4 normal volunteers. All vests were fitted to subjects in a manner resembling proper clinical application. Each volunteer was then subjected, one at a time, to each of 9 load types. See figure 3 for description. The load types are divided into three groups: 1) loads applied through the halo to the vest, 2) loads applied to the vest itself, and 3) loads applied by the subject to the vest. The first group was applied to simulate the loading which the head might apply to the vest, through the halo and upright linkage, via the physiological motions of flexion-extension, and lateral bend. Loads were applied to the halo, unattached to subjects head, with a load cell and resulting vest rotation on thorax monitored by photogrammetry. The load application sites, arrows A and B, and photographic markers are seen in figure 3. Loads were applied using a hand held load cell ranging from 0-40 N, while in 5 N increments load and photogrammetric data were simultaneously sampled by a microcomputer. Evaluation of vest grip on thorax was quantified by the second group of loadings and measured displacements at points of uniaxial translation of vest on thorax. Sagittal plane anterior/posterior load application at the level of sternal notch produced uniaxial translation, while coronal plane lateral loading at the level of the acromion produced uniaxial lateral translation. The load application and measurement sites, arrows C and D, are seen in figure 3. Loads were applied using a



hand held load cell ranging from 0-40 N, while in increments of 5 N load and displacement, using a linear potentiometer, were sampled. The third group of loadings were applied by the subject to the vest. This evaluated displacements a subject may require a vest to move through, by moving the shoulder girdle relative to the trunk, and transmitting loads to, if attached, the halo and across cervical spine. Each subject moved scapula maximally anterior, posterior, or cephalad, with resulting displacements monitored. These loadings are seen as arrows E in figure 3. Displacements were monitored, with a linear potentiometer positioned at sternal notch for anterior/posterior movement of scapulae, and for maximal elevation of scapulae displacement was monitored at the vertex with a linear scale.

For the first and second loading groups a load deflection relationship was developed and a linear regression performed. All proved to be highly linear, lowest was a correlation coefficient of .95. The slope of each regression equation served as quantification of vest fit. The larger the slope in magnitude the better vest fit. The third group of loadings used an average maximum displacement for each loading as a quantification of vest fit (the larger average displacement represents larger vest thorax movement).

### RESULTS

For each of the 9 loading types, for each subject, a) the data for the 8 vests were normalized by an arbitrarily chosen Index vest (Ace), b) the mean of the normalized values was calculated across the subjects and a rank ordering of the vests was performed. An overall score was defined as the mean of the rank order number across the 9 load types. The vest scores fell into three groups: high mobility (DePuy = 6.88, J.M.S. = 5.67), intermediate mobility (PMT = 4.56, Ace = 4.44, Camp = 4.22, Pope = 4.22, Bremer = 4.11), and low mobility (experimental = 1.89). Thus, the experimental vest has roughly twice as good a grip on the thorax as the intermediate mobility vests and three times as good a grip as the high mobility vests. See Table 1.

### CONCLUSIONS

The vest-thorax interface problems, for current commercially available vests, have been defined. The attachment sites used which are moveable relative to the rest of thorax (shoulder girdle, pectoralis muscle, and epigastrium) have proven to be poor "attachment sites". An experimental vest has been designed and developed and its improved fit on thorax comparatively assessed. This improvement has been accomplished in the following manner: 1) larger contact areas over those trunk surface sites which actually are part of thorax itself and thus by definition cannot move relative to the thorax. These sites are sternum, posterior aspect of the interscapular region, and lateral aspect of the trunk, along the mid-axillary line. 2) avoiding contact with sites which are moveable relative to the thorax. The rank ordering of the mean-normalized vest-thorax mobility has shown the experimental design to have improved attachment to thorax (1.9 vs. 4.1 6.9).

### References

1. Koch, R.A., Nickel, V.L., (1978) The Halo Vest An Evaluation of Motion and Forces Across the Neck. Spine 3(2):103-07.
2. Nickel, V.L., Perry, J., (1968) The Halo A Spinal Skeletal Traction Device. J. Bone Joint Surg. 50A:1400-1409.

FIGURE 1  
ANTERIOR VIEW

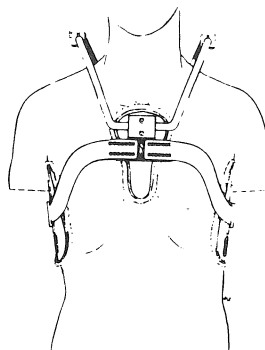


FIGURE 2  
POSTERIOR VIEW

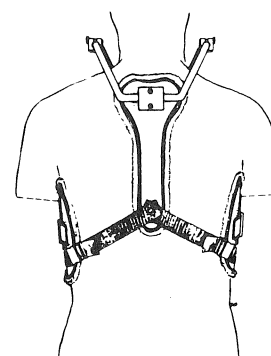


FIGURE 3

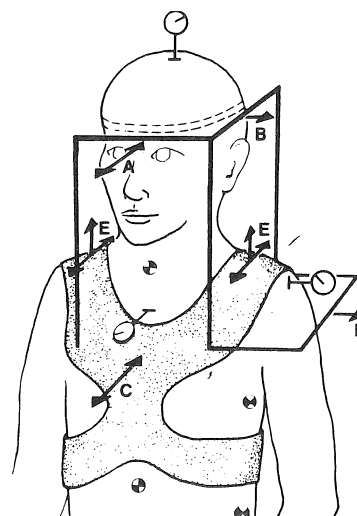


TABLE 1

RANK ORDERING OF MEAN NORMALIZED  
VEST-THORAX MOBILITY

VEST	A (ant)	A (post)	B	C (ant)	C (post)	D	E (ant)	E (post)	E (ceph)	SCORE
DePuy	8	7	7	4	6	7	8	8	7	6.88
JMS	5	4	6	5	8	8	4	3	8	5.67
PMT	6	3	8	7	5	6	2	2	2	4.56
Ace	3	6	4	3	2	5	6	6	5	4.44
Camp	2	2	2	6	4	2	7	7	6	4.22
Pope	4	8	1	8	1	3	5	5	3	4.22
Bremer	7	5	5	2	3	4	3	4	4	4.11
Exper.	1	1	3	1	7	1	1	1	1	1.89

# THE INFLUENCE OF PHYSICAL ACTIVITY ON BONE DENSITY

R.T. Whalen†, D.R. Carter‡, C.R. Steele\*

†Veterans Administration Medical Center, RR&D, Palo Alto, CA

‡Department of Mechanical Engineering, Design Division, Stanford University, Stanford, CA

\*Department of Mechanical Engineering, Applied Mechanics, Stanford University, Stanford, CA

## INTRODUCTION

Skeletal mass and bone density measurements of selected bone sites are often used to assess the condition of the skeletal system. The variety of body sizes and types, and physical activity levels makes the interpretation of these results difficult. Proper correlation between these variables and skeletal response is needed to identify the forces of remodeling and guide clinicians in the development of programs to prevent, reverse, or slow the loss of bone with ageing.

The overwhelming body of clinical and experimental evidence suggests that activity level and certain types of exercise are the dominant factors in bone metabolism. Athletic activities which involve significant increases in joint loads increase bone mass in the heavily loaded bones. The humerus of the playing arm of 84 world class tennis players showed pronounced hypertrophy [1]. Cross country runners were found to have a 20 % greater calcaneal density than a non-exercising control group [2]. On the opposite end of the loading spectrum, removal or reduction in the level of physical activity through immobilization or bed rest has consistently resulted in severe bone resorption.

In an earlier work we developed a mathematical expression for bone apparent density,  $\rho$ , as a function of a condensed daily loading history which retained the number of cycles and maximum effective stress per cycle as the two essential parameters. In this work we apply our formulation to the calcaneus for a range of lifestyles, differing in activity level, chosen to encompass a wide spectrum of the population. Expected bone densities for each activity level were calculated and compared to the literature. Our results indicate that bone density depends far more on daily stress levels than cycles of load per day.

## REVIEW AND THEORY

In an accompanying paper, we relate equilibrium bone apparent density,  $\rho$ , to a daily loading history as

$$\rho(x) \propto \left[ \sum_{i=1}^n n_i (\sigma_i)^m \right]_{\text{per day}}^{\frac{1}{2m}} \quad (1)$$

where  $\sigma_i$  is an effective stress measure which can be related to the ultimate failure stress. The value of  $m$  is a weighting factor for the relative importance between the effective stress per cycle and the number of load cycles. To calculate the relative density with respect to a reference, or 'normal' density, equation (1) becomes

$$\frac{\rho^l}{\rho^{\text{norm}}} = \left[ \frac{\sum_{j=1}^k n_j (\sigma_j)^m}{\sum_{i=1}^n n_i (\sigma_i)^m} \right]_{\text{per day}}^{\frac{1}{2m}} \quad (2)$$

Simplification of equations (1) and (2) occurs when applied to the calcaneus. All significant calcaneal boundary conditions are related to the ground reaction force. The orientation of the calcaneus with respect to the tibia and foot is relatively unaffected by activity, particularly at the point of maximum exertion, or near toe-off. Gait analysis studies for a wide range of velocities have shown that horizontal ground reaction forces are at most only 10-15 % of the vertical force [3,4,5]. More importantly, the peak force levels for each component do not occur at the same point in the gait cycle. Therefore, the horizontal forces do not contribute significantly to the maximum resultant force. Without losing significant accuracy, we retain only the vertical reaction force. The internal stress field now scales linearly with this force, and  $\rho$  can be related directly to the external ground reaction force,  $Gz$ , as

$$\frac{\rho^l}{\rho^{\text{norm}}} = \left[ \frac{\sum_{j=1}^k n_j (Gz_j)^m}{\sum_{i=1}^n n_i (Gz_i)^m} \right]_{\text{per day}}^{\frac{1}{2m}} \quad (3)$$

For this unique case, since  $\rho$  is not a function of the internal stress field, apparent density scales linearly and the spatial distribution of bone mass is constant. Other bones, with only one dominant loading orientation, would be expected to approximate this condition. It is interesting that trabecular orientation and distribution of apparent density in the proximal femora are similar among bones.

## METHODOLOGY

All loads on the calcaneus are assumed to result from walking/jogging/running. Dynamic load factors for other activities normally encountered, such as stair climbing, are close to 1.0. Their contribution to the loading history is not considered separately since one cycle for each of these activities is approximately equivalent to a single walking load cycle. Values for  $Gz$  versus gait velocity were gathered from the literature [3,4,5,6,7]. Table I lists a discrete set of gait velocities chosen to span the population. Table II, constructed from Table I, lists a sample set of hypothetical occupational activity levels again chosen to encompass the spectrum of lifestyle activity levels. Expected relative bone apparent densities with respect to the 'normal activity' lifestyle were computed for each activity level using Tables I and II and equation (3).

## RESULTS AND DISCUSSION

Apparent densities for the different lifestyles were plotted as a continuous function of the stress exponent,  $m$ . For  $m$  values below 2, bone density is overly dependent on the number of cycles experienced during the day. Beyond  $m=3$ , a clear pattern of relative apparent densities emerges among the

different lifestyles. As  $m$  increases to infinity, the bone apparent density converges to the value predicted from the single load cycle with the largest ground reaction force. Clearly, clinical observation does not agree with either of these extremes. Based on the observed range of bone densities,  $m$  must lie between 4 and 18. Interestingly, the value of  $m$  determined from *in vitro* fatigue testing of bone for different loading conditions ranges from 5 to 18. Recent compression fatigue tests yielded an  $m$  value of 12. We have chosen an  $m$  value equal to 12 to correlate the various studies in the literature.

To directly apply this model to running and exercise studies in the literature requires a knowledge of the individuals activity level and ground reaction forces developed during exercise. Since these are rarely given completely, we have had to make certain reasonable assumptions regarding jogging/running speeds and distance run. Given this, our model consistently predicted the increased bone density measured for cross-country runners [2,8].

### CONCLUSION

A method for predicting equilibrium bone apparent density has been developed and successfully applied to a specific bone site. Cellular mechanisms related to fatigue microdamage are strongly implicated as providing the remodeling stimulus. The bone apparent density is a continuous, monotonic function of the daily loading history. The technique can be applied to any bone to predict expected densities for various activity levels and exercises.

These results have clinical relevance, since a framework is provided for the relation of bone density and various physical activity levels. We suggest that prevention of bone loss with age may take the form of exercises tailored to promote and maintain high bone density throughout life. Stated briefly, high, cyclic loads appear to be the most effective means of increasing bone density. Jogging, which does not develop high ground reaction forces, is not very effective when compared to the time spent exercising. For example, we predict that, for a non-exercising individual, initiating a jogging program of 4 miles per day will increase calcaneal density by only 5 %. The benefit to the axial skeleton and upper limbs would be even less.

### References:

1. Jones, H., et al., *J. Bone Jt. Surg.*, **59-A**:204-208, 1977.
2. Dalen, N., et al., *Acta Ortho. Scand.*, **13**:383-390, 1980.
3. Alexander, N.R., et al., *J. Biomech.*, **13**:383-390, 1980.
4. Cavanaugh, P., et al., *J. Biomech.*, **13**:397-406, 1980.
5. Andriacchi, T.P., et al., *J. Biomech.*, **10**:261-268, 1977.
6. Rohle, H., et al., *J. Biomech.*, **17**:409-424, 1984.
7. Winter, D., et al., *J. Biomech.*, **16**:91-97, 1983.
8. Williams, et al., *Med. Sci. Sports. Exer.*, **16** #3:223-227, 1984.

Supported by NASA grant NAG 2-348, and the Veterans Administration.

ACTIVITY	GAIT VELOCITY (m/sec)	CYCLES PER MINUTE	GROUND REACTION Gz (BW)
Slow Walking	0.50	28	1.00
Normal Walking	1.25	48	1.15
Fast Walking	2.00	69	1.30
Slow Jogging	2.72	87	1.70
Distance Running	4.50	137	2.75

**Table I:** This table was constructed from gait analysis data taken from the literature. For walking, ground reaction forces increase slowly, but linearly with gait velocity. At the transition between walking and running ( $\approx 2.5$  m/sec), ground reaction forces increase more rapidly with increasing gait velocity.

OCCUPATIONAL ACTIVITY LEVEL	HOURS SPENT PER DAY			
	Slow Walking	Normal Walking	Fast Walking	Exercising
Sedentary	4	----	----	----
Sedentary + Exercise	4	----	----	.67*
Normal	----	4	4	----
Active	----	4	8	----
Active + Exercise	----	4	8	.67*
Athlete	----	4	4	.75**

\* 6.5 Km at a 2.7 m/sec jogging pace.

\*\* 12 Km at a 4.5 m/sec running pace.

**Table II:** The above set of hypothetical lifestyles was constructed to encompass a wide range physical activity. For example, a person with a 'sedentary occupational' level might be someone with a desk job and minimal additional outside activity. An 'active' person might be a waiter/waitress who is standing or walking much of the day.

# REGIONAL VARIATIONS IN THE COMPRESSIVE PROPERTIES OF HUMAN LUMBAR VERTEBRAL TRABECULAE: INFLUENCE OF TISSUE PHYSICAL CHARACTERISTICS

T.S. Keller  
Biomechanics Lab  
V.A. Medical Ctr.  
Nashville, TN 37203

T.H. Hansson  
Dept. of Orthopaedic Surgery  
Sahlgren Hospital  
Gothenburg, Sweden S413 45

M.M. Panjabi  
Yale Medical School  
New Haven, CT 06510

D.M. Spengler  
Dept. of Orthopaedics and Rehab.  
Vanderbilt University MCN  
Nashville, TN 37232

## INTRODUCTION

In osteoporosis and during aging, the earliest and most prevalent changes occur in the cancellous bone, where the trabeculae become thin and sparse (1). Later clinical manifestations may include compressed vertebral bodies, dorsal kyphosis, and chronic back pain. The trabeculae appear, therefore, to be the weakest component of the lumbar vertebrae in compression. The objective of this investigation was to examine the compressive properties of human lumbar vertebral trabeculae (LVT) on the basis of anatomical origin, bone density and intervertebral disk properties. Cubical specimens of LVT were prepared from 24 precisely determined anatomical regions of lumbar vertebrae and oriented cephalad during compressive testing. The significant findings were increased strength and stiffness of bone overlying the disk nucleus in comparison to bone adjacent to the disk annulus, and decreased strength and stiffness with decreasing bone density. The latter was proportional to strength to the one-half power, indicating that a decrease in bone density by 1/2 would result in a decrease in bone strength by 1/4. Although not significant, bone strength and stiffness also tended to increase with decreasing degree of disk degeneration and increasing segment level. These findings suggest an interdependence of disk and LVT properties and provide a means to clinically estimate vertebral strength from knowledge of *in vivo* measures of bone density.

## REVIEW AND THEORY

The compressive properties of LVT have been closely correlated with tissue physical characteristics such as porosity, apparent density, ash density (2,3,4,5,6) and more recently dual photon absorptiometry (DPA) determined bone mineral content BMC (7), the latter an *in vivo* measure of bone density. Changes in trabecular bone mechanical properties as a function of density are best represented by power law ( $y=ax^b$ ) relationships where the exponent  $b$  is approximately equal to 2 (2,3).

Less well understood is the correlation between the mechanical properties of LVT and those of the intervertebral disk. Studies by Lin et al. (8) indicate that the compressive mechanical properties of the disk tend to decrease as a function of increasing degree of disk degeneration. Since disk degeneration is often associated with or accompanied by changes in the LVT, we hypothesized that an interdependency of LVT bone strength and disk properties may exist. Furthermore, the material properties of LVT may reflect the tissue characteristics of the intervertebral disk.

## METHODOLOGY

Lumbar spines were obtained fresh from three human subjects with a mean age of 77.7 (S.D. 6.5)

years. DPA was used to determine the BMC of each segment ( $L_1-L_4$ ) such that the measurements would reflect conditions that simulated *in vivo* determinations of BMC. The spines were then sectioned into 12 segments and the exposed superior and inferior disks were graded according to their degree of macroscopic disk degeneration on a scale from I to IV (9).

Two hundred and thirty-one cubical specimens of LVT were prepared from 24 precisely determined anatomical regions of the 12 lumbar vertebrae. Following removal of the superior and inferior endplates, a precision band saw and specially designed cutting jig were used to cut one centimeter square by one centimeter thick cubes of trabecular bone. In this fashion, a 3x4x2 centimeter region of the vertebral bodies was sectioned into 24 cubes (12 cranial and 12 caudal). Some lumbar vertebrae were too small to obtain uniformly cubical specimens throughout the 3x4x2 region and were discarded. The cranial and caudal regions were identified as shown in Fig. 1.

Testing was performed in uniaxial compression on an Alvetron T-2000 universal testing machine at a constant cross-head speed of 5 mm per minute with the specimens oriented cephalad with respect to the axis of the applied load and with marrow *in situ*. Load versus deformation was recorded until a decrease in the load was noted, at which time the load was removed.

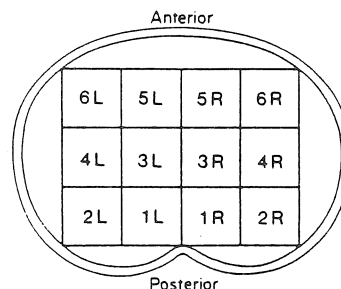


Fig. 1. Schematic diagram of the regions from which the LVT specimens were obtained, and the alpha-numerical identification of each region.

## RESULTS AND DISCUSSION

Figure 2 illustrates the log-log or allometric relationship obtained between compressive modulus  $E$  and apparent density  $\rho$ . Linear correlations did not yield as good a fit as determined by the correlation coefficient and the F-test. Similar allometric relationships were found between compressive strength  $\sigma_u$ , yield strength  $\sigma_y$ , and stiffness  $S$  and both apparent density (Table I) and BMC (Table II). Note that the power coefficient or exponent  $b$  was approximately equal to 2 for all the parameters as a function of density ( $\rho$  and BMC).

Figure 3 illustrates the relationships between density normalized compressive modulus  $nE$  and

specimen anatomical position. In general, the modulus of the center regions (1 and 3) was significantly ( $P < 0.05$ ) greater than the outer regions (2,4-6). The former region may be analogous to the cancellous bone overlying the disk nucleus, while the outer region may be more representative of the properties of the disk annulus. Similar results were obtained for the parameters  $n\sigma_u$ ,  $n\sigma_y$  and  $nS$ , indicating that the cancellous bone overlying the nucleus is stronger and stiffer than cancellous bone overlying the annulus. No significant differences between cranial and caudal parameters (mechanical and densitometric) were found, although the trend was an increase with increasing segment level. A trend for decreasing strength and stiffness with increasing degree of disk degeneration was also noted, but was not statistically significant.

TABLE I. Allometric Relationships for Log Parameter as a Function of Log Apparent Density.

Parameter	Intercept	Exponent (b)	Correlation Coefficient
E (MPa)	2.85	1.91	0.83
$\sigma_u$ (MPa)	1.85	2.21	0.86
$\sigma_y$ (MPa)	1.93	2.24	0.87
S (N/mm)	3.72	1.89	0.84

TABLE II. Allometric Relationships for Log Parameter as a Function of Log BMC.

Parameter	Intercept	Exponent (b)	Correlation Coefficient
E (MPa)	0.36	2.13	0.91
$\sigma_u$ (MPa)	-0.89	2.25	0.87
$\sigma_y$ (MPa)	-0.94	2.24	0.87
S (N/mm)	1.30	2.00	0.90

#### CONCLUSIONS

Lumbar vertebral trabecular bone strength and stiffness were found to increase with increasing density, the latter proportional to strength and stiffness to the one-half power, indicating that decrease in density by 1/2 would result in a decrease in strength and stiffness on the order of 1/4. Regional variations within each segment were found, the most prevalent differences occurring in regions overlying the disk nucleus in comparison to regions overlying the disk annulus. Slight differences in strength and stiffness were found as a function of segment level and degree of disk degeneration, but were not statistically significant. These findings suggest an interdependence of disk and LVT properties and provide a means to clinically estimate vertebral strength from knowledge of *in vivo* measures of density.

#### References

1. Salter, R.B. Williams and Wilkins, p. 152-153, 1970.
2. Bell, G.H., et al. Calcif. Tis. Res. 1:75-86, 1967.
3. Carter, D.R., et al. JBJS 59A:954-962, 1977.
4. Galante, J. Spine 5:147-153, 1981.
5. Lindahl, O. Acta Orthop. Scand. 47:11-19, 1976.
6. Weaver, J.K., et al. JBJS 48A:289-299, 1966.
7. Hansson, T.H., et al. Spine 5:147-153, 1981.

8. Lin, H.S., et al. J. Biomechan. 11:1-14, 1978.
9. Nachemson, A. Acta Orthop. Scand. (Suppl.) 43:1-104, 1960.

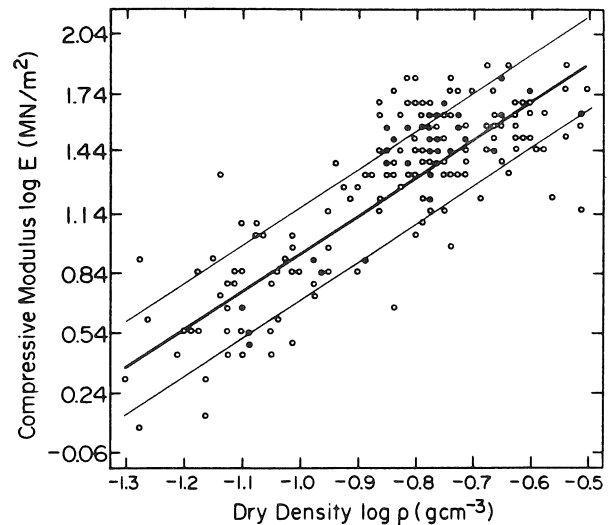


Fig. 2. Log compressive modulus versus log specimen apparent density. The open circles represent one data point, closed circles represent two or more data points. Best fit linear regression line shown (see Table I).

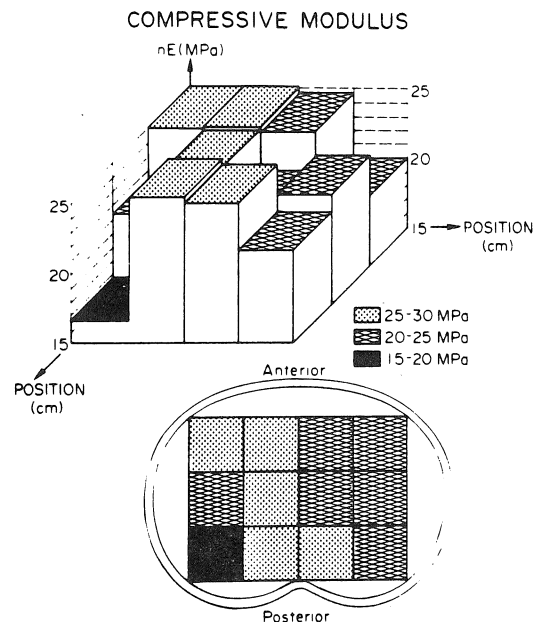


Fig. 3. Mean normalized compressive modulus as a function of anatomical position. The data have been normalized to the mean density ( $\bar{\rho} = 0.15$  g/cm³) for the specimens of this study. Three stress ranges have also been qualitatively assigned and the data shown in both 2-D and 3-D perspectives.

MORPHOLOGICAL AND MECHANICAL  
RESPONSES OF LONG BONE TO WEIGHTLESSNESS

S. Shaw, R. Zernicke, A. Vailas, & R. Grindeland\*  
Department of Kinesiology, UCLA, Los Angeles, CA 90024 and  
\*NASA-Ames Research Center, Moffett Field, CA 94035

INTRODUCTION

Exposure to a weightless environment and reduced loadbearing on bones during spaceflight are associated with a rapid and progressive loss of calcium from the skeleton (1). The etiology of bone changes resulting from spaceflight, however, has not been fully explained, and researchers continue to investigate the mechanisms which may mediate the response of bone to weightlessness. Studies, generally, have not reported correlated biomechanical and morphological results on the same bones that were exposed to spaceflight conditions. The present study does this by comparing these characteristics in humeri and tibiae from three groups of young rats: young controls (60 days old), age-matched simulated controls (67 days old), and age-matched spaceflight rats (67 days old). Significant alterations were found among long bone mechanical properties and morphology as a result of weightlessness.

REVIEW AND THEORY

Previous data from rapidly growing rats that had flown in space indicate that growth and maturation were delayed by weightlessness. Morey and Baylink (2) correlated decreased periosteal bone formation with the appearance of histological arrest lines in the diaphysis of appendicular bones. Subsequently, Morey (3) localized the primary defect in bone turnover during weightlessness to the process of calcification. Roberts et al. (4) have observed a pre-osteoblast depletion with an increase in less differentiated cells which may indicate not only a lack of differentiation, but also a lack of proliferation or enhanced cell death as well. Jee et al. (5) also demonstrate a decline in osteoblast population with no change in osteoclast population, while Simmons et al. (6) suggest that spaceflight causes a delay in the normal maturation of bone mineral content and organic matrix.

In contrast to periosteal appositional processes, endosteal resorption seems little affected by weightlessness. Jee et al. (5) report a decrease in trabecular bone mass and an increase in marrow fat content, but suggest that an unchanged osteoclast population coupled with a lack of change in medullary canal width in the tibial diaphysis (2) indicates that bone resorption is unaltered during spaceflight (7). The torsional stiffness, strength, and energy to failure data from rats flown 18.5 days in space indicate that normal increases in these mechanical properties fail to occur in sedentary flight animals, while in-flight centrifugation at 1 g promotes a more nearly normal development of these properties (8).

METHODS

A pre-flight, control group (n=6), a simulated control group (n=6), and a spaceflight group (n=6)

of rats were used. The pre-flight laboratory controls were sacrificed at age 60 days, whereas the remaining two groups were sacrificed (67 days) at the end of a 7-day flight of the space shuttle. The simulated control group was maintained for the 7 days duration of the flight in isolated, caged conditions which simulated the cabin of the space shuttle. Immediately after the landing of the shuttle, the flight animals and the simulated controls were also sacrificed. Limbs were immediately removed from the sacrificed animals and frozen in hermetically sealed containers. On the day of mechanical testing, the limbs were thawed, and bones were dissected and equilibrated in a buffered solution (50 mM potassium phosphate,  $37 \pm 1^\circ \text{C}$ , pH 7.4). Bone lengths were measured with a micrometer. Three-point bending to failure tests (Instron 1122) were done as each bone was maintained in a test-chamber circulating bath of buffered solution (9). Load-deflection curves were digitized to determine force, deformation and energy at yield, maximum, and fracture loads, bending stiffness, tensile yield stress (determined at proportional limit), and non-linear displacement (bone deflection between proportional limit and maximum load).

Following the failure test, a 1 mm thick cross section was milled (EMCO Unimat 3) from the mid-diaphyseal region of each bone to determine morphological characteristics of each specimen. The 1 mm cross sections were photographed with a 35 mm camera (Olympus OM2S, 50 mm flat-field lens, Asanuma auto bellows), color slides were rear-screen projected, and cross-sectional images were digitized (Numonics 1220) via microcomputer to determine bone morphology and geometry using a modified version of SLICE (10).

Univariate analyses of variance with post hoc comparisons were used to detect differences among group means. A significance level of  $p = 0.05$  was accepted for all statistical tests.

RESULTS AND DISCUSSION

Those morphological and mechanical properties which showed significant differences among the pre-flight control, simulated control, and spaceflight rats for tibiae are given in Table 1 and for humeri are given in Table 2. In these rapidly-growing rats tibial and humeral longitudinal growth rates were suppressed as a result of weightlessness. For both bones, the 67-day simulated controls had significantly longer bones than their age-matched flight rats. Further, the tibiae and humeri for both the simulated and the flight groups were significantly longer than the 60 days old pre-flight control group bones.

In general, the effects of weightlessness appeared to be more pronounced in the tibia than in the humerus, as was apparent from the number of significant changes in properties shown in Table 1 versus Table 2. The tibia is stiffer and stronger than the

humerus, nevertheless, both bones showed many of the same relative changes in structural properties as a result of weightlessness. The bending stiffnesses of tibiae and humeri of both the pre-flight and flight groups were significantly less than the simulated group, but no statistical differences were found between the stiffnesses of tibiae and humeri of the 60-day pre-flight group and the 67-day flight group. The loads at yield point (proportional limit), maximum, and fracture for both tibia and humerus were significantly greater in the simulated group than in either the pre-flight controls or the flight group. Weightlessness significantly affected the amount of non-linear displacement of the tibia. Tibiae of the flight rats showed significantly smaller non-linear deformations between the yield point and the maximum load than either the pre-flight group or simulated groups, which displayed no difference in their amounts of non-linear deformations.

The cross-sectional morphologies of the tibiae and humeri of the different groups did not, generally, show any statistical differences among groups. Mid-diaphyseal area moments of inertia about the bending and non-bending axes, endosteal and periosteal circumferences, medullary areas, anterior-posterior and medial-lateral cortical and medullary diameters, and regional (anterior, posterior, medial, and lateral) cortical thicknesses all did not reveal any statistical differences among any of the three groups.

#### CONCLUSIONS

Our data indicated that longitudinal growth rates of the tibia and humerus were suppressed as a result of exposure to a weightless environment. The tibial mechanical properties appeared to be affected to a greater degree than those of the humerus. However, the bending stiffnesses of tibiae and humeri of both the pre-flight and flight groups were significantly less than the simulated group, but no statistical differences were found between the stiffnesses of tibiae and humeri of the younger pre-flight group and the one-week older flight group. The loads at yield point, maximum, and fracture for both tibia and humerus were significantly greater in the simulated group than in either the younger pre-flight controls or the flight group.

#### References

1. Wronsky, T.J., et al. Med. Sci. Sports Exerc. 15:410-414, 1983.
2. Morey, E., et al. Science 201:1138-1141, 1978.
3. Morey, E. BioScience 29:168-172, 1979.
4. Roberts, B., et al. Physiologist 24(6):Suppl. 75-76, 1981.
5. Jee, A., et al. Am. J. Physiol. 244:R310-R314, 1983.
6. Simmons, J. et al. Physiologist 23:Suppl. 87-90, 1980.
7. Wronsky, T., et al. Am. J. Physiol. 244:R305-R309, 1983.
8. Spengler, D., et al. Proc. Soc. Exp. Biol. Med. 174:224-228, 1983.
9. Matsuda, J.J., et al. J. Appl. Physiol. in press.
10. Nagurka, M.L., et al. J. Biomech. 13:59-64, 1980.

Table 1

Tibia: Morphology and Mechanical Properties

VARIABLES	PRE-FLIGHT	SIMULATED	FLIGHT
Length	33.0 (0.4)	36.6 (0.4) <sup>a</sup>	35.5 (0.6) <sup>c</sup>
Cortical Area	2.4 (0.1)	2.9 (0.3)	3.1 (0.2) <sup>a</sup>
Bending Stiff.	8.2 (0.7)	11.3 (1.0) <sup>a</sup>	9.3 (1.3) <sup>b</sup>
Disp. Yield	0.2 (0.0)	0.2 (0.0)	0.3 (0.0) <sup>c</sup>
Load Yield	36.1 (2.7)	48.4 (4.7) <sup>a</sup>	49.7 (1.7) <sup>a</sup>
Non-Lin.Disp.	0.4 (0.1)	0.3 (0.1)	0.2 (0.1) <sup>c</sup>
Load Maximum	49.4 (2.6)	67.3 (4.3) <sup>a</sup>	60.0 (2.7) <sup>c</sup>
Disp. Max.Load	0.6 (0.1)	0.5 (0.1)	0.4 (0.1) <sup>a</sup>
Load Failure	38.5 (15.4)	60.6 (8.0) <sup>a</sup>	53.0 (11.0)

Values are means (s.d.)

<sup>a</sup>significantly different from pre-flight (p = 0.05)

<sup>b</sup>significantly different from simulated (p = 0.05)

<sup>c</sup>significantly different from both pre-flight and simulated groups (p = 0.05)

#### Units of measurement:

Length = mm

Cortical Area = mm<sup>2</sup>

Bending Stiffness = kN mm<sup>-1</sup>

Displacement at Yield Point = mm

Load at Yield Point = N

Non-Linear Displacement = mm

Maximum Load = N

Load at Failure = N

Table 2

Humerus: Morphology and Mechanical Properties

VARIABLES	PRE-FLIGHT	SIMULATED	FLIGHT
Length	22.6 (0.2)	25.0 (0.3) <sup>a</sup>	24.1 (0.3) <sup>c</sup>
Bending Stiff.	4.6 (1.2)	7.4 (0.6) <sup>a</sup>	4.8 (1.0) <sup>b</sup>
Load Yield	23.9 (1.1)	35.7 (7.0) <sup>a</sup>	23.3 (6.9) <sup>b</sup>
Load Maximum	33.0 (4.4)	48.7 (4.3) <sup>a</sup>	35.3 (5.8) <sup>b</sup>
Load Failure	32.2 (3.4)	47.9 (4.5) <sup>a</sup>	35.2 (5.8) <sup>b</sup>

Values are means (s.d.)

<sup>a</sup>significantly different from pre-flight (p = 0.5)

<sup>b</sup>significantly different from simulated (p = 0.5)

<sup>c</sup>significantly different from both pre-flight and simulated groups (p = 0.5)

#### Units of measurement:

Length = mm

Bending Stiffness = kN mm<sup>-1</sup>

Load at Yield = N

Maximum Load = N

Load at Failure = N

## MECHANICAL PROPERTIES OF BONE ALLOGRAFTS

K. Cowling, J. Mukherjee, R. W. Soutas-Little, R. Hubbard  
Department of Biomechanics  
Michigan State University  
East Lansing, Michigan 48824

J. Forsell  
Michigan Tissue Bank  
Edward Sparrow Hospital  
P.O. Box 30480  
Lansing, Michigan 48909

### INTRODUCTION

The study of the mechanical properties of cancellous bone is of great clinical significance to the use of bone allografts in orthopedic surgery (1-9). Of particular interest is the effect of storage procedures on these properties (5, 10, 11). Freeze-drying is one common method of bone preservation used by tissue preparers as once dried and sterilized, the allografts can be stored for a long time if properly packaged. This process requires rehydration before use of the tissue and, at present, the effect of rehydration time on the mechanical properties has not been studied. The optimum rehydration time may depend upon bone density, considering the relationship between density and strength.

The effect of sterilization procedure is another variable in the strength of the allografts. Sterilization may vary from boiling or autoclaving to chemical sterilization to use of radiation.

This pilot program in cooperation with the Michigan Tissue Bank at Sparrow Hospital in Lansing, Michigan, considered the Cloward plugs used in cervical spine fusions. Plugs were taken from the condyles of human donors and differences between fresh, frozen, and freeze-dried with different rehydration times were analyzed. A parallel study considered irradiated and non-irradiated allografts. Results of these studies will be of interest to tissue banks and orthopedic surgeons as well as researchers in tissue biomechanics.

### REVIEW AND THEORY

Cloward plugs of 1.4 cm diameter and approximately 2.0 cm in length were tested in compression perpendicular to their long axis. Use of the Flamant solution from elasticity (12) shows that the stresses in the cylinder should be inversely proportional to diameter and length.

$$\sigma \approx \frac{P}{DL}$$

where P is the diametrically applied compressive load, D is cylinder diameter and L is the length of the cylinder. Load deformation curves may be used to determine peak load and 2% offset stiffness.

### METHODOLOGY

Six Cloward 1.4 cm diameter plugs were taken from both the left and right femoral condyles of human donors. Sample locations were as shown in Figure 1. Each sample was tested after a predetermined treatment schedule. The treatment pattern included fresh samples, frozen and freeze-dried with rehydration times of 0, 30 minutes, 2 hrs., 8 hrs., and 24 hrs. In addition, the parallel study of freeze-drying with two-hour rehydration comparing irradiated and non-irradiated samples has been initiated. Samples were tested in an Instron testing machine using plexiglass fixtures cut with a 1.4 cm half circle to ensure proper loading. All samples

were compressed diametrically at a 1.6% per second strain rate to a 33% strain and the load recorded. Volume measurements were taken and dry ash density will be determined later.

### RESULTS AND DISCUSSION

Figure 2 shows typical output curves for samples tested after different preparation procedures. In general, samples taken from the posterior, sites 1 and 4, showed higher peak loads than those from 3 and 6. Preliminary results of the effects of irradiation are shown in Figure 3. The irradiated samples were subjected to cobalt 60 gamma radiation at a flux 5 for 776 minutes for an approximate dosage of 2 megarads. All samples were first freeze-dried and rehydrated for 2 hours prior to testing. Samples were grouped such that six were taken from each limb on the same donor and one group irradiated, and the second group used as a control.

Figure 2 shows a minimal dependency of stiffness on the preparation procedure but a strong dependency of peak load on rehydration time. Freeze-dried samples approached the properties of fresh bone with up to 18 hours of rehydration in saline solution. Continued rehydration produced a consistent loss in mechanical properties with significant loss in strength after 24 hours' rehydration. Samples with less than 2 hours rehydration time were weaker and failed in a brittle fracture mode.

Figure 3 shows insignificant variation in peak load or stiffness after irradiation although there was an increase in the scatter of the data for the irradiated samples.

This study will be broadened to consider the dependency of the mechanical properties on donor sex, age and anatomical location of bone allograft, as well as rehydration and irradiation. Preliminary results show that with proper rehydration, bone tissue transplants may be freeze-dried and stored and maintain properties of fresh bone.

### References

1. Carter, D. E., et al. J. Bone and Joint Surg. 59-A:954-962, 1977.
2. Chalmers, J., et al. J. Bone and Joint Surg. 48-A:299-308, 1966.
3. Galante, J., et al. Tissue Res. 5:236-246, 1970.
4. Gibson, L. J. Biomech. 18(5):317-328, 1985.
5. Lindahl, O. Acta Orthop. Scan. 47:11-19, 1976.
6. Pelker, R. R., et al. Clin. Orthop. 174:54-57, 1983.
7. Reilly, D. T., et al. J. Biomech. 7:271-275, 1974.
8. Townsend, P. R., et al. J. Biomech. 8:199-201, 1975.
9. Weaver, J. K., et al. J. Bone and Joint Surg. 48-A:289-299, 1966.
10. Evanoff, J. AORN Journ. 37(5): 972-980, 1983.
11. Jonck, L. M. S.A. Med. Journ. 12:428-430, 1981.
12. Little, R. W. Elasticity, Prentice-Hall, Inc.: 188-189, 1973.



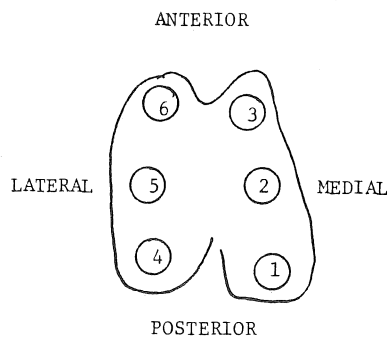


Figure 1. View of distal end of right femur with sample locations.

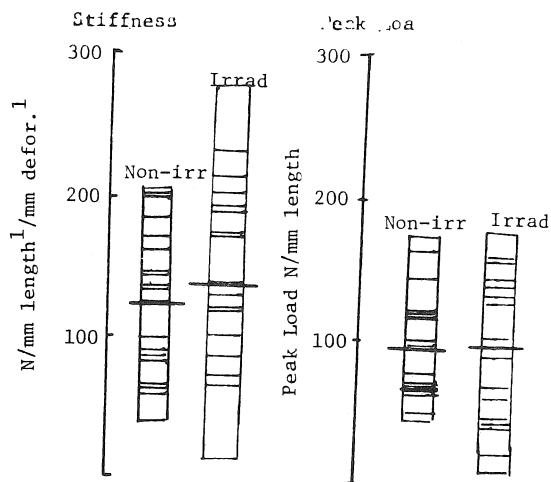


Figure 3. Stiffness and peak loads of non-irradiated and irradiated samples.

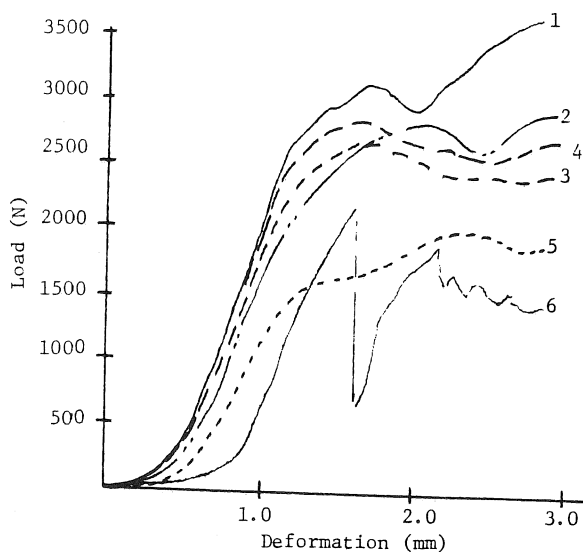


Figure 2. Load-deformation response of fresh (1), freeze-dried-2 hr. rehydration (2); f-d with 12-hr. rehyd. (3), f-d with 18-hr. rehyd. (4); f-d with 24-hr. rehyd. (5); and f-d with no rehydration (6).

# THE VISCOPLASTIC BEHAVIOR OF CORTICAL BONE

M. Fondrk, E. Bahniuk, D. T. Davy, C. Michaels, P. Pallone  
Orthopaedic Engineering Laboratory  
Case Western Reserve University  
Cleveland, Ohio 44106

## INTRODUCTION

The absence of complete constitutive equations has often been an obstacle to understanding biological structures in an engineering context. This is the case for the post yield behavior of cortical bone, where complete stress-strain relations have not been developed. Our study addresses the subject by performing a test sequence on human and bovine cortical bone samples. The test enables total strain to be decomposed into elastic, anelastic, and plastic components. The results indicate that a well defined stress threshold exists; above which rate effects dominate material response and below which behavior is primarily viscoelastic, with rate effects playing only a secondary role. The stress threshold represents a creep limit, i.e., failure will eventually occur if loads are held above the threshold for a sufficient period of time. A constant stress above the threshold produces a constant steady state creep rate, with the magnitude of the creep rate being an exponential function of stress magnitude. Furthermore, even when creep strains are substantial, much of the deformation is recovered upon unloading.

## REVIEW AND THEORY

A simple tensile test is not adequate to determine if a material is plastic, viscoelastic, viscoplastic, or nonlinear elastic. The question is better addressed by using a multiple loading test as described several places in the literature, e.g., Rabotov (1) or Cristescu (2). A modification of this approach was adopted for our investigation. It consists of the following sequential elements: a one second ramp-up in load, a sixty second hold at constant tensile

load, a one second ramp-down, and a sixty second hold at zero load. The sequence is repeated several times on the same specimen, using a greater value of maximum load on each successive cycle. The response during the constant load period reveals the extent and nature of any viscous effects, while the response to the unloading shows if any permanent plastic strains have developed.

## METHODOLOGY

A total of 31 specimens were tested; 25 from bovine metatarsals (8 fresh and 17 fresh frozen), and 6 from the fresh frozen human femur of a 21 year old male. The structure of the bovine samples was mature plexiform. The human samples were fully developed haversian. Machining and testing was performed under constant water irrigation. The specimens were nominally 1.6mm by 6.3mm by 51mm, with a 1.6mm by 3.2mm symmetrically reduced gage section. Their longitudinal axes coincided with the long direction of the bones. Testing was performed at room temperature, using a IBM PC based data acquisition system to record extensometer and load cell voltages.

## RESULTS AND DISCUSSION

The results were qualitatively similar for all samples. Figures 1 and 2 show typical results from the tests performed on human bone. The first 5 cycles produced closed stress-strain loops (figure 1). During the hold at constant load, the same 5 cycles produced strain-time curves that stabilize at an equilibrium strain (figure 2). These two attributes are indicative of a viscoelastic material with fading memory. The magnitude of the viscous effects can be

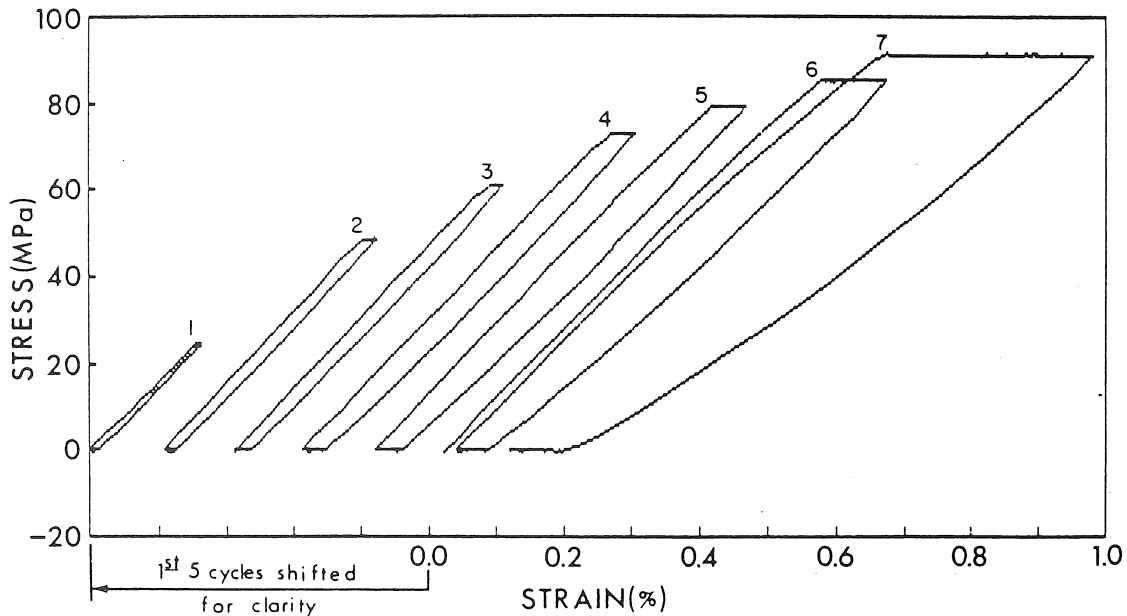


Figure 1. Stress-strain response of human bone to multiple creep load sequence.

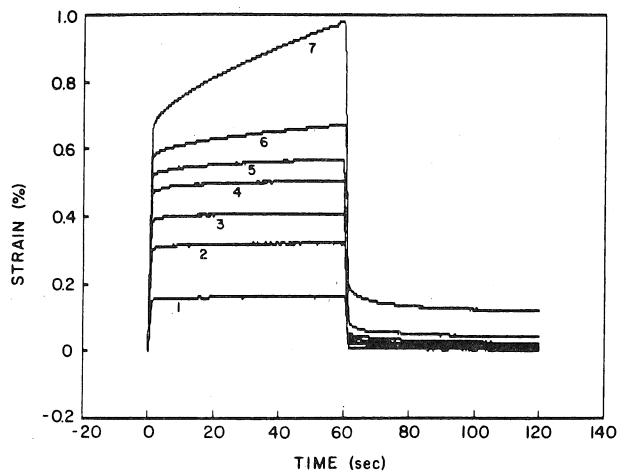


Figure 2. Strain history of the test shown in fig. 1.

judged by the size of the top-horizontal portion of the loops. For the first 5 cycles the effects are relatively small. The last two cycles, in contrast, do not form closed stress-strain loops. Additionally, during the constant load period, their strain-time curves, instead of stabilizing at a constant level, asymptotically approach a straight line with positive slope. In the last cycle, 0.36% anelastic strain develops, of which 78% was recovered after unloading. For the total sample population, it was found that at least 74% of the anelastic deformation was recovered after unloading. This was true even for samples showing anelastic strains of over 1.5%.

Two regimes of behavior exist. In the regime associated with lower stresses, strains are completely recoverable and stabilize under a constant load. In the regime associated with higher stresses, plastic strains develop and a constant creep rate is produced by a constant load. To distinguish between the regimes, we used a  $10 \mu\text{strain/sec}$  creep rate criterion, i.e., the stress that produces a steady state creep rate of  $10 \mu\text{strain/sec}$  is considered to be the boundary between the two regimes. This stress, which we refer to as the creep threshold, was found to be 73MPa (S.D.=5MPa) for the human samples and 117MPa (S.D.=10MPa) for the bovine samples. The steady state creep rate was plotted as a function of load to determine if the creep threshold represents a sharp boundary. Figure 3 shows such a plot for two typical specimens. It is clear that the creep rates increase rapidly for stresses above the creep threshold. The  $10 \mu\text{strain/sec}$  value was intentionally chosen to be small. It is interesting to note, however, that loads producing creep rates as low as  $10 \mu\text{strain/sec}$  will

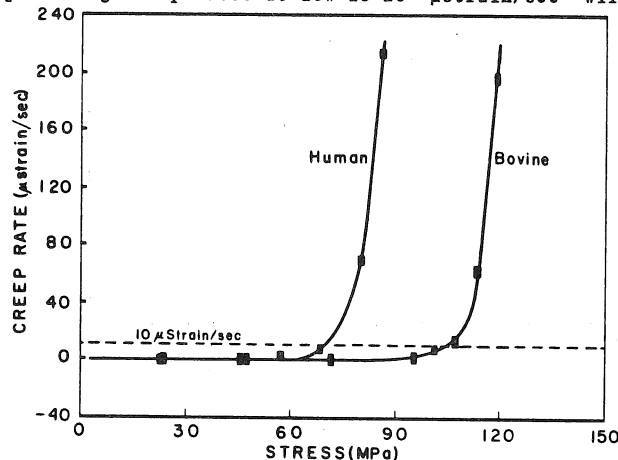


Figure 3. Creep rate as a function of constant load.

eventually cause rupture. This was shown by holding several specimens at the creep threshold for an extended period of time. Figure 4 shows the results for such a test performed on a bovine sample. The creep rate remained relatively constant for over 50 minutes until rupture occurred at a final strain of 3.5%.

Several of the specimens that experienced substantial creep strains without rupture were retested as if they were virgin specimens. Creep threshold values calculated from the second test sequence were within 1% of the values produced by the initial test. The retested specimens did, however, have different properties in the prethreshold region. This is shown in figure 5, where the equilibrium stress-strain curve is plotted for two test sequences performed on the same bovine specimen. These curves contain one point from each cycle; that point being the stress magnitude during the constant load period, plotted against the equilibrium strain reached during that period. The instantaneous modulus (the slope of the actual stress-strain curves at zero load), which is also shown in figure 5, was the same for both sequences. The equilibrium stress-strain curve, however, showed a definite softening.

Supported by NIH Grants AM-32405 and AM-0705.

#### REFERENCES

1. Cristescu, N., et al. Viscoplasticity. M. Nijhoff, The Hague (1982).
2. Rabotov, Y., Elements of Hereditary Solid Mechanics. Mir, Moscow (1980).

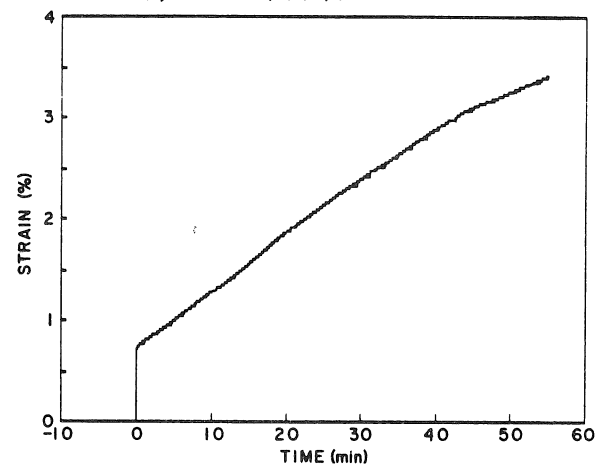


Figure 4. A single long term test at a creep rate of  $10 \mu\text{strain/sec}$ .

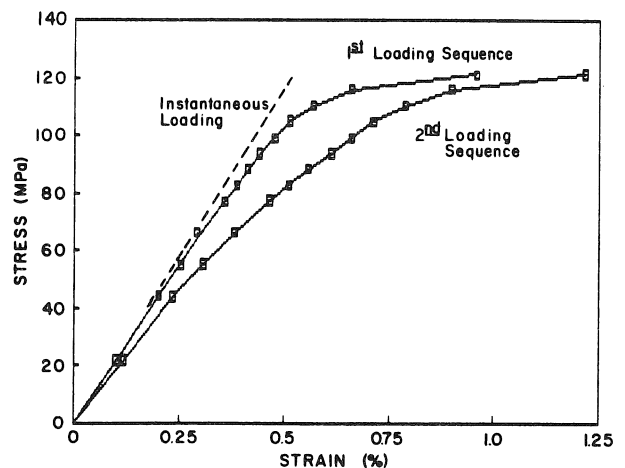


Figure 5. Equilibrium stress-strain curves for two sequences of tests performed on the same specimen.

E. Schneider, P. Weber, B. Gasser, S.M. Perren

M.E.M.-Institute for Biomechanics,  
University of Bern, Murtenstr. 35,  
CH-3008 Bern, Switzerland

## INTRODUCTION

The treatment of fractures as well as other diseases of the musculo-skeletal system is often subject to considerable uncertainty, if one attempts to base clinical decisions on estimations of the mechanical situation from x-rays. For example, the planning of early removal of implants due to infection (based on radiological evaluation of the fracture zone) is difficult.

Knowledge of the in vivo three-dimensional distribution of the mechanical properties of bone is further useful for cases requiring custom-made implants. The design-process of the implant and an appropriate stress analysis could both benefit from input data from the specific case. Computed tomography (CT) is a non-invasive technique readily available in many hospitals which might prove suitable for this purpose. While the technique has been used with quantitative scanners of high accuracy to assess bone mineralization [e.g. 1], its correlation to mechanical parameters has barely been approached. Because the CT scanners available in clinical practice are optimized for discrimination and imaging rather than quantitative measurements, the question is as to the accuracy of this technique.

The goal of this study is 1) to compare measurements acquired from quantitative computed tomography with results obtained from digitizer and standard materials tests for two specific geometrical and mechanical parameters (cross-sectional area and Young's modulus of cancellous bone), and 2) to investigate the variability of mechanical parameters due to osteoporosis.

## MECHANICAL PARAMETERS OF BONE FROM CT-MEASUREMENTS

Quantitative computed tomography produces planar images of the attenuation of x-rays due to absorption in the human body. The absorption coefficient at the  $i$ -th point in the pixel matrix is defined (in Hounsfield units, HU) as

$$\mu_{i, \text{rel}} = \frac{\mu_i(\text{bone}) - \mu(\text{water})}{\mu(\text{water})} \cdot 1000 \quad (1)$$

If it is assumed, that the absorption coefficient is proportional to physical density, that Young's modulus may be estimated according to [2] by the density to the third power, and that the material within the voxel (elementary volume) of the scanner is homogeneous and isotropic, a relative Young's modulus may be determined as

$$E_{i, \text{rel}} = \frac{(\mu_i - \mu_{\min})^3}{(\mu_{\max} - \mu_{\min})^3} \quad (2)$$

with  $\mu_{\min}$  and  $\mu_{\max}$  being the lowest and highest coefficients of absorption of the particular type of CT-scanner. Based on this relative modulus, the following mechanical parameters may then be determined for each cross section:

axial stiffness  $\alpha$ , torsional stiffness  $\gamma$  and bending stiffness in medio-lateral  $\beta_x$  and antero-posterior direction  $\beta_y$ :

$$\alpha = \int E_{i, \text{rel}} \cdot dA_i \quad (3)$$

$$\gamma = \frac{1}{2(1+\nu)} \int (x_i^2 + y_i^2) \cdot E_{i, \text{rel}} \cdot dA_i \quad (4)$$

$$\beta_x = \int y_i^2 \cdot E_{i, \text{rel}} \cdot dA_i \quad (5)$$

$$\beta_y = \int x_i^2 \cdot E_{i, \text{rel}} \cdot dA_i \quad (6)$$

where  $dA_i$  is denoting the infinitesimal area and  $\nu$  Poisson's ratio. These "stiffnesses" are in fact the weighted cross sectional area ( $\alpha$ ), the weighted rotational ( $\gamma$ ) and the weighted linear moments of inertia ( $\beta$ ). They are all relative and therefore have arbitrary units.

## METHODS AND MATERIALS

For this study, 5 normal ( $62 \pm 22$  yrs,  $63 \pm 8$  kg) and 5 osteoporotic femora ( $86 \pm 3$  yrs,  $48 \pm 9$  kg) were used. Subjects were classified as being osteoporotic by the pathologist at time of removal, if their spinal bodies were "easily impressable". This classification was found to be closer to the clinical definition of impression fractures than the use of the Singh index [3].

The bones were moistened, sealed immediately after removal in polyethylene bags and stored at  $-20^\circ$  Celsius until measurements were made. A SOMATOM SF (Siemens) scanner was used for the tomographic measurements. The distal 20 % of the femora were scanned continuously with a slice thickness of 2 mm. Additional scans were taken between 25% and 80% of total length. A 460 mAs product at a tube voltage of 125 kV and an image matrix of  $256 \times 256$  elements were used.

For the comparative analysis of geometrical and mechanical properties, one of the specimens, the femur of a 60 year old male (bodyweight=59 kg) with no evidence of osteoporosis was analyzed further. Cross-sectional area was determined 10 times from a photographic enlargement of a cross-section through the diaphysis and through the condyles by means of a digitizer (TALOS 8000) as well as from the corresponding CT-measurements.

Young's modulus  $E_{CT}$  of cancellous bone was estimated from the CT-measurements as the above described relative Young's modulus, averaged over the pixel elements contained in  $1 \text{ cm}^3$  at 29 selected locations in the distal femur.

Young's modulus  $E_{\text{exp}}$  was determined on an INSTRON 1026 materials testing machine under compressive loading. The distal femur was cut into five slices 1 cm thick and 29 cubes of cancellous bone of identical dimensions were cut from them at the locations analyzed by CT. Samples were tested at a strain rate of  $0.008 \text{ s}^{-1}$ , in three orthogonal directions and not exceeding 5% strain in any direction.  $E_{\text{exp}}$  was then taken as the average of the three orthogonal values.

## RESULTS

For the cross-sectional measurements, the following values (mean  $\pm$  1 standard deviation) were found:

	CT-scanner	Digitizer
Diaphysis	$6.41 \pm 0.02 \text{ cm}^2$	$6.21 \pm 0.01 \text{ cm}^2$
Condyles	$48.01 \pm 0.02 \text{ cm}^2$	$48.00 \pm 0.03 \text{ cm}^2$

The Young's moduli as determined by the two methods are presented as a scatter plot with the appropriate regression line and parameters in Fig. 1.

Figure 2 shows axial and torsional stiffness, and figure 3 bending stiffness in 2 orthogonal planes for the normal and osteoporotic group. Although the units are arbitrary, care was taken to present the same parameters in identical magnifications. Axial and bending stiffness is highest at the condyles, whereas torsional stiffness is comparable at diaphysis and condyles for both groups. Axial stiffness is reduced in the osteoporotic group by 45% at mid diaphysis and by 40% at the condyles. Torsional stiffness is reduced by 50% and 43% respectively. Bending stiffness in x-direction is reduced by 55% at mid diaphysis and by 45% at the condyles, bending stiffness in y-direction is reduced 45% throughout.

## DISCUSSION

The determination of the cross-sectional area shows, that CT-measurements overestimate the true values, mainly as a consequence of the partial volume effect. This error may be reduced by using a pixel matrix with more elements, presently available on most scanners. There might be room for further improvement by using edge detection algorithms (e.g. 4) rather than threshold criteria as used in this study.

The correlation between Young's moduli as determined by the two techniques ( $R^2=0.88$ ) is high enough to make this a useful technique with reasonable accuracy. Further investigations, however, including other sites and bone conditions, are warranted. Further improvement of the accuracy achievable is likely to occur, if phantom measurements are included, later generation scanners and their dual-energy options are used.

The wide separation between the values found for the two groups with respect to their mechanical properties shows, that the method is sensitive. It might be speculated, that these results could be useful for the estimation of the risk, certain patients may have to fracture their bone.

## References

1. Rügsegger, P., et al. J. Bone Joint Surg. 66-A (7): 1015-1023, 1984.
2. Carter, D.R. and Hayes, W.C. J. Bone Joint Surg. 59-A (7): 954-962, 1977.
3. Singh, M., et al. J. Bone Joint Surg. 52-A (3): 457-467, 1970.
4. Seitz, P., et al. IEEE Trans. Med. Imag. MI-2 (3): 136-141, 1983.

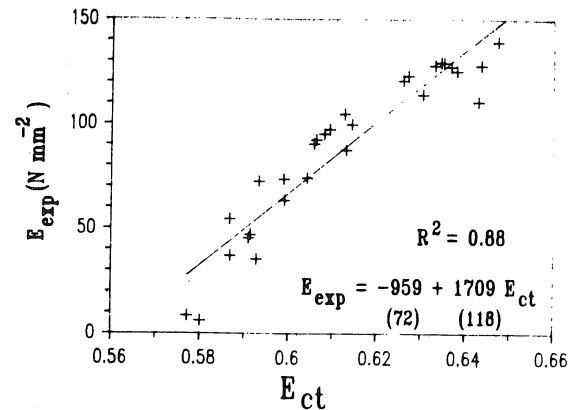


Figure 1. Scatterplot and regression equation for Young's modulus as determined by mechanical testing ( $E_{\text{exp}}$ ) and CT-measurements ( $E_{\text{CT}}$ ).

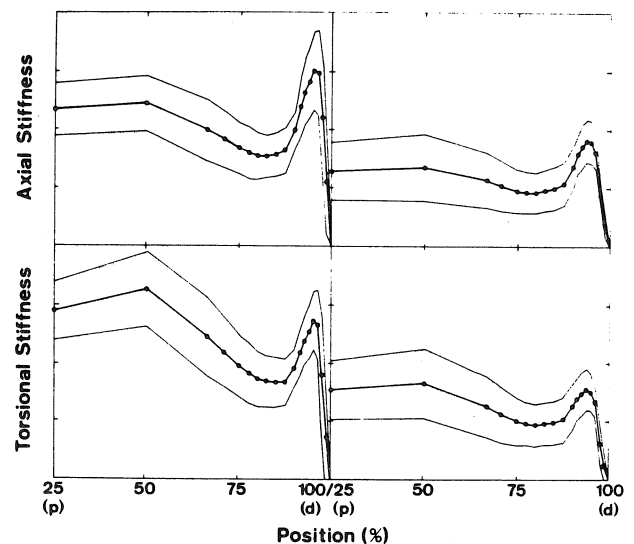


Figure 2. Average and confidence interval ( $1\sigma$ ) of axial and torsional stiffness of normal (left) and osteoporotic group (right) with respect to the relative position along the femur (p=proximal, d=distal).

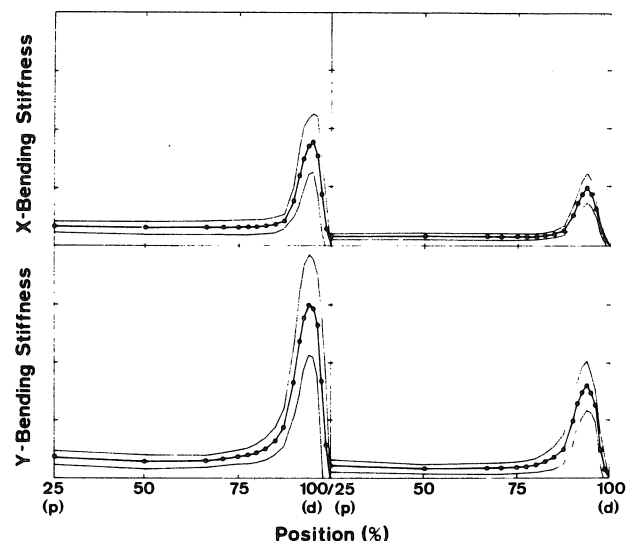


Figure 3. Average and confidence interval ( $1\sigma$ ) of bending stiffness in m-l (x) and a-p (y) directions of normal (left) and osteoporotic group (right) with respect to the relative position along the femur.

# A BIOMECHANICAL ANALYSIS OF GRAFT FATIGUE FRACTURE IN A RESECTION ARTHRODESIS

N.R. Williamson, C. Tylkowski, G. Piotrowski, G. Miller, D. Springfield, Gait Analysis Laboratory

University of Florida, Department of Orthopaedic Surgery, Box J-246 JHMC, Gainesville, FL 32610.

**INTRODUCTION:** A biomechanical analysis incorporating the methods of gait analysis, computed tomography, finite element analysis, and nonlinear optimization was performed to investigate the cause of graft fatigue fractures following "tibial turnback" knee resection arthrodeses. This surgical procedure(1) uses autogenous cortical grafts from the anterior tibia and the ipsilateral fibula to bridge the femoral defect created by the resection. An intramedullary (IM) rod is used to provide fixation.

Fatigue fractures of the posterior grafts have occurred primarily in resections longer than 12 cm and have led to concerns regarding the long-term reliability of this procedure. The effects of graft length, leg (tibia plus grafts) rotation, and IM rod size on the stresses in the graft and IM rod were analyzed.

**METHODS:** The physiological loads on the fused limb during walking were obtained at the University of Florida Gait Analysis Laboratory. The methods used to obtain these data are well developed and yield reliable quantitative information(2,3). The motion and ground reaction force data thus acquired were used to calculate the quasi-static axial and bending loads on the arthrodesis structure. The specific loads applied to the distal end of the model occurred during the early single limb stance of one subject; the type of loading seen by the graft structure was, however, general throughout the gait cycles of the three subjects surveyed.

Computed tomography (CT) scanning of a sham resection arthrodesis was used to obtain the cross-sectional geometry of the structure. A Philips CT scanner was employed to scan the fused limb at 6.2 mm intervals over its length for a total of 132 transverse sections. The CT images were optimized for cortical-cancellous bone contrast(4,5). A full scale window width (CT# = 3200), centered at the average radiographic density of the cortical and cancellous bone (CT# = 900), minimized the error in reproducing the load-bearing cortical thickness in each section. Due to the gradual transition from cortical to cancellous bone, the best precision to which cortical thickness could be measured was found to be approximately 1 mm; this agrees with other reports(6).

Each transverse section CT image was traced and discretized into radially disposed elements. The discretized tracings were then digitized to obtain the three-dimensional nodal coordinate values. These nodal coordinates were used to define the geometry of a finite element model of the structure.

Three-dimensional isoparametric solid elements were used to model the tibia. Twenty elements per transverse section were used to model the tibial cortex. The cancellous bone of the tibial plateau was modelled in four concentric layers with twenty elements each for a total of eighty elements per transverse section. The fully incorporated grafts were modelled in a manner consistent with radiographic observations of the healed structures: three-dimensional beam elements were used to model

the anterior graft, while the posterior graft was modelled using three-dimensional cylindrical elements. Callus formation was taken into account in both cases. The additional information required for these elements (e.g. area moments of inertia) was obtained by applying the SCADS computer program to the graft cross-sectional images(7). The fluted intramedullary rod was modelled as a right circular cylinder, using cylindrical elements and geometrical information derived from Miller(8); the effects of the flutes were included in the element specifications. Material properties for the model were taken from the literature.

The CT images were also used to determine the regions of cortical intramedullary support for the IM rod. Proximally these regions were modelled by placing appropriate displacement constraints on the rod: axial translation of the rod was permitted; AP and ML displacements were restricted according to the support seen to occur in the femur. Cortical support of the IM rod in the distal tibia was modelled using three-dimensional interface elements at points of bone-rod contact. These elements allowed the rod to slide on, and separate from, the supporting cortical bone while transmitting only compressive forces across the bone-implant interface. The stiffness specification for this interface was taken from Miller(8). The complete finite element model consisted of 847 elements with 4700 degrees of freedom. Parametric simulations were performed varying graft length, leg position, and IM rod size. A computer program for the constrained non-linear optimization of these variables, minimizing graft stress, was developed and implemented.

**RESULTS & CONCLUSIONS:** A prominent von Mises stress peak was found to occur proximally in the posterior graft. This correlated well with the radiographically determined predominant in vivo fatigue fracture location.

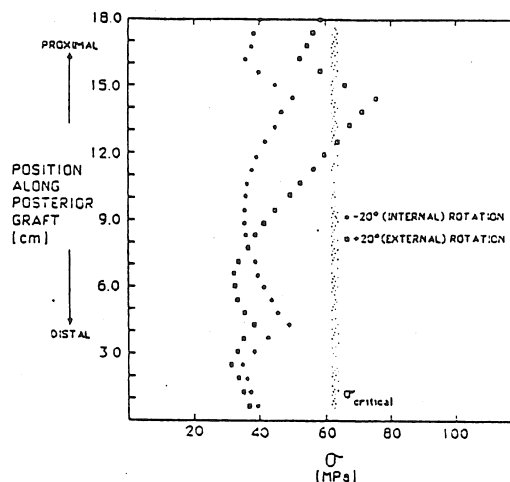


Figure 1

Figure 1 shows the von Mises stress distribution along the length of an 18 cm graft. The peak stress occurred at the interior border of the proximal callus and exceeded the graft's critical stress level with external leg rotation. This peak was minimized in the model for all resection lengths by placing the leg (tibia plus grafts) in approximately 20 degrees of internal rotation with respect to a neutral femur.

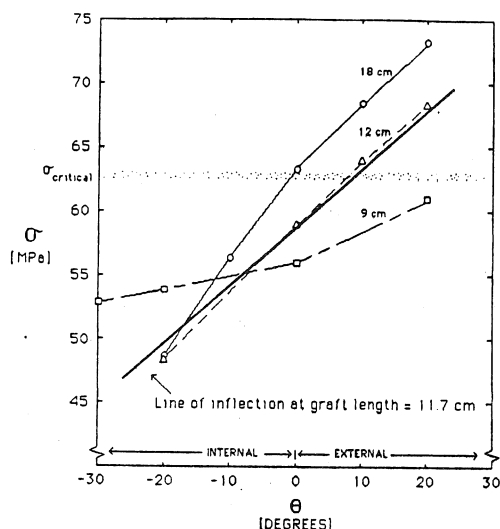
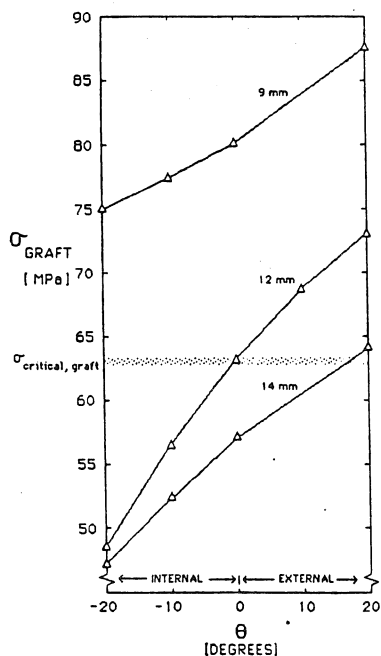


Figure 2

A strong relationship was found between resection length and graft stress. Figure 2 shows the relationship between the proximal von Mises stress peak in the posterior graft and the position of the leg with respect to a neutral femur for three resection lengths. The stresses were generally greater and more sensitive to leg position in grafts longer than 12 cm, correlating well with the clinically observed "12 cm length effect". The increased sensitivity of longer grafts was emphasized by a line of inflection which occurred on the analytical response surface at a graft length of 11.7 cm.

Figure 3



IM rod size had a strong effect on the stresses in the posterior graft. Figure 3 shows the relationship between the proximal von Mises stress peak in the graft and the position of the leg (tibia plus grafts) for three IM rod sizes in an 18 cm resection. The 9 mm diameter rod provided insufficient support, resulting in graft peak stresses which exceeded the critical stress for all leg positions. This result correlated well with clinical experience. The stiffest IM rod studied (14 mm), combined with internal leg (tibia plus grafts) rotation, minimized the likelihood that fatigue fracture of the posterior graft or the IM rod would occur in the model.

The combined use of Gait Analysis, finite element analysis and engineering optimization proved to be an effective method of analyzing graft fatigue failure in the knee resection arthrodesis and suggested corrective measures to obviate these clinically observed problems.

#### REFERENCES:

1. Enneking WF. in *Attualita in Chirurgia Ortopedica*, 57-63, ed. Aulo Gaggi, Bologna, 1982.
2. Simon SR, Nuzzo RM, Koshinen MF: *Bulletin of the Hospital for Joint Diseases*, 38:1, 1977.
3. Tylkowski CM, Simon SR, Mansour JM: In *The Hip: Proceedings of the Tenth Open Scientific Meeting of the Hip Society* (J.P. Nelson, ed.) 89-125, CV Mosby, St. Louis, 1982.
4. Baxter BS, Sorenson JA, *Investigative Radiology*, 16:337-348 1981.
5. Koehler PR, Anderson RE, Baxter B, *Radiology*, 130:189-194, 1979.
6. Rohlmann A, Bergmann G, Kolbel R: *Z Orthop* 118:122-131, 1980.
7. Piotrowski G, Wilcox GA. *J Biomech* 4:497, 1971.
8. Miller GJ, Ph.D. Dissertation, U of Fla., 1977.

#### ACKNOWLEDGEMENTS:

This research was aided by a grant from the Orthopaedic Research and Education Foundation.

## ANALYSIS OF BONE MODEL MATERIAL FOR EXTERNAL FRACTURE FIXATION EXPERIMENTS

T. J. Hein, A. Perissinotto, R. N. Hotchkiss, and E. Y. S. Chao  
Orthopedic Biomechanics Laboratory  
Mayo Clinic/Mayo Foundation  
Rochester, MN 55905

### INTRODUCTION

In the biomechanical testing of various orthopedic devices, the geometry and physical property of the bone model plays a key role in determining the performance of the device. Fresh cadaver bones have often been used, but their high variability can greatly affect the test results. When pins or screws are interfaced to bone, nonuniform models may introduce additional variables and produce inconsistent test data with large deviations. The aim of this study was to identify a consistently reproducible material for synthetic bone models which has physical properties similar to fresh bone. Using such a model, external fixators and different bone pin designs can be compared objectively.

### MATERIALS AND METHODS

The performance of three different materials was compared to fresh humeral bone. These included 2.54-cm solid rods made of "RK-100" foam (.72 gm/cc) (Daro Products, Inc.), kiln dried "white oak" dowel, and "Lexan" polycarbonate. To establish statistical significance, five specimens of each material were used to compare with five fresh humeri. The study consisted of three parts. First, the specimens were tested and compared to intact humerus. The second test consisted of creating a midshaft osteotomy in each model to examine the rigidity of the reduced segments after the application of a small Orthofix unilateral external fixator. And, finally, each material was examined for its mechanical properties at the pin-bone interface when an external fixator was applied.

Intact bone models (Fig. 1A) were tested on an MTS machine under torsional loading, A-P bending, and lateral bending. Load was applied at a rate of 15 deg/min and 226.8 N/min for torsional and bending tests, respectively. Force versus displacement curves were recorded on an x-y recorder and used to derive the structural stiffness values for each model.

The bone models were cut at the midshaft, and the segments were fixed with an Orthofix external fixator using 6 half pins with tapered threads. The pin holes were predrilled to the manufacturer's recommendation of 3.2 mm in diameter using an alignment jig. An instrumented torque wrench was used to record the maximum insertion torque. A gap of 1 cm was maintained during the testing process in order to transmit all load to the pin-bone interface. All components of the fixator were tightened using consistent torque on the fixation screws. The identical fixator configuration was maintained for each bone model, so that changes in stiffness could be attributed only to bone model variation. The bone fracture fixation model (Fig. 1B) was then mounted on the MTS machine and tested under axial compression, torsion, and A-P and lateral bending at the same loading rates to establish the stiffness properties of the entire structure involving different bone models.

To examine pin tract characteristics, maximum pin insertion torque was compared to pin loosening torque after completing the loading test for each bone model. To further study pin-bone interface behavior, an indentation test was performed on five, 10-mm thick cross-sectional specimens of each material, including humeral diaphyseal bone. Each specimen was loaded on the MTS machine using a 3.175-mm diameter indenter in specific zones of the cross section at a rate of 226 N/mm. The "Brinell" hardness was then calculated for each material using the force versus displacement data.

### RESULTS

When comparing intact structural stiffness values, the "oak" model behaved closest to intact humerus. However, because of its irregular grain structure and the inhomogeneity of the wood, large standard deviations were observed. When testing the fixator/bone models, the "RK-100" foam model exhibited structural properties similar to humeral bone under all loading configurations (Table 1). The oak model had similar pin insertion torque values of the humerus, but the "RK-100" foam more closely simulated the pin removal torque observed in the humerus (Table 2). The RK-100 foam also had similar results as compared to the humerus in pin insertion/removal torque ratios.

The indentation test revealed that the humeri, RK-100 foam, and white oak have zones of different hardness magnitude (Fig. 2). White oak has alternative parallel zones with two distinct mechanical properties, depending upon the grain density and orientation. The dense zone hardness value is an order of magnitude larger than the more porous zone. The humeri and RK-100 foam have concentric zones of varying hardness, the maximum hardness being on the outer circumference and decreasing towards the center, the humerus hardness values being much larger. In addition, the foam model had the least standard deviation in raw test data.

### DISCUSSION

For comparative study of structural stiffness properties in external fixation, the "RK-100" foam material appears to be a suitable model to simulate the humerus. The solid structure of the model tends to make up for the lack of material strength as compared to cortical bone. The concentric hardness distribution, with a higher value on the surface layers, provides a cortical-cancellous bone property to better simulate the pin/bone interface behavior in the metaphyseal region of a long bone. Finally, changing the material density during the molding process may also provide additional control of the required mechanical performance in this model.



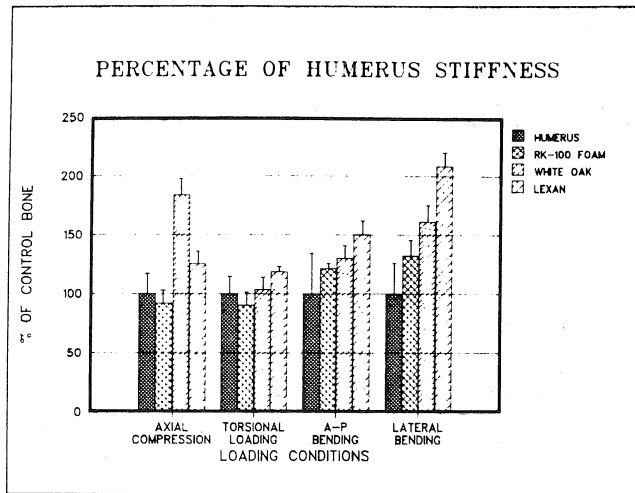


Table 1. Fixator/bone stiffness comparison of bone models to control bone humerus.

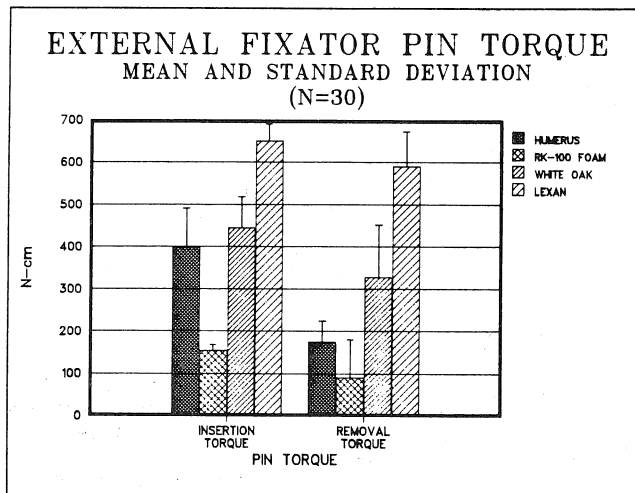


Table 2. Pin insertion and loosening torque value comparison.

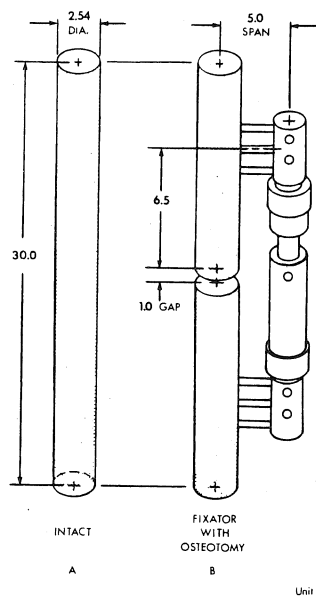


Fig. 1 Bone model geometry. A) Intact bone model dimensions. B) Fixator/bone model configuration.

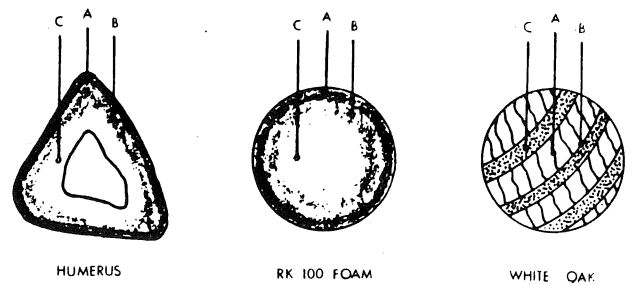


Fig. 2 Indentation test cross-sectional specimens. Zone A is zone of maximum hardness. Zone B is zone of intermediate hardness. Zone C is the least hard.

## MECHANICAL PERFORMANCE OF PROPHYLACTIC KNEE BRACES

S. Meyer, D. Anderson, M. Jimenez, T. Brown, and R. Brand  
Department of Orthopaedic Surgery, Biomechanics Laboratory  
The University of Iowa, Iowa City, Iowa 52242

Increasing interest and participation in athletics has been accompanied by a predictable rise in musculoskeletal trauma, particularly to the knee. For a number of years, knee stabilizing orthoses have been used to return previously injured individuals back to the playing field. Lately, several new prophylactic knee braces have been developed. To date there has been a paucity of well-controlled investigations of knee braces in general, and of prophylactic models in particular [1]. This study determined the effects of prophylactic braces on reducing or limiting knee ligament strain under specified dynamic loading conditions, and directly compares the mechanical efficacy of the Am Pro knee orthosis with the Anderson knee orthosis.

Data were collected from seventeen fresh-frozen (thawed) cadaver legs, each dissected away from the pelvis, and completely intact from femoral head to foot (six paired females, two paired males, and one single male limb). Each femur was denuded five inches at its proximal end and potted in a metal cylinder using methyl methacrylate. The knee was then incised in a medial curvilinear fashion from the superior aspect of the patella to the medial flare of the tibial condyle. Great care was taken to preserve as much musculature and knee capsule as possible. Liquid metal strain gauges (LMSGs) were sutured to the midsubstance of both the anterior (long) and posterior fibers of the medial collateral ligament (MCL). LMSGs have proven quite reliable under dynamic loading conditions [2]. We used a loading apparatus designed to secure the leg for testing while allowing appropriate (physiologic) motion at the knee joint (Figure 1). A feature necessary to simulate physiologic conditions, as shown by Hsieh and Walker [3], is the ability to generate axial loading. Pneumatic loading of the femoral support assured that appreciable "weight-bearing" compressive force (nominally 100 pounds) was developed across the knee. Specimens were preloaded until the LMSG output rose quasilinearly with valgus load, suggesting full MCL engagement. To simulate the "clipping" type injury in football, a dynamic blow was then delivered laterally to the preloaded knee, producing further rapid valgus angulation. To achieve this, we used an MTS materials testing machine. Feedback from the load cell to the MTS servo mechanism guaranteed delivery of a load of the desired magnitude. Each cadaver specimen was evaluated in the braced and unbraced state, all other parameters being equal, permitting a direct calculation of strain attenuation for each brace.

Data captured during a typical valgus blow are shown in Figure 2. Medial deformation increased linearly with time (MTS stroke control), leading to nonlinear overall load uptake. During this interval, the output from the LMSG also rose, in general nonlinearly, due to MCL distension. The criterion for blow termination was attainment of a specified load level. The testing sequence used

involved triads of tests performed at each of several progressively increased load termination levels (dashed line in Figure 2). For each specific load termination level, the test sequence began with the Am Pro brace, followed by the Anderson brace, and finally by the unbraced knee. Repeating this sequence at progressively higher termination loads until specimen failure, we found that four specimens failed (at higher loads) with Am Pro braces installed, while failure of two specimens occurred with the Anderson brace at load levels successfully protected against by the Am Pro brace, and five unbraced specimens failed at load levels successfully protected against by both braces. Recordings from six of the specimens were not included in the overall tabulated results either because of unexplained trial-to-trial irreproducibility, because of uncontrollable specimen rotation during loading, or because of excessively weak or atrophic ligaments.

The series-wide mechanical performance data are summarized in Table 1. Both the Am Pro and Anderson braces showed a marginally significant strain attenuation in the MCL ( $p < 0.05$  and  $p < 0.1$ , respectively) with respect to no bracing, while the Am Pro showed a mild but not very significant ( $p < 0.25$ ) trend of greater MCL strain attenuation than that seen with the Anderson device. In terms of mean strain attenuation as a percentage of unbraced MCL strain, the Am Pro device demonstrated a 14.6% attenuation, while the Anderson showed 10.4%. However, there was no significant change in gross stiffness with either brace compared to the unbraced knee. There was considerable intra-specimen variability with respect to leg length, joint stiffness, and unloaded varus/valgus knee angles. Also, gross dissection after mechanical testing revealed various modes of MCL failure, including complete mid-substance rupture (mop-end effect), partial deep substance ruptures, and partial ligament end avulsions.

Both of the braces studied appeared to afford possibly clinically significant degrees of MCL strain reduction; the Am Pro device seemed to perform marginally better in this regard than did the Anderson. There was no doubt that bracing prevented several MCL failures that would otherwise have occurred without bracing, and in two instances the difference between the brace designs turned out to be critical. We would strongly emphasize, however, that these findings pertain only to the case of purely valgus deformations, for which specimen rotation/flexion is negligible. In the many instances during which the specimens spontaneously rotated and flexed to various degrees during the loading pulse, there was no evidence that brace attachment was efficacious in reducing MCL load uptake. Since this latter situation is probably the more representative of actual injury conditions, additional study of brace performance under conditions of flexion and rotation appears to be warranted.

## References

1. DeHaven, K. AAOS Knee Brace Seminar pp 10-14, 1984.
2. Brown, T.D, et al. TORS 10:39, 1985.
3. Hsich, H.H., et al. JBJS 58-A:87-93, 1976.

Acknowledgement: Financial assistance was provided by American Prosthetics, Inc. We appreciate the laboratory assistance of Mr. J. Van Hoeck and Mr. R. Shelman.

Table 1

	Absolute MCL % Strain+	Relative Strain Attenuation (per cent)	Gross Stiffness (N/mm)	Valgus Failure Load (N)
Unbraced	15.2,7.86*	----	9.8,4.2	1019,273
AmPro	12.7,6.8	14.6,31.5	9.7,3.8	1025,818
Anderson	13.9,7.5	9.4,27.5	9.1,3.9	750,35.4

\*Values listed as mean, S.D.

+Beyond preloaded configuration

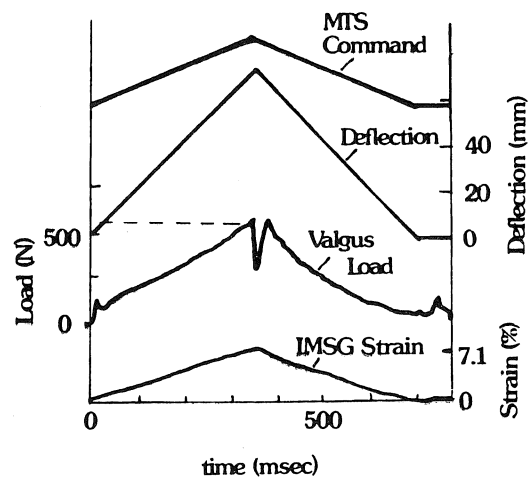


fig. 2

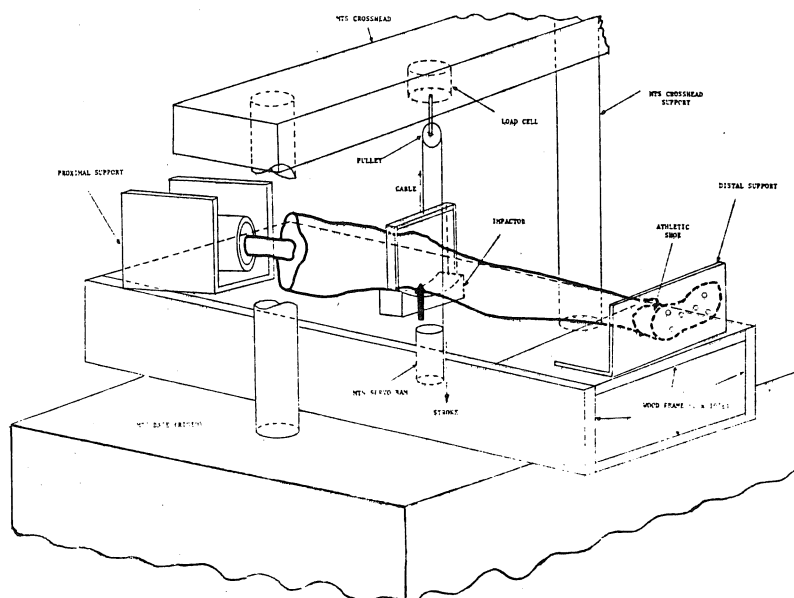


fig. 1

# FRACTURE GAP MOTION IN EXTERNAL FIXATION

B. Fleming, T. Kristiansen, G. Neale, S. Reinecke, M. Pope  
Department of Orthopaedics & Rehabilitation, The University  
of Vermont, Burlington, VT 05405

## ABSTRACT

Eight different external fixation frames were mounted on acrylic cylinders across a simulated fracture gap and their mechanical properties compared. Displacements of the fracture gap and overall frame stiffness were measured under different loading conditions. Significantly different motion patterns were exhibited at the fracture site by the different frames. Some were highly shear resistant; others were highly resistant to axial compression.

## INTRODUCTION

There have been many studies examining the mechanical properties of external fixateurs. Burny et al., 1982, has promulgated the concept of elastic fixation, suggesting that up to a point decreased frame stiffness leads to rapid union and substantial callous. Perren, 1979, has theorized that bone healing is a function of the strain tolerance of the fracture callous. Work by Panjabi, 1979, and Goodship et al., 1985, show evidence that compressive micromotion will accelerate fracture healing, while Seligson et al., 1982, have suggested that shear is deleterious. Although useful insights have been gained through stiffness evaluations of external fixateurs, attention should be focussed on the motion patterns at the fracture site. As a step toward investigating these theories, we designed an experiment to simultaneously measure the displacement at the fracture gap and the stiffness characteristics of various commercially available external fixation frames under different loading conditions.

## METHODS

Eight frames were tested, five unilateral and three bilateral systems. All frames were mounted on acrylic tibias and loaded by an MTS materials testing system. Testing was performed in lateral and AP bending, torsion and axial compression loading. A system of strain gauged extensometers and linear displacement potentiometers were utilized to measure gap closure and shear respectively.

## RESULTS AND DISCUSSION

The data demonstrates that different motion patterns were exhibited at the fracture site. (Figure 1 illustrates how two fixateurs with a similar bending stiffness may differ in fracture gap movement.) Certain fixateurs demonstrated a high shear resistivity (fig. 2) while others maximize gap

closure (fig. 3). The bilateral half pin external fixateurs provide maximum shear stiffness while permitting some compressive motion. The results suggest that overall fixateur stiffness is not a definitive or clinically relevant means for evaluating an external fixateur system. These types of data, by means of an in vivo study, could be useful in examining existing theories of fracture healing in response to different fracture gap motion.

## CONCLUSIONS

External fixateurs with similar stiffness characteristics could exhibit different motion patterns at the fracture site. Previous investigators indicate that compressive motion accelerates fracture healing, whereas shear is detrimental. For a complete mechanical evaluation of an external fixation system one should consider fracture gap motion patterns as well as overall stiffness.

Fig. 1  
Motion characteristics at the fracture site.

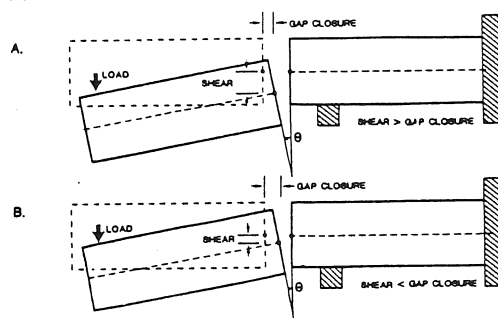


Fig. 2: SHEAR COMPARISON

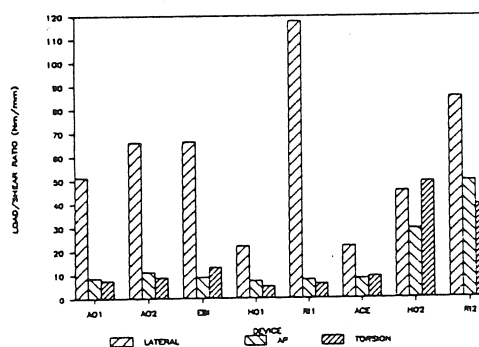
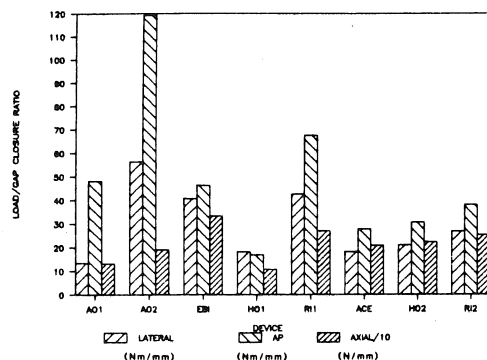


Fig. 3: GAP CLOSURE COMPARISON



### References

1. Burny, F., Bourgois, R., Donkerwolke, M.: Elastic External Fixation: A Biomechanical Study of the Half Frame. In Seligson, D. and Pope, M. (eds.): Concepts in External Fixation. New York: Grune & Stratton, 1982, pp 13-39
2. Goodship, A.E., Kenwright, J.: The Influence of Induced Micromovement upon the Healing of Experimental Tibial Fractures. *J. Bone Jt. Surg.* 67B:650, 1985
3. Panjabi, M.M., White, A.A., Wolf, J.W.: A Biomechanical Comparison of the Effects of Constant and Cyclic Compression on Fracture Healing in Rabbit Long Bones. *Acta Orthop. Scand.* 50:653, 1979.
4. Perren, S.M.: Physical and Biological Aspects of Fracture Healing with Specific Reference to Internal Fixation. *Clin. Orthop.* 138:175, 1979.
5. Seligson, D., Blitzler, A.S.H., Pope, M.H.: The Biology of Fracture Healing with External Fixation. In Seligson, D. and Pope, M.H. (eds.): Concepts in External Fixation. New York: Grune & Stratton, 1982, pp 41-65.

## Fatigue Evaluation of a New Spinal Fixation Device

M. H. Krag, B. D. Beynon, M. H. Pope, J. W. Frymoyer, L. D. Haugh

The Vermont Rehabilitation Engineering Center  
The University of Vermont, Burlington, Vermont 05401

### INTRODUCTION

A new spinal implant has been developed, and biomechanically evaluated, which is intended for application to "short-segment" spinal defects such as disc degeneration, fracture, spondylolisthesis, or tumor (2). Major improvements over currently available implants include: (1) minimal length of spine involvement (only two to three vertebrae are spanned); (2) three-dimensional control of involved spine segments is provided before and after locking of implant; and (3) primary graft sites are not covered, as they are with Harrington and Luque instrumentation, allowing accessibility to laminectomy sites, lumbosacral and thoracolumbar junctions. The implant, the Vermont Spinal Fixator (VSF) shown in Figure 1, uses a posterior approach. Trans-pedicle screws, made of 316L S.S., are placed bilaterally in vertebral bodies above and below the involved region. These screws are connected longitudinally with rods and specifically-designed clamps which allow three-dimensional adjustment prior to locking. The work presented here is the last biomechanical assessment in the course of implant development, the fatigue evaluation of implant, with particular concern for pedicle screws.

### REVIEW AND THEORY

Design and development of the VSF has taken the following course: (1) definition of vertebral morphometry, using CT scanning, specifying the major diameter screws permissible for pedicle screw application; (2) pedicle screw design, through the independent optimization of pitch, minor diameter and tooth profile, using screw pull-out strength from vertebral body as an assessment measure; (3) establishing a relationship between depth of screw penetration and strength of fixation; (4) designing and mechanical evaluation of the compact, three-dimensionally adjustable, non-loosening clamp; and, presented here, (5) fatigue evaluation of the implant, focussing on evaluation of the "weak-link", the pedicle screw.

Most current clinically used spine implants have had some type of fatigue evaluation(3), either in the form of in vivo clinical trials or experimental testing, simulating the in vivo environment. However, none of the work performed may be used to predict fatigue performance of the VSF, since vastly different biomechanic principles are used to achieve spine stabilization. The VSF achieves fixation through rigid

attachment to involved spinal segment, much like an external fixation device applied to long bone fractures, while most other implants rely on a compressive or distractive interface between implant and spine. Kasman et al. (1) evaluated the performance of external fixator screws in an experiment designed to resemble clinical application. This work is only applicable to prediction of an external fixator's performance in which multiple screws are used, and not the performance of an individual screw. Zand et al. (4) studied the fatigue performance of cortical bone screws applied to compression plates. This work is only applicable to screws which are subject to cyclic shear stress loading and not applicable to a cyclic bending stress environment, the stress environment of the pedicle screw. The present study was undertaken since there exists no single, controlled study of fatigue performance of a screw subject to a bending stress environment.

### METHODS

A unilateral portion of the VSF, shown in Figure 2, was tested in a manner resembling the single most demanding in vivo load environment, and thus stress state, that imparted by the physiological motions of flexion/extension. Specifically-designed pedicle screws (5.0mm major diameter, 4.0mm minimum diameter, 2.0mm pitch, buttress thread profile) were anchored in low density polyethylene blocks, which simulated vertebral bodies. Superior and inferior screw/block constructs, aligned perpendicular to axis of load cell travel, were joined using articulating clamps and longitudinal rod. Load was applied to the screw/ block system through points simulating center of vertebral body rotation. A load application assembly forced the fixator to deflect and rotate about the chosen centers of rotation. The implant was subjected to fully reversed sinusoidal cycling, about zero load, at a frequency of 1.0 Hz, using a Materials Test System. A constant load test, or constant stress, was chosen to assess fatigue performance (number of cycles to failure), and to develop a load vs. cycles-to-failure relationship. This was accomplished by choosing different stress (load application) levels at which the implant was cycled to fracture. Tests were run at, theoretically calculated, constant stress levels (of .3%, .5%, .7% and .9% yield stress). At each stress level seven screws were tested. Experimental design followed ASTM protocol and statistical analysis in development of load vs. cycles-to-failure relationship.

## RESULTS

In all tests, the fully-reversed bending stress environment produced fracturing of the pedicle screw at the first thread, the simulated point of entry to a vertebral body. The relationship of applied load to screw vs. cycles to failure (N) may fit different distributions. The two distributions considered were (1) log normal distribution and (2) Weibull distribution. A maximum likelihood analysis was used to test each distribution for "goodness of fit". The log normal distribution was found to provide the best fit at each load level tested. Additionally, the variance was found to be constant over the range of loads tested, indicating a random sampling of dimensionally similar screws. Since the data were log normally distributed, a linear regression was performed and prediction intervals determined. This relationship, linear with a corr. coeff. = .8, is depicted in Figure 3. The regression relationship is only applicable between the yield stresses of .5% and .9%, a common stress range the implant will experience under in-vivo conditions. At the level of .3% yield stress, runnout occurred. At runnout (10<sup>6</sup> cycles), implant cycling was terminated, no failure evident on the pedicle screw indicating that a fatigue limit is approached. These data points may not be combined with those in which specimens failed, since the outcome measures differ.

## CONCLUSIONS

A new spinal implant has been designed, developed, and biomechanically evaluated. The final step in the course of development has been fatigue analysis of implant. Testing was performed on a uniquely designed pedicle screw. A load controlled, or constant stress, test subjected the implant to the single most demanding environment to be experienced in vivo, the loads applied to the implant by the physiological motions of flexion/extension. This was simulated by applying a fully reversed, about zero load, sinusoidal loading to implant. In all cases fatigue evaluation has produced implant failure at the site of first thread on pedicle screw, the point of screw entry into vertebral body. The fatigue data has been demonstrated to fit a log normal distribution best. A log(applied load) vs. log(cycles to failure) relationship has been developed, with corresponding prediction intervals, and has proven to be a linear one (correlation coefficient = .8). From this relation, and predicted loads transmitted across an involved spinal region, an estimate of device life may be predicted.

## REFERENCES

- 1) Kasman, R.A., Chao, E.Y.: Fatigue Performance of External Fixator Pins. *J. Orthopaedic Res.* 2(4):377-84, 1984
- 2) Krag, M.H., Beynon, B.D.: An Internal Fixator for Posterior Application to Short Segments of the Thoracic, Lumbar, of Lumbosacral Spine design and testing. *Clinical Orthopaedics.* 203:75-98, 1986.

- 3) Nasca, R.J., Hollis, J.M., Lemons, J.E., Cool, T.A.: Cyclic Axial Loading of Spinal Implants. *Spine*, 10(9):792-798, 1985.
- 4) Zand, M.S., Goldstein, S.A., Matthews, L.S.: Fatigue failure of Cortical Bone Screws. *J. Biomechanics*, 16(5):305-311, 1983.

Figure 1

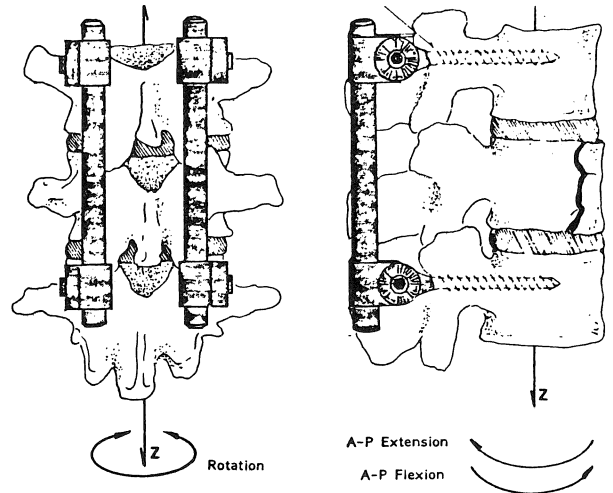


Figure 2

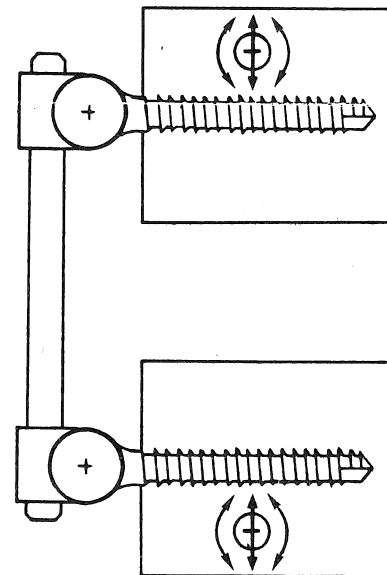
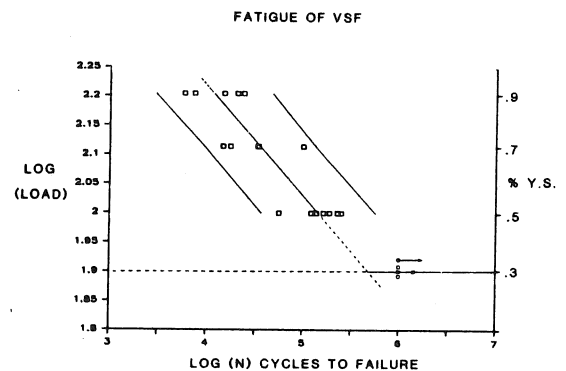


Figure 3





## Index List of Contributors

Akre, F.	55	Charteris, J.	<b>224,299,305</b>	Fondrk, M.	153
Alexander, J.	259	Chase, J.	275	Forsell, J.	151
Allard, P.	<b>185,197,271</b>	Chehade, A.	55	Frank, J.	141
Anderson, D.	161	Chen, S.M.	21,251	Frazer, M.	99
Andersson, G.	89	Cheung, T.K.	181	Frymoyer, J.W.	165
Andrews, J.G.	13,207	Choi, K.W.	125	Fujikawa, H.	293
An, K.N.	15,97	Chuinard, R.	29	Furnée, E.H.	273
Bahniuk, E.	153	Chyan, D.	51	Fyhrie, D.P.	131
Baratta, R.	71	Clouse, S.D.	177	Gagnon, M.	55,81
Barbeau, H.	269	Cooke, T.D.V.	281	Gasser, B.	155
Bates, B.T.	<b>179,195,215,307</b>	Cooper, L.B.	<b>249,295</b>	Gilbertson, L.G.	87,115
Bejjani, F.J.	51,57,117	Costigan, P.A.	27	Glover, R.	193
Beynnon, B.D.	143,165	Cowling, K.	151	Godfrey, C.M.	201
Bhattacharya, A.	259	Cresswell, A.G.	25	Goldstein, S.A.	125
Bjerkreim, I.	109	Dansereau, J.	253	Gomez, M.A.	101
Bobbert, M.	69	Dapena, J.	37,291	Gordon, M.E.	247
Borra, H.	99	Davy, D.T.	153	Gotzen, L.	129
Borra, R.J.	226	Day, B.	31	Gracovetsky, S.A.	91
Bramble, D.	3,169	Degnore, L.	125	Gravel, D.	11,183
Brand, R.	13,161	Denoth, J.	<b>193,213</b>	Griffin, M.P.	27
Broman, H.	89	Derby, D.	39	Grindeland, R.	149
Brooks, S.	259	Desjardins, S.	11	Groenendyk, J.S.	303
Brouwer, B.	185	DeVita, P.	215	Gross, T.S.	191
Brown, J.	141	Dickey, J.P.	219	Haas, N.	129
Brown, T.	13,161	Dick, R.W.	233	Hafex, A.A.M.	181
Bullard, S.K.	181	Dimnet, J.	107	Halpern, N.	57
Bunch, R.P.	191	DiMonte-Levine, P.	277	Hamill, J.	<b>195,215</b>
Burkowski, F.	31	Dowling, J.J.	243	Hamilton, N.	47
Burleson, E.M.	101	Drouin, G.	85,121,127	Hanna, A.	123
Burns, S.A.	226	Duhaime, M.	271	Hansson, T.H.	147
Byrne, K.B.	87,105,115	Dumas, G.A.	81,127	Hart, T.J.	77
Cady, C.T.	247	D'Ambrosia, R.	29,71	Haseganu, E.	39
Cahalan, T.D.	63	Engin, A.E.	21,251	Haugh, L.D.	87,165
Cairns, B.	283	Engsberg, J.R.	207	Hayes, K.C.	73
Carter, D.R.	131,133,135,145	Enneking, W.	221	Hay, J.G.	43
Cavanagh, P.R.	<b>205,209,233,287,297</b>	Feltner, M.E.	37,291	Hein, T.J.	159
Chang, W.	51	Fillion, M.	11,261,263	Herzog, W.	59
Chao, E.Y.S.	15,63,97,159	Finch, L.	269	Hill, D.L.	53,111
Chapman, A.E.	45	Fleckenstein, S.J.	255	Himeno, S.	15,97
Charbonneau, N.	127	Fleming, B.	163	Holden, J.P.	209

\* Bold characters refer to pagination of volume II





Hollis, J.M.	101	Maki, S.	141	Ounpuu, S.	265
Hoshizaki, T.B.	17	Malouin, F.	257	O'Connor, W.	267
Hotchkiss, R.N.	159	Manley, M.T.	279	Pallone, P.	153
Hoy, M.G.	95,247	Martin, P.E.	41,229	Panjabi, M.M.	147
Hubbard, M.	151,217,293	Matthews, L.S.	125	Parnianpour, M.	117
Huk, O.	271	McBride, I.	281	Patel, P.	259
Hurley, P.	279	McCarthy, L.	141	Paterson, E.G.	217
Iacono, S.	91	McCaw, S.T.	307	Patla, A.E.	65,79,177
Inoue, M.	101	McFadyen, B.	31,241	Patt, N.	113
James, D.F.	19	McGill, S.M.	113	Pavlidis, L.	117
Jefferson, R.J.	285	McGuirk, T.	295	Pederson, D.	13
Jensen, R.K.	227	McIntyre, G.	121	Perissinotto, A.	159
Jimenez, M.	161	McIvor, J.B.	111	Perren, S.M.	155
Johnson, G.B.	115	McNeill Alexander, R.	7,173	Petty, R.W.	275
Jorneus, L.	89	Meller, B.T.	279	Piette, V.	11,261
Jovanovic, M.	81	Meyer, S.	161	Pijanowski, G.J.	226
Kekosz, V.	283	Michaels, C.	153	Pinzur, M.	277
Keller, T.S.	135,147	Mikosz, R.P.	23	Piotrowski, G.	157
Kemp, F.	55	Miller, G.J.	157,221,223,275	Pope, M.H.	49,89,107,119,163,165
Kirby, R.L.	255	Miller, J.A.A.	43,109	Poulin, M.J.	81
Knutzen, K.	179	Miller, L.	115	Pratt, T.J.	19
Krag, M.H.	87,105,115,143,165	Miller, M.K.	195	Préfontaine, J.	257
Krettek, C.	129	Moeinzadeh, M.H.	226	Raso, V.J.	111
Kristiansen, T.	163	Moorman, R.P.	289	Reid, J.G.	103
Kumar, S.	53	Moreland, M.S.	253	Reinecke, S.	49,163
Ku, J.L.	125	Morlock, M.	231	Riach, C.L.	73
Labelle, H.	185,271	Morton, D.J.	103	Ricard, M.D.	195
Ladin, Z.	139	Motriuk, H.U.	203	Richards, C.L.	11,183,261,263
Laible, J.P.	253	Mueller, R.T.	249	Rivard, C.H.	127
Levine, W.S.	247	Mukherjee, J.	151	Robbins, S.E.	123
Limbird, T.	99	Mungiole, M.	229	Robertson, D.G.E.	235,239
Lin, J.L.	289	Naumann, S.	283	Roberts, E.M.	181,289
Liu, S.H.	63	Neale, G.	163	Rodgers, M.M.	205
Loo, W.	197	Neal, R.J.	35,211,303	Roy, B.	81
Lortie, M.	55	Nigg, B.M.	193	Rozendal, R.H.	69
Luethi, S.	187	Nordin, M.	117	Russell, G.G.	111
MacIntyre, D.	239	Normand, M.C.	263	Sanderson, D.J.	297
MacKinnon, C.D.	201	Norman, R.W.	113,243	Schieb, D.A.	199
MacLeod, D.A.	255	Olney, S.J.	27,281	Schmidt, R.A.	77
Main, J.A.	135	Orcutt, A.E.	217	Schneider, E.	155

\* Bold characters refer to pagination of volume II

Schneider, K.	77	Trimble, J.	277
Schot, P.	179	Tsumura, H.	15,97
Schultz, A.B.	83,109	Turnbull, G.I.	224
Scott, P.A.	305	Tylkowski, C.M.	157,221,223,275
Segesser, B.	187	Vagenas, G.	17
Selker, F.	133	Vailas, A.	149
Seroussi, R.E.	105,107,119	Vaillancourt, H.	121
Shadwick, R.E.	137	Valiant, G.A.	295
Shaw, S.	149	van der Woude, L.H.V.	69
Sherman, R.	277	van Ingen Schenau, G.J.	69
Shiavi, R.	99	Voloshin, A.S.	189
Shirazi-Adl, A.	85	Vrahas, M.	13
Shoji, H.	71	Wainberg, M.	269
Shorten, M.R.	249	Wall, J.C.	224,299,305
Siler, W.L.	41	Watson, G.	39
Singer, K.P.	25	Weber, P.	155
Sirin, A.V.	65	Weisman, G.	49
Smith, A.W.	301	Wells, R.	61,75
Snyder, C.W.	35	Whalen, R.T.	131,145
Solomonow, M.	29,71	Wheeler, D.L.	223
Soutas-Little, R.W.	151	White, S.C.	67
Spengler, D.M.	135,147	Whittle, M.W.	285
Sprigings, E.	39	Wilder, D.G.	89,105,107
Springfield, D.	157,221	Williamson, N.R.	157,221
Steele, C.R.	145	Williams, K.R.	287
Steen, H.	109	Wilson, B.D.	35,211,303
Stein, S.	125	Winter, D.	31
Stevenson, P.J.	245	Winter, D.A.	5,31,67,171,219,237,241,265,301
Stifter, A.	49	Wood, G.A.	25
Stokes, I.A.F.	93,253	Woo, S.L-Y.	101
Strauss, A.M.	135	Wyss, U.P.	27,281
Stüber, E.N.	61,75	Yamaguchi, G.T.	95
Stuessi, E.	187	Yang, J.F.	237
Sveistrup, H.	17	Yeadon, M.R.	33,231
Svensson, M.	89	Yoshia, S.	279
Tannenbaum, H.	197	Zajac, F.E.	95,245,247
Tepperman, P.	283	Zernicke, R.F.	77,149
Topp, E.L.	245,247	Zhou, B.-H.	71
Trausch, I.	105		
Triano, J.	83		

\* Bold characters refer to pagination of volume II



### List of Exhibitors

---

Advanced Mechanical Technology, Inc.  
141 California Street  
Newton, MA  
USA 02158  
(617) 964-2042

Chattecx Corporation  
101 Memorial Dr.  
P.O. Box 4287  
Chattanooga, TN  
USA 37405  
(615) 870-2281

Holt, Rinehart and Winston  
of Canada Ltd  
55 Horner Avenue  
Toronto, Ontario  
Canada M8Z 4X6  
(416) 255-4491

Intertechnology, Inc.  
3675 Blvd. des Sources, Suite 105  
Dollard-des-Ormeaux, Québec  
Canada H9B 2T6  
(514) 683-0930

Kistler Instrument Corporation  
75 John Glenn tr.  
Amherst, NY  
USA 14120  
(716) 691-5100

The Langer Biomechanics Group Inc.  
21 E. Industry Court  
Deer Park, NY  
USA 11729  
(516) 667-1200

Northern Digital  
415 Phillip Street  
Waterloo, Ontario  
Canada N2L 3X2  
(519) 884-5142

Oxford Metrics, Inc.  
14206 Carlson Circle  
Tampa, FLA  
USA 33625-2803

Selspine AB  
Selective Electronic, Inc.  
1233 Chicago Road  
Troy, MI  
USA 48083

### Extraneous Activities

---

ISB Council Meeting

Working group on the definitions, terms and conventions for use in research of human gait (Joint effort of CSB and ISB).

### **Acknowledgements**

The Organizing Committee of the North  
American Congress on Biomechanics  
acknowledges the generous support of the  
following institutions:

**DÉPARTEMENT D'ÉDUCATION PHYSIQUE  
UNIVERSITÉ DE MONTRÉAL**

**CANADIAN HOWMEDICA, LTD**

**NATIONAL SCIENCES AND ENGINEERING  
RESEARCH COUNCIL OF CANADA**

**EMPLOYMENT AND IMMIGRATION CANADA**

